EFFECTS OF TURBULENT SHEAR STRESS ON PLANT CELL SUSPENSION CULTURES

by

Darika Darlene Sowana

Thesis submitted for the degree of
Doctor of Philosophy

in

Adelaide University, Australia
Department of Chemical Engineering
Faculty of Engineering

October 2001

This work contains no material which has been accepted for the award of any other degree or diploma in any university or other tertiary institution and, to the best of my knowledge and belief, contains no material previously published or written by another person, except where due reference has been made in the text

I give consent to this copy of my thesis, when deposited in the University Library, being available for loan and photocopying.

SIGNED: .....

DATE: 23/7/02

ACKNOWLEDGEMENTS

I would like to express my gratitude to my supervisors Dr David Williams, Dr Brian O'Neill and Dr Bassam Dally. Their guidance, patience and encouragement have been most appreciated throughout the project. I would like to thank Professor Eric Dunlop for his initiative advice and help on this project. I would also like to thank Dr David Fletcher at the Department of Chemical Engineering at University of Sydney for his invaluable advice and support on the computation fluid dynamic work.

I am most indebted to Mr Jason Peak and Mr Peter Kay at the departmental workshop for their advices and the construction of the experimental apparatus. I would like to acknowledge Mr Stan Woithe at Civil and Civil and Environmental Engineering for his assistance with the assembly of electronic parts, and the School of Molecular Biology and Immunology at the Department of Molecular Bioscience for allowing me to share their equipment. I am most grateful to Mr Chris Mansell for his technical assistance in the biochemical engineering laboratory, and Mrs Mary Barrow and Mrs Elaine Minerds for their support throughout the difficult time.

This project had the financial support from the Australian Research Council, Australian Postgraduate Awards and Departmental of Chemical Engineering at Adelaide University. The Research Abroad Scholarship from Adelaide University is also gratefully acknowledged.

The encouragement from everyone at the Department of Chemical Engineering during the degree was also most appreciated. I would especially like to thank all the postgraduate students and my friends outside the university for their friendships, encouraging words and valuable discussion.

Finally, I would like to thank my mother, father and Ben for their advice, love and encouragement. This work would not have been possible without their unwavering support.

"*But we should be looking for unifying principles that will order our facts into some understanding.*"

Alfred G. Gilman

SUMMARY

The potential of plant cell culture technology has been extensively considered in the commercial production of numerous valuable plant products, including pharmaceuticals, flavour enhancers and fragrances. However, successful scale-up application of various plant cell cultures has been limited by their shear sensitivity to turbulent shear stress in commercial bioreactors. Shear sensitivity is one of the prime factors that compromise productivity in large-scale fermentation. Consequently, ongoing research into plant cell cultures is being directed towards understanding the rate limiting steps in the biosynthesis pathway associated with the problem of shear sensitivity.

The studies presented in this thesis aim to

(i) improve the characterisation of the biological response of plant cell subject to shear stress,

(ii) expand the understanding of the interaction between cells and the turbulent eddies,

(iii) investigate how the cell-eddy interaction influenced calcium transient in the sublytic response, and

(iv) investigate if the effect of turbulent eddies could be moderated using shear-protective polymers.

The local profiles of energy dissipation rate and shear stress were simulated using computational fluid dynamics (CFD). The information obtained from the CFD calculations was implemented in the modelling of the effects of the local fluid forces on cell aggregates, leading to various sublytic responses mediated by calcium signalling.

Shearing experiments were performed in a novel turbulent shear apparatus, consisting of an annulus bowl and a cylindrical stirrer. The cylindrical stirrer rotated to generate turbulent wakes. The average energy dissipation generated ranged from 2 to 5.5 W/kg, which corresponded to the Reynolds number range of 4690-7040. The average energy dissipation rates were comparable to the values generated in a conventional stirred tank bioreactor. The maximum energy dissipation rates obtained from the CFD simulation varied from 29 to 122 W/kg. *Daucus carota* (wild carrot) cell suspension cultures were

subjected to a range of turbulent shear intensities and exposure time. The indicators of the biological responses included the relative mitochondrial activity, aggregate size and membrane integrity. The kinetics of these responses exhibited an initial lag phase, followed by a first-order decay.

A statistical analysis indicated that the biological responses of carrot cells strongly depended on both time and energy dissipation rate. The results also confirmed that the cumulative energy dissipation varied significantly with the shear environment. Further analysis demonstrated that a more appropriate parameter for shear-sensitivity studies should include the energy dissipation rate, fluid circulation time and impeller geometry.

Characterisation of cell aggregates confirmed the complex morphology of carrot cells. The cell geometry deviated substantially from a spherical shape. Larger cell aggregates were found to be less tolerant to shear and break preferentially to form smaller, more shear-resistant aggregates. The modelling of turbulent shear stress on the cell surface using CFD results confirmed that larger aggregates experienced significantly higher shear stress. The stretching of the cell membrane caused by these fluid forces exceeded 2%, which was sufficient to open the mechano-sensitive calcium channels.

Modelling of cell membrane stretching highlighted the role of calcium in sublytic responses. Abnormal activity of mechano-sensitive calcium channels can lead to an increase in cytosolic calcium ion concentration. A mathematical model was developed to describe the calcium transient associated with shear damage mechanisms in plant cells. The model predicted that the membrane stretching resulted in calcium transients that resembled the reported responses to cold shock and wind in tobacco and Arabidopsis seedlings. Furthermore, these predicted calcium transients strongly agreed with the calcium response pattern observed in endothelial cells subject to fluid shear stress. These results also confirmed that mitochondria have an essential role in regulating cellular calcium. Unfortunately, there has been no reported results for calcium transients in plant cells subjected to shear.

The preliminary factorial studies of the effects of shear-protective agents on carrot cells demonstrated that the damaging effect of turbulent shear could be moderated. Significant improvement in the mitochondrial activity was observed for carrot cells grown in a

medium supplemented with the surface-active polymer, Pluronic F-68 (PF-68). However, the protective effects of a viscosity-enhancing polymer, carboxymethyl cellulose (CMC) was insignificant. These results indicated that shear-protective mechanism of PF-68 was achieved by physical interaction between PF-68 and the cell membrane. This interaction could strengthen cell membrane fluidity or form a protective layer surrounding the cell to moderate the fluid tension exerted on its extracellular matrix.

This study introduced several key factors that assist the understanding of how fluid shear stress affected the biological responses in plant cells. It also highlighted that the local fluid-cell interaction is of crucial importance in characterising shear damage, allowing predictions to be made on how fluid stress might be perceived locally by the cells. Reducing this cell-fluid interaction has been shown to moderate the damage sustained by the cells. It was also confirmed that the extracellular matrix is an important gateway to stress signal transduction in plant cells. These results enhance the current understanding of the cellular responses of plant cells to hydrodynamic shear.

TABLE OF CONTENTS

LIST OF FIGURES

LIST OF TABLES

CHAPTER 1

INTRODUCTION

1.1. Background

Plants currently supply in excess of twenty thousand valuable compounds including pharmaceuticals, pigments and other fine phytochemicals (Zhong et al., 1995). In 1983, the US Congress reported that plant derived pharmaceuticals and metabolites constituted an annual market of nine billion US dollars at the consumer level, compared to the aroma components, which represented a worldwide market of only 1.5 billion dollars (OTA, 1983). Many commercial plant-derived products are too complex to synthesise chemically. Consequently, many compounds are currently extracted from natural and cultivated whole plants, which are subject to diseases, variable climatic conditions and genetic instability. Plant cell culture technology is an attractive alternative to the conventional plantation. Processes involving extraction from whole plants are experiencing difficulty in satisfying the growing demand for these valuable compounds, and fermentation is considered an attractive alternative route. Fermentation has the advantage of producing a higher yield of consistent quality chemicals (Sajc et al., 2000). An additional benefit for the industrial-scale plant cell culture mode is the conservation of threatened plant species.

Unfortunately, production of plant cell cultures in large-scale fermenters also encounters significant difficulties. Even though the fermentation technology is well established for microorganisms, its direct application to plant cell cultures has not proved as simple or as fruitful. Since the first commercial production of shikonin was successfully produced from *Lithospernum erythorhizon* cell cultures, many attempts have been made to produce phytochemicals from various other cell lines (Fujita and Tabata, 1987). Current commercially successful plant cell culture processes include shikonin, ginsenosides and berberine, but other cell cultures are still produced for research purposes under laboratory conditions in shake flasks rather than in a stirred bioreactor (Sajc et al., 2000). The major

constraint that restricts large-scale production of plant cell cultures is poor yield of products due to their shear sensitivity. Slow growth rates and rapid sedimentation also lead to limitation in mass transfer and susceptibility to contamination by other microorganisms. Consequently, the continuous fermentation of plant cell cultures has proven to be nearly impossible (Guardiola et al., 1995).

Although the hypersensitivity of plant cells to shear has been well recognized, surprisingly few reports are available on the effect of hydrodynamic shear forces on their growth and viability (in comparison with their mammalian counterpart) (Ho et al., 1995). However, the key to improved reactor design is to identify the rate limiting steps in the biological pathways that control the sensitivity of plant cells to fluid forces. The shear sensitive nature of plant cells means that significant problems are encountered particularly in attaining homogeneous suspension and good oxygen mass transfer in a fermenter using the conventional arrangement for microbial cell growth. Unfortunately, adequate mass transfer requires vigorous agitation, which compromises growth and viability of plant cells in the bioreactor.

A number of studies have quantified the viability of various species of plant cell cultures cultivated in stirred tank bioreactors (Wagner and Vogelmann, 1977; Scragg et al., 1988; Zhang et al., 1994; Rodrigues-Monroy and Galindo, 1999). Their results have been reported in terms of shear rate, shear stress and impeller speed. However, these variables are highly system-specific and they are not universally applicable to other bioreactor configurations. Adoption of the optimal operating conditions for a given cell culture cannot guarantee similar performance with other cell lines. A lack of universal design parameters has prompted studies on the suitability of various impeller geometries for different plant cell applications (Doran, 1999).

In parallel to these studies, advances in biotechnological expertise have focussed growing attention on studies of stress signalling pathways. It is hoped that this work may reveal how the cell responds to hydrodynamic stress, and how these pathways may be manipulated to produce shear-tolerant cells. Plant cells exposed to a shear environment sustain serious physiological damage prior to the occurrence of any physical signs or cell death (Dunlop et al., 1994). These sub-lethal conditions precede the onset of irreversible damage and they may be early indicators of metabolic malfunction.

While the transduction of hydrodynamic stress signals within plant cells are not fully understood, the studies of sub-lytic effects play a role in elucidating shear damage mechanisms (Kieran et al., 2000). One of the proposed hydrodynamic stress transduction mechanisms is through the ion channels. The hydrodynamic stress signals are transduced into plant cells through second messengers, particularly calcium ions (Takeda et al., 1997). Evidence suggests that mechanical stresses, such as tension, compression and variation of turgor pressure can cause cytosolic calcium ion concentration to rise abnormally (Knight et al., 1992; Trewavas and Knight, 1994). Hydrodynamic shear stress results in a similar form of mechanical stretching of the cell membrane, which can activate ion channels known as stretch-activated ion channels (Schroeder and Thuleau, 1991; Ding and Pickard, 1993). These channels are suspected to be responsible for increasing calcium ion transport into cells during exposure to shear stress. An oversupply of intracellular calcium ions may lead to mitochondrial damage, cytoskeletal alteration, and other metabolic dysfunctions (Campbell, 1985; Malek and Izumo, 1996; LoSchiavo et al., 2000). These phenomena are ultimately linked to sub-lytic effects in plant cells. They can retard growth and cause eventual cell death (Aloi and Cherry, 1994). Despite the widely speculated hypothesis on the damage mechanisms, the stress transducing mechanisms of biological responses in plant cells remain unclear.

Successful development of plant cell processes clearly requires appropriate modifications to existing fermenter technology. Therefore, ongoing research on various physiological responses of plant cells in bioreactor systems must be maintained. While the bulk behaviour of the fluid can be reasonably estimated, it is difficult to predict the microscale structure of the fluid. Unfortunately, this is where the majority of the energy is dissipated. Many studies have characterised the local and maximum energy dissipation rate in bioreactors (Wu and Patterson, 1989; Zhou and Kresta, 1996a, 1996b). In a bioreactor, the intense vortex motion, and the regions of high shear and energy dissipation are localised in or near the impeller region rather than the bulk of the fluid (Cutter, 1966). The impeller region is likely to cause more significant damage to cells. The local energy dissipation rate is difficult to determine as the volume in which the energy decays varies from one location to another. A recent study has successfully simulated the local turbulent flow structure in a small-scale rapid extensional flow using computational fluid dynamics (Gregoriades et al.,

2000). This technology combined with further experimental studies may uncover the unknowns of transduction of mechanical stress signal at a cellular level.

1.2. Objectives of the Studies

The focus of the current work is to refine the characterisation of turbulent shear stress and its effects on the biological activity of plant cells. It also aims to establish mathematical models to elucidate the effect of turbulent shear stress on calcium transients during sublytic responses of plant cells.

Wild carrot or *Daucus carota* cells were subjected to turbulent shear fields in a novel stirring apparatus. The shear-sensitivity studies focus on four main aspects. Firstly, the hydrodynamic structures were quantified using a computational fluid dynamic (CFD) software package. Visualisation of the complex turbulent flow profiles provided vital information regarding the local flow conditions. These results are integrated in the development of the models describing the surface shear stress and strain rate on irregular cell aggregates of various sizes.

Elevated levels of calcium are often implicated in cell damage mechanisms. The cell membrane stretching generated by fluid forces is a critical factor, which influences calcium signal transduction during sublytic responses in plant cells. The mechano-sensitive calcium channels have been reported as the primary gateways, through which excess calcium ions enter the cell (Ding and Pickard, 1993). Unfortunately, the transduction pathway of calcium in stress signalling remains unclear, as changes in calcium level are extremely difficult to detect in plant cells. Kinetic modelling of calcium transients in plant cells could enhance our understanding of their transient behaviour. Consequently, this work also aims to develop a kinetic model to predict this calcium transient using the results obtained from the CFD simulations and the surface strain rate model.

Finally, a number of studies have discussed the benefit of polymer additives as shear protective agents for animal and insect cells (Michaels et al., 1992; Zhang et al., 1992b; Michaels et al., 1995; Palomares et al., 2000). Surfactant compounds, such as Pluronic alcohols were found to alter cell membrane fluidity and increase its tolerance to

hydrodynamic stress. The potential of these agents has not yet been explored in plant cells. Hence, this work also investigated whether these compounds could alleviate the effect of surface shear stress. The four aspects of the shear-sensitivity studies explored in this thesis are summarised in Figure 1.1.

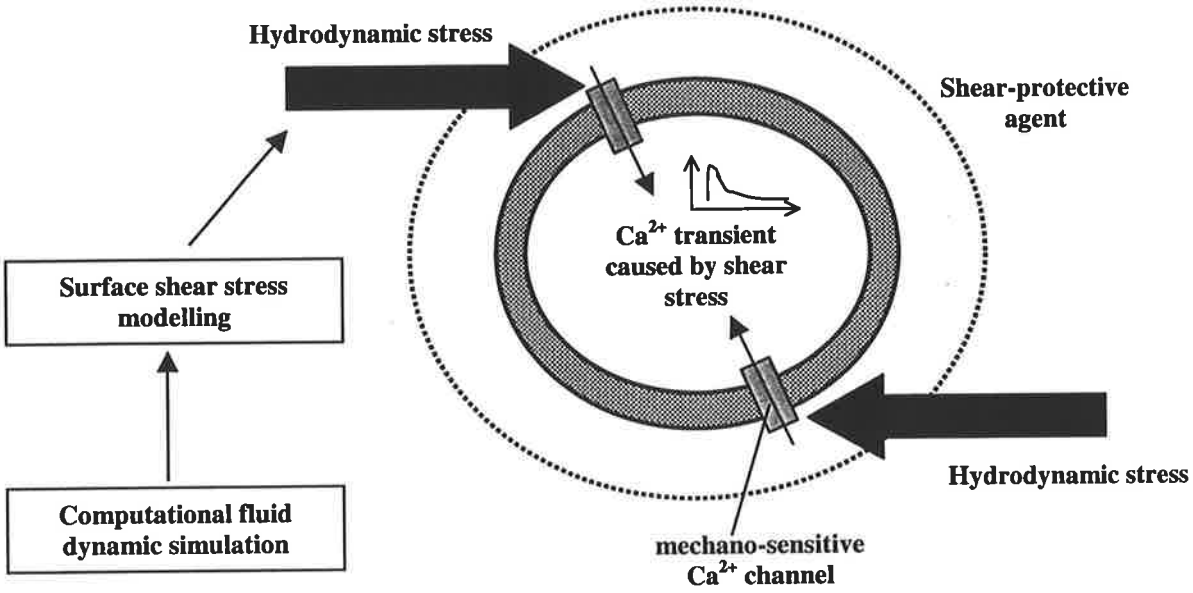

Figure 1.1. A summary of the four objectives of the project

In summary, the aims of this work are to (i) quantify the complex turbulent structures using computational fluid dynamics (CFD), (ii) use the information from CFD to describe how cells are locally affected by turbulent shear stresses, (iii) predict the influence of local turbulent shear stress on calcium transient, which plays an important role in sublytic responses in plant cells, and (iv) investigate techniques to alleviate the effects of shear stress on plant cells.

1.3. Thesis Organisation

Chapter 2 highlights the background information on the development of plant cell technology, limitations of the scale-up systems, and previous studies in this area.

Techniques of determining biological responses are also summarised. Hypotheses on biological responses leading to sub-lytic effects are presented. Various techniques applied in the studies of the effects of hydrodynamic shear stress on plant cells are also discussed.

The experimental design and procedures are outlined in **Chapter 3**, where the experimental and biological assay techniques are described in detail.

The hydrodynamic parameters, describing the flow regime in the experimental apparatus are presented in **Chapter 4**. The 'local' flow structures were numerically modelled using a computational fluid dynamic software package, CFX. The relationships between local and average parameters, such as the energy dissipation rate established from the simulations will be presented.

Chapter 5 presents the results on the effects of turbulent shear stress on biological responses of carrot cell cultures. The data confirm a strong dependence on time and energy dissipation rate, which highlights the need for better understanding and correlations. The biological responses were quantified in terms of bulk and local hydrodynamic properties. A more global parameter for defining the hydrodynamic in shear-sensitivity studies will be proposed. In addition, the kinetics models characterising the change in viability of plant cells exposed to turbulent shear stress will also be discussed.

The complexity of plant cell aggregates is investigated in **Chapter 6**. Several shape factors were calculated to demonstrate that their morphology differs substantially from simple spherical particles. Hence, the level of shear stress applied on the cell surface varies with the morphology of individual cell aggregates. This chapter will also present a mathematical model, which is developed to define a variable that describes the irregularity of cell aggregates. This model implements the results from CFD calculations from Chapter 4 to enhance the evaluation of the surface shear stress and membrane stretching experienced by the cells.

The membrane stretching calculated in Chapter 6 suggests that a significant increase in cytoplasmic calcium concentration is associated with the sublytic responses in damaged plant cells. A kinetic model to predict this cytosolic calcium transport is proposed in **Chapter 7**. The model is based on a system of differential equations obtained from mass

balances of calcium ion in a cell. The kinetics of cytosolic calcium concentration is described by damped oscillations of a typical feedback control system, which can be simulated using the Matlab-Simulink software package.

A possibility of alleviating the damaging effects of turbulent shear stress will be discussed in **Chapter 8**, where the potential role of polymers, Pluronic F-68 and carboxymethyl cellulose as shear-protective agents for plant cells is investigated. The experiments are performed following a complete two-level, three-factor factorial design strategy. The main effects and their interactions are statistically analysed and discussed.

Finally, the results of these studies will be summarised in **Chapter 9**, where future work will also be recommended.

CHAPTER 2

LITERATURE REVIEW

The initial development of plant cell culture produced a means for the study of the physiological and biochemistry of plants. As culturing techniques developed, the commercial potential of plant cell culture was realised. It was a potential source of a wide range of enzymes, secondary metabolites and compounds which are characteristic of the original plants (Scragg, 1995). Various examples of these compounds and their potential applications are shown in Table 2.1.

Table 2.1: Plant Metabolites and Their Applications (Meijer, 1988; Sharp et al., 1995).

Products	Plant Compounds	Application
Pharmaceuticals	ajmalicine	anti-hypertensive, circulatory problems
	codeine	analgesic
	digitalis	cardiatonic (heart disorder)
	quinine	malaria
	shikonin	anti-inflammatory and pigment
Fragrances	jasmine oil	perfume
	rose oil	perfume
Food Flavours	mint oils	mint flavour
	vanillin	vanilla flavour
	crocin	saffron
	quassin	bittering agent
Insecticides	nicotine	insecticide
	pyrethrin	insecticide

Commercial-scale production normally requires a large volume of plant cell culture to be grown in a bioreactor. Unfortunately, its competitive advantage compared to the traditional agricultural and chemical synthesis will remain only if the production targets high value added compounds produced in relatively small quantities. Examples of compounds available from plant cell cultures include shikonin from *Lithospermum erythrorhizon*, ginsenosides from *Panax ginseng* (Kieran et al., 1997) and taxol or Paclitaxel. Taxol is considered one of the most successful treatments for breast, ovarian and lung cancers (Alexander, 2001). Unfortunately, taxol is only available in small amounts from the bark of a rare Pacific yew species (Nicolaou et al., 1996). Furthermore, its chemical synthesis is complex requiring many expensive synthesis steps (Scragg, 1995; Alexander, 2001). Consequently, taxol is an ideal candidate for plant cell culture technology.

Although other plant tissue or differentiated cultures, such as roots, embryos and hairy roots can provide alternative processing modes, plant cell suspension culture still has more immediate potential for industrial application. Extensive knowledge and expertise exists for processing suspension cultures. A significant fraction of the investment in plant cells has been directed toward the commercialisation of plant cell suspension culture rather than other tissue and organ cultures, as these are constrained by novel techniques and expensive equipment (Kieran et al., 1997).

This chapter provides an overview of the commercial development of plant cell suspension culture technology. It focuses on the limitations of the process, specifically the hydrodynamic shear sensitivity. Recent outcomes from the studies on shear sensitivity of plant cells are also reviewed to elucidate improved and advanced techniques to accurately identify the damage mechanisms in plant cell cultures exposed to hydrodynamic shear.

2.1. Commercial Development

Industrial-scale processes for plant tissue culture processes have been considered for the past four decades. However, it was not until the early 1980s that such processes achieved commercial success. The success of the shikonin process from *Lithospermum erythrorhizon* by Mitsui Petrochemical Industries, Ltd. in Japan in 1983 (Su, 1995)

spawned increased interest in plant cell culture. Research into such processes has become an active area of study, both commercially and academically. Numerous commercial developments have occurred in Japan, with minor successes in the United States and Europe. Examples of promising patents granted in the area of plant tissue culture technology between 1988-1992 are presented in Table 2.2.

Table 2.2: Japanese Patents in Plant Tissue Culture Technology (Sharp et al., 1995; Su, 1995).

Year	Title of invention	Assignee	Remarks
1988	Production of cultured plant cell containing anti-oxidative substance	Kobe Steel Ltd.	Sesame culture
1988	Production of albumin	Shiseido Co. Ltd.	Biotransformation of hydroquinone by *Catharanthus roseus*
1989	Agent for suppressing blood pressure	Kao Co.	Callus culture of *Musci* or *Hepaticae*
1989	Culture of herb plant tissue	Mitsubishi Heavy Ind. Ltd.	Production of essential oil
1989	Production of antiulcer agent	Nitto Denko Co.	Cell culture of a pea family plant
1990	Anticancer agent	Kao Co.	Acidic heteropolysaccharides from cell culture of the genus *Polianthes* L.
1991	Production of taxol in cell culture	US Secretary of Agriculture	Cell culture of *Taxus brevifolia* to produce taxol and related alkaloids
1992	Production of plant gum material using tissue culture	Bio Polymers Pty Ltd. and Commonwealth Scientific and Industrial Research Organisation	Gum-secreting plant cells in tissue culture. Gum can be recovered from the culture medium

In recent years, numerous potentially attractive compounds have been discovered and extracted from various species of plant cells. Plant cell products with significant potential for commercialisation are shown in Table 2.3. Many compounds can be produced at high yields. Unfortunately, the bulk of these are not commercially desirable. Valuable products have been produced at laboratory-scale using shake flasks rather than in commercial bioreactors (Scragg, 1995). However, slow growth rate and poor yields often occur in large-scale bioreactors. Furthermore, production from large-scale processes is often irreproducible, due to susceptibility of plant cells to hydrodynamic forces, particularly the turbulent shear stress. These problems coupled with the requirement for sufficient mixing in a bioreactor are responsible for the reduction in overall productivity experienced by the industrial-scale plant cell tissue culture bio-processes.

Table 2.3: Productivity and price for plant cell culture products

Product	Application	Plant Source	Productivity (g/L/day)	Price* ($US/kg)	
Berberine	drug	*Coptis japonica*	0.60	3250	(Fujita et al., 1987)
Codeine	sedative	*Papaver somniferum*		17000	
Digoxin	heart stimulant	*Digitalis lanata*		3000	
Diosgenin	steroid	*Dioscorea deltoidea*	0.028	1000	(Sahai et al., 1985)
Morphine	drug	*Papaver somniferum*		0.34M	
Quinine	anti-malarial	*Cinchona ledgeriana*		500	
Sanguinarine	antibiotic	*Papaver somniferum*	0.034	4800	(Park et al., 1992)
Shikonin	anti-bacterial	*Lithospermum erythrorhizon*	0.15	4500	(Fujita et al., 1987)
Taxol	anti-cancer	*Taxus brevifolia*		0.6M	
Vanillin	flavour	*Vanilla planifolia*		1000	
Vincristine	anti-leukaemic	*Catharanthus roseus*		20M	

*Data from (Curtin, 1983; Sahai et al., 1985; Scragg, 1995; Verpoorte et al., 1993)

2.2. Bioreactor Design

The behaviour of plant cell culture in bioreactors has been the subject of study for many years. Numerous workers have attempted to rectify the difficulties involved in scale-up of

processes. Most of the successful fermentation processes were developed for microbial systems. Unfortunately, the use of microbial technology to grow plant cells frequently led to failure. A successful bioreactor system for plant cell cultures requires the appropriate specifications, which address the problems of insufficient mixing, as well as shear sensitivity of plant cells.

A number of workers have focussed on the response of cellular system to hydrodynamic forces under cultivation conditions in a bioreactor. However, many of these studies were highly system-specific. The stirred-tank reactor is primarily employed in the study of shear effects on plant cells (Kieran et al., 2000).

The hydrodynamic characteristics of flow in a bioreactor are normally quantified in terms of the agitation rate, the rotation speed, and the impeller tip speed (πND). However, none of these parameters are suitable for comparative purposes across different reactor geometries. The total cumulative energy dissipation has recently been identified as more appropriate parameter (Dunlop et al., 1994; Kieran et al., 2000).

In agitated bioreactors, the bulk flow is turbulent. This turbulence is generated by impeller agitation and sparging. The velocity gradient responsible for liquid mixing also induces shearing in the fluid. For laminar flow, the shear rate is directly proportional to the shear stress. However, fluid motion during turbulence is more complex and is characterised by three-dimensional velocity fluctuations of random frequencies at a single point (Nienow, 1998). The instantaneous turbulent velocity is the summation of a time-averaged velocity component and the fluctuating velocity component. The interaction between the velocity fluctuations in different directions introduces turbulent Reynolds stresses in turbulent flow. These cause significantly more damage in cell culture than laminar shear stress of the same magnitude (Rosenberg, 1989). Clearly, plant cells may be more susceptible to specific characteristics of the turbulence, in particular, the random turbulent forces and their frequencies rather than the mean turbulent motion.

Turbulence phenomena have been widely studied for many decades. However, its complexity means that it has not yet been accurately characterised. Relatively few

theoretical studies consider turbulence in bioreactors. In addition, the bulk of these works are based on single-phase Newtonian fluids with low viscosity. Unfortunately, plant cell cultures at high cell concentration behave as inhomogeneous non-Newtonian fluids. This introduces higher levels of complexity to the system. Many empirical correlations from these studies inadequately describe the multiphase fluid-solid turbulent flow phenomena. The most common approach to model the bioreactor fluid mechanics is to apply Kolmogorov theory of isotropic turbulence (Dunlop et al., 1994; Joshi et al., 1996). Turbulent flow is assumed to consist of large primary eddies whose initial length scale approximately equal to the diameter of the impeller in the case of a stirred tank reactor or the diameter of rising gas bubble in a bubble column (Caulet et al., 1996). These primary eddies are unstable and tend to decay, transferring the energy to the smaller eddies. During the latter stages of decay, information concerning the direction of energy transfer is lost. Consequently, energy transfer occurs equally in all directions. This stage is known as isotropic turbulence where the energy transfer is statistically independent of the direction. The microscale eddies in isotropic turbulence are defined as the Kolmogorov scale eddies (Joshi et al., 1996).

In the turbulent region, eddies that are significantly larger than the cell particles entrain the particles, whereas eddies that are much smaller than the particles flow over the particles surfaces. Most damage on the cell is caused by eddies with comparable sizes to the cell (Croughan et al., 1987; Rosenberg, 1989). A significant fraction of the energy is transferred to the cell only when the sizes of these microscale eddies are comparable to the cells (Mufti et al., 1995).

Despite simplification in the Kolmogorov's theory, the theoretical results cannot be completely verified with empirical results due to the chaotic nature of turbulence in a bioreactor (Kawase et al., 1990). The need to understand such a complex flow structure in turbulence has resulted in techniques that allow turbulent parameters to be measured. Hot film and laser Doppler anemometry have become the essential tools for measuring variations in the flow structures in bioreactors. Unfortunately, these techniques involve complex equipment and complicated analysis (Nienow, 1998). Computational fluid dynamic (CFD) has also been introduced to aid the study of complex fluid-flow process, where particle motion can be simulated using three-dimensional numerical techniques. A

number of CFD software packages are now routinely implemented in the simulation of velocity, temperature profiles and pressure gradients in many complex chemical engineering applications, including pipe flow, turbines, gasification, fluidised beds and stirred tank reactors (CFX, 1997). Recently, the damage to microcarrier cell cultures by an extensional flow was simulated and quantified in terms of local flow parameters using CFD tools (Gregoriades et al., 2000). However, despite the extensive studies in the area of computational fluid dynamics, there have not yet been any extensive CFD studies involving plant cell cultures.

2.3. Limitations in the Scale-Up Processes

Scale-up of plant cell culture bio-processes normally results in a reduction in the overall system productivity (Hooker et al., 1989; Rosenberg, 1989; Dunlop et al., 1994; Kieran et al., 1995; Namdev et al., 1995; Wongsamuth et al., 1997). The principal problems limiting the performance of plant cell cultures are the difficulties in achieving sufficient nutrient transfer to the cells, their tendency to aggregate, their shear sensitivity, and problematic product extraction (Joshi et al., 1996). Plant cell cultures are also highly susceptible to contamination compared to other micro-organisms given their slow growth rates. On average, plant cells have doubling times from 20 to 200 hours making the fermentation cycle time vary from 15 days to a few months compared to 4 to 5 hours for micro-organisms such as *Escherichia coli* (Sahai et al., 1985).

The majority of plant metabolites are contained within cell vacuoles rather than in the extracellular surroundings (Sahai et al., 1985). This storage site complicates the extraction and recovery of the metabolite products in large scale processing. The rate of metabolite recovery can be enhanced, but the process complexity increases. For example, Sahai et al.(1985) reported that an increase in the recovery of metabolites by altering the membrane permeability of plant cells. The recovery rate could also be improved by using activated charcoal to adsorb the excreted metabolites and by inducing a cyclic change in the medium pH (Sahai et al., 1985).

The selection of the impeller, agitation speed and bioreactor configuration primarily depends on the shear sensitivity of the plant cells, mass transfer, and cell aggregation (Dunlop et al., 1994; Joshi et al., 1996). Impellers are usually operated at high speeds to ensure complete suspension of the cells and sufficient mixing to ensure high mass transfer rate. However, intense mechanical agitation contributes to high hydrodynamic shear stress. This results in severe damage to the cells. Hence, ideal scale-up design for stirred tank bioreactors where high mass transfer rate can be achieved without compromising cell growth and product yield is exceptionally difficult to achieve.

Due to difficulties in achieving maximum cell growth in large-scale bio-processes, a demand is clearly evident for further studies on the improvement of cell culture growth in different types of bioreactors. Individual bioreactor designs, such as stirred tank reactors (STR), air lift and bubble columns exhibit different fluid dynamic characteristics. Modifications of the bioreactors have been developed from the study of the effects of exhaust gases, dissolved oxygen and nutrient limitation on cell growth and secondary metabolites (Schlatmann et al., 1994; Ho et al., 1995). Other modifications of a conventional STR have been implemented for plant cell culture production by inducing aeration and modifications of the impeller designs to mitigate the level of hydrodynamic forces generated (Hooker et al., 1990).

Current understanding of turbulent conditions in bioreactors may not provide sufficient guidance to significantly improve the performance of plant cell culture bio-processes. Further study of the effects of hydrodynamic stress in bioreactors on the physical and biological responses of plant cells is necessary for the appropriate modifications to be made on the existing equipment and processes.

2.4. Damage of Cells by Hydrodynamic Stress: Sublytic Effects

When biological cells are subjected to fluid forces, they produce various adaptive metabolic and physical responses. Studies have demonstrated signs of biological responses of plant cells prior to cell lysis, known as the sublytic responses. The interests in the sublytic effects increases with the growing need to identify mechanisms, through which

cell metabolisms are affected by shear stress and the stress signals (Kieran et al., 2000). The sublytic responses cannot be detected with the conventional methods, such as the measurement of lysis, which indicates a complete destruction of the cells. Such level of damage is inappropriate for detection of sub-lethal responses.

A range of sublytic responses is induced by shear exposure of plant cell cultures. The early signs of sublytic damage include a decrease in growth rates, loss in ability to grow, and a decrease in mitochondrial activity (Dunlop et al., 1994; Wongsamuth et al., 1997). These symptoms normally indicate damages to the cellular functions. These damages are often accompanied by a release of intracellular metabolites, such as proteins and phenolic compounds (Wagner et al., 1977; Abu-Reesh et al., 1989; Hooker et al., 1989; Meijer et al., 1993; Namdev et al., 1994; Takeda et al., 1994; Al-Rubeai et al., 1995).

An advanced stage of sublytic damages is often indicated by a reduction in average cell aggregate size, a loss in membrane integrity, and a severe alteration of cell morphology and cytoskeletal network (Rosenberg, 1989; Takeda et al., 1998). Additionally, productivity of secondary metabolites often declines with decreasing viability (Wagner et al., 1977; Zhang et al., 1994).

Sublytic responses are believed to be associated with fragility of plant cells to shear stress. The shear sensitivity of the plant cells has been attributed to the large cell size, their tendency to aggregate, and the presence of rigid cell walls and large vacuoles within the cells (Joshi et al., 1996). Plant cells are large in size for suspended cell culture; individual plant cell size usually ranges between 20 to 100 μm (Kieran et al., 1997). Furthermore, aggregation of cells is rather common, owing to failure of cells to completely separate during cell division. Cell aggregates can consist of up to 100 cells and can be many several millimetres in diameter. Higher agitation rates are required to suspend these aggregates in order to optimise mass transfer.

Cell viability is lost at hydrodynamic stress levels two to three orders of magnitude below the degree required to cause significant physical damage or lysis to the cells (Rosenberg, 1989; Dunlop et al., 1994). The contents of DNA and ATP in cells, respiratory activity, and

cell membrane integrity deteriorate with increasing agitation intensity. However, these responses occur at different stages of cell damage. These cellular responses are believed to follow a certain hierarchy. Studies have confirmed this finding and reported that membrane integrity was less affected by shear stress than other characteristics at the same energy dissipation rates (Rosenberg, 1989; Dunlop et al., 1994). This indicates that cell physiology is damaged prior to any observable cell destruction by hydrodynamic stress (Abu-Reesh et al., 1989; Takeda et al., 1994; Takeda et al., 1997).

A direct indication of the ability of cells to regrow or cell viability is the regrowth measurement. Regrowth is commonly performed in petri-plates with agars and feed plates, where viable cells are counted (Horsch et al., 1980; Rosenberg, 1989). However, other available techniques are by immobilising cells in transparent agarose beads (Schroeder et al., 1989; Wong, 2001) or growing cells in suspension in shake flasks. Unfortunately, regrowth assays have provided inconclusive results. While Rosenberg (1989) reported regrowth ability to be the most sensitive attribute in plant cells, Wong (2001) found that regrowth was relatively insensitive to hydrodynamic shear stress. Additionally, the cells showed a strong recovery rate once they were removed from the sheared environment (Wong, 2001). The disadvantage of the regrowth technique is its highly complex and time-consuming procedure. An assay requires at least 2 weeks to complete, and slow-growing plant cells are often contaminated.

Integrity of the cytoplasmic cell membrane provides an indirect measure of the loss of cell viability. Staining is the most common technique due to its simplicity. The basic requirement for the assay is a fluorescent dye, such as fluorescein diacetate or phenosafranin (Kieran et al., 2000). More advanced methods include dielectric spectroscopy (Markx et al., 1991) and isotope labelling techniques (Parr et al., 1984).

A more sensitive indication of the response to stress is to detect cellular activity. The most common method is to measure the ability of living cell to reduce tetrazolium salts (TTS) in its mitochondria. This technique has been successfully used to quantify the viability of plant cells in many shear studies (Hooker et al., 1989; Rosenberg, 1989; Dunlop et al., 1994; Takeda et al., 1994; Zhong et al., 1994; Takeda et al., 1998). However, TTS results can be very sensitive to factors, such as pH, buffer, salt concentration, incubation time

(Towill et al., 1975; Kieran et al., 2000), as well as the age and condition of the suspension. These factors have been studied and optimised in the project to ensure minimum variability of the results.

The detection of ATP and NAD(P)H level, as well as the actin filaments contents are less common approaches. Nevertheless, they have been applied successfully to measure sub-lethal responses in plant cells (Takeda et al., 1998). Both ATP and NAD(P)H are fundamental to normal cell maintenance and growth. Lower levels of these substances usually indicate that the cells are weak. Takeda et al. (1998) reported a decrease in the intracellular ATP and NAD(P)H contents in eucalyptus and safflower cells grown in a stirred tank reactor. An increase in cytosolic calcium concentration was also found responsible for reduction of these metabolic substances in cells subjected to shear stress (Aloi et al., 1994).

2.4.1. Stress-Protein Expression

Cells often respond to environmental stress by the rapid acceleration of the synthesis of certain proteins, known as the stress proteins (Namdev et al., 1995). The response of the cells to shear stress may be related to specific genes which are repressed or enhanced when the cell is stressed (Rosenberg, 1989). Stress-response phenomena in cells are commonly known to generate abnormal stress proteins or activate particular stress-induced genes, which ultimately change the properties of the cells. When cells are exposed to temperatures above their normal range, they produce the so-called heat shock proteins, which have an ability to denature the abnormal proteins and protect them from further physiological damage. These genes are not only activated by heat, but also other stimuli and stress (Anathan et al., 1986; Namdev et al., 1995). It has been demonstrated that production of a large quantity of abnormal proteins in *Escherichia coli* could activate the production of heat shock proteins, which increases the capacity of the bacteria to degrade abnormal proteins (Anathan et al., 1986).

Mature cells have been reported to respond differently to stress than younger cells of certain species. A higher level of phenolics concentration has been detected after shearing

more mature cells. This may have resulted from an increase in secondary metabolites production brought about by growth or wounding. The phenolic secretion is intensified by cell membrane permeabilisation as shear stress increases. However, experimental evidence indicated that cells respond to stress by boosting the level of extracellular phenolics rather than merely boosting the rate of its production implying that the level of phenolic secretion was directly proportional to the degree of shear rate (Sahai et al., 1984). As a response to hydrodynamic stress, *Beta vulgaris* suspension cultures were found to secrete more proteins into the medium when grown in a stirred tank than when grown in a shake flask. A considerable reduction in turbulence was observed as the medium viscosity increased as a result of accumulation of extracellular compounds. These compounds may have a similar role in shear protective effect that polymers such as Pluronic F-68, methylcelluloses, and bovine serum albumin provide in animal cell cultures (Rodrigues-Monroy et al., 1999).

2.4.2. Osmo-regulation

Plant cell regulates its turgor pressure and cell wall composition through a mechanism known as osmo-regulation. Although plant cell walls are considered to be relatively rigid and inflexible during the non-growth phase, an increase in cell size during growth and expansion can cause the cell wall to weaken. Consequently, plant cell cultures in late exponential growth phase are relatively shear-sensitive compared to those in lag and stationary phases (Hooker et al., 1989; Rosenberg, 1989; Al-Rubeai et al., 1995; Namdev et al., 1995).

Various results have been reported on changes in cell wall strength as a function of the applied shear stress. A decrease in cell wall strength in *Nicotiana tabacum* with shear has been related to increase cell permeability and an intensification of phenolic metabolites release (Hooker et al., 1989). However, other workers have reported contradictory results. Tanaka et al. (1988) found an increase in cellular contents of *Catharanthus roseus* cell walls, implying that cell wall strength increased after being cultivated under mild mixing condition. Variations in cell wall strength and turgor pressure are also observed in other cells under both low and high agitation rates (Namdev et al., 1995).

These substantial differences in strength may depend primarily on the species of plant cells and the conditions under which they are grown. Many plant species become more robust, as they develop shear resistant characteristics after a period of subcultivation. *Catharanthus roseus* and *Nicotiana tabacum* are suspected of possessing repair mechanisms that allow lesions or ruptures in the cell walls to heal (Meijer et al., 1994). An improvement in the shear-tolerance and growth was observed in *Picrasma quassioides* cultures after a year of exposure to hydrodynamic stresses in stirred tank and airlift bioreactors (Scragg et al., 1988). The culture was initially slow growing under shearing conditions, but eventually developed a tolerance to shear after a year of cultivation. This observation may explain the variation in shear sensitivity of different plant cell species, particularly the gradual shear tolerance acquired during successive subculture of some plant species (Scragg et al., 1988). Clearly, while many plant species remain highly sensitive to shear, other cell lines may develop resistance to shear following long periods of cultivation (Wagner et al., 1977; Scragg et al., 1988).

An oxygen burst is another phenomenon which has recently been linked to cell damage by shear (Kieran et al., 2000). The active oxygen species are responsible in the oxidative cross-linking of hydroxyproline-rich glycoproteins in plant cell walls. An increase in these active oxygen species can result in a toughening of the cell wall in response to mechanical stimulation (Cazalé et al., 1998). A reported increase in cellulose level in *Catharanthus roseus* suspension in shake flasks confirmed that this cell wall strengthening mechanism is available in some plant cells (Tanaka et al., 1988).

2.4.3. Morphological Changes of Aggregates

Plant cells commonly exist as aggregates due to their failure to sufficiently separate during cell division. This causes problems with nutrient distribution, as well as suspension problems and increased settling velocity of the clumps (Kieran et al., 1997). Problems with shear sensitivity are further compromised, as higher agitation rates are required to maximise mass transfer rate and avoid growth limitation due to oxygen uptake.

Plant cells are not homogenous. Cell aggregates of various sizes mean that individual cells experience different levels of shear stresses. Older cell cultures may be more susceptible to hydrodynamic shear stress, mainly due to increased cell size with the culture age (Markx et al., 1991).

A decrease in the aggregate size due to cell breakage does not merely imply a mechanical injury of cells (Tanaka et al., 1988; Kieran et al., 1997). Studies have shown that there are strong links between the aggregate size and metabolite production (Kinnersley et al., 1980; (Kieran et al., 2000). Aggregate size has been shown to alter secondary metabolites, phenolic levels, intracellular RNA, DNA, protein levels as well as wall integrity and cell viability (Namdev et al., 1995). A decrease in cell size has recently been related to apoptosis phenomenon in animal cells (Meneses-Acosta et al., 2001). Unfortunately, plant cell aggregate size and the number of cells per aggregate are not consistent enough to be quantified statistically. Differing degrees of cell breakage cause a wide range of effects on viability. The mechanisms of breakage and subsequent damage remain unclear and require further investigation.

2.4.4. Calcium Ion as a Secondary Messenger

Plant cells interact with the extracellular environment through various physiological receptors. Likewise, mechanical stress is perceived through a range of mechanisms. Many ion channels are believed to be activated by mechanical forces. They open and pass specific ions when the cell is mechanically stressed. The hydrodynamic stress signals are transduced into plant cells in a similar manner through second messengers such as calcium ions (Takeda et al., 1997). Evidences suggest that plants suffer from different types of mechanical stresses. Tension, compression and variation of turgor pressure can equally cause cytosolic calcium level to rise abnormally (Knight et al., 1992; Trewavas et al., 1994). Calcium ion channels are suspected to be triggered by mechanical stress and influence the rate of calcium influx from extracellular source.

Calcium ions play a significant role in signal transduction of cells, as they act as secondary messengers. They regulate cell metabolic activity as they are introduced from the

extracellular medium through various types of Ca^{2+}-permeable channels, such as voltage-dependent channels (Trewavas et al., 1994; Thion et al., 1996; Takeda et al., 1997). The level of cytosolic calcium ion concentration is usually maintained at approximately 10^{-7} M (Anderson et al., 1991). When the cell is stimulated, calcium is transported into the cytosol from extracellular solution or intracellular store, such as the mitochondria, endoplasmic reticulum (ER) or vacuoles. Studies have demonstrated an increase in the cellular [Ca^{2+}] following an exposure of Sf-9 insect cells to laminar and turbulent shear in a capillary flow system (Dunlop et al., 1994). A similar pattern was reported for eucalyptus and safflower cells, where the cellular cytosolic calcium concentration increased as the hydrodynamic shear rate intensified (Takeda et al., 1998).

Cytosolic calcium ions are responsible for regulating several metabolic pathways. They activate many protein kinases by combining with compounds, such as calmodulin (CaM) to form a CaM-Ca^{2+} complex. The protein kinases are activated to produce inositol triphosphate, which in turn increases the permeability of endoplasmic reticulum to calcium ions, permitting more movement of Ca^{2+} into the cytosol. Several other protein kinases bind with the CaM-Ca^{2+} complex, which triggers various biochemical responses (Anderson et al., 1991). This phenomenon is directly responsible for regulation of the NAD(P)H reduction, as well as reduction in ATP and NAD(P)H level in plant cells. Abnormal levels of ATP and NAD(P)H could severely upset the respiratory activity of the cells (Takeda et al., 1998).

Certain chemical pathways involving calcium ions and calmodulin can be established by chemically blocking Ca^{2+} or CaM complex from participating in the metabolic reactions. The most common calcium ion blocking compound are ruthenium red, verapamil and EGTA (Takeda et al., 1998), whilst calmidazolium, compound 48/80, trifluoperazine, and N-6(aminohexyl)-5-chloro-a-naphthalenesulfonamide (W-7) have been successfully used in inhibiting calmodulin-related pathways (Kumar et al., 1991).

Hydrodynamic shear stress is believed to stimulate calcium ion transport in cell through a certain type of Ca^{2+}-permeable channels, known as the stretch-activated (SA) channels. These SA channels are mechanosensitive. The presence of SA Ca^{2+} channels has been detected in several types of plant cells. For instance, Ding and Pickard (1993) identified SA

Ca^{2+} channels in onion epidermal cells, whilst Cosgrove and Hedrich (1991) reported Ca^{2+}-permeable SA channels in the plasma membrane of the guard cell protoplasts of *Vicia faba*.

Numerous studies have demonstrated flow-induced elevation in cytosolic [Ca^{2+}] in endothelial cells exposed to laminar shear stress (Schwarz et al., 1992; Yao et al., 2000). Evidence confirms that the cytosolic calcium rise results primarily from extracellular Ca^{2+} entry rather than intracellular release from internal stores (Yao et al., 2000). The rise in flow-induced cytosolic [Ca^{2+}] was completely eliminated by the chemicals that blocked the mechanosensitive Ca^{2+}-permeable channels in the plasma membrane (Yao et al., 2000). However, contradictory results have been reported for insect cells. Aloi et al. (1994) demonstrated that fluid forces solely affected the signalling process rather than activating SA channels. These insect cells were found to have increased calcium ions concentration even though there were no free calcium ions available in the extracellular environment (Aloi et al., 1994). Under the reported conditions, the energy demand to regulate the level of calcium ions would be sufficient to interfere with energy available for other metabolic processes.

Intense fluid forces can activate the SA channels and trigger a cascade of events involving rising calcium ion concentration, mitochondrial damage, and cytoskeletal alteration. These phenomena ultimately result in sublytic effects in plant cells. They can retard growth and cause eventual cell death (Aloi et al., 1994). An energy dissipation as low as $2\times10^{4}J/m^{3}$ could cause an increase in cytosolic [Ca^{2+}] in cells (Namdev et al., 1995). Physiological processes, such as cell wall material secretion, cell division, osmo-regulation and membrane damage are essentially mediated through transient calcium ion level (Namdev et al., 1995). Variations in calcium levels have been reported to cause changes in actin filament network in plant cell suspension. [Ca^{2+}] exceeding $10^{-7}M$ can result in an onset of fragmentation of actin filaments in the cytoskeleton (Alberts et al., 1994). Malek and Izumo (1996) demonstrated that endothelial cells undergo morphological change and actin network remodelling following exposure to fluid shear stress. Takeda et al. (1997) reported a reduction in F-actin filament content in eucalyptus and safflower cells as calcium level increased. In addition, the cell require more energy to remove the excessive Ca^{2+} and less energy is consequently available for regular cell maintenance. While Ca^{2+} plays a crucial

role in normal cell growth processes, any excess can interfere with cell maintenance and productivity, and is likely to cause death.

Ca^{2+} has also been implicated in physiological cell death, including apoptosis and necrosis (Smaili et al., 2000). In living cells a large amount of calcium ions is taken up by the mitochondria, which require its presence to activate a series of metabolic reaction including ATP synthesis (Rizzuto et al., 2000). An increase in cytosolic calcium results in Ca^{2+} uptake into mitochondria. Ca^{2+} overload of mitochondria has been shown to be involved in cell death process. Large flux of Ca^{2+} induced by excitotoxicity has been linked to mitochondrial overload and cell damage. High mitochondrial $[Ca^{2+}]$ can result in impairment of the membrane permeability and leading to collapse of membrane potential, abnormal ATP synthesis and mitochondrial dysfunction (Smaili et al., 2000). The phenomena of apoptosis and necrosis have been well characterised in mammalian cells (Meneses-Acosta et al., 2001). Some hydrodynamic stress-responses of insect cells are believed to be a programmed death process (Aloi et al., 1994). The most distinctive features of apoptosis in animal and insect cells are a decrease in cell size, loss in sphericity and swelling of endoplasmic reticulum (Meneses-Acosta et al., 2001). These features may be readily detected by laboratorial equipment. However, they may not be as distinctive or easy to detect in plant cells due to severe aggregation. The cell death phenomena will be further discussed in Chapter 7.

2.5. Assessment of Shear Sensitivity of Plant Cell Cultures

Studies on the effects of hydrodynamic shear on plant cell cultures usually involve both laminar and turbulent regimes (Rosenberg, 1989 and Dunlop et al, 1994). A decrease in cell viability with increasing shear and exposure time was reported in both flow regimes. Hypersensitivity of cells under the turbulent conditions was evident compared to laminar conditions. For the same degree of damage, the magnitude of turbulent stress is much lower than that for the laminar stresses. This indicates that the cells may be particularly sensitive to certain aspects of the turbulence, such as the time-dependent Reynolds shear stresses and their frequencies. In addition, the cell-cell and cell-impeller collisions in the

laminar flow field are negligible. By contrast, in turbulent flow, these may predominate (Rosenberg, 1989; Dunlop et al., 1994).

Measurements of biological responses and cell damage by hydrodynamic stresses are usually related to the viability of the cells (Wagner et al., 1977; Rosenberg, 1989; Dunlop et al., 1994; Namdev et al., 1994; Ho et al., 1995; Kieran et al., 1995; Wongsamuth et al., 1997). Viability is defined as a measure of the ability of a cell to grow and divide when placed in favourable conditions. It is often estimated by membrane integrity and permeabilities, and mitochondrial activities. On the other hand, cell death is directly related to lysis, which is usually accompanied by a release of DNA or other acidic intracellular materials and a reduction in pH (Wagner et al., 1977; Scragg et al., 1988).

The two principal techniques for studying the effects of shear stress on biological systems are characterised according to the type of stress environment generated, as well as the period at which cells are exposed to shear (Prokop et al., 1992). The first method is a direct investigation using agitated and/or sparged bioreactors with various anemometric techniques (Scragg et al., 1988; Takeda et al., 1994; Kieran et al., 1995; Joshi et al., 1996) and the second relies on a device to generate well-defined laminar or turbulent flow (Rosenberg, 1989; Prokop et al., 1992; Dunlop et al., 1994; Kieran et al., 1995). The critical factors include the type of forces, their effect on the cell structure and physiology, and the duration of these forces (Prokop et al., 1992).

2.5.1. Long-term Studies of Shear Sensitivity of Plant Cells

Long-term study focuses on the effects of shear stresses on cells under growth condition. The cultures are studied in stirred tank configuration for both batch and continuous culture (Meijer et al., 1994). The main disadvantage of this system is the turbulent mixing regime produced under actual growth conditions. The flow field within a bioreactor is highly complex. The flow structure varies enormously from one location to another. It is very difficult to accurately measure the shear stresses. Consequently, the appropriate characterisation of cell response to different levels of shear stresses become problematic.

A reduction in cell growth and viability are usually observed in mildly agitated vessels (Wagner et al., 1977; Takeda et al., 1994; Zhang et al., 1994; Rodrigues-Monroy et al., 1999). An investigation of hydrodynamic damage of *Carthamus Tinctorius* or sufflower cell cultures in a stirred tank reactor showed a decrease in cell viability and relative ATP levels with hydrodynamic stress without cell lysis. The extent of damage on respiratory activity was also much greater than that of membrane integrity; indicating cell physiology is damaged prior to any observable cell physical destruction by hydrodynamic stress (Takeda et al., 1994).

Takeda et al. (1998) provided suggestions on the signalling of hydrodynamic stress and its communication into metabolism of plant cells (Takeda et al., 1997). The eucalyptus and safflower cell suspensions were grown in a stirred tank reactor with the average energy dissipation ranging between 0.5 to 2.3 m^2/s^3. The results indicated that the relative ATP content, respiratory activity and NAD(P)H levels can be improved by an addition of a calcium ion channel blockers or calmodulin blockers such as verapamil and W-7. In addition the test for filamentous actin content to determine changes in membrane integrity demonstrated that the formation of actin filaments was suppressed by external stress.

Most studies agree on the shear sensitivity of plant cells. However, the results of some studies imply that many plant cell lines may not be as sensitive to shear as first imagined. Cell lines have become resistant to shearing after a long cultivation in shake flasks conditions (Scragg et al., 1988). For instance, *Nicotiana tabacum* was found to be sensitive to short-term exposure (less than 5 hours) to shearing, but they were tolerant to long-term exposure to shearing environment (Scragg, 1995). Other species of shear resistant cell lines include *Catharanthus roseus*, *Helianthus annuus* and *Vitis vinifera* (Scragg et al., 1988; Markx et al., 1991).

Despite a relative large number of studies, the results from the long-term tests remain very system-specific (Kieran et al., 2000). Many provide contradictory outcomes. Empirical models obtained are not universal and vary substantially with operating factors, such as the type of impellers, cell line, culture age, and culture medium. Most researchers fail to agree on the magnitude of energy dissipation rate measured within different bioreactor regions.

Some of these differences are summarised in Tables 2.4 and 2.5. The notation ε_{bulk} is the bulk energy dissipation rate, ε_{ave} refers to the average energy dissipation rate, ε_{imp} is the impeller region, and $\varepsilon_{discharge}$ refers to the impeller discharge region.

Table 2.4: Typical values for energy dissipation rates in terms of average rate.

Correlation	Value	References
$\varepsilon_{bulk}/\varepsilon_{ave}$	0.26	(Cutter, 1966)
$\varepsilon_{bulk}/\varepsilon_{ave}$	0.25	(Tomi et al., 1978)
$\varepsilon_{discharge}/\varepsilon_{ave}$	50	(Tomi et al., 1978)
$\varepsilon_{discharge}/\varepsilon_{ave}$	9.4	(Zhou et al., 1996a; Zhou et al., 1996b)
$\varepsilon_{imp}/\varepsilon_{ave}$	5.16	(Placek et al., 1985)
$\varepsilon_{imp}/\varepsilon_{ave}$	5.4	(Tomi et al., 1978)
$\varepsilon_{imp}/\varepsilon_{ave}$	4.5	(Zhou et al., 1996a; Zhou et al., 1996b)

Table 2.5: Percentage of total energy being dissipated in different regions in a stirred vessel with standard six-blade impeller (expressed as % of total energy dissipated)

Impeller region (%)	Impeller discharge stream (%)	Bulk region (%)	References
20	50	30	(Cutter, 1966)
30	30	40	(Wu et al., 1989)
15	28	57	(Zhou et al., 1996a; Zhou et al., 1996b)

2.5.2. Short-term Studies of Shear Sensitivity of Plant Cells

Numerous fundamental studies have been conducted using short-term shear application of stress. Plant cells are exposed to a well-defined flow field in a small volume for a fixed period (typically less than 10 hours). Various configurations for generating the short-term shear field are summarised in Table 2.6. Examples of such techniques include capillary tubes, cylindrical tubes, and submerged jet devices (Zhang et al., 1993; Al-Rubeai et al., 1995; Kieran et al., 1995; Joshi et al., 1996; Kieran et al., 1997; MacLoughlin et al., 1998). Alternative configurations are viscometers, such as parallel plates, plate and cone viscometers, and more commonly the couette rheometers (Hooker et al., 1989; Rosenberg, 1989; Prokop et al., 1992; Dunlop et al., 1994; Joshi et al., 1996). The principal advantage of this technique is the flow regime is more reproducible in relatively smaller volume. However, the experiment can only be carried out over a short period and it is not possible to monitor the long-term responses of the cells.

Table 2.6: Examples of experiments on shear sensitivity of plant cells

Equipment	Type of cells tested	Reference
Capillary tube flow	*Morinda citrifolia*	(Kieran et al., 1995)
Couette viscometers	*Daucus carota*	(Rosenberg, 1989; Dunlop et al., 1994)
	Nicotiana tabacum	(Hooker et al., 1989)
	Perilla frutescens	(Zhang et al., 1994)
Submerged jet flow	*Morinda citrifolia*	(MacLoughlin et al., 1998)
Rotating drum reactor	*Perilla frutescens*	(Zhang et al., 1994)
Stirred tank reactor	*Catharanthus roseus*	(Scragg et al., 1988)
	Helianthus annuus	(Scragg et al., 1988)
	Morinda citrifolia	(Wagner et al., 1977)
	Beta vulgaris	(Rodrigues-Monroy et al., 1999)

The couette shear flow has been studied for *Daucus carota* and *Nicotiana tobacum* cultures (Hooker et al., 1989; Rosenberg, 1989; Dunlop et al., 1994). The shear stress developed in this device ranged from 0.5 N/m^2 to 10,000 N/m^2. The turbulent energy dissipation rate ranged from 3.1×10^{-4} to 4.3 W/kg (Rosenberg, 1989). The critical shear stress level which *D. carota* cell ceased to regrow was 50 N/m^2 (Dunlop et al., 1994). The damage to mitochondrial activity began at much lower energy dissipation of 100 J/m^3 and became significant at around 10^4 J/m^3 (Dunlop et al., 1994). A sign of damage to the aggregates appeared at much higher energy dissipation of 10^5 J/m^3. This evidence provides further support that plant cells are damaged metabolically prior to any observable physical damage.

Another commonly applied apparatus for creating reproducible laminar and turbulent flow is the capillary flow device. A study of the turbulent effects on *Morinda citrifolia* suspension culture involved a capillary system with various capillary lengths and diameters. The average shear stress generated ranged between 25 and 350 N/m^2, which covers a smaller range than the viscometer studies (Kieran et al., 1995). The energy dissipation rate generated by such a configuration is often of many orders of magnitude greater than the typical dissipation rate found under normal bioreactor operating conditions (Kieran et al., 2000). Results from this study confirmed a first order model of the reduction of the relative viability of the cells with the exposure time. Chain length and cell size were confirmed as critical factors, determining cell-survival rates. A linear relationship between cell death and energy dissipation verified the observation that cell viability decreased with increasing exposure time.

A submerged jet flow is another technique used for shearing *Morinda citrifolia* cells. Cell suspension is injected from a jet nozzle beneath the surface of a reservoir of the same fluid (MacLoughlin et al., 1998). The first-order death rate constant confirmed a linear dependence on the average energy dissipation rate, which ranged from 10^3 to 10^5 W/kg. The relative chain length damage corresponded reasonably well with other literature values (Dunlop et al., 1994). The first-order, cell-death rate constant was directly proportional to the average energy dissipation rate for both capillary and jet flow.

Figure 2.1 compares biological damage of plant cells exposed to various hydrodynamic shear environments. *M. citrifolia* cell cultures were subject to flow in the capillary and submerged jet, whilst *D. carota* cells were studied in a viscometer. Damages to *M. citrifolia* cultures occur at much greater energy dissipation than *D. carota*. However, *M. citrifolia* viability was determined with Evans Blue staining technique, which only highlights deceased cells. Consequently, it is not sensitive enough to detect changes at a cellular level, and can only indicate damage to the cell membranes in a very advanced stage.

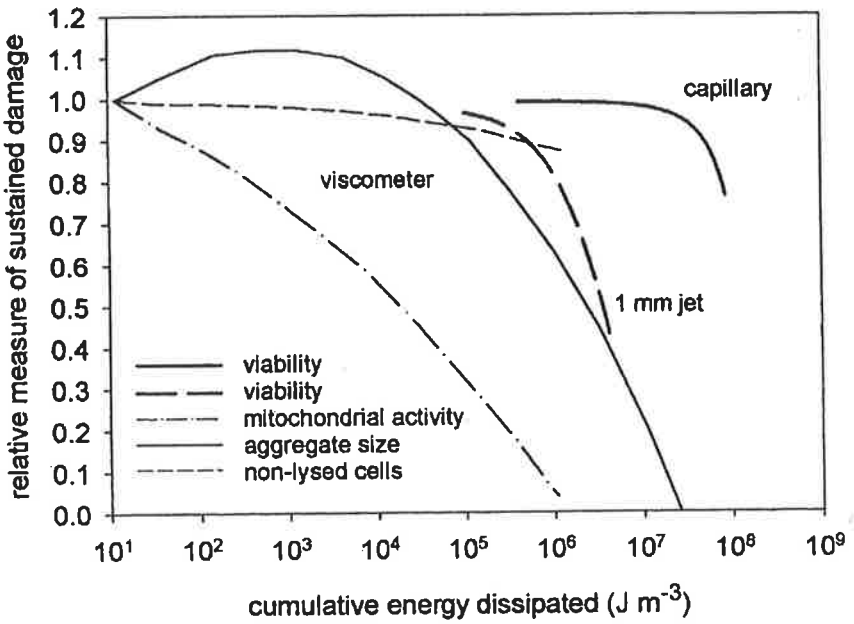

Figure 2.1. The effect of cumulative energy dissipation on plant cell viability, adapted from Kieran et al. (2000). The two lines marked as 'viability' represent *Morinda citrifolia* cultures, which were exposed to capillary flow and submerged jet (1mm nozzle) (MacLoughlin et al., 1998; Kieran et al., 2000). The remaining plots are for *Daucus carota* cells, which were studied in a viscometer (Dunlop et al., 1994)

Cumulative energy dissipation is the most common design parameter used in specification of plant cell culture processes. Unfortunately, the variation in these results highlights the difficulty involved in global characterisation of shear-sensitivity of plant cells. In addition, the effects of energy dissipation rate or exposure time cannot be individually expressed in the total energy dissipation. A high total energy dissipation may result from either a low

shear level for longer exposure time, or a high level of shear stress for a shorter period. Unfortunately, biological responses of plant cells vary significantly with the level of shear stress applied.

Although the existence of turbulence phenomena has been acknowledged for many decades, it has not yet been fully characterised and quantified. Empirical measurements of the Reynolds stresses and energy transfer phenomenon among the turbulent eddies are not simple. Numerous studies attempted to establish a parameter, which adequately describes the turbulent environment. Unfortunately, parameters, such as shear rate, shear stress or total cumulative energy dissipation can only characterise bulk fluid motions (Wagner et al., 1977; Dunlop et al., 1994; Zhong et al., 1994; MacLoughlin et al., 1998).

The local flow structures have been long established as more appropriate correlation factors for the turbulent regime. Hence, the models involving solely shear rate or shear stress would not be expected to adequately describe the physical nature of the system. The energy dissipation rate has proven far more superior to other variables, such as shear rate, in describing influence of hydrodynamic shear stress (Liu, 2000). Recently Jüsten et al. have overcome the problem of variation in energy dissipation rate in a bioreactor, by introducing a factor to for the local energy dissipation in the impeller volume, the circulation frequency and the impeller geometry. They found that the damage to *Penicillium chrysogenum* and mycelial cells in stirred bioreactors was poorly correlated by the local energy dissipation rate. However, the damage in various bioreactor configurations correlated well with the new factor, which includes the specific energy dissipation rate in the impeller swept volume, recirculation time and the geometry of the impeller (Jüsten et al., 1996). This parameter will be exploited in the analysis in Chapter 5.

2.6. Conclusions

This chapter summarises various potential benefits and the commercial developments of plant cell culture technology. Unfortunately, significant progress of this fermentation technology is severely hindered by poor performance of the shear-sensitive plant cells in intense shear environments. Limitations of the current technology highlight the needs to

improve the existing equipment in order to optimise plant cell production. Such an improvement may only be possible when the mechanisms involved in shear-sensitivity of plant cells are fully understood.

Shear sensitivity of plant cells is strongly associated with their biological and physical characteristics. This chapter also describes some of the sublytic responses detected in shear-injured plant cells prior to cell lysis. Various techniques for measuring these biological changes are also discussed. Several mechanical stress-transduction pathways have been postulated. However, evidences strongly suggested a possible involvement of calcium ions and stretch-activated channels in response to mechanical stress.

Finally, various shear configurations previously used in the shear-sensitivity studies are summarised. The hydrodynamic criteria and results obtained from the literature are generally comparable. However, these values are system-specific and their magnitude tends to vary substantially depending on the type of shear environment. Selection of appropriate critical design parameters for plant cell processes is a difficult task. Hence, there is the need for developing a more global hydrodynamic parameter to describe responses of plant cells in various shear conditions.

In the next chapter, a novel turbulent shear apparatus will be presented and an accompanying experimental methodology is also summarised.

CHAPTER 3

MATERIALS AND METHODS

3.1. Plant Cell Cultures

Wild carrot cultures (*Daucus carota*) were provided by the Commonwealth Scientific and Industrial Research Organisation (Sydney, Australia). The cultures were grown in wild carrot medium (WCM) on a gyratory shaker at 100 rpm in the dark at 27°C. They were subcultured fortnightly using 10% inoculum volume. The ingredients for WCM are industrial grade with an exception of sucrose, which was food grade. These ingredients are listed in Appendix A. Cell cultures were maintained at 50mL in 250mL Erlenmeyer flasks. Individual flasks were closed with cottonwool-cloth stoppers to allow oxygen permeation. The medium was prepared with Milli-Q water and adjusted to pH 5.4 prior to sterilisation in an autoclave at 120°C for 20min.

3.2. Cell Culture Preparation

During the growth cycle, plant cells are more susceptible to damage during late-exponential phase or early stationary phase (Wagner et al., 1977). Consequently, cell suspension cultures for the shear experiments were harvested in their late exponential growth phase (12 days). Particles size distribution was controlled by pre-screening the suspension culture consecutively through 40 mesh (380 μm) and 60 mesh (230 μm) stainless steel screen cups (Sigma Aldrich). The filtrate was centrifuged at 40×g for 10 min to separate the cell pellets and the conditioned medium. The final cell concentration was then adjusted to 0.05 g (fresh weight) per mL. The average density of the suspension was 1013 kg/m^3.

3.2.1. Cultures Rheology

The rheological properties of the pre-screened cell cultures were determined with a parallel plate viscometer (CVO). The parallel plates were 40mm in diameter and the gap size was 500μm. The experiments were controlled at 25°C. Figure 3.1 illustrates a slight thixotropic nature of the suspension. A normal least square analysis indicated that the viscosity data exhibited a power law behaviour, which is described by

$$\tau = k\dot{\gamma}^n \tag{3.1}$$

where τ denotes the shear stress, γ is the shear rate, k refers to the power law coefficient, and n represents the power law index. A power law index value of 1 corresponds to a Newtonian fluid.

Figure 3.2 presents the relationship between shear stress and shear rate for the pre-screened carrot suspension. The shear stress was found to follow the power law relationship:

$$\tau = 2.84\times10^{-3}\dot{\gamma} \tag{3.2}$$

The power law index of 1 indicated that the suspension followed Newtonian behaviour. The apparent viscosity of the suspension was 2.84×10^{-3}Pa.s, which is almost three times higher than viscosity of water. However, the apparent viscosity only represents the bulk behaviour of the suspension. For the calculations involving microscale structures, the viscosity of the suspending fluid (ie water) should be assumed.

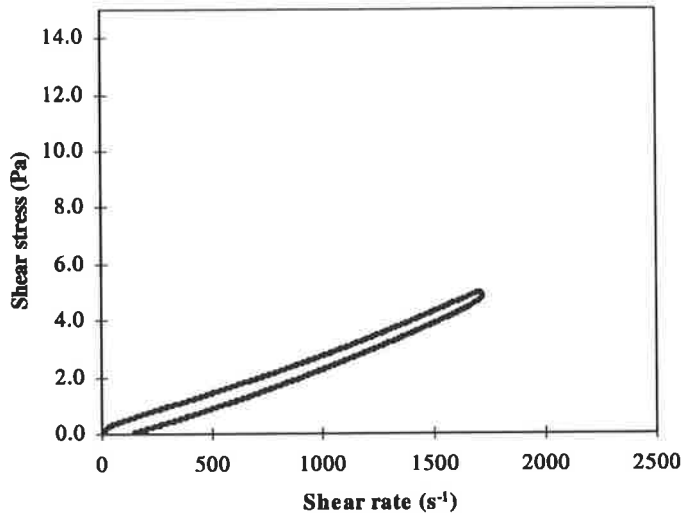

Figure 3.1. A hysteresis curve, showing a slight thixotropic behaviour of pre-screened carrot suspension cultures

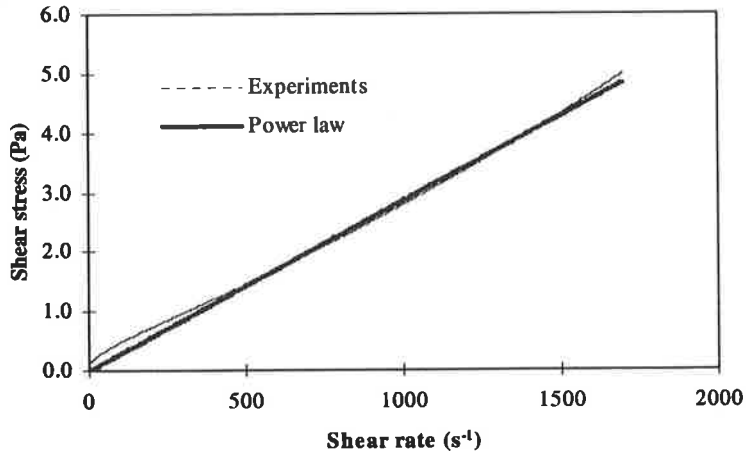

Figure 3.2. The relationship between shear stress and shear stress for the pre-screened carrot cultures.

3.3. Shearing Device

The shearing environment was generated in an apparatus illustrated in Figure 3.3. The experimental apparatus design was primarily based on a combination of a couette viscometer and a stirred tank bioreactor. The schematic and complete assembly are presented in Figures 3.4 and 3.5 respectively. It consists of a cylindrical stainless steel annulus with a cylindrical stirrer. This stirrer rotates inside the annulus, generating turbulent wakes and providing a turbulent shear flow within the gap.

The concentric cylinders have an outer diameter of 110mm and an inner diameter of 87mm. Both cylinders are 60 mm in height. The cylindrical rod diameter is 3mm. Eight pairs of cylindrical baffles (3mm diameter) are attached to the internal walls of the annulus (refer to Chapter 4, section 4.3). On rotation, the cylindrical stirrer generates shear due to wake behind the cylinder, and couette motion between the rotating rods and the walls of tank. The equipment was sterilised in an autoclave at 120°C for 20min prior to every experiment. Both control and sheared samples were maintained at 20 °C.

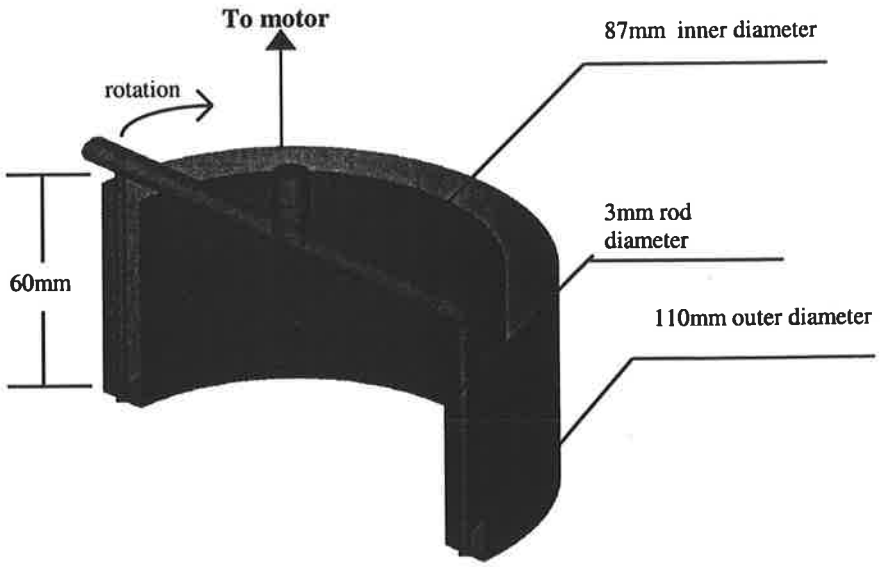

Figure 3.3. A cross-section diagram of the annular shearing device

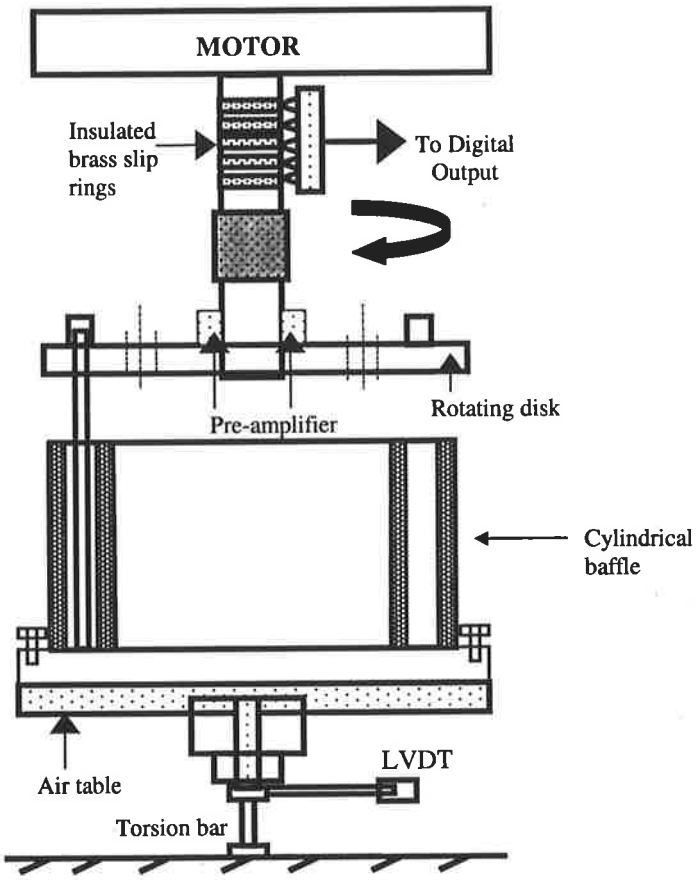

Figure 3.4. Schematic of the construction of annular shearing device

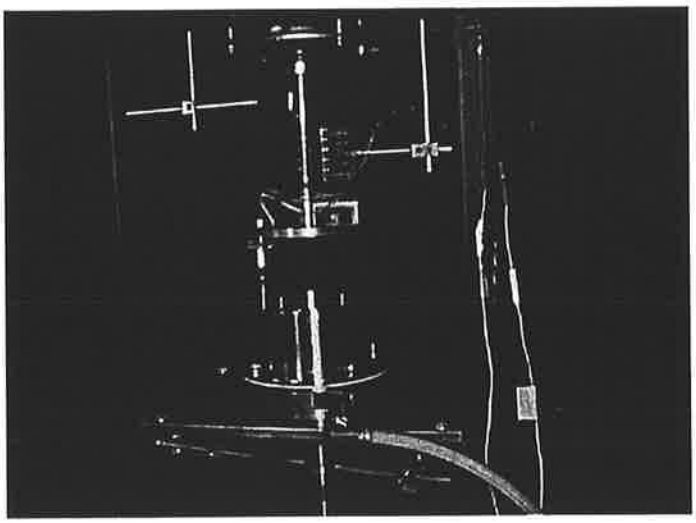

Figure 3.5. A complete assembly of the apparatus

The annulus bowl rests on an air bearing with a shaft connected to a linear variable differential transformer (LVDT). The air bearing ensures that the annulus bowl has a frictionless contact with the base. The LVDT measures the average change in torque applied to the annulus, and hence to the entire flow system. The LVDT is also connected to an amplifier. The amplified signals are digitised in a Maclab panel.

The average energy dissipation rate is directly related to the power input into the system,

$$\varepsilon_{ave} = \frac{P_T}{\rho V_T} \tag{3.3}$$

where ε_{ave} is the average dissipation rate (W/kg), P_T is the total power input (W), ρ is the fluid density (kg/m^3) and V_T is the total volume of the fluid (m^3).

The total power supplied to the annulus system is the product of torque and rotational speed. The shear stress τ experienced by the fluid particles can be derived from the measured energy dissipation rate using the following correlation (Matsuo et al., 1981; Rosenberg, 1989);

$$\tau = 2.46\left(\rho\varepsilon^{2/3}d^{2/3}\right) \tag{3.4}$$

3.4. Biological Assays

Biological responses of plant cells to hydrodynamic shear stress are measured in terms of viability, which includes mitochondrial activity, membrane integrity, change in average aggregate size, and regrowth ability. Common techniques used in the analysis of plant cell viability are outlined in Table 3.1. The three assay techniques selected for the experiments are for mitochondrial activity, membrane integrity and aggregate size.

Table 3.1: Various techniques for biological assays

Biological Property	Assay Technique
Regrowth ability	Plating regrowth technique (Horsch et al., 1980), agarose bead (Schroeder et al., 1989) or suspension regrowth
Mitochondrial activity	Triphenyltetrazolium chloride staining (Towill et al., 1975)
	Oxygen uptake rate (Wong et al., 2000)
Aggregate size	Malvern particle analyser Series 2600
Membrane integrity	Fluorescein diacetate staining (Widholm, 1972)

3.4.1. Fresh and Dry Cell Weight

Five mL of cell suspension is placed in a preweighed tube and centrifuged at 3000×g for 10 min. The supernatant is pipetted out without disturbing the cell pellet. The remaining cell pellet is weighed to determine fresh cell weight, and dried in an oven overnight at 60°C to obtain dry cell weight.

3.4.2. Suspension Growth Rate

The growth rate of the suspension follows the relationship

$$\frac{N}{N_0} = e^{\mu t} \qquad (3.5)$$

where N_0 is number of cells initially present, N is the number of cells after time t (days), and μ is the growth rate (day^{-1}). The ratio of number of cells is assumed to be proportional to the ratio of the corresponding fresh cell weights.

Cell suspensions were grown in 250mL Erlenmeyer flasks. Fresh cell weight was determined by the technique described in section 3.4.1. Growth rate is represented by the slope of a semi-logarithmic plot of the relative fresh cell weight against time.

3.4.3. Mitochondrial Activity

The oxidative respiratory electron transport activity or the mitochondrial activity was determined by 2,3,5-triphenyltetrazolium (TTC) staining technique (Towill et al., 1975; Rosenberg, 1989; Benson, 1994). The measurements are expressed as the absorption of the UV-VIS light at 485nm. TTC solution was obtained by diluting TTC powder (Sigma Aldrich) in 0.05M sodium phosphate solution buffered at pH 7.5. The TTC had been optimised at pH 7.5. The TTC concentration for optimum absorbance intensity was approximately 0.8% w/v for wild carrot cultures as shown in Figure 3.6.

For the assay, two mL of cell suspension was added to 4 mL of TTC solution. After incubating in the dark at 25°C for 18 hours, the cells were harvested by centrifugation at 3000×g for 15 min, and washed in Milli-Q water. Extraction of formazan dye was carried out with 3mL of 95% ethanol (Sigma Aldrich). The cell-ethanol solution was incubated in a shaker-waterbath at 60-65°C for 60 min to completely extract the dye. Red formazan was obtained by separating the solution from the cell pellets in a centrifuge at 3000×g for 15 min. The absorption of the supernatant at 485 nm corresponds to the quantity of formazan present in the cells, which indicates their mitochondrial activity. The absorbance was expressed per g (fresh weight).

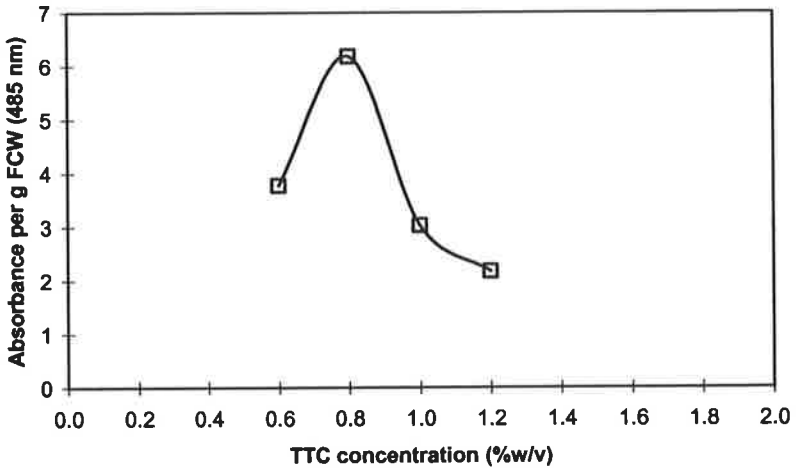

Figure 3.6. Variation in UV absorbance of formazan dye by wild *Daucus carota* with TTC concentration.

3.4.4. Membrane integrity

Fluorescein diacetate (FDA) staining technique detects living cells (Widholm, 1972; Benson, 1994). The diacetate solution reacts with esterases within the cells to form fluorescein, which fluoresces under the microscope.

The FDA stock solution was prepared by adding 0.1 g of fluorescein diacetate (Sigma Aldrich) to 100 mL acetone. A few drops of the stock solution were added to 10 mL of fresh medium to make 0.01% dye solution. 1mL of suspension culture cells was pipetted on to a microscope slide with a small drop of 0.01% FDA solution. Prior to viewing, the slide was incubated for 15 min to allow dye to diffuse. Cell samples were viewed under an inverted microscope (Olympus IX50) and the fluorescent light, which is provided by a mercury (Hg) lamp with blue/violet filter (Olympus). Only live cells fluoresce under blue/violet UV light. The images were recorded onto a computer and analysed with Scion image software (US National Institute of Health).

3.4.5. Aggregate Size Distribution

The size distribution of the cell cultures was measured in a Malvern Particle and Droplet Size Analyser (series 2600). The 2%(w/v) sucrose solution with Milli-Q water used as the background solvent for particle size analysis. The solution was sterilised in an autoclave at 121°C for 20min. The background noises were calibrated with blank solution prior to the cell measurement. Sheared samples were measured against the control samples and the results expressed in terms of average geometric mean diameter relative to control.

3.5 Dissolved Oxygen in the Shearing Device

The shearing unit consisted of a cylindrical rod rotating within a circular cylindrical annulus. The primary fluid motion is governed by the turbulent wake behind a cylinder.

The concepts of a turbulent wake generated behind a cylinder is known as free turbulent shear flow. However, the turbulent wake expansion within the annulus gap is slightly affected by the wall boundaries. The vortices may not spread as freely as wake flow with no wall boundary effect. However, the majority of the fluid behind the cylinder is affected by the shear stress distribution within the wake. The flow profile of the shearing device will be discussed in more detail in Chapter 4.

The calculations of dissolved oxygen in the shearing device required an estimation of the fluid velocity profile. The calculations were based on a two-dimensional representation of a wake behind a cylinder shown in Figure 3.7.

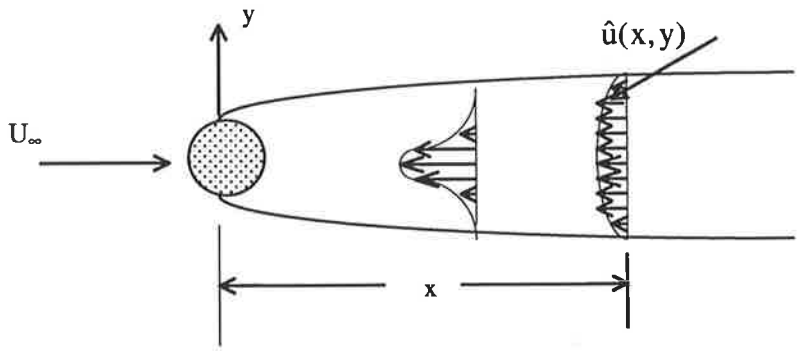

Figure 3.7. Two-dimensional wake behind a cylinder, for the estimation of fluid velocity behind a cylindrical wake. The symbols x and y represent the distance in the x and y direction, respectively.

The central wake region is considered to be continuous turbulent whereas the region near the boundary of the wake becomes more and more intermittent (Hinze, 1975). The statistical distributions of the velocity fluctuations of the wake in the central region are nearly Gaussian, which indicates isotropic turbulence (Townsend, 1947).

The energy of mean flow into turbulent energy occurs by diffusion along the velocity gradients on each side of the wake centre. This includes the diffusion inwards toward the centre of the wake and the outwards towards the outside fluid. The turbulent intensity at the wake centre is generated from the diffusion of turbulent energy from the regions of shearing motions, which is predominantly the movement in the y direction (Townsend, 1947). Consequently the transport of the v fluctuations occurs more rapidly than the transport of other fluctuating component u and w, where u, v and w are turbulent velocity fluctuation in x, y and z direction respectively.

The flow in the wake of a cylinder is symmetric about the x-axis. The velocity approaches the free stream velocity far from the cylinder. According to the mixing length theory, the velocity U at a location (x, y) behind the cylindrical wake can be expressed as follows: (Schlichting, 1968; Wilcox, 1998)

$$U(x,y) = U_\infty - 1.38\sqrt{\frac{C_D}{\rho x}}\left(1-\left(\frac{y}{\delta(x)}\right)^{3/2}\right)^2 \qquad (3.6)$$

where U_∞ is the free stream velocity and C_D is the drag of the body per unit width, which is approximately 1.1 (Cantwell et al., 1983), or 0.6-0.85 from the experimental measurements. The half width of the wake $\delta(x)$ is approximated by (Wilcox, 1998)

$$\delta(x) \approx 0.805\sqrt{\frac{C_D x}{\rho U_\infty^2}} \qquad (3.7)$$

The average velocity at a fixed x position within the far wake region can be calculated by

$$\overline{U}_x = \frac{\int_{y_1}^{y_2} U(x,y)dy}{\int_{y_1}^{y_2} dy} \qquad (3.8)$$

where y_1 and y_2 are the edges of the wake.

From equation (3.6), if

$$k = 1.38\sqrt{\frac{C_D}{\rho x}} \qquad (3.9)$$

Substitution of k into equation (3.6) yields

$$\overline{U}_x = \frac{1}{y_2 - y_1}\int_{y_1}^{y_2}\left[U_\infty - k + 2k\left(\frac{y}{\delta}\right)^{3/2} - k\left(\frac{y}{\delta}\right)^3\right].dy \qquad (3.10)$$

Due to the symmetry of the velocity profile, an integration over the gap of the annulus, where y_2-y_1 = 0.0114m becomes

$$\overline{U}_x = \frac{1}{0.0114}\left(2\int_{y=0}^{y=0.0114/2}\left[U_\infty - k + 2k\left(\frac{y}{\delta(x)}\right)^{3/2} - k\left(\frac{y}{\delta(x)}\right)^3\right].dy\right)$$

$$\overline{U}_x = \frac{2}{0.0114}\left[(U_\infty - k)y + \frac{4}{5}k\delta\left(\frac{y}{\delta(x)}\right)^{5/2} - k\frac{\delta}{4}\left(\frac{y^4}{\delta(x)^3}\right)\right]_0^{0.0057}$$

$$\overline{U}_x = \frac{2}{0.0114}\left[(U_\infty - k)y + 0.8k\delta\left(\frac{y}{\delta(x)}\right)^{5/2} - 0.25k\left(\frac{y^4}{\delta(x)^3}\right)\right]_0^{0.0057} \qquad (3.11)$$

The oxygen uptake rate (OUR) in the shearing apparatus was approximated to be equal to the uptake rate of cells grown in shake flasks. The equation for oxygen mass balance in a biological system can be described as

O_2 accumulation = (O_2 In) – (O_2 Out) + O_2 production – O_2 consumption

The dynamic oxygen balance in a batch culture can be expressed as (Cooney et al., 1985)

$$\frac{dC_L}{dt} = k_L a\left(C^* - C_L\right) - q_{O_2} x_D \qquad (3.12)$$

where

C_L = dissolved oxygen concentration in liquid (mmol/L)

C^* = dissolved oxygen concentration in equilibrium with existing oxygen in gas phase

k_La = overall mass transfer coefficient (1/s)

q_{O2} = specific rate of oxygen uptake (mmol O_2 /g(dry wt) /s)

x_D = cell dry weight (g/L)

The differential equation (3.12) can be expressed as

$$\frac{dC_L}{dt} + k_L a C_L = k_L a C^* - q_{O_2} x$$

$$\frac{dC_L}{dt} + k_L a C_L = A \qquad (3.13)$$

where

$$A = k_L a C^* - q_{O_2} x \qquad (3.14)$$

The general solution for C_L is:

$$C_L = \frac{A}{k_L a} + Be^{-k_L at} \qquad (3.15)$$

where B is a constant and can be expressed as:

$$B = \left(C_0 - C^* + \frac{q_{O_2} x}{k_L a} \right) \qquad (3.16)$$

The typical value of C* is 0.25 mM at atmospheric pressure (Cooney et al., 1985), and C_o equals C^* initially as the cells are resuspended in fresh medium. As the fluid level is low (3.5cm), the fluid was assumed to be uniformly mixed. The value of k_La was be approximated using the expression for surface aeration correlation for a flowing stream (Bailey et al., 1986);

$$k_La = \left(\frac{D_{O_2} \overline{U}}{\pi h^3} \right)^{1/2} \qquad (3.17)$$

where

D_{O2} = oxygen diffusivity which is 2.25 x 10^{-5} cm^2/s in water (Bailey et al., 1986)
2 x 10^{-5} cm^2/s dilute suspension (Rosenberg, 1989)

$\bar{U}$ = average velocity of fluid (cm/s)

h = depth of the stream (cm)

The minimum mixing speed of 50 rpm (0.26 m/s) was considered to represent the worst scenario. The operating velocity range was 300-450rpm, which was well above the minimum speed considered. The k_La profiles estimated from equation (3.17) for the fluid velocity of 50 rpm and 400 rpm are presented in Figure 3.8. The average values of k_La for 50 rpm and 400 rpm are 0.00448 s^{-1} and 0.01505 s^{-1}, respectively.

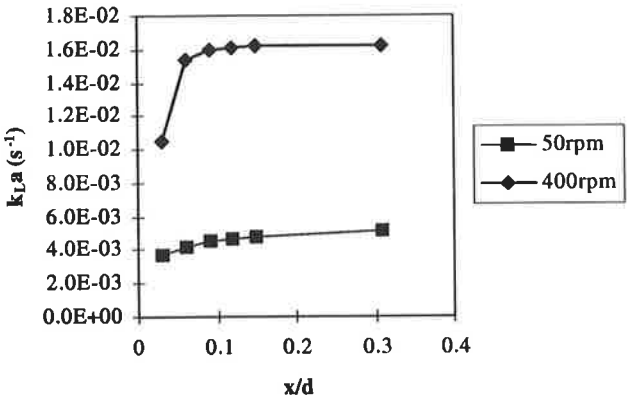

Figure 3.8. Mass transfer coefficient (k_La) profiles at two different operating speeds. x/d denotes the dimensionless downstream distance as ratio of stirrer diameter d.

The final expressions for dissolved oxygen (DO) are:

$$C_L = 0.25 - 4.40 \times 10^{-2}(1 - e^{-0.00448t}) \qquad \text{(50rpm)} \qquad (3.18)$$

$$C_L = 0.25 - 1.31 \times 10^{-2}(1 - e^{-0.01505t}) \qquad \text{(400 rpm)} \qquad (3.19)$$

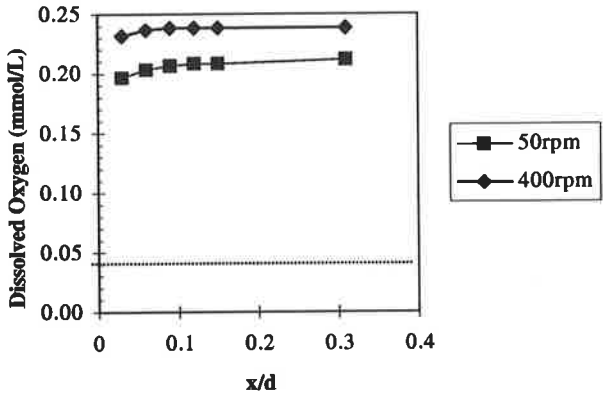

Figure 3.9. The dissolved oxygen profile downstream of the cylindrical stirrer, after 5 hours at two different speeds. x/d denotes the dimensionless downstream distance as ratio of stirrer diameter d.

A decrease in OUR of plant cells exposed to very intense shear stresses has been previously reported (Wong 2001). However, for the purpose of this calculation, the uptake rate was estimated to be constant at 1.97×10^{-4} mmol O_2 $g^{-1}dw$ s^{-1} as measured for 7-day old cultures (Pepin et al., 1995). The critical dissolved oxygen concentration for exponential growth of *Daucus carota* culture is 0.04 mmol O_2 L^{-1} (Kessell et al., 1972). The DO profiles at 50 rpm and 400 rpm after 5 hours in Figure 3.9 demonstrates that the DO level remains higher than the critical oxygen concentration after the duration. This indicates that the oxygen supply to the cells should remain abundant during the shear experiments.

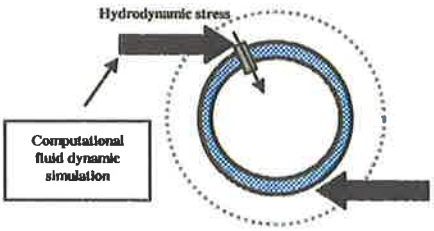

CHAPTER 4

COMPUTATIONAL MODELLING OF TURBULENCE QUANTITIES

Characterisation of turbulent shear stress and its interaction with plant cells are essential factors in the study of the shear damage mechanisms in plant cells exposed to shear flow. Modelling of the complex turbulent shear fields can improve our understanding of how plant cells are affected by these fluid forces. This chapter is dedicated to computation fluid dynamic (CFD) modelling of the flow in the shearing apparatus. This technique has several advantages over traditional theoretical and analytical predictions and complicated experimental techniques. The mathematical models derived to theoretically correlate fluid particle interaction usually involve numerous assumptions and they may also over-simplify crucial parameters, which are difficult to measure experimentally. Furthermore, these correlations represent the bulk properties of the flow rather than 'local' flow conditions. On the other hand, measurement of complex fluid profiles usually involves complicated procedure and analysis. The CFD technique can overcome these problems and provide an good and inexpensive approach to characterise the fluid-particle interaction in the studies of shear sensitivity in plant cells.

4.1. Modelling of the Flow Field

The 'local' flow structures are numerically modelled using CFX (Version 4.3, AEA-Technology, Oxfordshire, UK), which was available at the University of Adelaide. The CFX software solves the Reynolds-averaged continuity and momentum equations using a finite volume method. In this study, the flow field is simulated as a two-dimensional

axisymmetric flow. The rheological properties of cell cultures at low concentration were assumed to be approximately equal to water (Rosenberg, 1989). Turbulence is modelled using the low Reynolds number k-ε model, which has been developed to simulate the detailed flow in the boundary layers and has been validated for this type of application.

The continuity equation is,

$$\frac{\partial \rho}{\partial t} + \nabla.(\rho U) = 0 \tag{4.1}$$

and the momentum equation is

$$\frac{\partial \rho U}{\partial t} + \nabla.(\rho U \otimes U) - \nabla.(\mu_{eff} \nabla U) = -\nabla p + \nabla.\left(\mu_{eff} (\nabla U)^T\right) + B \tag{4.2}$$

where ρ and U are the average fluid density and velocity, B is the body force and μ_{eff} is the effective viscosity defined as the sum of the average laminar viscosity μ and turbulent viscosity μ_T.

$$\mu_{eff} = \mu + \mu_T \tag{4.3}$$

The turbulent viscosity in the low Reynolds number k-ε model is given by

$$\mu_T = C_\mu f_\mu \rho \frac{k^2}{\varepsilon} \tag{4.4}$$

where C_μ is the drag coefficient, the function f_μ is an exponential function of the local turbulence Reynolds number and provides damping near walls. The turbulent kinetic energy, k, and energy dissipation rate, ε are obtained from the solution of conservation equations (Launder and Sharma, 1974; CFX, 1997). No modifications to the equations or the "standard" model constants were made.

A schematic diagram of the shearing apparatus is presented in Figure 4.1. Its construction was described in detail in Chapter 3. It is consisted of an annular bowl and a cylindrical stirrer. The stirrer rotates to generate turbulent wake in the annular gap.

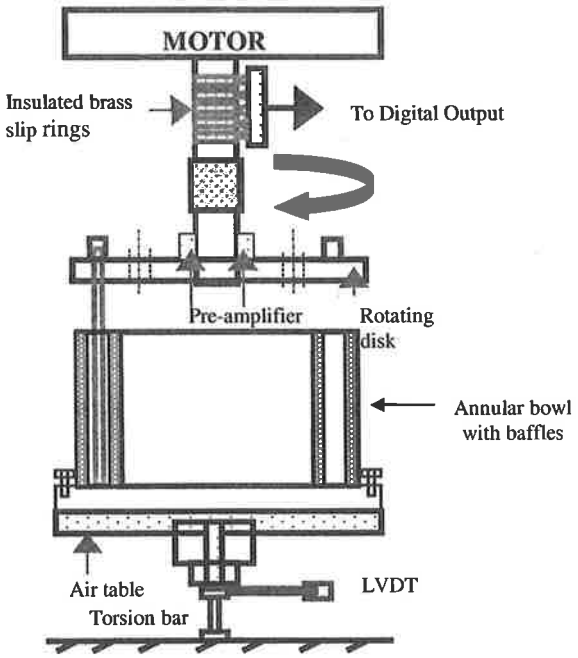

Figure 4.1. Schematic of the construction of annular shearing device

The flow profile inside the annulus is represented by two-dimensional axisymmetric flow. Two geometries considered include (i) the annular bowl excluding baffles and (ii) the annular bowl with baffles.

4.2. Simplified Model: Annular Bowl without Baffles

Figure 4.2(a) represents the overall mesh construction for the annular bowl without baffles. A detailed mesh construction around the cylindrical stirrer is shown in Figure 4.2(b). The model was simplified by excluding the baffles. The cartesian mesh was built from two blocks and the flow domain was represented by 15750 cells. A statistical analysis of the mesh construction indicated that cell volume ranged from 1.01×10^{-11} m^3 near the stirrer to approximately 1.1×10^{-8} m^3 further away from the stirrer. Grid expansion ratio of the mesh ranged from 1 to 1.55, indicating that the overall mesh quality was reasonably consistent (Refer to Appendix E for the CFX code).

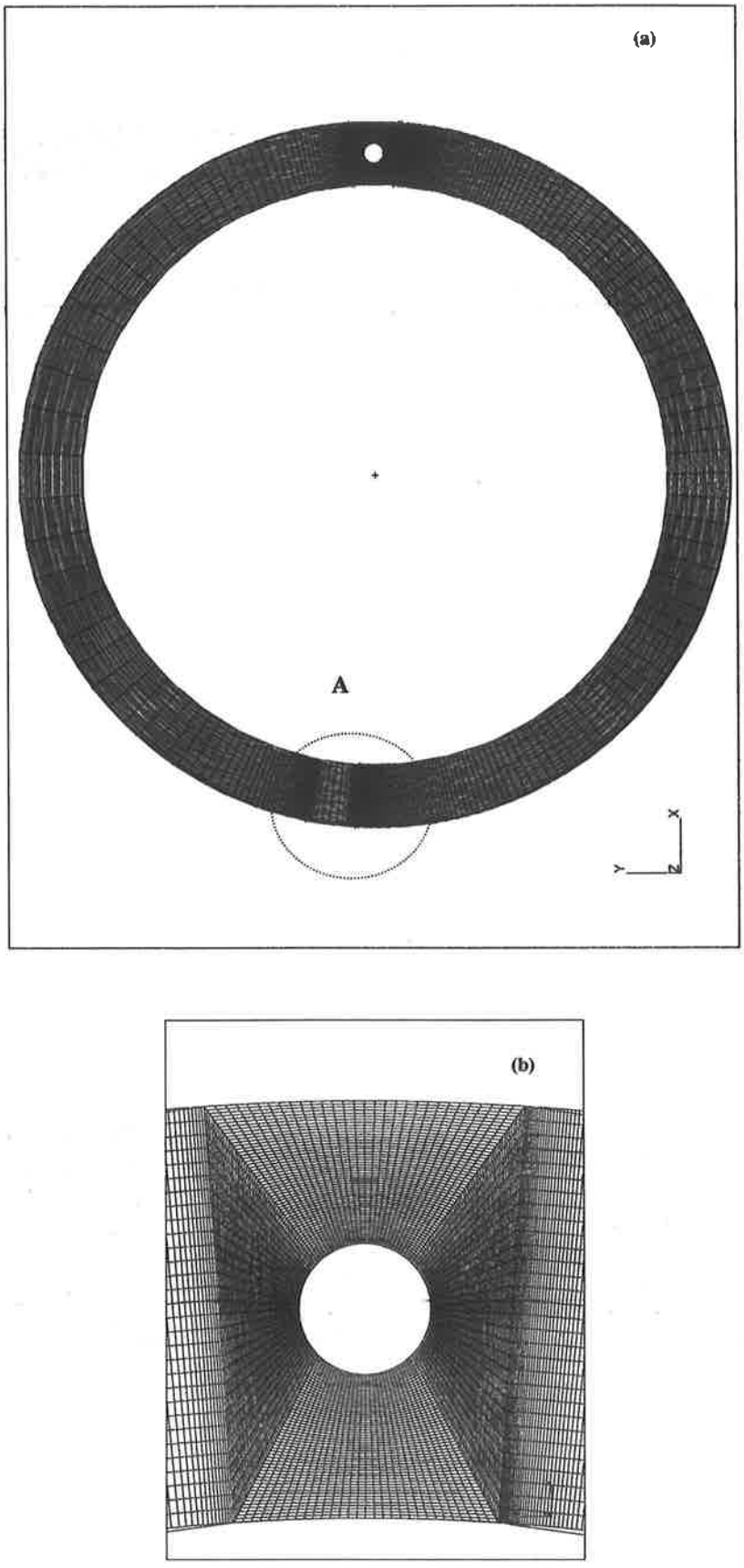

Figure 4.2. (a) Grid construction for the simulation of turbulent flow generated by a rotating cylinder **(b)** Detail grid construction around the cylindrical rod

Section A in Figure 4.2(a) is a section that was added to improve the overall mesh quality. Analysis showed that this section had orthogonal deviation of 0.03 and grid expansion ratio of 1, confirming that the mesh quality in this section was consistent with the rest of the geometry, and hence it did not influence the calculations near the stirrer.

The non-linear equations were solved using an Algebraic Multi-Grid (AMG) algorithm for all variables, except for turbulence quantities which were solved using a line-solver algorithm. The hybrid differencing scheme was used for all equations, except for U and V velocities (velocity component in the x and y direction, respectively), which employed the quadratic upwind differencing scheme (QUICK). These differencing schemes are the basis of finite-volume method. Both hybrid and QUICK scheme are modifications of the same fundamental method. The hybrid differencing scheme is the default scheme and it gives first-order accuracy, whilst QUICK scheme is third-order accurate and it can eliminate the overshoot of the solutions (CFX, 1997).

The transient run was started from a partially converged steady state solution, which was assumed as an initial guess. Transient convergence control was conditioned on the pressure. To simulate the rotation of the stirrer, the entire geometry was rotated about the z-axis while the annulus walls were set to rotate at the same velocity but in the opposite direction. The resultant model represented a stationary annulus walls with a rotating cylinder.

The reliability of the mesh construction was verified by applying the same simulation to the geometry at two different mesh densities. The original geometry consisted of 15750 elements and the new geometry had 19140 elements, which was the maximum number of cells that could be run on the available machine. This increase represents a 22% increase in the total number of elements. Figures 4.3 and 4.4 compare the energy dissipation rate and average shear stress at 550rpm at different downstream positions. No significant changes in the results were obtained for a 22% increase in mesh density. These results confirmed that the model construction was independent of the grid size.

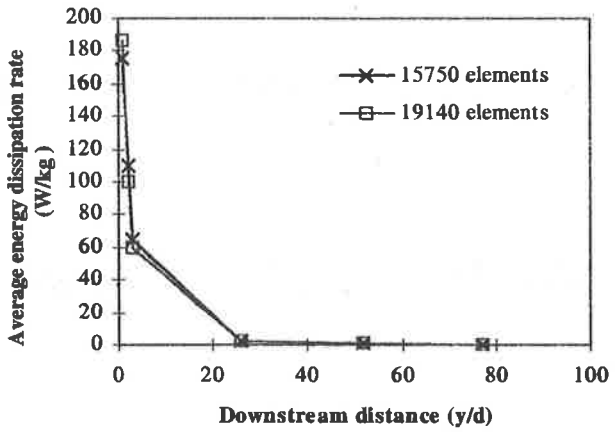

Figure 4.3. A comparison of the average energy dissipation rate at different monitoring points for different grid density at 550 rpm.

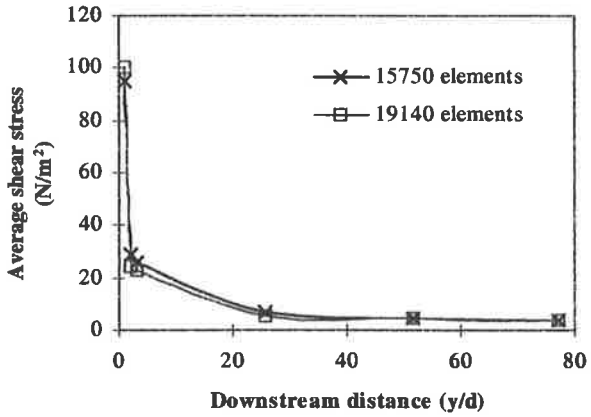

Figure 4.4. A comparison of the average shear stress at different monitoring points for different grid density at 550 rpm.

Turbulent wake behind a cylinder can be observed at Reynolds number (Re) greater than 1000 (Bloor and Gerrard, 1966; Cantwell and Coles, 1983). The operating speed range of the shear apparatus is 300-600rpm, which corresponds to the stirrer Reynolds number of 4200-7500. The transient parameters were evaluated by an adaptive time-stepping method, where the convergence was ensured by manipulation of the time step size. A total of 3200 time steps were calculated for each simulation. Each iteration was deemed to reach convergence when the pressure residual was less than 0.5 N/m^2.

4.2.1. Results from Simulations

Figures 4.5 and 4.6 show the resultant velocity profiles in the z plane at the stirrer rotational velocity of 350rpm and 600rpm, respectively. It is evident that the vortices are strongest in the flow domain approximately two stirrer-diameters (d_s) downstream of the cylinder. High velocity gradients in this region generate correspondingly high shear stresses. The average residence time of cell particles in this region is in the order of 10^{-3} s. The downstream vortices are damped by the walls and dissipate rapidly resulting in a significant fall in shear stress beyond $25d_s$ downstream.

The corresponding energy dissipation distributions are presented in Figures 4.7 and 4.8 for 350rpm and 600rpm, respectively. Intense energy dissipation rates are also observed in the region where shear stresses are high. These results confirm that the region of intense shearing responsible for severe damage to the cells is immediately behind the stirrer. As the shear stress and the energy dissipation rate weakens downstream, the degree of cell damage is expected to become less significant.

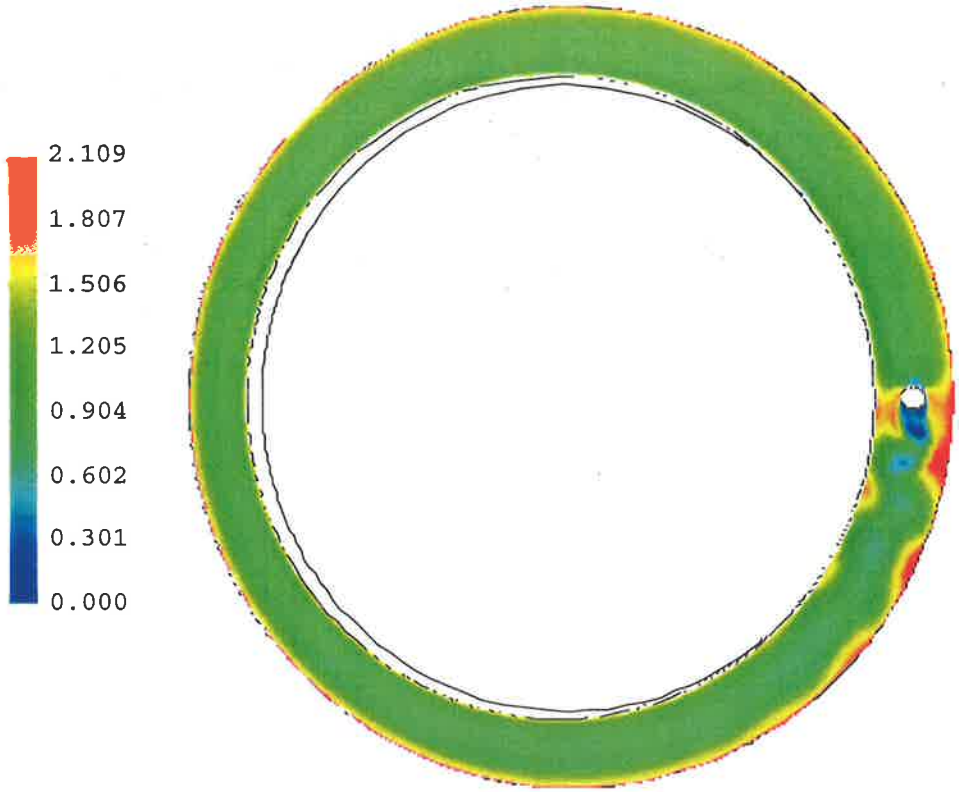

Figure 4.5. Resultant velocity profile at 350rpm (m/s)

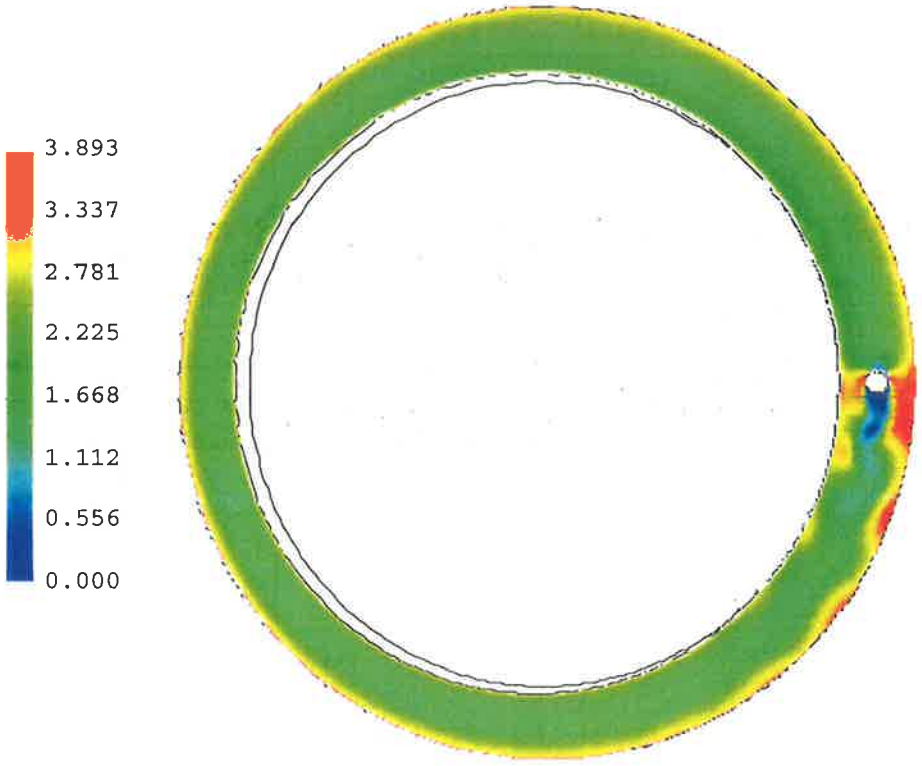

Figure 4.6. Resultant velocity profile at 600rpm (m/s)

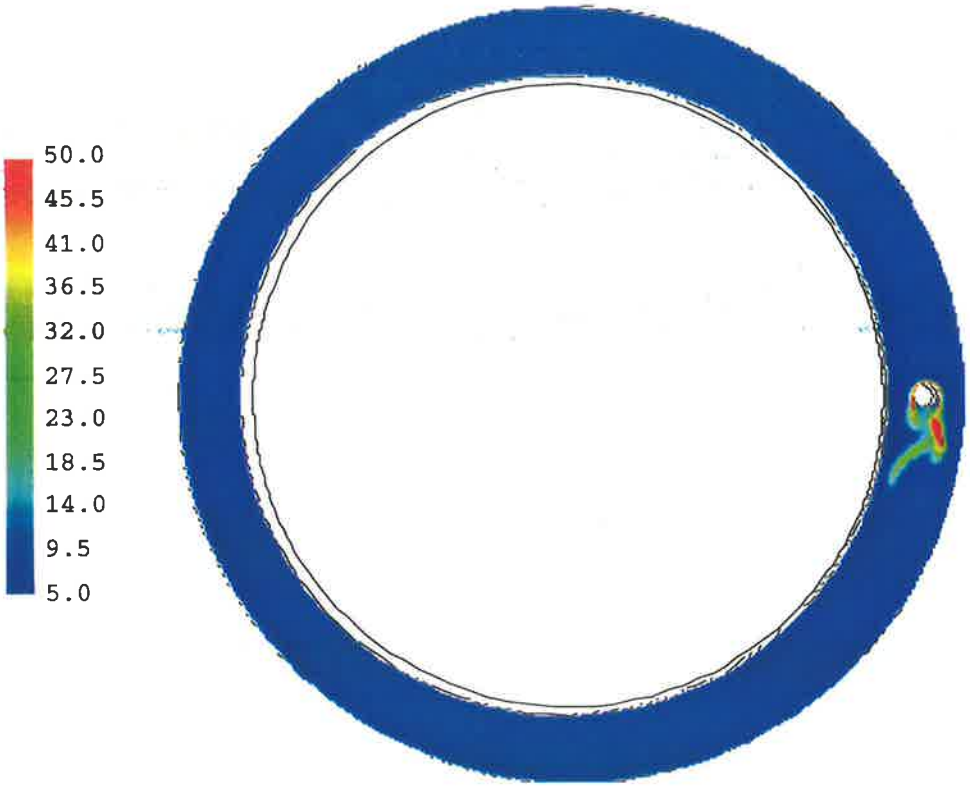

Figure 4.7. Energy dissipation distribution for an operating velocity of 350rpm (W /kg)

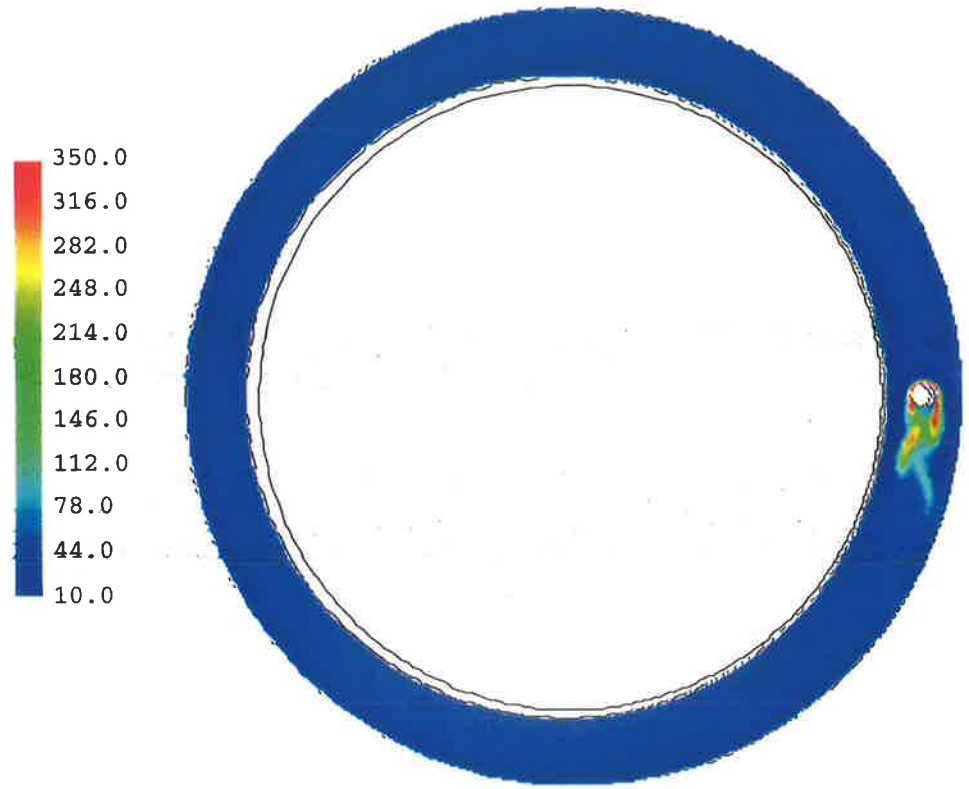

Figure 4.8. Energy dissipation distribution for an operating velocity of 600rpm (W /kg)

Table 4.1 summarises values of maximum and average shear stress, as well as energy dissipation rates downstream of the cylindrical stirrer. Both shear stress and energy dissipation rate were averaged over six downstream points of d_s (a stirrer diameter), $2d_s$, $3d_s$, $26d_s$, $52d_s$, $77d_s$. The simulated results for shear stress and the empirical data are compared and presented in Figure 4.9. The empirical shear stresses were obtained from the measured energy dissipation rate and equation (3.4). The simulated results are in good agreement with the empirical results up to the maximum operating velocity of 500rpm.

Table 4.1: Numerical results for the operating range.

Velocity (m/s)	Maximum shear stress (N/m^2)	Average shear stress (N/m^2)	Maximum energy dissipation rate (W/kg)	Average energy dissipation rate (W /kg)
1.441	51.5	4.2	28.8	4.05
1.801	75.1	10.0	55.2	10.97
2.316	100.5	18.9	121.6	30.72
2.831	137.7	23.5	227.4	63.09

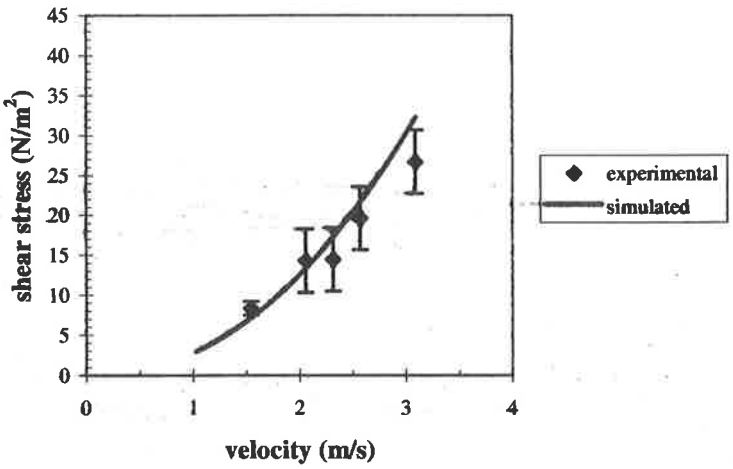

Figure 4.9. Comparison of average shear stress from experiments and simulations. The error bars represent the estimated errors obtained from the experimental data.

Given the information on the 'local' hydrodynamic conditions, the effect of shear damage can now be related directly to the microscopic structure of fluid, as well as the bulk fluid properties. Results from the simulations allow the local shear flow to be further characterised by the relationship between the shear stress ratio and the velocity shown in Figure 4.10. This relationship can be described by

$$\frac{\tau_{max}}{\tau_{ave}} = 16.48 u_c^{-1.09} \qquad (4.5)$$

where the shear stress ratio is defined as a ratio between maximum and average shear stresses, and u_c is the tangential velocity of the stirrer.

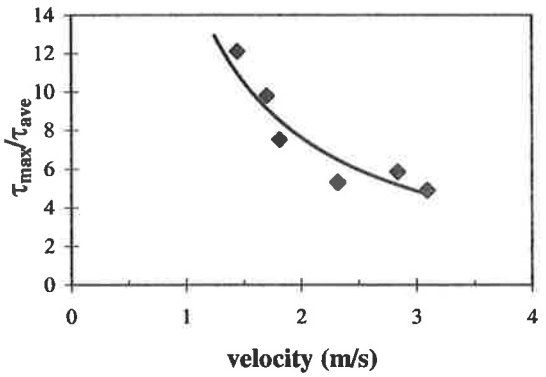

Figure 4.10. The relationship between the shear stress ratio and the tangential velocity. The shear stress ratio is expressed as the ratio between the maximum and the average shear stress. The curve represents equation (4.5).

In addition, the maximum dissipation rate is approximated by a linear function of ε_{ave} for a range of $4 \le \varepsilon_{ave} \le 100$ W /kg, where

$$\varepsilon_{max} = 3.27\varepsilon_{ave} + 20.44 \qquad (4.6)$$

The local dissipation rate in a control volume containing the region two stirrer diameters downstream is

$$\varepsilon_{local} = 2.33\varepsilon_{ave} + 14.75 \qquad (4.7)$$

The preliminary results of shear-sensitivity of *Daucus carota* demonstrate that cell viability is well correlated by the maximum energy dissipation rate. These data are presented in a plot of cell viability of *Daucus carota* as a function of maximum energy dissipation in Figure 4.11.

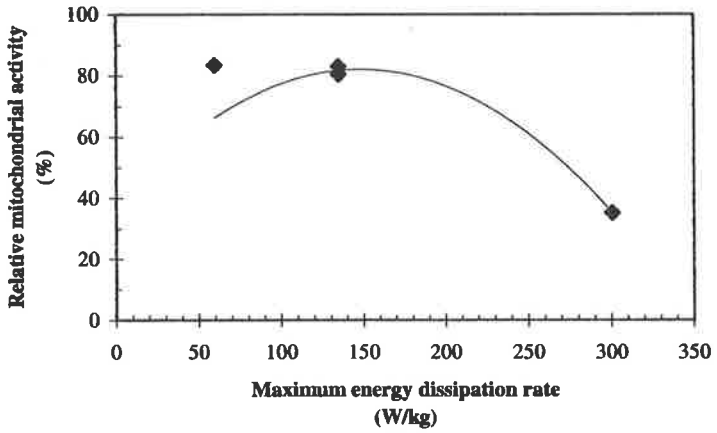

Figure 4.11. The relative cell viability of *Daucus carota* as a function of maximum energy dissipation from simulated results

The results have demonstrated that the characterisation of the turbulent effect on plant cell damage can be potentially refined with CFD modelling. Both microscopic (eg. 'local' dissipation rate) and macroscopic structure of turbulence (eg. total energy dissipation) can now be determined and used to quantify the effects of turbulence. Although further verification is required for the proposed shear damage relationship with other plant species, these results provide valuable information for the design of fermentation systems for plant cell cultures.

The model developed in Section 4.2 was further modified to accommodate the presence of baffles. The detail and outcome of this modification are presented in the next section.

4.3. Modified Model: Annular Bowl with Baffles

The geometric construction of this modified model with an addition of eight pairs of stainless steel cylindrical baffles with 3mm nominal diameter on the annular walls. These baffles were included to enhance mixing of the suspension. The 2D Cartesian mesh was constructed from 7 annular blocks. The cylindrical stirrer is located in an innermost annular section, which is defined as a 3D patch (USER3D). The boundaries of this USER3D patch are unmatched boundaries, which represent the interface where the sliding movement of the cylindrical stirrer occurs. To simulate the rotation of the stirrer, the USER3D patch was rotated about the z-axis while the annulus walls remained stationary. The resultant model simulated a stationary annulus walls with a rotating cylinder.

The flow domain was represented by 46536 cells. Figures 4.12 (a) and (b) represent the overall grid construction and the detail construction of the stirrer region, respectively. The run was modelled as a transient system with sliding mesh using unmatched boundaries. Transient convergence control was conditioned on the U velocity (velocity component in the x direction). The total run time was 1s, and the minimum residual for control parameter U velocity was set at 10^{-5} m/s.

The non-linear equations for sliding mesh model were solved with a General Algebraic Multi-Grid algorithm for all variables, except for k and ε which were solved using a line-solver algorithm. The 'van Leer' differencing scheme was used for all equations, except for U and V velocities (velocity component in the x and y direction, respectively), which employed the quadratic upwind differencing scheme (QUICK) (CFX, 1997).

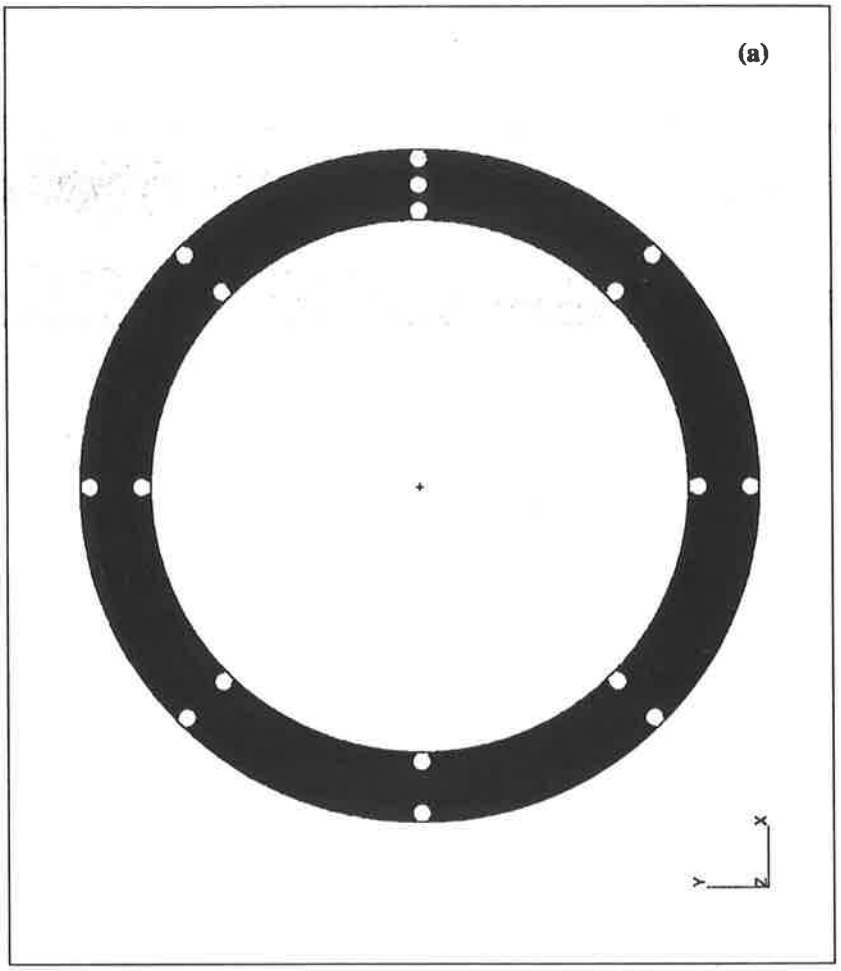

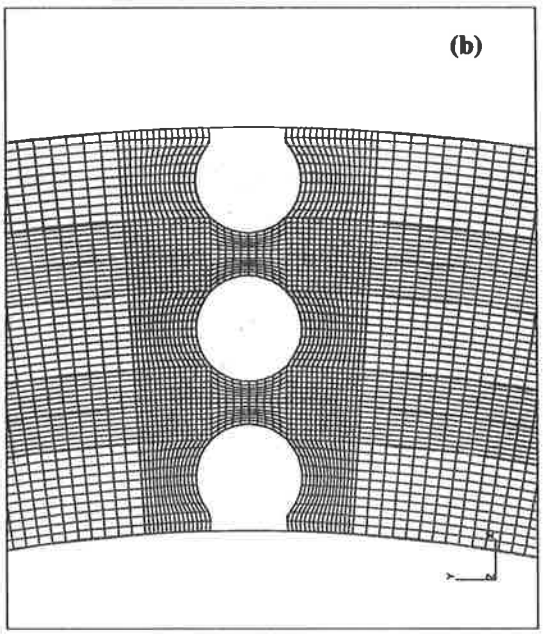

Figure 4.12. **(a)** Mesh construction for sliding grid model and **(b)** detail grid construction for sliding grid model with baffles

4.3.1. Simulation Results

4.3.1.1. Sliding Mesh with Baffles

Figure 4.13 shows the energy dissipation distribution for operating velocity of 400rpm after 2 revolutions (t = 0.3s). The local maximum dissipation rate is 0.06 W/kg, which is extremely low compared to the previous model (244 W/kg). This dissipation range is not consistent with the velocity profile in Figure 4.14, which indicates significant velocity gradients behind the cylindrical stirrer. The velocity gradients obtained should result in higher energy dissipation range. This unexpected outcome prompted further investigation to validate the sliding mesh model using a simplified (no baffle) geometry.

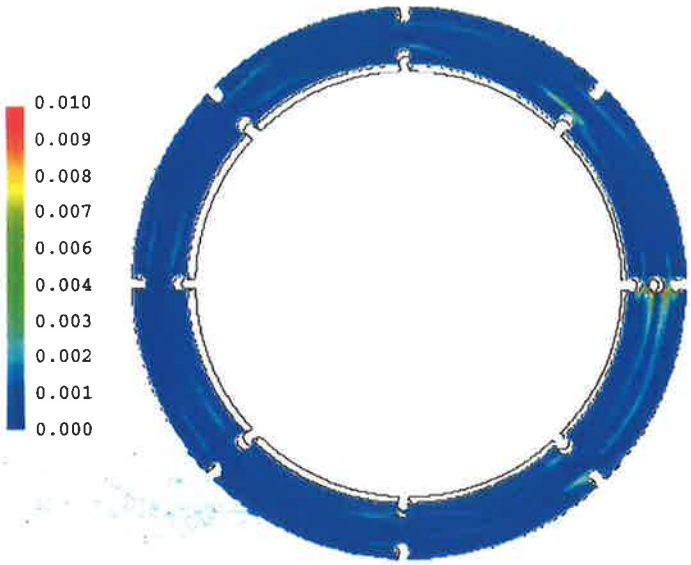

Figure 4.13. Energy dissipation profile at 400rpm for sliding mesh model with baffles (W/kg)

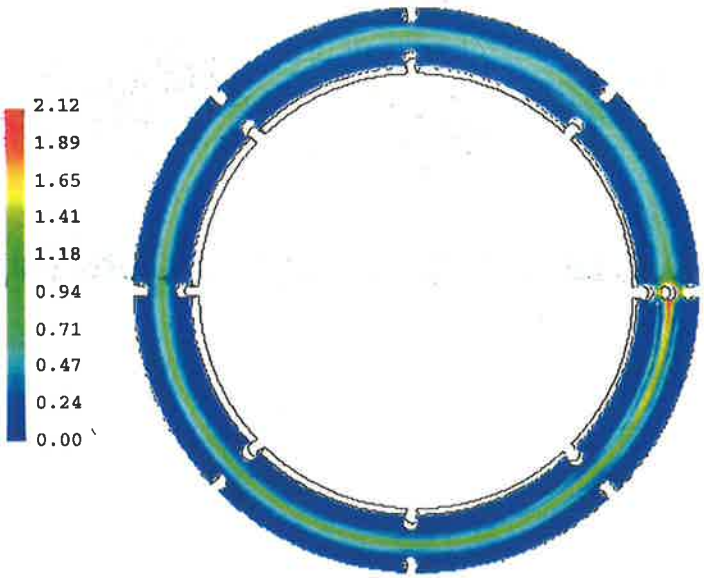

Figure 4.14. Velocity profile at 400rpm for sliding mesh model with baffles (m/s)

4.3.1.2. Sliding Mesh without Baffles

This model was generated to validate the accuracy of the sliding mesh regime for the given geometry without baffles. Figure 4.15 represents a detail construction of the model, which is similar to the case with baffles. The geometric mesh is represented by 68430 elements. Numerical methods for this model were based on the same principles and assumptions as those for the sliding mesh model with baffles.

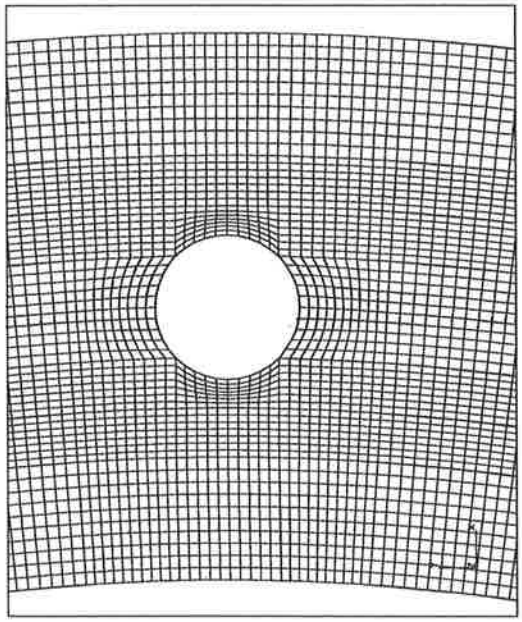

Figure 4.15. Detail grid construction for sliding mesh model without baffles.

The simulation results for this case were validated against the simulated results from the model without baffles using rotating coordinates. Figure 4.16 (a) shows the energy dissipation profile at 400rpm for sliding mesh model, whilst Figure 4.16 (b) represents the energy dissipation distribution at 400rpm from previous model using rotating coordinates. The range and profile are in general agreement; similar energy dissipation ranges were obtained from these models. However, vortex-shedding pattern was not observed in Figure 4.16 (a) for sliding mesh model. In addition, the dissipation was confined within a small annular section behind the stirrer. The reason behind this discrepancy may be due to the grid resolution in the boundary layer section, and therefore, finer grid size was required for vortex shedding to be observed. However, further reduction in mesh size would substantially increase the random access memory (RAM) requirement and this could not be achieved due to some limitations in the current computing resources, as well as the time constraint.

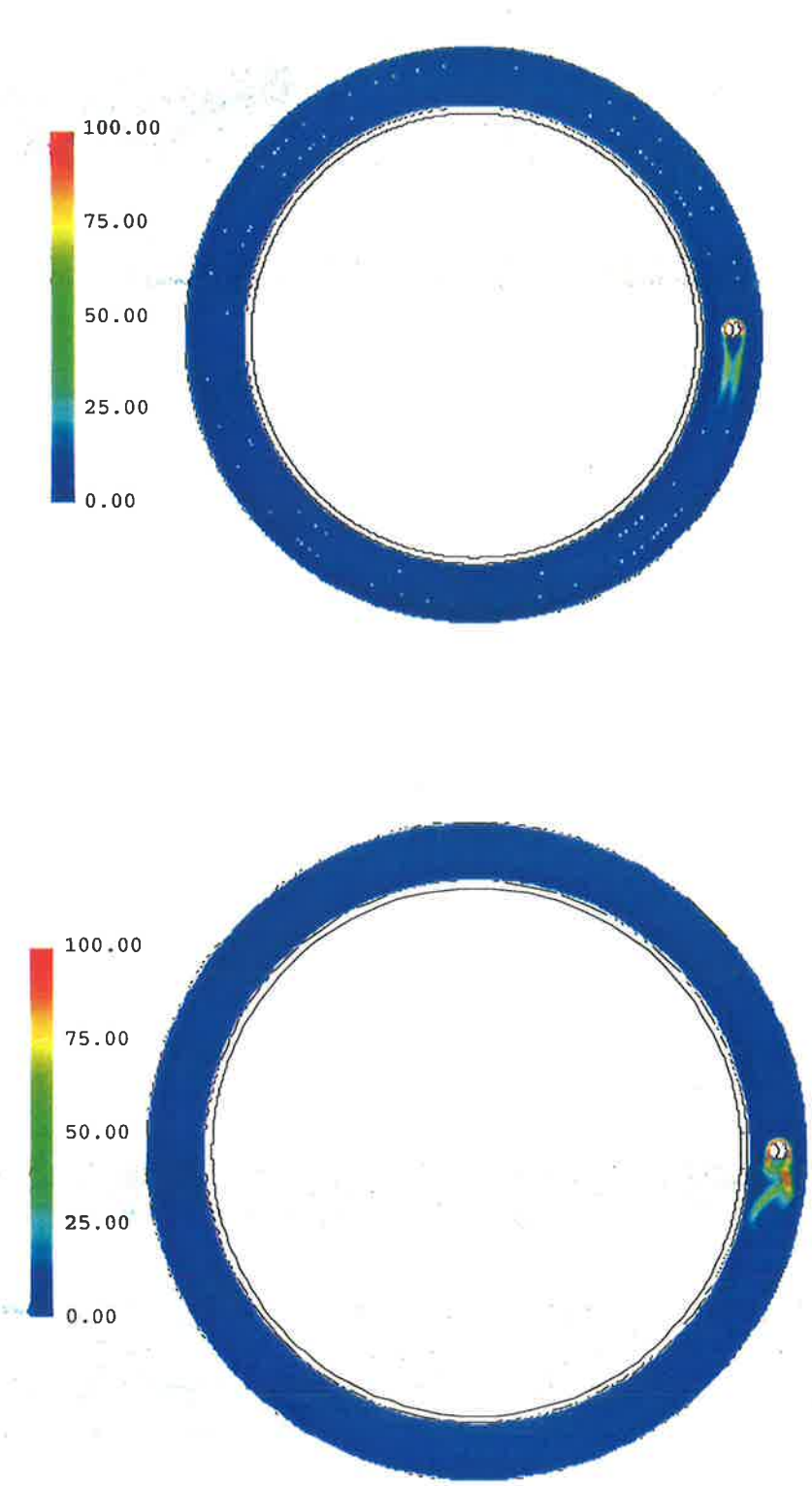

Figure 4.16. **(a)** Energy dissipation profile for the model with no baffles using sliding mesh, and **(b)** energy dissipation profile using rotating coordinates (stationary mesh). Both profiles were recorded for 400rpm at t = 1s, the energy dissipation rate is expressed in W/kg.

It was observed in Figure 4.16 (b) that dissipation of energy (in the vortices) spreads over a wide area behind the stirrer, indicating that vortex shedding also occurs on the interface between the sliding meshes. Consequently, any vortices generated in the proximity of the sliding mesh interface could not be accurately evaluated. This may explain the erroneous results from the sliding grid simulation with baffles (Figure 4.13). To overcome this problem, the sliding mesh boundaries must be moved further away from the vortex shedding motion. However, due to the scale of the geometry and the presence of baffles, it is difficult to relocate the sliding mesh boundaries. Relocating the sliding boundaries any further would result in inaccuracy of the finite difference calculations for moving mesh. Therefore, it was concluded that sliding mesh model was not suitable for the current geometry with baffles. Unfortunately, the sliding mesh model is the only approach available by CFX software package that could appropriately model the transient flow conditions with baffles. Consequently, it was also concluded that the current state of the software was not suitable for the modelling of this complex geometry.

4.4. Conclusions

This chapter has illustrated the application of CFD to the study of a flow field and its interaction with a biological system. The simplified two-dimensional simulations of the flow field in the experimental apparatus showed a strong agreement with the empirical results. The region of most severe cell damage was confined within two stirrer diameters downstream of the stirrer, where the most intense energy dissipation rates were observed. A linear relationship was found between the maximum and average energy dissipation rates. The extent of cell damage correlated reasonably well with both the 'local' turbulent dissipation rate and the bulk total energy dissipation. Further investigation is required to verify the relationships between cell damage, residence time, and stirrer frequency.

The simplified model was further modified by an addition of baffles. Due to the presence of baffles, this geometry could only be modelled by the sliding mesh model. However, the simulated results for energy dissipation by sliding mesh were found to be inconsistent with the velocity profiles obtained, indicating some erroneous results, which may be due to the grid construction near the boundary layer regions. In addition, vortex shedding was found

to occur on the interface between the sliding meshes, resulting in inaccurate calculations near this region. Unfortunately, correction of this geometry was difficult due to the presence of baffles and the geometric scale. Consequently, it was concluded that the current state of the CFX software package was not appropriate for modelling the flow conditions with baffles.

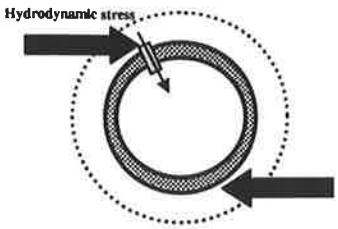

CHAPTER 5
PARAMETRIC STUDY OF THE EFFECTS OF TURBULENT SHEAR STRESS ON BIOLOGICAL RESPONSES

The understanding of the mechanisms involved in plant cell response to hydrodynamic shear stress requires the quantification of cell responses from several plant cell species. Unfortunately, studies have demonstrated that biological responses of plant cells can vary substantially with the shear environment, defined by system operating parameters, such as impeller type, vessel geometry and impeller speed. Furthermore, plant cells experience differing levels of physiological damage when exposed to fluid shear flow. For example, viability loss occurs prior to apparent mechanical signs of damage, such as aggregate break up or membrane damage (Dunlop et al., 1994). The degree of shear-tolerance also depends on the cell line and their growth stage (Wagner et al., 1977; Scragg et al., 1988). Consequently, proper characterisation of their response to hydrodynamic shear is subjected to several shortcomings. This chapter aims to address some of these problems and limitations.

Cell damage is commonly characterised in terms of average quantity, but evidence has confirmed that it is highly dependent on local conditions. Critical shear condition that plant cell can withstand varies significantly, depending on the cell line and type of cell cultures. For plant cell suspension cultures, damage is correlated in terms of energy dissipation, shear stress, shear rate, or impeller speed. However, these parameters change significantly depending on shear configurations. Clearly, there is a need to characterise cell damage using a more universal parameter that is applicable to all types of growth vessels and impeller types. In this chapter, the biological responses of cultured carrot cells (*Daucus carota*) are evaluated in a novel turbulent shearing apparatus (described in Chapter 3). The

experiments were performed over a range of rotational velocities to characterise cell damage over a range of shear conditions. Biological responses were quantified in terms of the mitochondrial activity, aggregate size and membrane integrity, relative to a control. The hydrodynamic conditions were expressed in terms of bulk and local variables. Bulk properties, such as average energy dissipation rates were measured experimentally, while the local conditions were determined from the input power and impeller swept volume. Finally, death kinetics models are proposed for better characterisation of cell viability in plant cells.

5.1. Preliminary Study

The measured physiological responses include the mitochondrial activity (reflecting respiratory activity), aggregate size (detecting the extent of break up of aggregates) and membrane integrity (indicating the damage on cell wall plasma membrane). All responses were expressed relative to the control samples (under normal growth condition, not subject to shear experiments). Table 5.1 summarises the average energy dissipation at different stirrer speeds in the shearing apparatus. The average energy dissipation range is typical of stirred tank bioreactors (Illing, 1996; Zhou et al., 1996a; Illing et al., 1999). The experiments were performed at 1, 2, 3, 4, 5 and 6 hours of shearing duration. The total number of 33 experiments (18 experiments per replicate with 15 experiments as partial replications).

Table 5.1: Energy dissipation rate in the shearing apparatus

Speed (rpm)	Average energy dissipation rate (W/kg)
300	2.15
400	4.56
450	5.47

Figure 5.1 shows the exponential decrease of biological responses to total applied energy dissipation. The hierarchy of the indicators of cell damage is the mitochondrial activity, aggregate break up and membrane integrity. As noted in literature, mitochondrial activity is

most sensitive to shear stress, and is damaged at much lower energy dissipation compared to other responses. Mitochondrial activity of *D. carota* was affected by total cumulative energy dissipation of 10^6-10^8 J/m^3, which is similar to the values observed for *Morinda citrifolia* and *Atropa belladonna* cells in turbulent conditions (Wongsamuth et al., 1997; MacLoughlin et al., 1998). From the data, the critical energy dissipation for 90% sustenance of cell viability was estimated to be 9.5×10^6, 1.76×10^7, 4.5×10^7 J/m^3 for mitochondrial activity, aggregate break-up and membrane integrity respectively. Approximately 50% biological response was maintained at 3.2×10^7, 1.28×10^8, 2.4×10^8 J/m^3 for mitochondrial activity, aggregate break-up and membrane integrity respectively. The critical energy dissipation for 90% viability is approximately equal to 10^7 J/m^3, which has recently been adopted as the criteria for designing an impeller system for optimum performance of plant cell cultures (Doran, 1999).

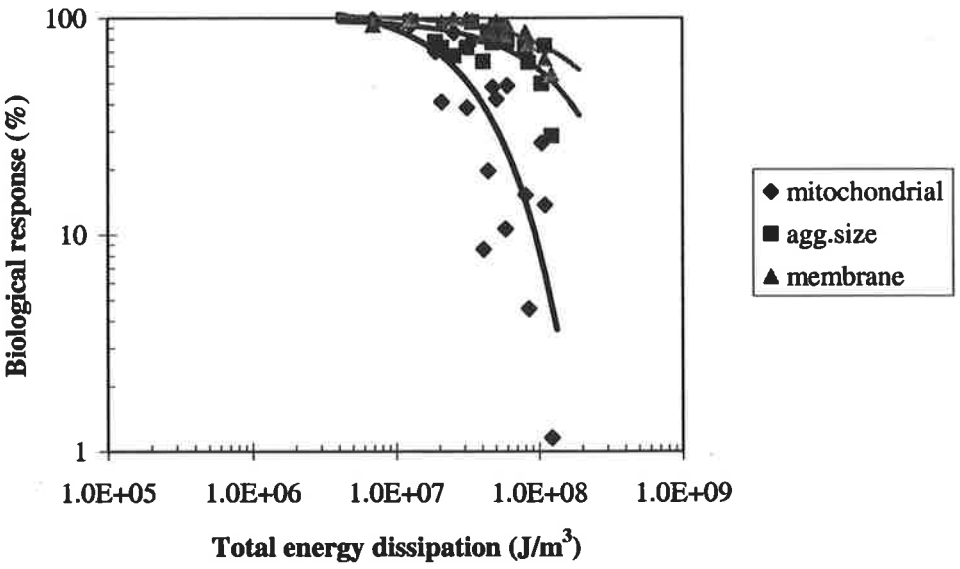

Figure 5.1. General biological response for *Daucus carota* in turbulent shear regime. The units are expressed as % of control responses.

Previous studies confirmed that the critical value of total energy dissipation strongly depends on cell types. Even though total energy dissipation has been suggested as the key design parameter for impellers and bioreactors (Doran, 1999), a global critical dissipation limit may not be optimum for all types of cells. Many investigators have demonstrated

more gradual damage over several orders of magnitude of energy dissipation (Dunlop et al., 1994; MacLoughlin et al., 1998). However, the recent study by Wong et al. (2000) found the onset of damage to occur at an order of magnitude higher. Figure 5.2 presents a comparison between the current experimental results for turbulent conditions with the literature values for *Daucus carota* for laminar (Wong et al., 2000) and turbulent flow (Dunlop et al., 1994) in couette viscometers. Biological damage occurred rapidly over a relatively shorter range of energy dissipations. The exponential decay models fitted to these data showed that the rate of the exponential deactivation was two orders of magnitude higher for turbulent compared with laminar data. As expected, very slight turbulent shear stress can cause comparable damage as that at high laminar shear stress. Approximately 30% of the cells became unviable when exposed to laminar energy dissipation of 2×10^{10} J/m^3, but the same damage level was caused by 6×10^{7} J/m^3 in turbulence regime. The major difference between laminar regime data from Wong et al. (2000) and that of Dunlop et al. (1994) could be due to shear hypersensitivity as a result of oxygen starvation. Plant cell subjected to oxygen starvation may become extremely weak, and hence, they may be more susceptible to shear stresses. Wong et al.(2000) reported that shear tolerance was markedly improved when the oxygen limitation problem was eliminated.

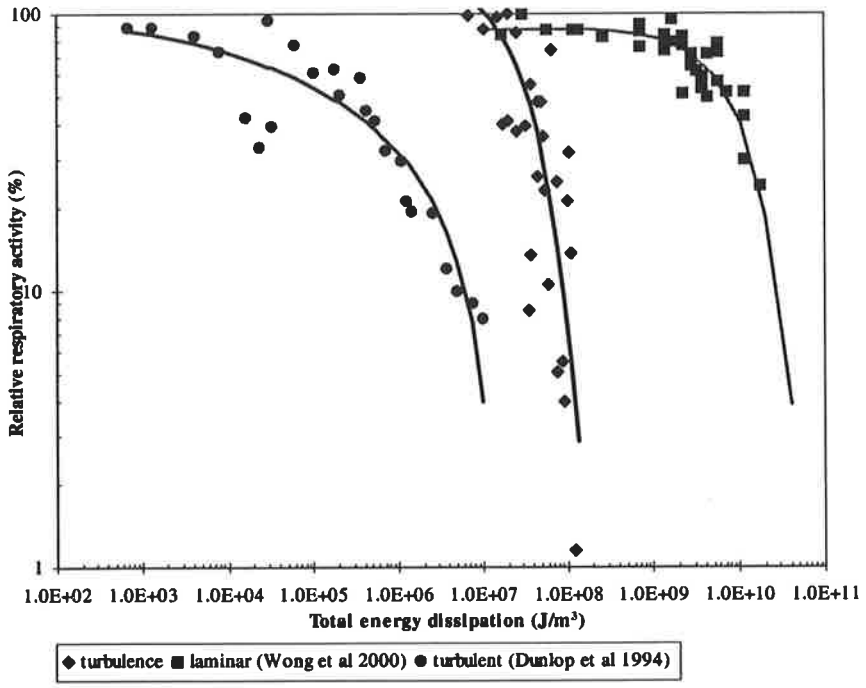

Figure 5.2. Mitochondrial activity relative to control as a function of total energy dissipation from turbulent shearing unit for *D. carota* in comparison to literature results.

Turbulence results in highly complex flow structures. Hence, it is difficult to characterise and reproduce. Studies quantify turbulence in terms of various hydrodynamic parameters, including shear stress, shear rate, and impeller speed. However, the cumulative energy dissipation has so far proven to be the most useful variable. Unfortunately, the main disadvantage of the total energy dissipation parameter is its strong dependence on both time and energy dissipation rate. Hence, the individual effects cannot be distinguished from each other. Wong (2001) suggested that cell damage may be cumulative and time may play an important role at different levels of shear stresses. A high energy dissipation level result from either exposure to high shear for a short time, or equivalently low shear for longer exposure time. As plant cells respond more strongly to maximum rather than average shear stress (Doran, 1993), they will undoubtedly show different responses at high and low shear conditions. In addition, flow regime in a typical suspension bioreactor varies enormously from highly turbulent near the impeller to slightly turbulent in the bulk flow. Hence, the region near the impeller is likely to provide predominant effect on how cells survive in bioreactors.

Rosenberg (1989) reported that mitochondrial activity decreased linearly with shearing speed at constant time. The time and energy dissipation rate dependence of *D. carota* cells is presented in Figure 5.3. The smooth curves are fitted so that the data sets can be readily identified, and do not have any statistical significance. The current results obtained deviate slightly from the expected linear relationship at lower exposure time between 1-2 hours, and became non-linear at higher shearing time. It is concluded that even though cell damage mechanisms are strongly dependent on both the time and dissipation rate, the interaction of these parameters is complex. Clearly, each variable should be considered individually.

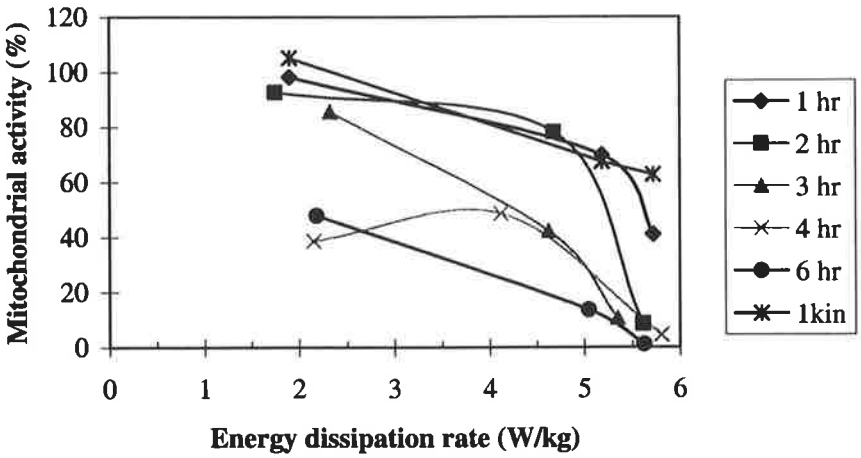

Figure 5.3. Changes in relative mitochondrial activity with respect to energy dissipation rate after different exposure time.

As a consequence of this deviation from a linear dependence, the individual effects of energy dissipation rate and exposure time were further investigated. Each biological response indicator was analysed in terms of 3D linear regression model against energy dissipation rate and time. The models aimed to verify whether the individual effect of ε and t was insignificant. If ε and t had no significant effects, then the model would produce a horizontal plane with the model F-value less than the critical F-value ($F_{critical}$).

The full proposed linear model is

$$Y_i = \beta_0 + \beta_1 \varepsilon + \beta_2 t + \delta_i \qquad (5.1)$$

where Y_i refers to the biological response, β_i represents the regression coefficients, ε and t denote the energy dissipation rate (W/kg) and time (hour) respectively, whilst δ_i represents the residual. If either ε or t had insignificant effect, then the corresponding coefficient β_i should be insignificant.

The coefficients at 5% level for all biological responses are presented in Table 5.2(a), where Y_1, Y_2 and Y_3 refer to relative mitochondrial activity, aggregate size, and membrane

integrity respectively. The Anova results in Table 5.2(b) verified that all F-values to be significantly greater than $F_{critical}$. Full results from the regression analyses are presented in Appendix C. Hence, the linear regression model estimated for mitochondrial activity is

$$Y_1 = 129.6 - 12.36\varepsilon - 10.60t + \delta_i \qquad (5.2)$$

Table 5.2(a): Regression coefficients for three biological responses ($\alpha = 0.05$)

Coefficients	Y_1	Y_2	Y_3
β_0	129.6	122.9	120.7
β_1	-12.36	-6.711	-3.880
β_2	-10.60	-5.565	-5.097

Table 5.2(b): Anova results for the 3D regression models ($\alpha = 0.05$)

Response	*F-value*	*significance F*
Y_1	18.97	7.81×10^{-5}
Y_2	9.783	0.0019
Y_3	14.19	0.00043

The level of significance of the regression analyses confirmed strong dependence on both time and energy dissipation rate (at 95% confidence level). This prompted further investigation into other appropriate parameters to model the shear response of plant cells.

Jüsten et al. (1996) proposed an alternative design parameter, the rate-ratio, which is a ratio between the energy dissipation rate and the circulation time, defined by

$$\frac{P}{\rho k' D_i^3} \frac{1}{t_c} \qquad (5.3)$$

where P is the power input by impeller, ρ is the fluid density, D_i is the impeller diameter, k' is the geometric factor and t_c is the circulation time (Jüsten et al., 1996). This parameter

possesses the advantage of accounting for both the level of shear and the frequency at which the cells are exposed to shear. Additionally, the constant k' represents a geometric factor, which describes the impeller size and type, the vortex shedding pattern and the impeller swept volume (Jüsten et al., 1996). In a bioreactor, the rate-ratio accounts for the power input per unit volume swept by the impeller, which is equivalent to the local-average energy dissipation rate. Hence, this parameter is independent of the operating volume. It showed consistent correlations for mycelial cells grown under various agitation conditions, and was recommended as a reasonable parameter to correlate from bench scale to pilot plant (Jüsten et al., 1996). Doran (1999) has also recommended the rate-ratio as a potential design parameters for selection of impeller type for various plant cell systems in stirred vessels.

Despite the unresolved question on the uniformity of energy distribution in stirred vessels, the consistency of the experimental results obtained by Jüsten et al. (1996) confirmed the potential of such a parameter. Determination of the parameter's general applicability depends on the outcome of future experiments on various plant systems.

Based on the above considerations, two design parameters are proposed and compared. As energy dissipation does not account for the frequency at which cells are exposed to stress, both parameters included the circulation time factor (t_c). In the proposed turbulent shearing system, the circulation time is equivalent to a reciprocal of the rotational speed.

The first proposed parameter is the ratio between the energy dissipation and the circulation time (ε_{ave}/t_c), which is a bulk property (Equation 5.4). The second parameter is based on the local power dissipation as described by Jüsten et al. (1996) (Equation 5.5).

$$Y_i = \beta_0 + \beta_1 \frac{\varepsilon_{ave}}{t_c} + \beta_2 t + \delta_i \qquad (5.4)$$

$$Y_i = \beta_0 + \beta_1 \frac{P}{\rho k' D^3 t_c} + \beta_2 t + \delta_i \qquad (5.5)$$

The linear regression analyses in Table 5.3 for the proposed parameters showed a marked improvement in the t-statistics following introduction of the circulation time. The *P*-values of the regression coefficients using ε_{ave}/t_c were almost half of the values obtained from the regression with ε_{ave} alone.

Table 5.3: *P*-value for the regression coefficients using different independent variables (ε_{ave} vs ε_{ave}/t_c)

Response	*P-value* for regression coefficient based on different independent parameters			
	Time	ε_{ave}	Time	ε_{ave}/t_c
Y_1	0.00069	0.00054	0.00046	0.00031
Y_2	0.0089	0.0060	0.0068	0.0036
Y_3	0.00049	0.0095	0.00031	0.0052

The linear plots of mitochondrial activity against the "energy dissipation/circulation" functions; (ε_{ave}/t_c) and $(P/(\rho k'D^3.t_c))$ are presented in Figure 5.4. The error bars represent standard errors. The value of $(k'D^3)$ in this case is based on the sweeping volume of the stirrer; ie the product of the stirrer diameter, height of the liquid and the distance of one revolution. Both models demonstrated reasonable correlation with correlating coefficients $R^2 = 0.92$. The y-intercepts for both parameters are 82.0, with different slopes of –1.45 and –0.38 for (ε_{ave}/t_c) and $(P/\rho k'D^3.t_c)$ respectively. The destruction rate in terms of (ε_{ave}/t_c) was an order of magnitude faster than $(P/\rho k'D^3.t_c)$. These results are similar to those reported by Jüsten et al. (1996). The apparent discrepancy between these two parameters arises from the swept volume factor, which accounts for the smaller contact volume where high shear is localised. Additionally, shear damage characterised by ε_{ave}/t_c varied significantly with the size and type of the impeller. Jüsten et al. (1996) found that the use of a larger Rushton turbine or paddle impeller resulted in less damage than that for a smaller pitched-blade impeller. Clearly, local energy dissipation rates would provide considerably more accurate results.

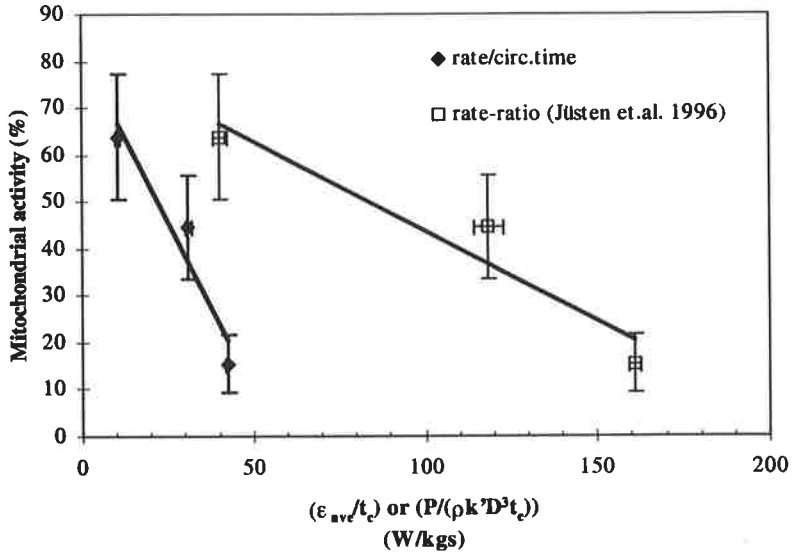

Figure 5.4. Comparison between (i) rate/circulation time (ε_{ave}/t_c) and (ii) rate-ratio ($P/\rho k'D^3.t_c$) as described by Jüsten et al.(1996). The error bars represent standard errors. The correlating coefficients for both plots is $R^2 = 0.92$.

Linear regression models were fitted to the responses data using the normal least square method. The two independent parameters are the time and the rate-ratio $(P/\rho k'D^3)(1/t_c)$. The regression coefficients are summarised in Table 5.4, and the 3D representation of the surface regression models are presented in Figures 5.5, 5.6 and 5.7 for Y_1, Y_2 and Y_3 respectively. These surfaces highlight strong interdependence of cell damage with time and the energy dissipation rate. As well, they present a method for predicting how the cell will maintain its viability in various scale of energy dissipation rates. This technique incorporates the frequency at which the cells are subjected to high stresses near the stirrer. The local forces which the cells are exposed to when they enter this high-shear zone are accounted for. The fundamentals remain the same whether the shearing device is a small apparatus or a large-scale stirred tank reactor. According to the findings by Jüsten et al. (1996), the relationship between cell morphology (*Penicillium chrysogenum*) on $(P/\rho k'D^3)(1/t_c)$ was consistent over a wide range of operating conditions. They could model all of their morphological data for mycelial cells with a single linear correlation, despite the fact that these cells were grown in various vessel volumes and impeller geometries. These results indicate that the biological response of any particular plant cell line should be modelled reasonably by a single 3D surface using these parameters.

Unfortunately as plant cells exhibit enormous variability in their biological activity, individual cell lines would undoubtedly be characterised by unique models. Such results require verification with further experiments. Each cell line would require numerous tests prior to any reliable characterisation. These correlations would consequently provide a detail insight into how the cells behave, while their applications would facilitate development of improved bioreactor designs for plant cell systems.

Table 5.4: Regression coefficients for 3D models.

	Regression Coefficients		
	Y_1	Y_2	Y_3
β_0 : Intercept	119.28	117.69	117.93
β_1 : $(P/\rho k'D^3)(1/t_c)$ (W/kg.s)	-0.3797	-0.2097	-0.1237
β_2 : Time (hour)	-10.714	-5.626	-5.161

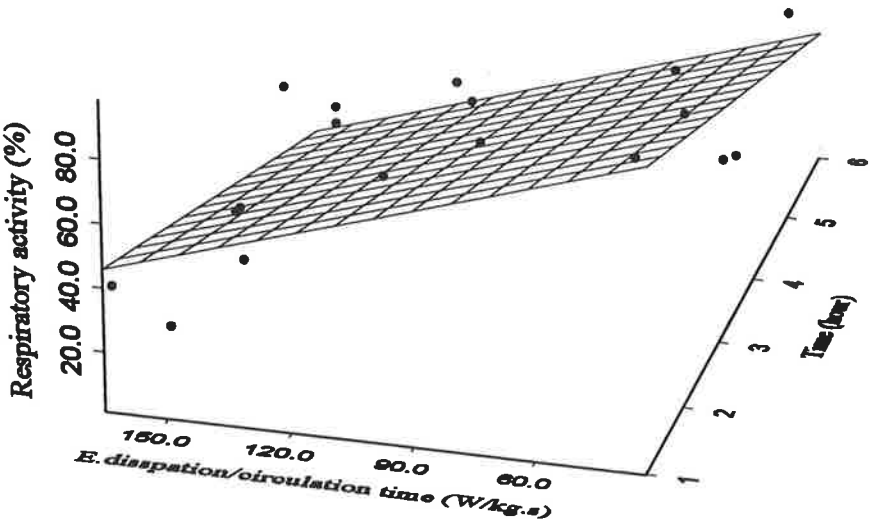

Figure 5.5. The 3D regression model for mitochondrial activity (Y_1) in terms of time and $(P/\rho k'D^3)(1/t_c)$.

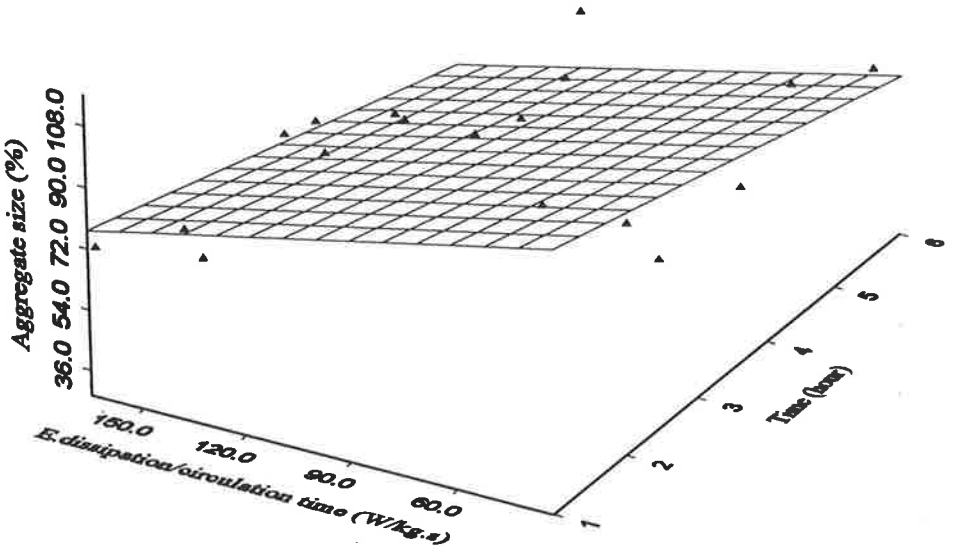

Figure 5.6. The 3D regression model for aggregate size (Y_2) in terms of time and $(P/\rho k'D^3)(1/t_c)$.

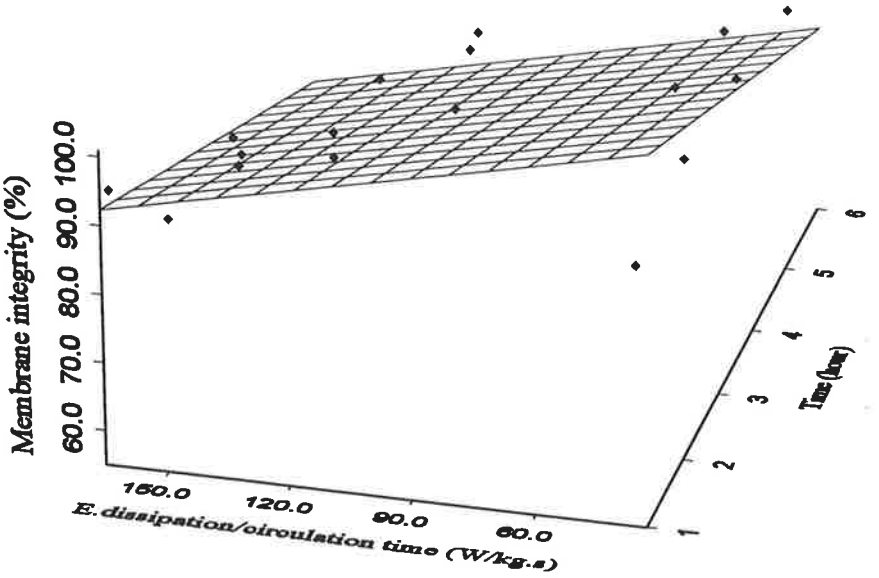

Figure 5.7. The 3D regression model for membrane integrity (Y_3) in terms of time and $(P/\rho k'D^3)(1/t_c)$.

5.2. Cumulative Sensitivity to Shear Stress

Experimental evidence confirms that the damage mechanism in plant cells is a cumulative phenomenon (Dunlop et al., 1994; Wong, 2001). Wong (2001) reported that the (coupled) oxygen uptake rate increased with cell damage, indicating that as cell viability deteriorates, more energy is required for additional processes invoked in responses to hydrodynamic stress. This rapid increase in energy demand may apply additional stress on cell metabolisms. This can eventually lead to an onset of cell death processes such as apoptosis or necrosis (Cowger et al., 1999).

Intermittent agitation will introduce a pause in the cumulative damage and thereby allow the cells to recover. Hence, a study was designed to investigate the possible recovery of cells subject to various degrees of shearing. The aim was to determine whether invoking an

intermediate rest phase for the plant cells during the shear experiments could improve their viability. If cell viability improved under such conditions, then it is possible then their health can be prolonged by growing them alternatively in high and low shear environments.

Carrot cells were sheared for 2 hours at a constant speed, then rested for 1-2 hours in a shaker incubator prior to a subsequent shearing at the same speed for 2 hours. The cells exposed to this treatment should sustain less damage if the recovery time was sufficient. The treated cells were compared to the cells exposed to 4 hours of continuous shearing.

The mitochondrial activity for cells with and without resting is presented in Figure 5.8. Similar results for relative aggregate size and membrane integrity are shown in Figures 5.9 and 5.10 respectively. Interestingly, Figure 5.8 shows that the mitochondrial activity of cells subjected to continuous shearing slowly declines initially, but the slow process is followed subsequently by a more rapid decay. A similar decay trend was observed in mammalian cells experiencing apoptotic death (Jiang et al., 1994; Cowger et al., 1999).

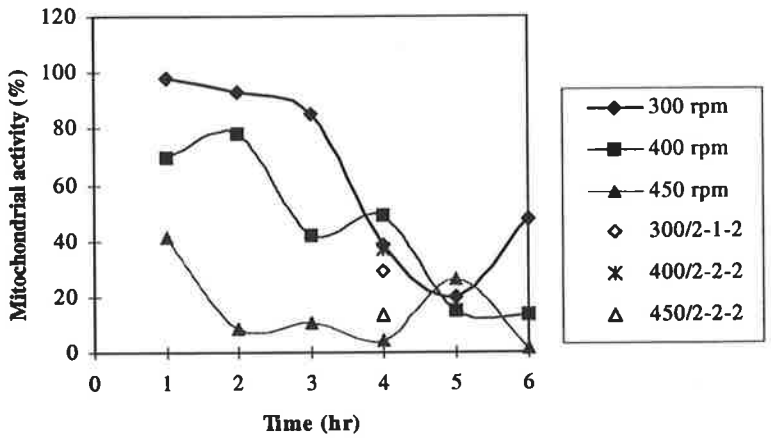

Figure 5.8. Comparison of the mitochondrial activity as a function of time, at fixed operating velocities. The individual points represent the cells exposed to various synergistic treatments; e.g. 300/2-1-2 refers to exposure to 300rpm for 2 hours, with 1 hour resting and 2 more hours of subsequent shearing.

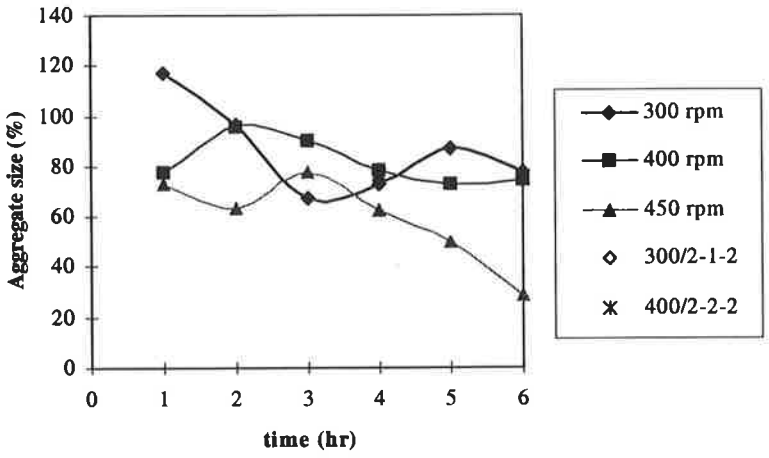

Figure 5.9. Comparison of the aggregate size as a function of time, at fixed operating velocities.

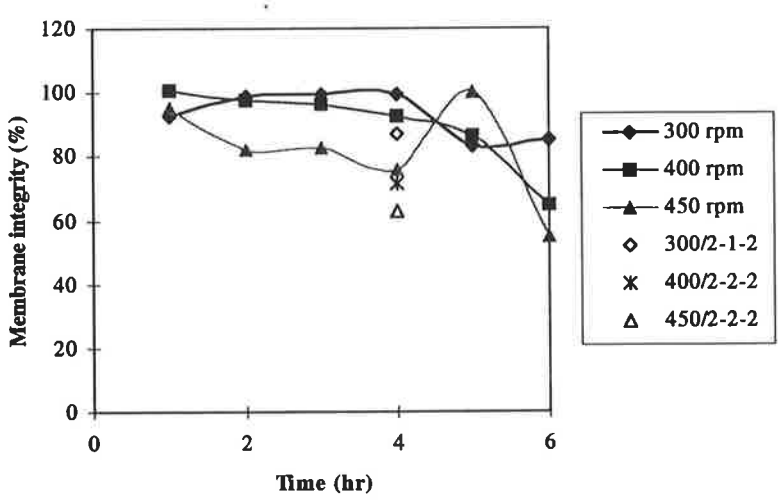

Figure 5.10. Comparison of the membrane integrity as a function of time, at fixed operating velocities.

For cells subject to intermediate resting, the mitochondrial activity (Figure 5.8) shows no improvement at 300-400 rpm. However, the cells subjected to 450 rpm may have improved survival prospect when rested intermediately for 2 hours. Similarly, no significant improvement was observed in aggregate size and membrane integrity in Figures 5.9 and 5.10.

Nevertheless, as the experimental time was limited, it remained uncertain whether the recovery time allowed in these experiments was sufficient for cellular metabolic recovery. Further extension of the recovery time would be impractical, especially when large-scale processes are considered. In addition, other operating factors, such as high cell mass, nutrient mass transfer limitation and sedimentation of aggregates would severely affect the performance of these cells in resting state with low shearing.

5.3. Deactivation Kinetics

The relative mitochondrial activity, aggregate size and membrane integrity responses in Figures 5.8, 5.9 and 5.10 seemed to deteriorate more rapidly as shear stress increased. At lower shear, the onset of the damage began slowly. However, as the shearing progressed, the damage rapidly increased. This behaviour can be commonly modelled by a number of deactivation kinetics models, but the Gompertz model, first-order model with lag phase were found to be more appropriate.

5.3.1. Gompertz Model

The Gompertz model is commonly used to describe deactivation kinetics of bacteria in sterilisation (McMeekin et al., 1993). The general expression of a Gompertz model is defined by

$$y = A + C\exp(-\exp(-B(t-M))) \qquad (5.6)$$

where A refers to the higher asymptote, and C is the difference between the highest and lowest value. B represents the relative slope at M, which is the inflection point. The actual slope at an inflection point of the Gompertz curve should theoretically correspond to the first-order decay. All coefficients of these models were estimated by least sum of squares method.

Figures 5.11, 5.12 and 5.13 represent the Gompertz models fitted to the relative mitochondrial activity, aggregate size and membrane integrity respectively. The relative mitochondrial activity and membrane integrity were well modelled at low energy dissipation rates, where the lag periods were more prominent. However, the relative aggregate size showed a rather poor fit, which may indicate that the decay preferentially follows the first-order kinetics.

Despite the reasonably good fit, the model is highly complex and involved four adjustable parameters. The number of data points was insufficient to guarantee model accuracy. Consequently, a simpler first-order kinetics model was adopted and is considered to be more appropriate statistically.

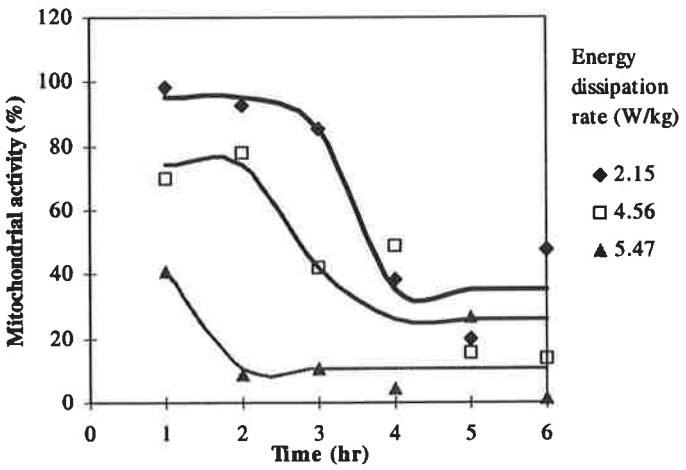

Figure 5.11. Gompertz decay model for relative mitochondrial activity as a function of exposure time. The points represent the experimental data and the lines are the Gompertz model fitted to the data.

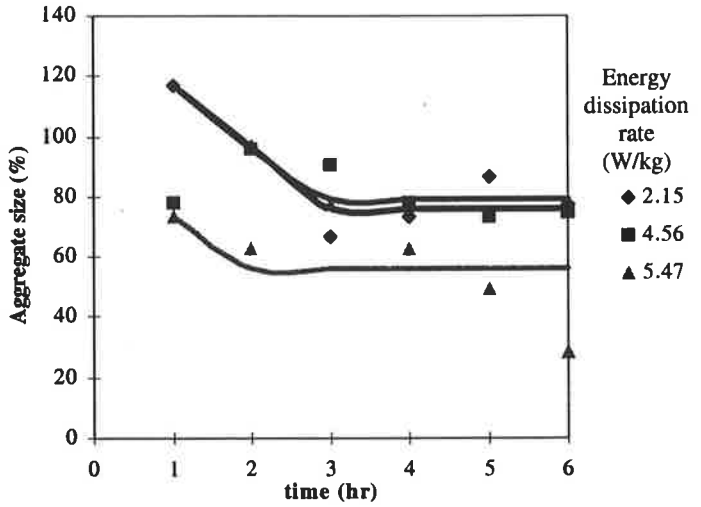

Figure 5.12. Gompertz model plot for deactivation of relative aggregate size against the exposure time.

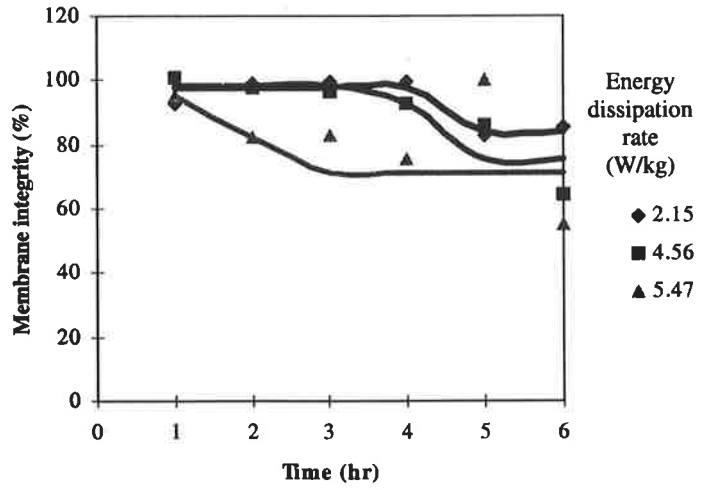

Figure 5.13. Gompertz kinetics model for relative membrane integrity as a function of exposure time.

5.3.2. First-Order Model

The first-order kinetic model is based on the deactivation model for bacteria during irradiation (Wu et al., 1993). Plant cell damage kinetics have also been extensively described by this model (Kieran et al., 1995; MacLoughlin et al., 1998; Kieran et al., 2000). The reasonable fit of the data by Gompertz equation indicated that some of the decaying responses had lag period. Consequently, the general first-order kinetics model was divided into two characteristic time periods. This pattern is often observed in bacterial deactivation, where the time is characterised by an earlier constant-viability (lag phase) and a first-order death phase (Wu et al., 1993).

The general relationship between the exposure time, t and relative cell viability (X/X_0) without lag phase is defined by

$$\frac{X}{X_0} = e^{-k\,t} \tag{5.7}$$

or

$$\ln\left(\frac{X}{X_o}\right) = -kt \tag{5.8}$$

The lag period is introduced into the first-order expression by using a breakpoint model (Potter et al., 1979). The breakpoint model is described by

$$y = a + \alpha b\left(t - t_{lag}\right) \tag{5.9}$$

where a is the y-intercept, b is the slope for first-order phase, and t_{lag} is the lag period. The control parameter which switches on the first-order term after the lag phase is α, where $\alpha = 0$ for $t < t_{lag}$ and $\alpha = 1$ for $t > t_{lag}$.

The breakpoint model for first-order kinetics becomes

$$\ln\left(\frac{X}{X_0}\right) = -\alpha k\left(t - t_{lag}\right) \qquad (5.10)$$

The relative cell viability (X/X_o) is expressed as a fraction of the control, t_{lag} represents the lag time, and the slope gives the decay rate.

Figures 5.14, 5.15 and 5.16 show the breakpoint-first-order model of the relative mitochondrial activity, aggregate size and membrane integrity respectively. The rate constants for these responses are represented in Figure 5.17. The deactivation rate constant for mitochondrial activity was 3-5 times higher than those of other responses. The rate of damage increased gradually until the average dissipation rate of approximately 4 W/kg. As the energy dissipation rate exceeded 4 W/kg, the damaging rate for both mitochondrial activity and aggregate size increased more rapidly. This confirmed a strong link between the aggregate break-up phenomenon and cell metabolic responses. The characterisation of aggregate structure during shear will be discussed in more detail in Chapter 6.

The deterioration rate for membrane integrity, however, showed no such rapid increase beyond the critical dissipation rate. This implied that membrane integrity assay might not be sensitive enough to describe cellular responses. The rate constant for mitochondrial activity ranged from 7.7×10^{-5} s^{-1} at 2.2 W/kg to 2.0×10^{-4} s^{-1} at 5.5 W/kg, while the maximum rate constant for membrane integrity was only 3.3×10^{-5} s^{-1}. The decay rate constants are relatively small compared to other reported values, as the average energy dissipation rates generated here are relatively milder than those in capillary or jet flows (Kieran et al., 1995; MacLoughlin et al., 1998).

Lag periods of the responses in Figure 5.18 vary with increasing energy dissipation rate. The relative membrane integrity showed the longest lag compared to the others, which further supported that membrane integrity is the least sensitive response. No lag was observed for mitochondrial activity and aggregate break-up when the average energy dissipation rate exceeds 5.5 W/kg. Interestingly, the aggregate break-up began at lower energy dissipation rate than mitochondrial activity, which indicated an early sign of damage in extracellular matrix prior to any injury in the intracellular activities. This

strongly supported the evidence that plant cell wall binds directly to the plasma membrane and the cytoskeleton elements. Such a continuum plays a significant role in several plant responses to the environmental stresses (Reuzeau et al., 1995). It is also evident that any impairment in extracellular stress receptors would hinder the ability of cells to detect stress. Hence, it would also impede their ability to regulate themselves against the invasive hydrodynamic stress.

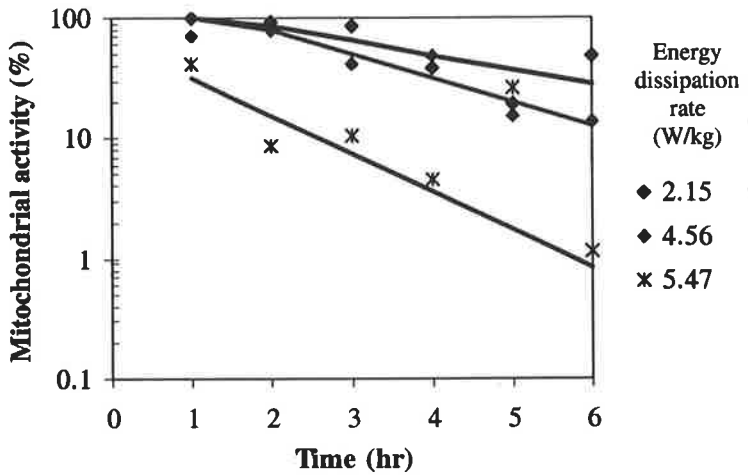

Figure 5.14. First-order decay model for relative mitochondrial activity against time. The lines represent the first-order decay model fitted to the experimental data.

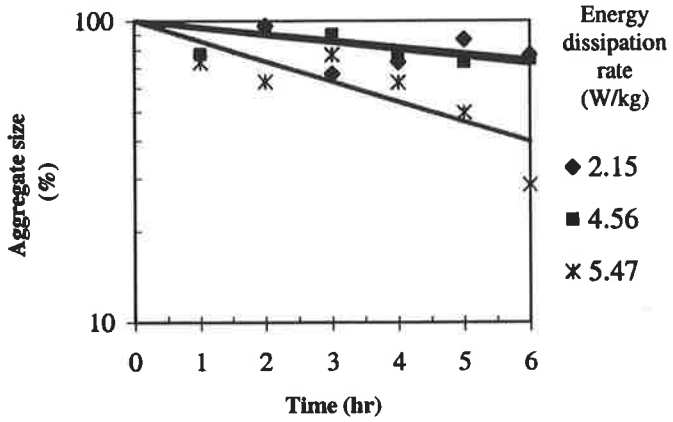

Figure 5.15. Plot of the first-order deactivation model for relative aggregate size versus time.

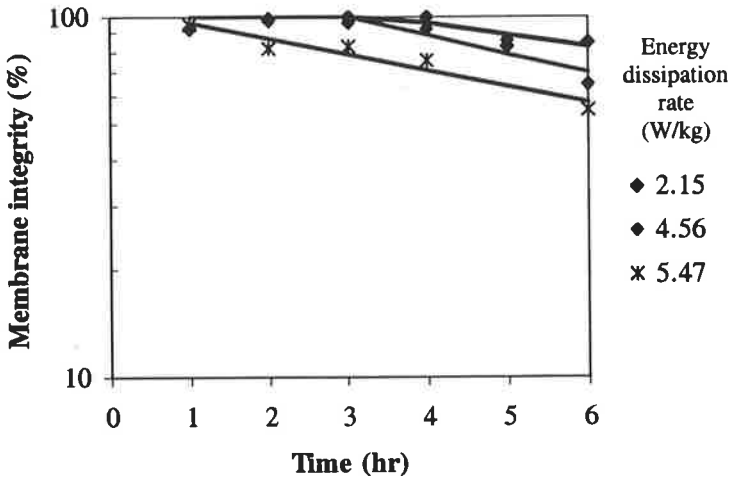

Figure 5.16. Plot of the first-order decay model for relative membrane integrity against time.

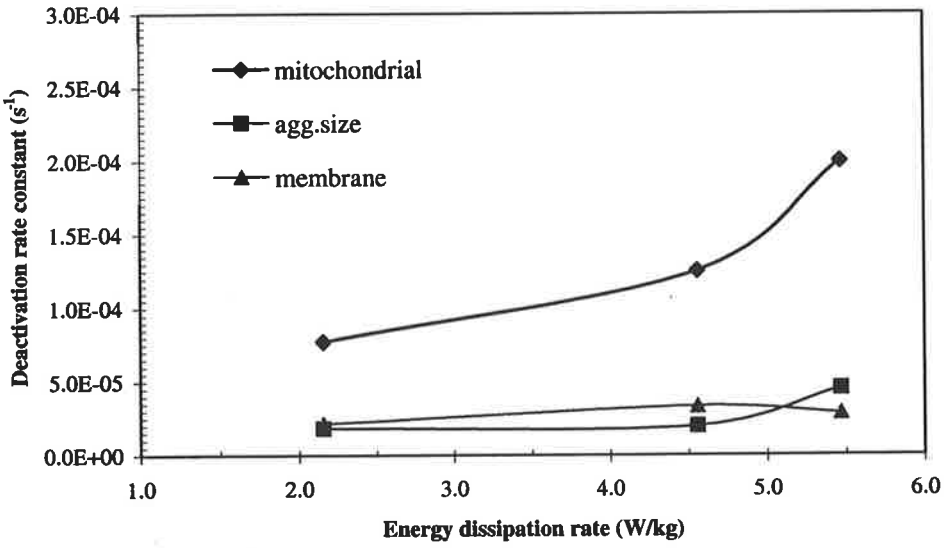

Figure 5.17. Deactivation rate constants for biological responses at different energy dissipation rates. All responses were fitted with first-order kinetics with lag phase. The coefficients were determined by least sum of squares method.

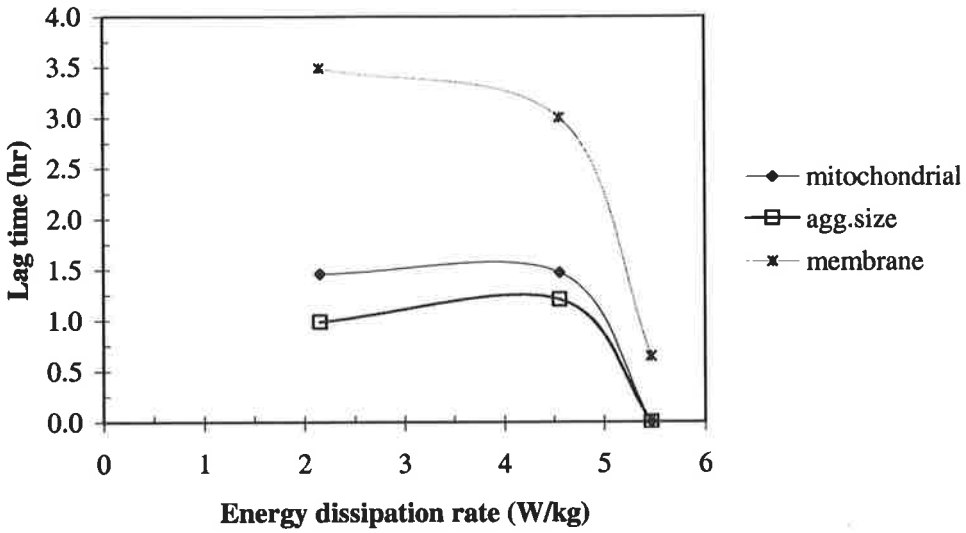

Figure 5.18. Variation in lag phase with energy dissipation rate, calculated from first-order model with lag period for mitochondrial activity, aggregate size and membrane integrity.

5.4. Conclusions

Studies of the effect of turbulence on cell viability of *Daucus carota* confirmed that the damaging energy dissipation ranged between 10^6-10^8 J/m^3. The turbulence shear regime was found to be two orders of magnitude more damaging than laminar regime. Membrane integrity was the least sensitive, while mitochondrial activity was most sensitive to shear. This confirmed that cells were damaged at a cellular level prior to signs of any physical injury.

As the current design parameters for plant cell processing are strongly system-specific, a new design parameter was proposed in terms of local energy dissipation and bioreactor configurations (Jüsten et al., 1996). This parameter may be applicable to other types of impellers and growth vessels. Further study with other impellers and vessels could confirm whether this is an ideal global design parameter.

It was observed that the damage mechanism in carrot cells resembled that of mammalian cells undergoing apoptosis. A study was undertaken to investigate whether allowing the

cells some shear-free recovery time could alleviate the damage. Unfortunately, 1-2 hours of recovery time was insufficient to relieve the damaging effects of shear stress.

Death kinetics was expressed as a first order process with lag period. The cell damage rate constant was highest for mitochondrial activity. However, it was possible that the onset of aggregate break-up occurred before a decay in mitochondrial activity. Consequently, a strong interrelation between aggregate break-up and cellular activity may exist, where the damage to the extracellular receptors could impair cell regulations.

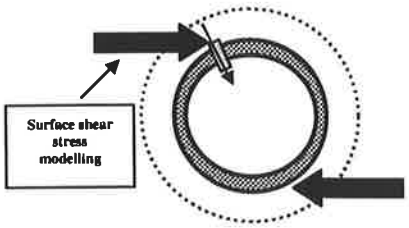

CHAPTER 6

CHARACTERISATION OF PLANT CELLS AND MATHEMATICAL MODELLING OF SHEAR STRESS ON PLANT CELL AGGREGATES

The extent to which hydrodynamic forces influence cells depends on the biological and physical characteristics of the organism (Mersmann et al., 1990). For plant cells, stress-sensitivity dictates several design and operating parameters of the equipment (Doran, 1993). In a bioreactor, the required levels of mixing and plant cell aggregate sizes are interrelated, as plant cell aggregates grow into various heterogeneous sizes and shapes. Consequently, the level of shear stress experienced by these aggregates strongly depends on their geometry.

Studies of the shear-sensitivity of plant cells are fundamentally complex due to the turbulent structure in a bioreactor. However, this problem is further complicated by variation in the shear stress level on different cell aggregates. Individual plant cells are significantly smaller than their aggregates. Hence, within an aggregate, individual cells experience unequal forces and shear stresses. Furthermore, irregular cell shapes are inadequately described by the normal assumption of a spherical particle. This chapter will address the issues regarding the complex morphology of plant cells and characterisation of shear stress experienced by the cells of various geometries.

Numerous correlations have been developed to describe the turbulent shear stress levels experienced by various cells (Cherry et al., 1990; Joshi et al., 1996; Takeda et al., 1998). These correlations involve the energy dissipation rate, the fluid viscosity and the average

particle diameter. However, these parameters are determined assuming spherical particles. They fail to account for heterogeneity of cell morphology. Plant cell aggregates are normally composed of several smaller cells forming an irregular shape. Larger aggregates will settle faster than individual cells. Hence, higher shear rates are necessary to maintain their suspension. The cells in the outer layer of an aggregate are exposed to higher shear stress than those on the inside of the aggregate. The number of cells in the outer layer is usually proportional the to individual cell size, as well as, the aggregate surface area (Illing et al., 1999). The number of exposed cells in an aggregate usually increases with increasing irregularity of the aggregate. Consequently, the rate of decrease in viability will depend on the number of cells exposed to a critical hydrodynamic shear environment.

This chapter presents means of characterising variation of plant cell morphology using a range of shape factors. The increased exposed surface area due to morphological irregularity of the cell can be approximated using these factors. The morphological characteristics of these cells can be incorporated into the modifications of expressions for surface shear stress on aggregates. The results from these modifications are also presented in this chapter.

6.1. Characterisation of Plant Cells

Plant cells aggregates result from incomplete separation during their growth phase. The heterogeneity of their geometry is primarily reflected in the variation of their sizes. A typical size distribution of the pre-screened carrot cultures is presented in Figure 6.1. The average diameter calculated from 18 experiments, using Malvern particle size analyser is 112.8 μm. Despite the maximum pre-screened size of 230 μm, larger cells were observed. These larger cells are suspected to be long ellipsoidal-shaped aggregates with minor axes less than 230 μm. Large aggregates with small minor axes would be able to pass through the filter.

The complexity of irregular particles can be characterised in terms of a variety of parameters. Geometric parameters, such as bio-volumes, diameter, and fractal dimensions have been used to describe proteins, bacteria and algal cell sizes (Billiones et al., 1999; Dziuba et al., 1999). Fractal dimension is a size-independent parameter, which measures

the ruggedness of the particle surface. Other size-dependent shape factors are elongation (ratio of the length (major axis) to the width (minor axis)), circularity (indicating how closely a particle resembles a circle relative to its perimeter).

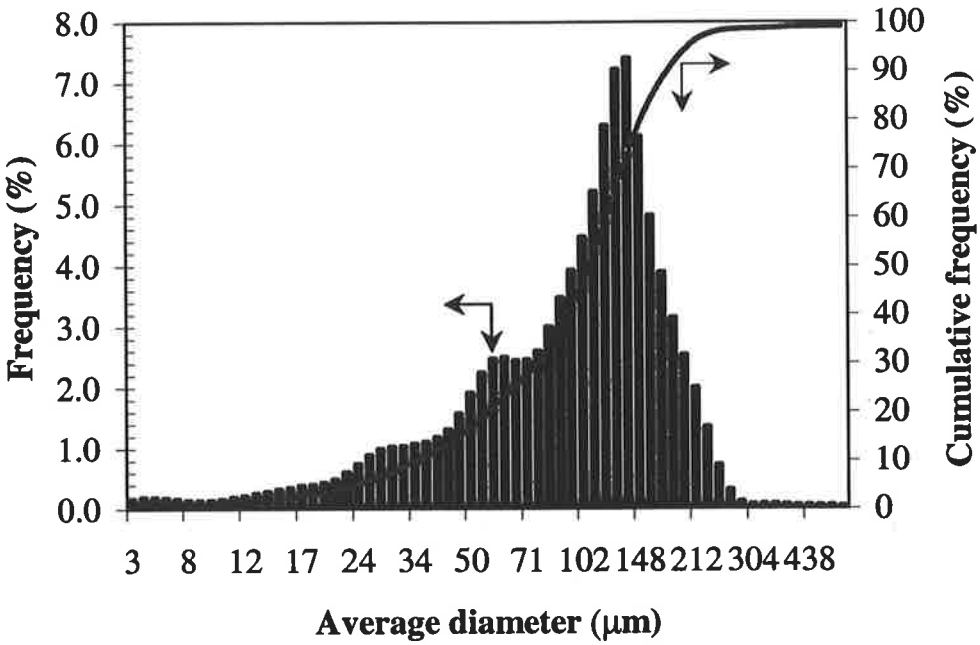

Figure 6.1. Particle size distribution of pre-screened 12-day old carrot cells. The mean diameter from 18 samples is 112.8 μm.

The complex morphology of a structure can be characterised by fractal dimension (Mandelbrot, 1983). Smaller fractal dimensions correspond to simpler structures. The fractal dimension is determined by examination of the perimeter of the structure. Several strategies have been developed for measurement of the fractal dimensions of an image. Two basic approaches will be examined. These are the box-counting (Jelinek et al., 1998) and perimeter-based fractal dimensions (Serra et al., 1998).

The box-counting method divides the object into a grid of boxes of variable size (r). A box containing the object's boundary called non-empty. For a fixed grid size, the number of non-empty boxes N(r) is counted. A logarithmic plot of N(r) versus log of (1/r) yields a line whose gradient corresponds to fractal dimension D_f (Jelinek et al., 1998). Values of D_f vary with the complexity of the morphology. Figure 6.2 presents a histogram obtained for

D_f from 100 carrot cell images, using grid size 1mm, 5mm and 10mm. Values of D_f obtained range from 1 to 1.7, indicating a mixture of round regular cells and highly irregular aggregates. The mean D_f equals 1.295, which represents a significant deviation from a spherical aggregate.

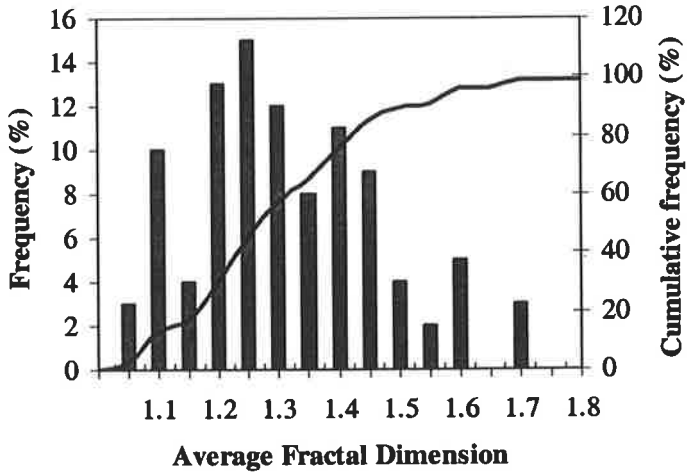

Figure 6.2. Fractal dimensions from box-counting method

The second method is the perimeter-based fractal dimension D_{pf}. It is based on the relationship between the cross-sectional projection area, A and the perimeter of its projection, P (Spicer et al., 1996; Serra et al., 1998);

$$A \propto P^{2/D_{pf}} \tag{6.1}$$

The slope of the logarithmic plot of A versus P is equal to $2/D_{pf}$. The value of D_{pf} ranges from 1, corresponding to a spherical particle to 2 for a linear aggregate. Value of D_{pf} close to 2 represents an open and irregular particle structure (Serra et al., 1998).

Figure 6.3 presents a logarithmic plot of the projected area versus the corresponding perimeter. The perimeter-based fractal dimension equals 1.294, which corresponds closely to the result determined by the box-counting method.

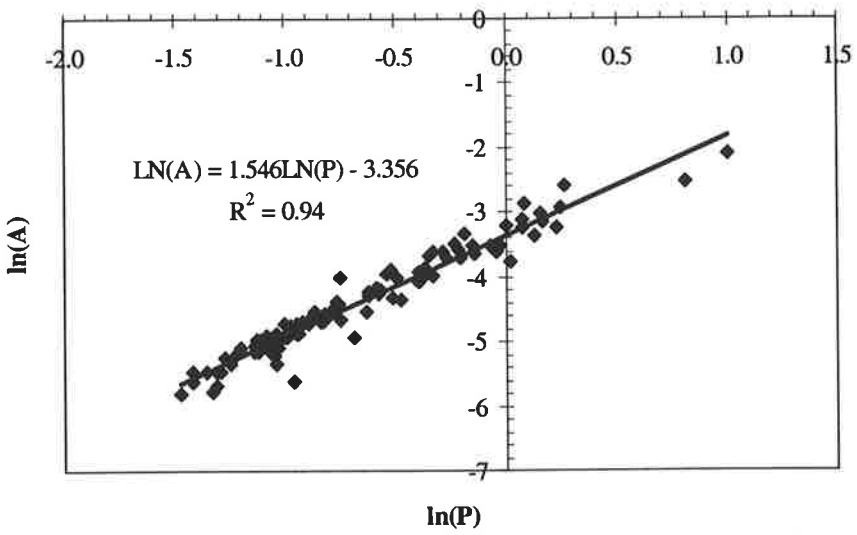

Figure 6.3. The perimeter-based fractal dimension 1.294, which agrees with the results from box-counting method.

Clearly, the fractal dimensions of carrot cells suggest significant complexity in the aggregate morphology. Figures 6.4 (a) and (b) illustrate a variation in the geometric shapes of pre-screened 12 day-old carrot cultures. These cells vary significantly in sizes and shapes. However, their morphology can be categorised into five principal groups characterised by distinctive features. The groups are summarised in Table 6.1. Different geometric shapes are best distinguished on a plot of equivalent diameter against the elongation as shown in Figure 6.5. Five distinct regions, each corresponding to a different geometric shape, are evident. The solid ellipses represent 2 standard deviations of the data groups.

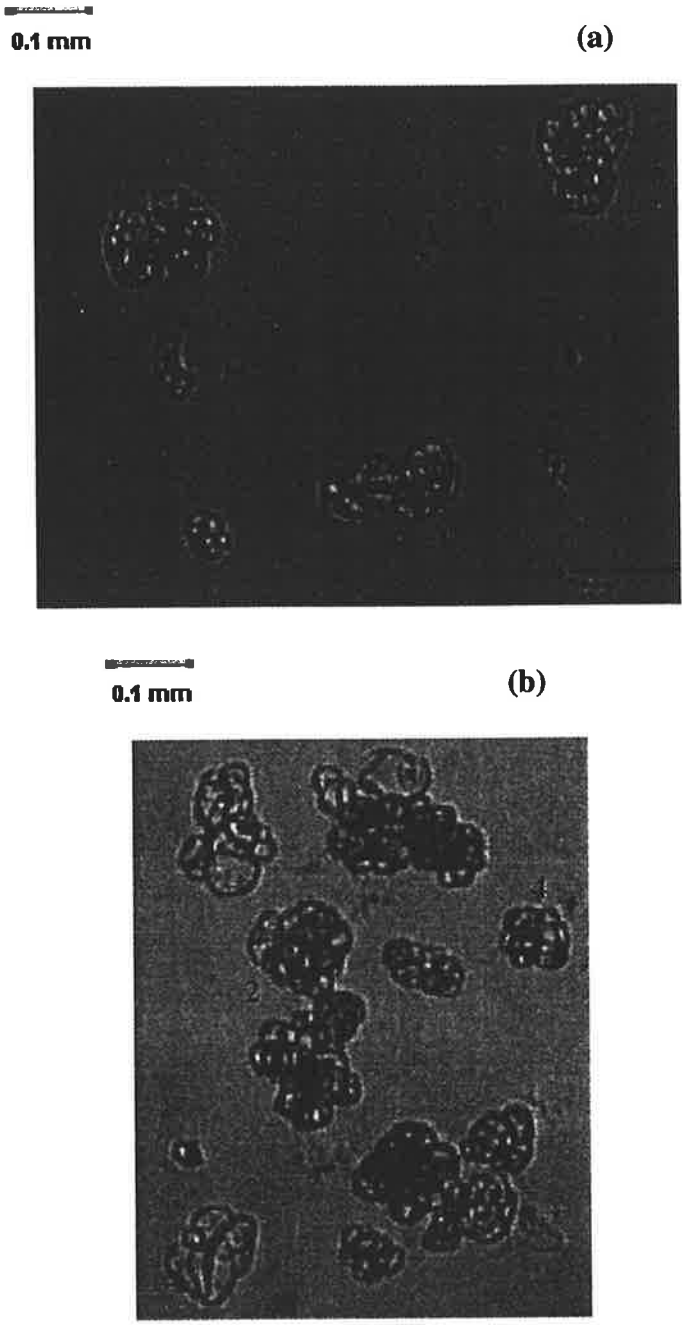

Figure 6.4 (a) and **(b).** Typical image of 12-day old *Daucus carota* cells for control samples.

Table 6.1: Classification of different geometric shapes

Group No.	Size	Geometric Shape
1	small	long aggregates
2	very large	irregular aggregates
3	large	long aggregates
4	small	round aggregates
5	medium	round aggregates

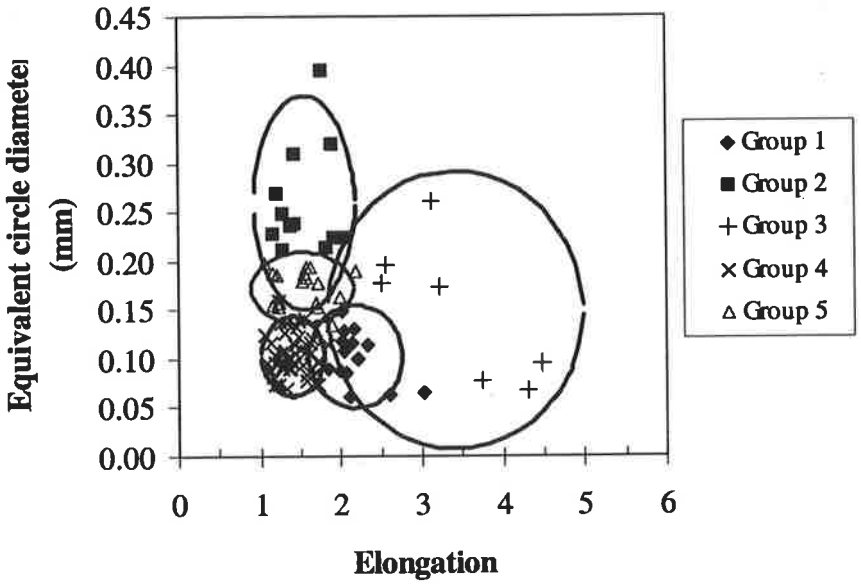

Figure 6.5. Characterisation of different geometric shapes in carrot cells. The group numbers are summarised in Table 6.1. Each ellipse's major and minor axes represent two standard deviations (95% confidence level) for the data group (Russ, 1994).

Group 1 represents the longer aggregates, while Groups 2 and 3 represent very long and large aggregates respectively with relatively high standard deviations. The cells represented by these latter groups have higher exposed surface area, and hence higher number of cells exposed to hydrodynamic shear. Group 4 is the most common geometric shape, representing small to medium round cell aggregates. Finally, Group 5 represents large round aggregates, consisting of increased number of cells.

Figure 6.6 summarises the transient change in carrot cells' morphology following exposure to 450rpm (ε_{ave} = 5.47 W/kg). After 1 hour of shearing, most large irregular aggregates (Group 2) were broken into smaller aggregates. The number of large irregular aggregates in Groups 2 and 3 decreases with increasing elapsed time, indicating that very large aggregates continuously break until the critical size range is reached. Smaller aggregates in Group 4 appear more stable and shear-resistant. After 6 hours, all large aggregates in Group 2 have been completely broken into smaller aggregates. The vast majority of the cells after 6 hours of shearing belong to Group 4 characteristics.

As expected, larger aggregates are more fragile and generally fracture readily to form smaller aggregates. This phenomenon has been observed in different plant cell morphology. Larger chains of shear-sensitive *Morinda citrifolia* cells exposed to turbulent jet flow broke preferentially to leave the more resistant smaller chains consisting of a few cells (MacLoughlin et al., 1998).

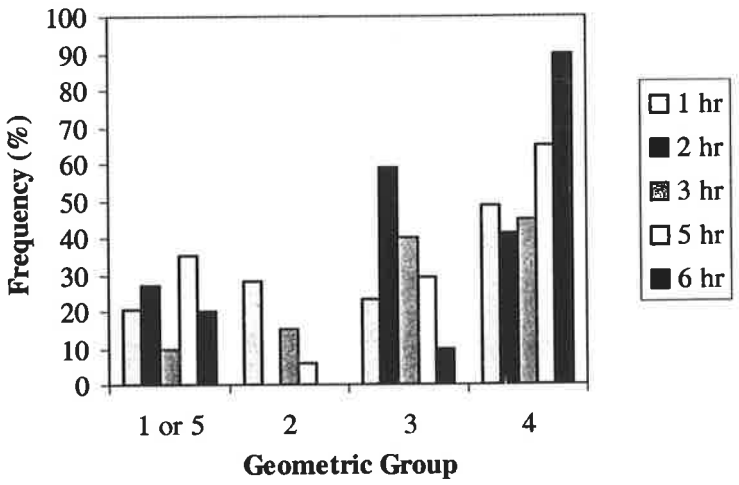

Figure 6.6. Transient change in carrot cell morphology when subject to shearing at 450rpm (ε_{ave} 5.47W/kg)

The change in cell geometric profile is mirrored in the mitochondrial activity, where a sharp decline occurred after 2 hours of shearing (viability < 20%). The maximum

equivalent diameter after 6 hours shearing at 450rpm is approximately 106 μm. However, the Kolmogorov eddy length scale at 450 rpm is approximately 20 μm. This confirms that the more damaging eddies lie in the inertial subrange rather than the viscous subrange.

The accuracy of shear stress calculations is influenced by the aggregate shape factor, as well as fluid flow parameters. If individual cells are approximately equi-sized, then the number of cells on the outer layer of the aggregate is proportional to the square of the aggregate diameter (Illing et al., 1999). This is equivalent to the surface area of the aggregate. The surface area of an object can be related to its cross-sectional area by a shape factor, known as circularity C. This was defined as follows (Billiones et al., 1999):

$$C = \frac{4\pi A}{P^2} \tag{6.2}$$

where A is a cross-section of the object's projected area and P is the perimeter. Hence, C equals to 1 for a circle. A particle with C<1 possesses larger perimeter than a sphere with equivalent projected area. The corollary of this relationship is the inverse proportionality between the perimeter and the square root of circularity;

$$P \propto \frac{1}{\sqrt{C}} \tag{6.3}$$

However, as the surface area of a sphere is proportional to its perimeter and diameter, it follows that the surface area is also inversely proportional to the square root of the circularity. The histogram in Figure 6.7 summarises the variation in circularity of carrot cells. All cell aggregates possess a C<1, indicating greater surface areas than the spherical particles of equivalent cross-sectional areas. The average circularity equals 0.616. These cell particles experience continuous morphological change and size reduction. The most severe case was observed for carrot cells exposed to ε_{ave} of 5.47 W/kg (450rpm) for 6 hours. The circularity of damaged cells is compared with the control samples in Figure 6.8. The average circularity after shear is 0.67. This is a slight 8.5% increase in the average value. However, the histogram indicates that the aggregate break-up shifts preferentially toward more spherical structures. These results confirm that more shear-resistant aggregates are smaller and more spherical. This finding is further supported by evidence

that some plant cells that can survive hydrodynamic shear stress by strengthening their cell walls are more likely to be smaller cells, which are subjected to lower force and require less energy to repair their cell walls (Takeda et al. 1998).

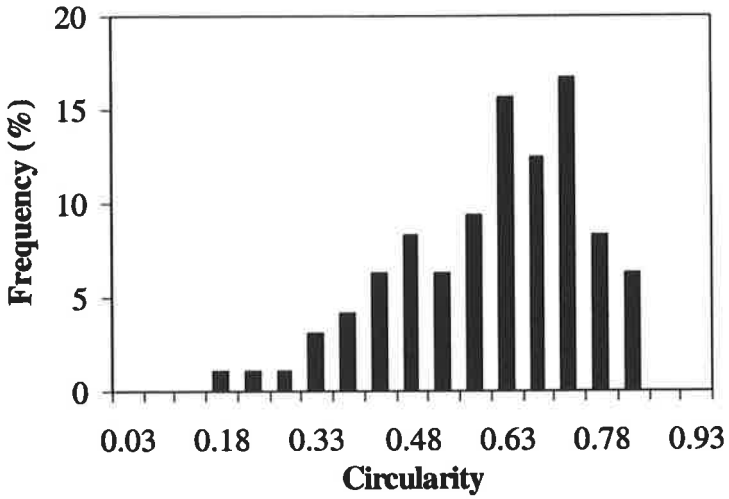

Figure 6.7. Histogram of the circularity of 100 normal carrot cells. The average circularity is 0.616.

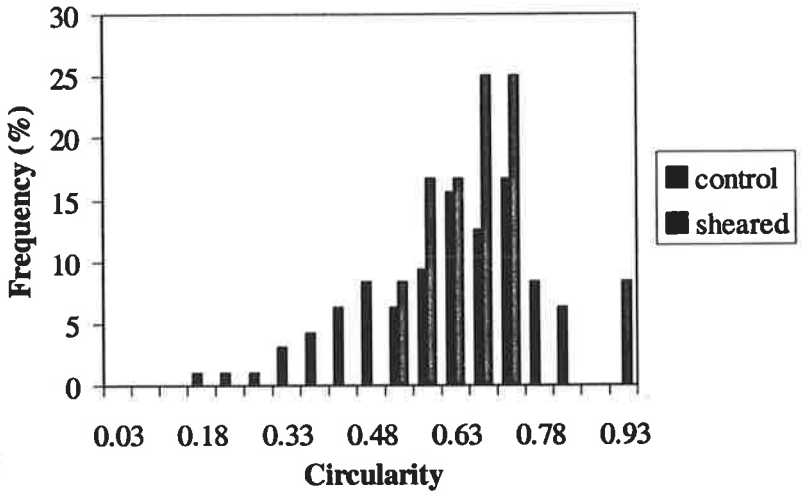

Figure 6.8. Histogram of the circularity of control sample compared with most severe case of shearing, sheared at ε_{ave} 5.47 W/kg for 6 hours. The average circularity is 0.67 and the total number of observation is 100.

6.2. Modification of Shear Stress Model and Calculations of Strain Rates

6.2.1. Theoretical Background

Turbulent flows are composed of large primary eddies typically characterised by a length scale approximately equal to the diameter of the mixing apparatus. This is independent of the model of mechanical power input, such as stirrer, impeller, or bubbles (Caulet et al., 1996). These primary eddies are unstable and decay, thereby transferring their energy to the smaller eddies in an energy cascade. These smaller, energy-containing eddies belong to the inertial and viscous subranges of the turbulent energy spectrum. During each step of energy transfer, the information regarding its directions is gradually lost. In this final stage of decay, the energy transfer is essentially independent of direction. Subsequently, the turbulence becomes isotropic (Papoutsakis, 1991).

Isotropic turbulence is the simplest form of turbulence since it is essentially homogeneous and a minimum number of relationships are required to describe its structure and behaviour. Despite this simplicity, isotropic turbulence is an idealisation, as actual turbulent flows never exhibit true isotropy. However, in many instances, isotropy of the turbulence is closely approached.

Despite the fact that these small eddies contain a relatively small quantity of energy, the continuous regeneration of small eddies from larger ones in turbulent flow causes a continuous energy dissipation to occur. Even though the turbulent flow field is anisotropic, when a very small volume is considered with dimensions much smaller than the fluid system, the fluctuating velocity components are equal. Hence, any small region of fluid, for example, the impeller region in a stirred tank bioreactor, can be considered to be "locally isotropic" (Kawase et al., 1990). It has been shown from theoretical considerations and confirmed by experimental evidence that the fine structure of most anisotropic turbulent flows is nearly isotropic, or locally isotropic. The fundamentals of isotropic turbulence may thus be applied to actual turbulent structures that are determined primarily by fine-scale turbulence (Kawase et al., 1990). At sufficiently high Reynolds numbers, the small-scale fluctuating velocity components in incompressible fluid turbulence are universal and locally isotropic (Nelkin et al., 1990).

Given its comparative simplicity, isotropic turbulence has been widely studied often by the use of correlations and spectrum functions. Although complete solutions for various correlations and spectrum functions are available, approximations can be applied if a few assumptions are made.

Figure 6.9 illustrates a relationship between the dissipated energy per unit mass of fluid and wavenumber, k, which represents the reciprocal of the eddy length scale. At high wavenumbers, the properties of turbulence are independent of the conditions of formation of the eddies. In other words, this region is not affected by the design of the apparatus or the impeller (Papoutsakis, 1991).

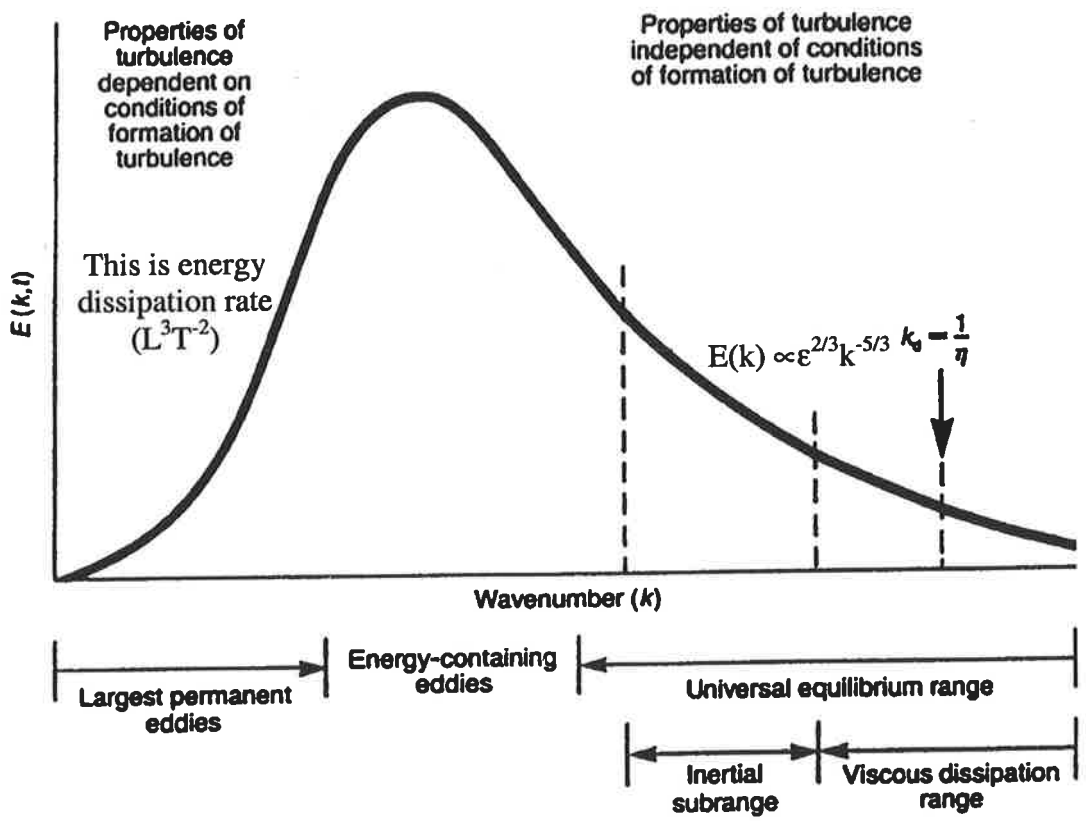

Figure 6.9. The energy spectrum of turbulent eddies as a function of wave number, from Papoutsakis (1991).

The energy containing eddies are smaller in size and belong to the inertial subrange and the viscous range. As eddy size decreases, the extent of energy dissipation by viscous effects increases. The smallest eddies in the energy dissipation range are characterised by a

Kolmogorov scale, η, defined by the local energy dissipation ε_{Local} and the kinematic viscosity ν, as in Equation (6.4) (Kawase et al., 1990; Frisch, 1995).

$$\eta = \left(\frac{\nu^3}{\varepsilon_{Local}} \right)^{1/4} \tag{6.4}$$

At the lower end of wavenumber range or large eddies, the frequency of these eddies is very small compared with the rate of decay of the total kinetic energy. At the higher end of the wavenumber range, the frequencies of the eddy motion are high compared with the relative rate of decay (Hinze, 1959). Hence, eddies in this range are also independent of the external conditions of formation, and can be determined by internal conditions alone. Since these smaller eddies obtain their energy by inertial transfer from larger eddies, it is possible that there is a continuous flux of energy dissipation increases with increasing wavenumber. The amount of energy transferred through eddies is large compared with their energy decay rate, so the eddies are considered in statistical equilibrium with each other. In this range the character of turbulence can be determined by the viscosity and the rate of energy dissipation as stated by Kolmogorov (Hinze, 1959).

A Kolmogorov microscale is essentially the transition between turbulent inertial and viscous regimes. The scale corresponds to when the eddy Reynolds number is equal to one, below which the viscous dissipation predominates and above this scale inertial forces predominate (Hinze, 1959; Kawase et al., 1990; Joshi et al., 1996). The Reynolds number of the Kolmogorov eddy is defined by

$$Re = \frac{\text{inertial}}{\text{viscous}} = \frac{\upsilon_e \eta}{\nu} \tag{6.5}$$

where eddy velocity or the velocity scale is

$$\upsilon_e = \frac{\nu}{\eta} = (\nu\varepsilon)^{1/4} \tag{6.6}$$

Within the inertial subrange, viscous dissipation is unimportant. If the Reynolds number is infinitely large, the energy spectrum in the subrange is independent of the viscosity and is determined only by the rate of energy dissipation per unit mass of fluid ε.

The interaction between particles and eddies depends on the particle characteristics, as well as the fluid flow. Eddies which are very much larger than the particles tend to entrain the particles. Conversely, the eddie smaller than the particles flow over their surfaces. Most interaction with and damage to cell particles is caused by eddies with comparable sizes to the particles (Croughan et al., 1987; Rosenberg, 1989). The typical magnitude of the Kolmogorov scale for eddies in the stirred tank reactor ranges from 25 to 200 μm. However, plant cell aggregates often grow to much larger sizes. Plant cell aggregate size commonly ranges from 100 to 2000 μm (Doran, 1999; Kieran et al., 2000). Hence, plant cells are more susceptible to eddies in the inertial subrange (Illing, 1996).

6.2.2. Maximum Strain Rate and Shear Stress on Cell Aggregates

Growing plant cells requires highly intense mixing due to the large aggregate size of plant cells. These aggregates will settle quite rapidly and require substantial energy to ensure suspension. However, the shear sensitivity problem requires the understanding of how the fluid forces on the cell affect its viability. The turbulent shear stress can be calculated from the correlation (Joshi et al., 1996):

$$\tau_k = \rho(u')^2 \tag{6.7}$$

However, the instantaneous velocity component u' is difficult to find without flow visualisation tools. Other theoretical correlations for u' have been derived using fluid particles interaction. The instantaneous maximum shear stress in the inertial subrange is given by (Matsuo et al., 1981):

$$\tau_i = \rho\left(1.57\varepsilon^{1/3}d_c^{1/3}\right)^2 \tag{6.8}$$

The instantaneous maximum surface stress in the viscous subrange is (Matsuo et al., 1981):

$$\tau_2 = 2\sqrt{\frac{2}{15}}\mu\left(\frac{\varepsilon}{\nu}\right)^{1/2} \tag{6.9}$$

Takeda et al. (1997) have also developed a correlation for turbulent shear stress on the cell, by modelling the cell walls using a Maxwell viscoelastic approximation. The cell-wall deformation rate of aggregates of size d_c by shear stress can be simplified in terms of Reynolds stress, τ_{Re} (Takeda et al., 1997) as:

$$\tau_{Re} = 3.72\rho\varepsilon^{2/3}d_c^{2/3} \tag{6.10}$$

An analysis of time-varying eddy-cell interaction showed that the maximum shear stress on microcarrier cells could be expressed using the correlation (Cherry et al., 1990) as:

$$\tau_{max} = 5.33\rho(\nu\varepsilon)^{1/2} \tag{6.11}$$

These correlations assume that cell particles are spherical, which is inaccurate for plant cells, which normally possess large and irregular shapes. The following section proposes a modification of the time-varying eddy-cell interaction model correcting for the irregularity of the aggregate's surface.

6.2.2.1. Modification of the Shear-Stress Model

The eddy-cell interaction model was developed by Cherry and Kwon (1990) for microcarrier cells. This approach describes the motion of a turbulent eddy and a particle's trajectory within the eddy. The model also assumes that the cells are spherical and the local shear rate in the eddy is constant over a distant comparable to the cell size. Eddies are long rotating cylinders of fluid, which are flexible and can stretch along their axes by bulk-flow motion. The eddy's motion or the stretching causes the fluid to move radially in and around the eddy. The velocities of these eddies in steady-state flow field can be described by Burgers vortex in cylindrical coordinates (Cherry et al., 1990), where

$$v_r = -\frac{1}{2}ar$$

$$v_z = az$$

$$v_\theta = \frac{2v\omega_o}{ar}\left[1-\exp\left(-\frac{ar^2}{4v}\right)\right]$$

The dimensionless radius R is defined by

$$R = \frac{ar^2}{4v} \qquad (6.12)$$

where v_r, v_z and v_θ are the velocity components in cylindrical coordinates, ω_o is vorticity parameter, the v is the kinematic viscosity, r is the eddy radius (m), and a is the strain rate parameter (s^{-1}) which can be calculated from the correlation:

$$a = 0.18\left(\frac{\varepsilon}{v}\right)^{1/2} \qquad (6.13)$$

An expression for local tangential shear rate γ can be estimated as

$$\gamma = \frac{\partial v_r}{\partial r} - \frac{v_\theta}{r} \qquad (6.14)$$

or equivalently $$\gamma = \omega_o\left[-\frac{1}{R}+\left(\frac{1}{R}+1\right)\exp(-R)\right] \qquad (6.15)$$

The local rate of energy dissipation within the eddy can be expressed in terms of the known bioreactor parameters using the following expressions (Cherry et al., 1990)

$$\varepsilon' = 3va^2 + v\left[\frac{v_\theta}{r} - \frac{\partial v_r}{\partial r}\right]^2 \qquad (6.16)$$

The flow field is assumed completely fills up the volume around individual eddy. The average energy dissipation within an eddy, ε is obtained by integrating ε' over the entire cylindrical volume of an eddy of length L;

$$\varepsilon = \frac{\int_0^z \int_0^L \varepsilon' r dr dz}{\int_0^z \int_0^L r dr dz} = \frac{\int_0^{L'} \varepsilon' dR}{\int_0^{L'} dR}$$

$$\varepsilon = 3\nu a^2 + \frac{\nu}{L'} \int_0^{L'} \gamma^2 dR$$

$$\varepsilon = 3\nu \left[0.18 \left(\frac{\varepsilon}{\nu} \right)^{1/2} \right]^2 + \nu \omega_o^2 \left[\frac{1}{L'} \int_0^{L'} \left[-\frac{1}{R} + \left(\frac{1}{R} + 1 \right) \exp(-R) \right]^2 dR \right] \qquad (6.17)$$

where L' is the maximum eddy radius which is of the same dimensionless unit of R. The expression is simplified by integration to

$$\varepsilon = 3\nu \left[0.18 \left(\frac{\varepsilon}{\nu} \right)^{1/2} \right]^2 + \nu \omega_o^2 \left[\frac{1}{L'} \left(\frac{1}{2} - \frac{\exp(-2L')(2(-1+\exp(L'))^2 + L'}{2L'} \right) \right] \qquad (6.18)$$

Rearrangement of the above expression yields an equation for the vorticity parameter, ω_o which can be used to find the shear rate γ.

$$\omega_o^2 = \frac{\varepsilon - 3\nu \left[0.18 \left(\frac{\varepsilon}{\nu} \right)^{1/2} \right]^2}{\nu \left[\frac{1}{L'} \left(\frac{1}{2} - \frac{\exp(-2L')(2(-1+\exp(L'))^2 + L'}{2L'} \right) \right]} \qquad (6.19)$$

Literature values suggest that the size of the smallest turbulent eddies range from 10-15η μm (Townsend, 1951; Cherry et al., 1990). The average diameter of carrot cells is 112.8 μm, and their size distribution ranges from 3-300μm, which corresponds to approximately 0.1-15η. Consequently, plant cell aggregates, which are smaller than 10η may not be severely affected by the turbulent eddies.

Other investigators suggest that the inertial-subrange eddies 12η in diameter are most active in the role of energy dissipation (Cherry et al., 1990). Plant cells are more likely to be damaged by the eddy in the inertial subrange, where the eddy sizes are comparable with cell diameters. Tomi et al. (1978) developed a criterion, which numerically determines whether an aggregate is predominantly influenced by inertial or viscous forces. This criterion R_d' is defined by the ratio of the inertial pressure fluctuation across an aggregate over the viscous pressure fluctuation, which is given by (Tomi et al., 1978):

$$R_d' = 2.7\varepsilon^{1/6} d^{2/3} \nu^{-1/2} \tag{6.20}$$

The inertial force dominates for $R_d' \geq 1$, and viscous force dominates when $R_d' \leq 1$. For the shearing apparatus described in Chapter 3, carrot cells of average diameter of 112.8 μm exposed to the average energy dissipation rate of 2.15 W/kg (300rpm) results in $R'_d = 7.16$. The values of R_d' is much greater than one, which confirms that the more damaging eddies are in the inertial subrange.

Maximum shear rate in the eddy occurs at R = 1.793 (Cherry et al., 1990), which corresponds to the eddy radius of 6.3η;

$$R = \frac{ar^2}{4\nu} = \frac{0.18\left(\varepsilon/\nu\right)^{1/2} r^2}{4\nu} \tag{6.12}$$

$$R = 1.793 = 0.045\frac{r^2}{\eta}$$

$$r = 6.3\left(\frac{\nu^3}{\varepsilon}\right)^{1/4} = 6.3\eta$$

Eddies in this size range will not affect particles that are smaller than 12.6η in diameter. Therefore, for cell diameter $d \geq 12.6\eta$, the maximum shear rate can be estimated at R = 1.793. However, for cell with diameter $d < 12.6\eta$, the corresponding shear rate can be estimated using $R = \frac{ar^2}{4v}$, where r equals the particle radius.

The analysis of the surface shear stress on a spherical microcarrier by Cherry and Kwon (1990) yields a simplified expression for shear stress τ;

$$\tau = \frac{5}{2}\mu\gamma\left|\cos(\gamma t)\right| \tag{6.21}$$

The maximum shear rate occurs at $\left|\cos(\gamma.t)\right| = 1$. Figure 6.10 shows the calculated results for maximum surface shear stress on spherical particles. The surface shear stress was calculated from the local energy dissipation rates from the correlation described in Chapter 4. Table 6.2 summarises both local and average energy dissipation rate at different operating speeds. The local energy dissipation rates were calculated from equation (4.7). The surface shear stress is approximately constant for cell diameter range up to 230 μm, and increases linearly with increasing cell size.

Table 6.2: Local and average energy dissipation rate at different speeds.

Speed (rpm)	Average energy dissipation rate (W/kg)	Local energy dissipation rate (W/kg)
300	2.15	19.8
400	4.56	25.4
450	5.47	27.5

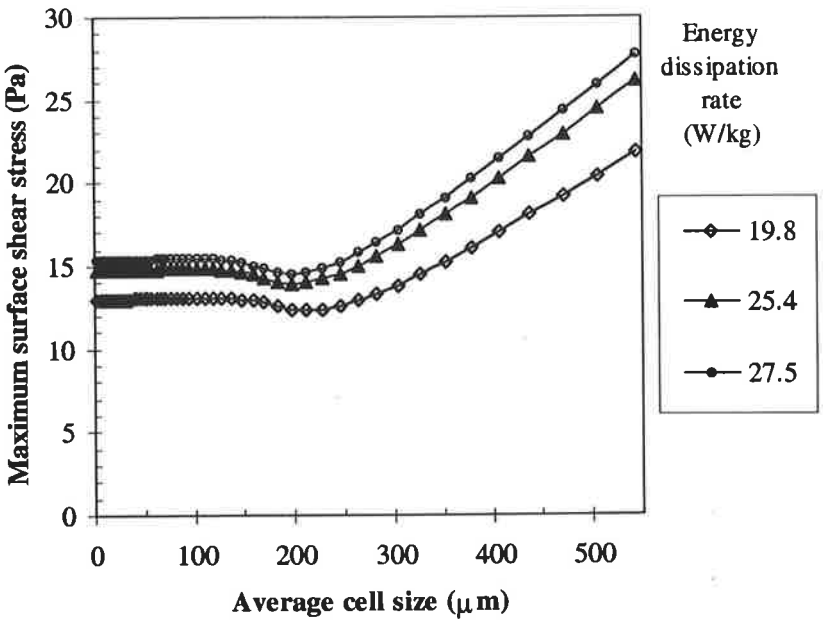

Figure 6.10. Maximum surface shear stress on different cell sizes. Cell particle diameters are assumed to be spherical.

The model for surface shear stress is further modified by an addition of the circularity term to account for an increase in exposed cell surface from their irregular shapes. Plant cells usually have large ratio between individual cell and aggregate sizes. It was suggested that the number of cells in the outer layer of the aggregate exposing to hydrodynamic forces is proportional to D_{agg}^2/d^2 (Illing et al., 1999). If individual cells are approximately equal in size then the number of exposed particles on an aggregate only depends on D^2_{agg}, which is proportional to the surface area.

The degree of damage is proportional to the number of cells exposed to the surface shear stress τ_s;

$$\tau_s \propto \text{aggregate surface area exposed to shear stress}$$

Hence, from the analysis in section 6.1 and equation (6.3)

$$\tau_s \propto \frac{1}{\sqrt{C}} \qquad (6.22)$$

For a spherical particle, the surface shear stress remains the same. However, shear stress increases for particle with larger exposed surface area. Figure 6.11 compares the values of τ_s with and without the surface area correction. The correction factor shifts the value of τ_s by 9-25% for cell particle > 230μm, but the difference is very small for cell diameter < 230μm. The values of τ_s at different local energy dissipation rates are shown in Figure 6.12.

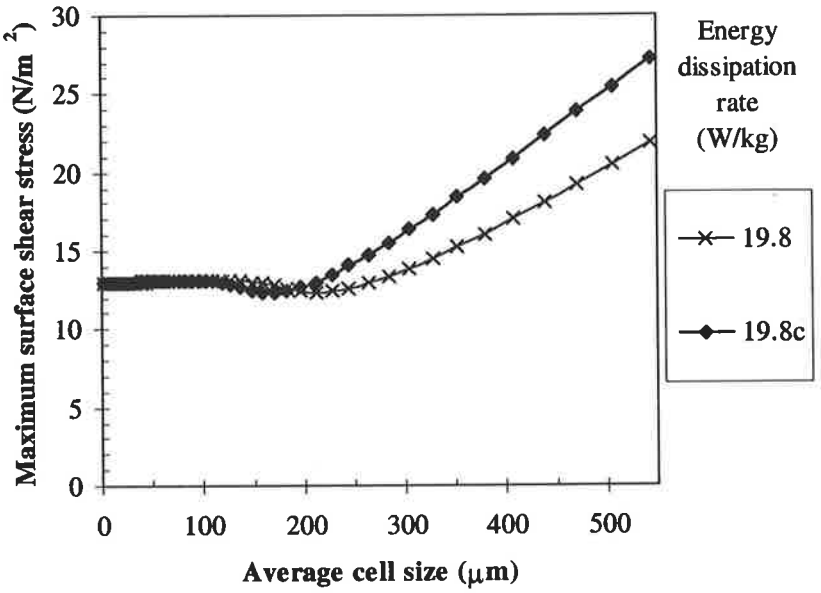

Figure 6.11. Comparison of maximum surface shear stress calculated with and without surface area correction at 300rpm. Letter c denotes shear stress with surface area correction.

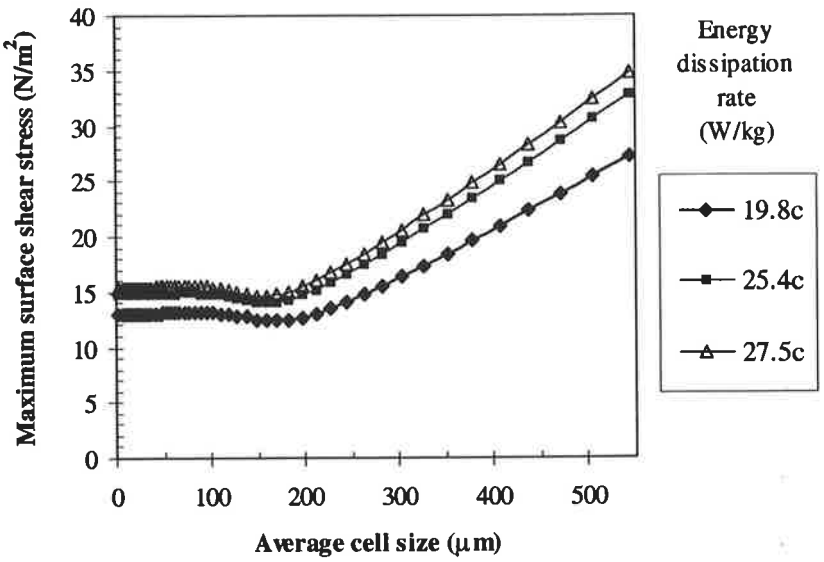

Figure 6.12. Maximum surface shear stress on different cell sizes. Cell particle diameters are corrected by perimeter based fractal dimension. Letter c denotes shear stress with surface area correction.

6.2.2.2. The Effects of Surface Stress on Stretch-Activated Calcium Channels

Plant cells perceive mechanical stress through a range of physiological mechanisms. The first step is usually through cell wall or the plasma membrane, which contains several stretch-activated (SA) ion channels, especially Ca^{2+} channels. It has been hypothesised that mechanical stimuli can activate these SA channels via the cytoskeletal network (Sackin, 1995). Cellular responses to mechanical stimuli differ for different cells due to variation in cell shapes.

Unfortunately, little is known about the mechanism involved in cytoplasmic $[Ca^{2+}]$ and the stretch-activated calcium channels in plant cells. A direct relationship between mechanical stimulation of cell membrane and the opening of stretch-activated calcium ion channels has been observed in various mammalian cell types (Stockbridge et al., 1988; Davidson, 1993). Human gingival fibroblasts showed no calcium response with a 1% mechanical stretch, but 2.8% stretch induced a transient calcium ion response (Arora et al., 1994). On the other

hand, 2% stretch was sufficient to open a calcium channel in embryonic chick skeletal muscle cells (Guharay et al., 1984). The amplitude of calcium ion responses to mechanical stretch differs for different cells as a consequence of the variations in cell shapes and cytoskeletal network. An increase in surface area between 2-2.8% corresponds to the critical strain rate for opening of the channels of approximately 1.4-1.7%.s^{-1}.

The degree of membrane stretching in plant cells is equivalent to the rate of membrane deformation. The relationship between deformation rate and turbulent shear stress can be calculated from (Takeda et al., 1998):

$$\mu_c \frac{de}{dt} = \tau_t \left(\frac{\theta_M}{\theta} + 1 \right) \tag{6.23}$$

where θ_M is the relaxation time of cell surface, θ is the time scale of turbulence fluctuation and τ_t is the turbulence shear stress. The turbulence shear stress is described by the surface shear stress previously calculated.

The cell volumetric elastic modulus for tobacco suspension cells ranges from 0.2-5.4 MPa (Dracup et al., 1986), compared to 2.0-5.0 MPa for *Chenopodium rubrum* suspension cells (Büchner et al., 1981). Others have reported the plant cell elastic modulus of 0.1-0.6 MPa (Rygol et al., 1983) and 0.19-4.6 MPa with an average of 1.38 MPa (Murphy et al., 1998). The values of elastic modulus vary with the turgor pressure of individual cells. Evidence also suggested that cell wall strength of plant cell could increase with increased exposure to hydrodynamic shear stress (Tanaka et al., 1988). Therefore, their elasticity modulus may alter during the course of shearing, resulting in variable strain rate.

The relaxation time of plant cell surface also differs for various cell lines and types. Nishitani and Masuda (1981) reported a relaxation time of 19.5 ms for the cell wall of azuki bean epicotyl. Others have reported relaxation time of 16.2ms for oat cell wall (Yamamoto et al., 1971) and 15.3ms for pea epidermal tissue (Masuda, 1978).

For simplification of the modelling, the elastic modulus is assumed to be approximately 1MPa, and the average relaxation time is 17ms. These values are summarised in Table 6.3.

Table 6.3: Estimated properties of cell wall for the calculations of surface shear stresses

Property	Average Value	References
Surface viscosity, E	1MPa	(Dracup et al., 1986) (Rygol et al., 1983) (Murphy et al., 1998)
Relaxation time, θ_M	17 ms	(Yamamoto et al., 1971; Masuda, 1978; Nishitani et al., 1981)

The strain rate is directly related to the surface shear stress. Figure 6.13 represents variation in strain rate at different cell sizes. For d < 230μm, the strain rate is approximately constant at 5.9, 7.5 and 8.2%.s^{-1} for 300, 400, and 450rpm respectively. The strain rate rapidly increases when cell diameter exceeds 230 μm. The maximum strain rate of 12.4, 16.8, and 18.5%.s^{-1} is obtained for ε_{local} of 19.8, 25.4, and 27.5 W/kg respectively. These strain rates are an order of magnitude greater than the stretching which opened mammalian SA ion channels (Guharay and Sachs, 1984). Hence, they are possibly sufficient to trigger an opening of stretch-activated ion channels in plant cells.

Furthermore, the majority of the pre-screened cells are less than 230 μm in diameter, indicating that they are subject to constant strain rate. Only 3% of the cells are larger than 230μm. After 1 hour at ε_{local} of 25.4 W/kg, the mitochondrial activity dropped to 70%. In such a short exposure time, the reduction in mitochondrial activity was possibly due to the damages on larger aggregates.

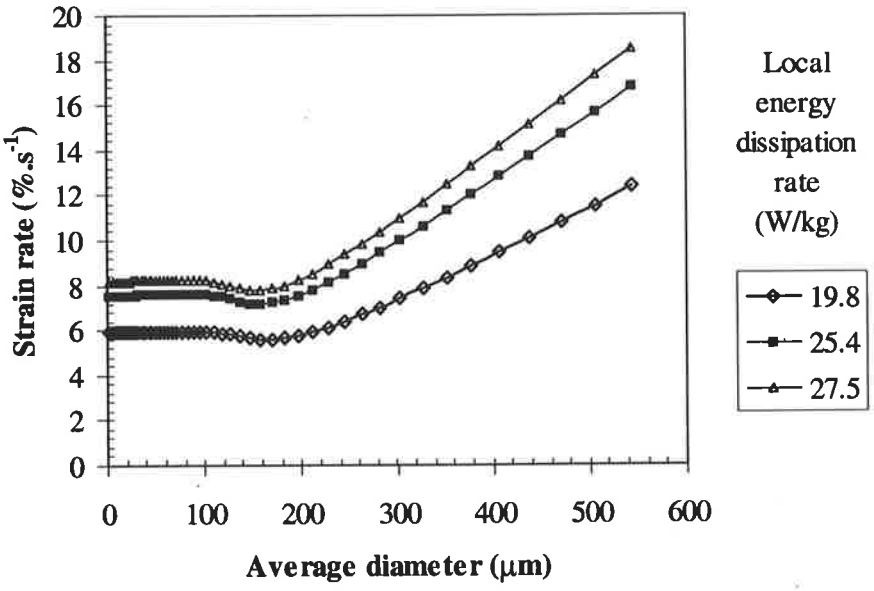

Figure 6.13. Variation of strain rate with cell diameter at different energy dissipation rates.

It was shown in Chapter 5 that the disruption of cell metabolism is a cumulative exponential decay function of energy dissipation rate. The results obtained for strain rate confirm this relationship. Figure 6.14 illustrates the exponential relationship between mitochondrial activity and strain rate. Figure 6.15 illustrates the slopes of the relationships in Figure 6.14. The slopes represent the changes of decay rate of mitochondrial activity with time. The rate of decay accelerates more rapidly with exposure time. The dimensionless cumulative straining of the cell surface in Figure 6.16 demonstrates a linear relationship with maximum cell diameter. This relationship implies that aggregate morphology is affected by the magnitude of the strain. For a fixed cumulative strain, there is a critical size range, which are more shear-resistant. Larger aggregates can endure only slight cell surface deformation compared with smaller aggregates.

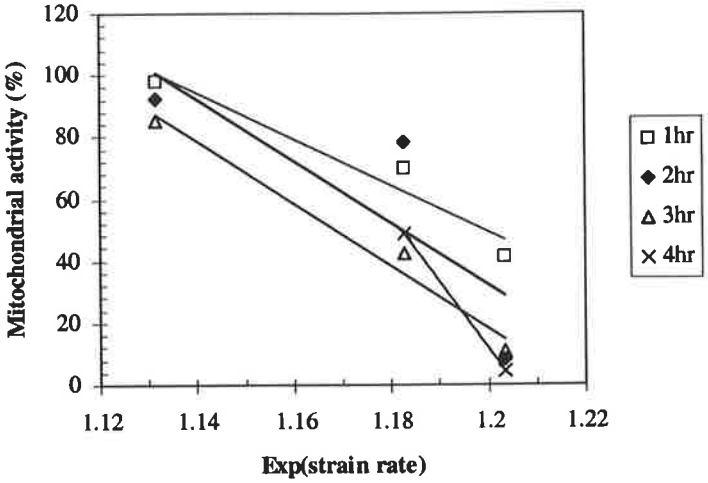

Figure 6.14. Exponential relationship between the relative mitochondrial activity and strain rate.

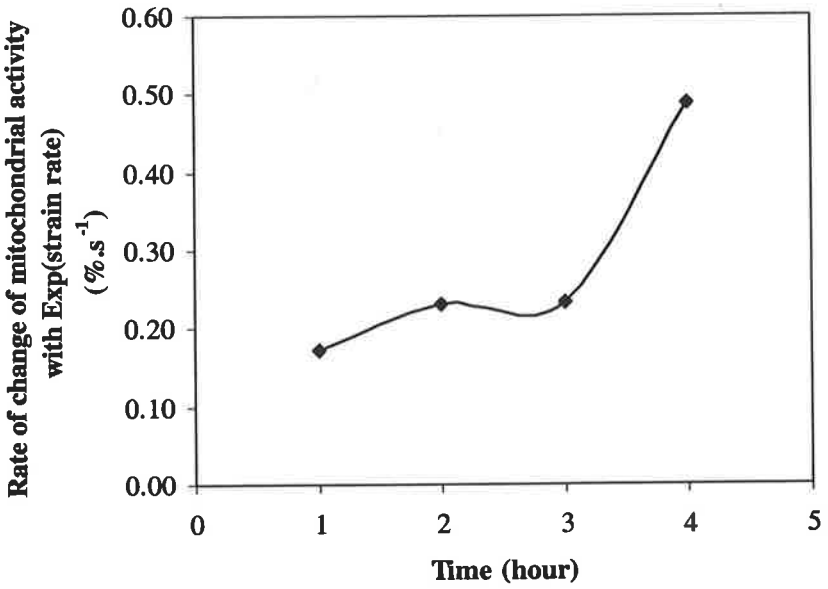

Figure 6.15. The change of the relative mitochondrial activity with strain rate increases more rapidly with time.

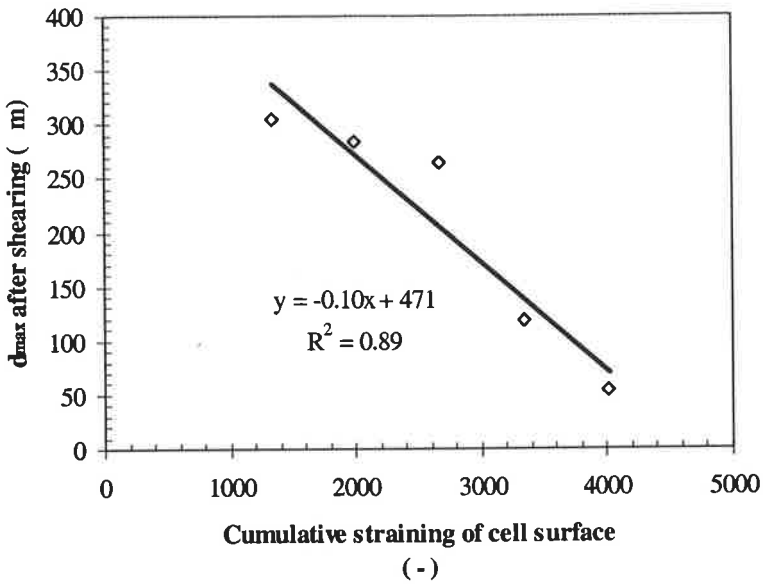

Figure 6.16. Linear relationship between maximum cell diameter and the cumulative surface strain. The values are for cells exposed to 450rpm at 5 different times. The dimensionless cumulative cell surface strain is a product of the exposure time (s) and maximum strain rate (s^{-1}). The solid line represents the linear regression of the data, where y is d_{max} and x is the cumulative straining of cell surface.

6.3. Conclusions

Studies of plant cell morphology showed that they exhibited different types of geometry. Fractal characterisations of the cells confirmed that their morphology is more complex than that of spherical particles. Irregularity of cell aggregates results in uneven exposure of individual cells in an aggregate to hydrodynamic shear stress. Mathematical models (Cherry et al., 1990; Takeda et al., 1998) were modified to describe the surface shear stress and strain rate on irregular cell particle using the circularity shape factor. The number of cells exposed to shear stress is proportional to the surface area of the aggregate, which depends on its circularity.

The results confirmed that larger aggregates are usually more irregular in shape, resulting in larger exposed cell surface. Hence, they experience higher surface shear stress and

strain, and more damage. Evidence also supported that large aggregates break down preferentially to form smaller, more shear-resistant aggregates.

The strain rate profiles indicated that the degree of stretching was sufficient to trigger the opening of stretch-activated Ca^{2+} channels. The mitochondrial activity decreased exponentially with increasing strain rate, confirming a cumulative biological response to mechanical straining. A linear dependence of maximum cell size on the cumulative strain also suggested the influence of aggregate size on the cell metabolic processes in combating stress signals. Nevertheless, it remains uncertain how plant cells perceive this mechanical insult. Next chapter will propose a simplified Ca^{2+} regulatory process and its involvement in the damage mechanisms, which can result in cell death.

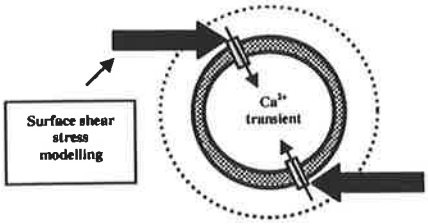

CHAPTER 7

MODELLING THE ROLE OF CALCIUM IN SHEAR DAMAGE AND DEATH

In the previous chapter, the predicted surface shear stress on cell aggregates suggested that the membrane stretching caused by the turbulent shear stress was sufficient to force the opening of stretch-activated calcium channels. It is known that the entry of excessive amount of extracellular calcium can trigger a range of sublytic responses. The understanding of Ca^{2+} transients in plant cells is essential in the study of their responses to hydrodynamic shear stress. This chapter is dedicated to the development of a kinetic model, which describes the effects of mechanical shear stress on intracellular calcium. The model is based on the fundamental species balances, including the Ca^{2+} regulatory functions of the mitochondria, endoplasmic reticulum and vacuole. The first section of this chapter provides the background information on the mitochondrial function and the role of calcium in cell damage and death processes. Several characteristic changes in Ca^{2+} concentration leading to the eventual cell death will be discussed. The latter section of this chapter presents the development of a mathematical model describing Ca^{2+} transients in the cells using existing data. This model introduces a novel approach in kinetic modelling by combining various fundamental engineering principles, including mass balances, linearisation of complex differential equations, and process control optimisation.

7.1. Introduction

Calcium is one of the essential signalling processes in all living systems. Calcium transients play an important role in sublytic responses of plant cells to hydrodynamic shear

stress. The role of Ca^{2+} remains critical and continues until the moment of cell death. Numerous studies have recognised the importance of Ca^{2+} signalling in metabolism, and have attempted to improve the understanding of its dynamics through measurement of intracellular Ca^{2+}. Several techniques are available for measurement of calcium concentration in cells, for examples, the Ca^{2+}-selective microelectrodes, radiotracer $^{45}Ca^{2+}$, and luminescent photo-protein aequorin (Read et al., 1993; Knight et al., 1996; Blatt, 1999). Recently, the direct measurement of intracellular $[Ca^{2+}]$ using fluorescence dyes has been successfully applied in mammalian cells. The technique involves loading a fluorescent Ca^{2+} indicator into the cell. The indicators bind with Ca^{2+} to form fluorescent compounds which are visible under a fluorescent microscope at different excitation wavelengths. The intensity of the fluorescence can be converted into the corresponding calcium ion concentration using the calibration parameters from fluorescence intensity obtained at various known calcium concentrations.

Despite the growing success of Ca^{2+} measurement in plant tissues and organs, there are still some inherent difficulties associated with measuring Ca^{2+} in intact single plant cells. Loading dye into plant cells is an extremely difficult task. It requires complete isolation of plant cells, or even a complete removal of the cell wall (Timmers et al., 1991; Read et al., 1993). Insufficient dye uptake by plant cells normally results from extracellular ester hydrolysis and incomplete internal dye hydrolysis (Williams et al., 1990). Consequently, it is necessary to use more invasive loading approaches, for examples, electroporation, acid loading, microinjection, or even using recombinant photo-proteins (Timmers et al., 1991; Read et al., 1993; Haley et al., 1995). These invasive techniques can potentially disrupt the cell's ability to regulate Ca^{2+} level and result in temporary loss of membrane function (Gilroy et al., 1986; Williams et al., 1990; Timmers et al., 1991). Cells sometimes remain viable after loading but cease to function normally (Read et al., 1992). Additionally, the procedure sometimes requires long incubation time (1-2 hours) and the measurement of calcium must be completed within a short period (< 1 hour) (Timmers et al., 1991; Read et al., 1992). Immobilisation of the cells is normally essential (Timmers et al., 1991). Hence, these current Ca^{2+} measurement techniques are considered impractical for on-line shear-sensitivity studies.

Substantial variation in the measurement of $[Ca^{2+}]_{cyt}$ has also been reported in plant cells. The resting level of $[Ca^{2+}]_{cyt}$ measured with luminescent proteins aequorin is

approximately 40nM, whilst the fluorescent dyes detect 150-200nM (Malhó et al., 1998). Furthermore, evidence has confirmed that $[Ca^{2+}]$ is not uniform in plant cells. Read et al. (1993) reported that $[Ca^{2+}]_{cyt}$ elevations are localised within different parts of the cytosol. Sequestration of Ca^{2+} dye into the organelles can prevent precise measurement of cytosolic Ca^{2+}(Read et al., 1992). Hence, accurate measurement of calcium transient remains difficult, particularly in plant cells suspended in complex flow conditions.

Current modelling of Ca^{2+} kinetics in plant cells remains confined to measurement of cells subject to stimuli, for example, wind, touch, temperature, and fungal infection. Unfortunately, there are problems associated with the lack of data for calcium kinetics in plant cells suspended in a hydrodynamic shear field. However, the data are more widely reported for mammalian cells, such as endothelial cells, as they are easier to measure and to immobilise. In addition, these cells are normally subject to relatively mild shear flow conditions (Schwarz et al., 1992; Shen et al., 1992; Malek et al., 1996; Wiesner et al., 1996). Nevertheless, researchers have recognised the need to introduce modelling to predict the experimental observations. Several models have been developed to estimate Ca^{2+} transients in endothelial cell responses to fluid flow (Wiesner et al., 1996). These were based on various complex reaction systems involving several proteins. However, plant cells models have not generated the same level of interest, primarily due to the lack of data. Consequently, the proposed model is intended as a first step of mathematically describing the effects of flow on intracellular Ca^{2+}. It is intended to demonstrate how a complex biological process can be simplified using a conventional control modelling approach. The calculations were based on calcium balances in a cell, consisting of the mitochondria, the vacuole, and the endoplasmic reticulum. The final solution was obtained from a Laplace transform approximation to the linearised calcium mass balances. This simple model is a valuable tool in bridging the understanding on the influence of shear stress on the complicated cellular Ca^{2+} processes. Further enhancement of the model to improve its predictive ability can be achieved by integrating other mechanisms that have a role in the cellular responses.

It has been suggested that mitochondria play an essential role in regulating calcium concentration in the cytoplasm (Boitier et al., 1999). Elevated levels of calcium ion in cellular response have been implicated in the mitochondrial dysfunction and consequential

cell death (Campbell, 1985). The next section summarises the roles of mitochondria in calcium regulation and their involvement in the events leading to cell death.

7.2. Role of Mitochondria

In a normal plant cell, approximately 90% of intracellular calcium ions (Ca^{2+}) are stored in organelles, for example the endoplasmic reticulum (ER), vacuole, and mitochondria (Campbell, 1985). The concentration of Ca^{2+} in these organelles is several magnitudes higher than that in the cytoplasm. Consequently, large concentration gradient exists across their semi-permeable membranes, which prevent the flow of calcium ions back to the cytosol. These intracellular organelles, particularly the mitochondria, play a crucial role in regulating the cytosolic $[Ca^{2+}]$.

The cytosolic free calcium $[Ca^{2+}]_{cyt}$ varies between 0.1-0.2μM in a cell at rest to 0.5-3 μM in an activated cell subject to extracellular signals (Alberts et al., 1994; Rizzuto et al., 2000). When the cell is damaged beyond repair, it cannot efficiently pump Ca^{2+} out of the cytosol and the level of cytosolic Ca^{2+} can rise to a dangerous level above 10 μM (Alberts et al., 1994). For a small rise in $[Ca^{2+}]$, the ions are pumped out of the cytosol into the endoplasmic reticulum. When the level of cytosolic Ca^{2+} becomes extremely high, the high capacity Ca^{2+} pump in the inner mitochondrial membrane is activated by an electrochemical gradient across the membrane.

Upon an increase of cytosolic $[Ca^{2+}]$, the mitochondria rapidly acquires sufficient amount of Ca^{2+} to increase the rate of metabolism. In a resting cell, a steady state exists between the uptake and efflux of Ca^{2+} by mitochondria. When the $[Ca^{2+}]_{cyt}$ increases, the mitochondria rapidly takes up Ca^{2+} until a new steady-state is reached. This steady-state is also called a balance point, where the uptake of Ca^{2+} equals the release. The balance point in an isolated mitochondrion is around 0.3-0.5 μM free Ca^{2+} (Campbell, 1985). The Ca^{2+} concentration profile in Figure 7.1 illustrates the regulation of cytosolic Ca^{2+} by the mitochondria.

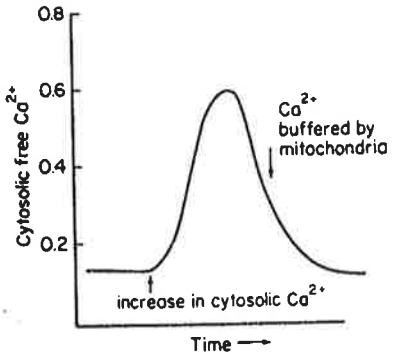

Figure 7.1. Response of mitochondria to an increase in cytosolic Ca^{2+} (Campbell, 1985)

In addition to regulation of cytoplasmic Ca^{2+}, the mitochondria also maintain other significant metabolic processes, for example, they supply 95% of the energy consumed by the cell by oxidative phosphorylation (Gunter et al., 2000) and they are responsible for the majority of ATP production (Alberts et al., 1994). The intra-mitochondrial calcium ions activate a number of processes in the Krebs cycles, including the electron-transport chains. Hence, they control the cell metabolic rates (Gunter et al., 2000). A respiring mitochondrion normally contains 0.25-1.0 μM of Ca^{2+} (Campbell, 1985).

The two mechanisms by which Ca^{2+} is transported into mitochondria involve the electrochemical gradient transport (uniporter) and the rapid mode. The rapid uptake mode is at least hundreds times faster than the uniporter (Gunter et al., 2000). These processes were found to be inhibited by ruthenium red, but the precise kinetics of these processes remains to be explored further (Gunter et al., 2000). A pulse increase in cytosolic Ca^{2+} can activate the rapid mode uptake (RaM) of mitochondria, which can range from 100 to 200nM in 0.75s (Rizzuto et al., 2000). The kinetics of the uptake rate by the uniporter can vary from hyperbolic to sigmoidal behaviour (Rizzuto et al., 2000).

The Ca^{2+} efflux from the mitochondria back to the cytosol follows two different ion-exchange pathways. These are either the Na^+/Ca^{2+} or H^+/Ca^{2+} exchanger, which trades Ca^{2+} for either Na^+ or H^+, and the efflux of Ca^{2+} through the permeability transition pore (Gunter et al., 2000). The Ca^{2+} efflux across the mitochondrial membrane requires energy due to the large internal negative membrane potential (Gunter et al., 2000). Approximately 33 kJ are rquired to remove 1 mole of Ca^{2+} from the mitochondria matrix space to the intermembrane space. This is comparable to the energy obtained from ATP hydrolysis with

a standard state free energy of 34.1 kJ mol^{-1}. In a normal cell, sufficient energy is supplied by a combination of substrate oxidation, ion gradient potentials, and ATP hydrolysis (Alberts et al., 1994; Gunter et al., 2000).

However, when the cell is injured, these membrane ion-transport systems may fail, and additional energy will be required to conduct the ion transports. Without the ion-gradient transports, the cell requires ATP to directly remove the excess Ca^{2+} out of the cytoplasm. The additional energy requirement will subsequently increase the oxygen requirement of the cell, as one oxygen molecule can only produce six ATP in the mitochondria (Campbell, 1985). An increase in oxygen uptake rate (OUR) has been observed in carrot cells following exposure to laminar shear, indicating that under hydrodynamic stresses, cells require additional energy to combat the stress signal, particularly the removal of excess cytoplasmic free Ca^{2+}. Failure of the mitochondria to supply sufficient amount of ATP during the healing process can lead to an onset of cell death, such as apoptosis and necrosis.

The calcium ion has often been implicated in cell death. A Ca^{2+} overload of the mitochondria has been shown to be involved in cell death processes and a large flux of Ca^{2+} induced by excitotoxicity has been linked to mitochondrial overload and cell damage (Smaili et al., 2000). Such overloading results in mitochondrial dysfunction and loss of ATP production. The amount of ATP produced in mitochondria depends on the electrochemical gradient energy utilised by Ca^{2+}-related reactions (Alberts et al., 1994). When the mitochondrial Ca^{2+} uptake exceeds a set point, the permeability transition pores in the mitochondria are impaired. This leads to a collapse of membrane potential with the ultimate consequence of failure to regulate ions. Consequently, the cells experience abnormal ATP synthesis, mitochondrial dysfunction, and finally, cell death (Gunter et al., 2000).

Several studies demonstrated that cell death signals during apoptosis and necrosis may be related to an increase in $[Ca^{2+}]_{cyt}$ (Trump et al., 1981; Wyllie, 1981; Campbell, 1985). Prolonged elevation of $[Ca^{2+}]_{cyt}$ may trigger a collapse in mitochondrial membrane potential, and the loss of mitochondrial membrane potential could be involved in the release of an apoptosis-inducing factor, as well as induction of necrotic death (Trump et al., 1981; Campbell, 1985; Smaili et al., 2000).

7.3. Cell Death: Apoptosis or Necrosis?

When a cell is subject to severe external insults, the two distinct types of cell death mechanisms could occur. These mechanisms are known as apoptosis and necrosis. Apoptosis is a rapid and deliberate gene-directed cellular self-destruction. On the other hand, necrosis is a degenerative but accidental event. It usually results from severe injuries caused by changes in environment (Kerr et al., 1991).

Under certain circumstances, the distinction between apoptosis and necrosis may not be apparent. A mild stress injury may lead to both apoptosis and necrosis. Some cells can produce toxins, which cause necrosis, as well as enhancing apoptosis (Kerr et al., 1991). However, an influx of Ca^{2+}, which is sufficient to trigger deliberate apoptosis, may not be sufficient to activate necrosis (Kerr et al., 1991).

Apoptosis is a progressive death. It is accompanied by contraction of cytoplasmic volume associated with loss of intracellular fluid (Wyllie, 1981), consequently, the organelles become more densely compacted in the cells. Usually apoptotic processes are results of induction of apoptotic gene expressions by the cells (Wyllie, 1981).

On the contrary, necrosis is a more gradual process. It develops more slowly by inhibition of oxidative phosphorylation of mitochondria followed by severe mitochondrial swelling, cytoskeletal alteration, rupture of plasma membrane and loss of recognisable organelles (Wyllie, 1981). At the commencement of necrosis, membrane injury may result from premature loss of the energy supply. Once the membrane is damaged, further injury inflicted on the mitochondria will remove the source of oxidative metabolism, and impede recovery of membrane-ion pumping activity, which regulates ion concentrations such as Ca^{2+}. A decrease in ATP concentration is a direct result of mitochondrial dysfunction. When the mitochondria cease to function, ATP contents becomes extremely low, and consequently, all energy-required systems fail to function (Wyllie, 1981).

Table 7.1: Characteristics of apoptosis and necrosis (Wyllie, 1981; Lockshin et al., 1991)

Characteristic	Apoptosis	Necrosis
morphology	cell shrinkage, fragmentation, condensation	eventual cell lysis
membrane integrity	persists till late	early failure
mitochondria	no effect	cell swelling Ca^{2+} overloading
ATP content	decreases in some cells	decreases

The primary difference between apoptosis and necrosis are summarised in Table 7.1. Unfortunately, the distinction between necrosis and apoptosis can sometimes be unclear. While the damage to mitochondrial functions is characteristic in necrotic bodies, Crompton (2000) reported a change in mitochondrial membrane following apoptosis by oxidative stress. Loss in membrane potential is also detected during the last phase of apoptosis. Consequently, some confusion remains over which damage mechanism prevails in cells exposed to hydrodynamic stress. Cowger et al. (1999) reported both necrotic and apoptotic death in insect cells grown in rotating vessels. Similarly, Singh et al. (1994) found that hybridoma and plasmacytoma cells exhibit signs of necrosis and apoptosis. Plant cells, like insect and animal cells, have been found to experience both apoptosis and necrosis, depending on the stress environment (LoSchiavo et al., 2000). Arabidopsis and carrot cell cultures experienced apoptotic death under oxidative stress (McCabe et al., 1997; Desikan et al., 1998); however, carrot cells subject to heat shock experienced death by necrosis (LoSchiavo et al., 2000).

Cells damaged by hydrodynamic shear fields exhibit several of the characteristic signs associated with necrotic bodies, such as reduced mitochondrial activity, decreased NAD(P)H level, abnormal increase in Ca^{2+}, reduced F-actin filaments contents, and cell

lysis (Dunlop et al., 1994; Takeda et al., 1998). A decrease in ATP content was also observed in eucalyptus and safflower cells in stirred tank studies (Takeda et al., 1998). The reduced ATP content indicates that additional energy is required for the injured cells to combat stress.

The change in mitochondrial [Ca^{2+}] during necrosis can be divided into two phases illustrated in Figure 7.2. The early phase occurs when [Ca^{2+}] increases 2-3 fold, resulting in $[Ca^{2+}]_{cyt}$ of approximately 10μM and a large uptake by mitochondria (Campbell, 1985). The damage occurring in this phase is usually reversible. If the accumulation of Ca^{2+} is sustained for longer than 30-60 min then mitochondria can experience irreversible damage and structural injury (Campbell, 1985). This will result in decrease in cell ATP, with values dropping to 5% of that in normal cell, causing severe cellular malfunctions. The chemical changes and their time course associated with cell death are summarised in Table 7.2, and a partial mechanism of necrosis is summarised in Figure 7.3.

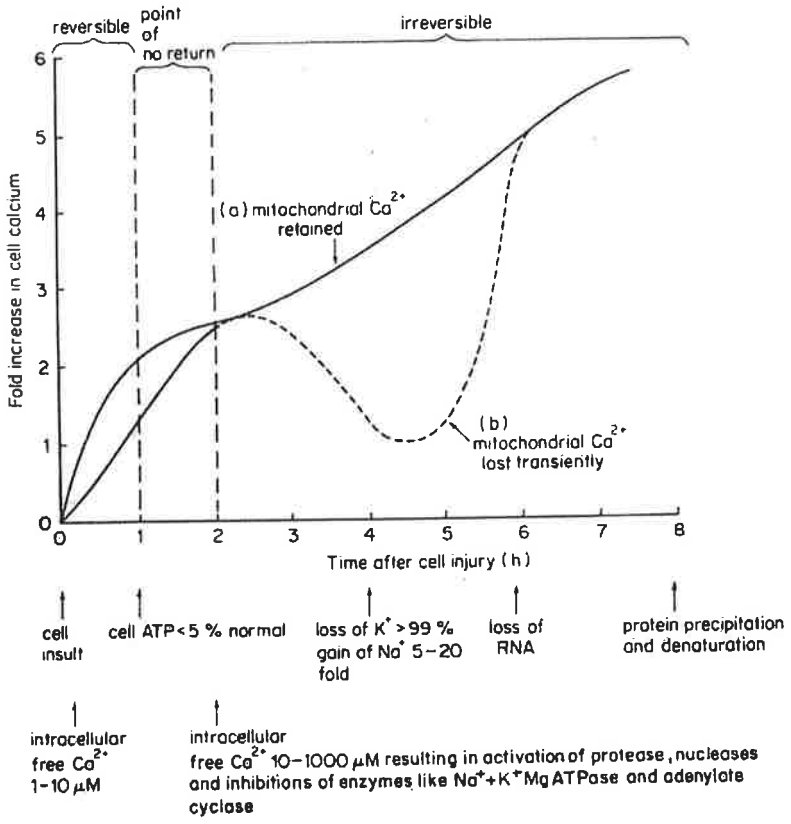

Figure 7.2. Biphasic changes in mitochondrial Ca^{2+} in necrosis, adapted from Campbell (1985).

Table 7.2: Chemical changes and the approximate time course in necrotic cells (Campbell, 1985)

Chemical Change	Approximate time after cell insult
Reversible changes	
1. Initial insult	0
2. Increase in cytosolic free Ca^{2+}	seconds-minutes
3. Loading of mitochondria with Ca^{2+}	minutes
4. Decrease in ATP, increase in ADP, AMP and adenosine	seconds-minutes
5. Activation of glycogen phosphorylase	minutes
6. Increase in intracellular Na^{+}, decrease in intracellular K^{+}, loss of membrane potential	minutes
Irreversible changes	
1. Irreversible damage to mitochondria	10-30 min
2. Cell swelling due to water uptake	30-60 min
3. Complete loss of intracellular K^{+} and membrane potential	30 min - 6 hours
4. Leakage of soluble proteins	30 min - 6 hours
5. Activation of proteases, phospholipases and nucleases	1 hour
6. Coagulation of intracellular protein	1-6 hours
7. Loss of RNA	1-6 hours
8. Degradation of protein and DNA	6 hours - days

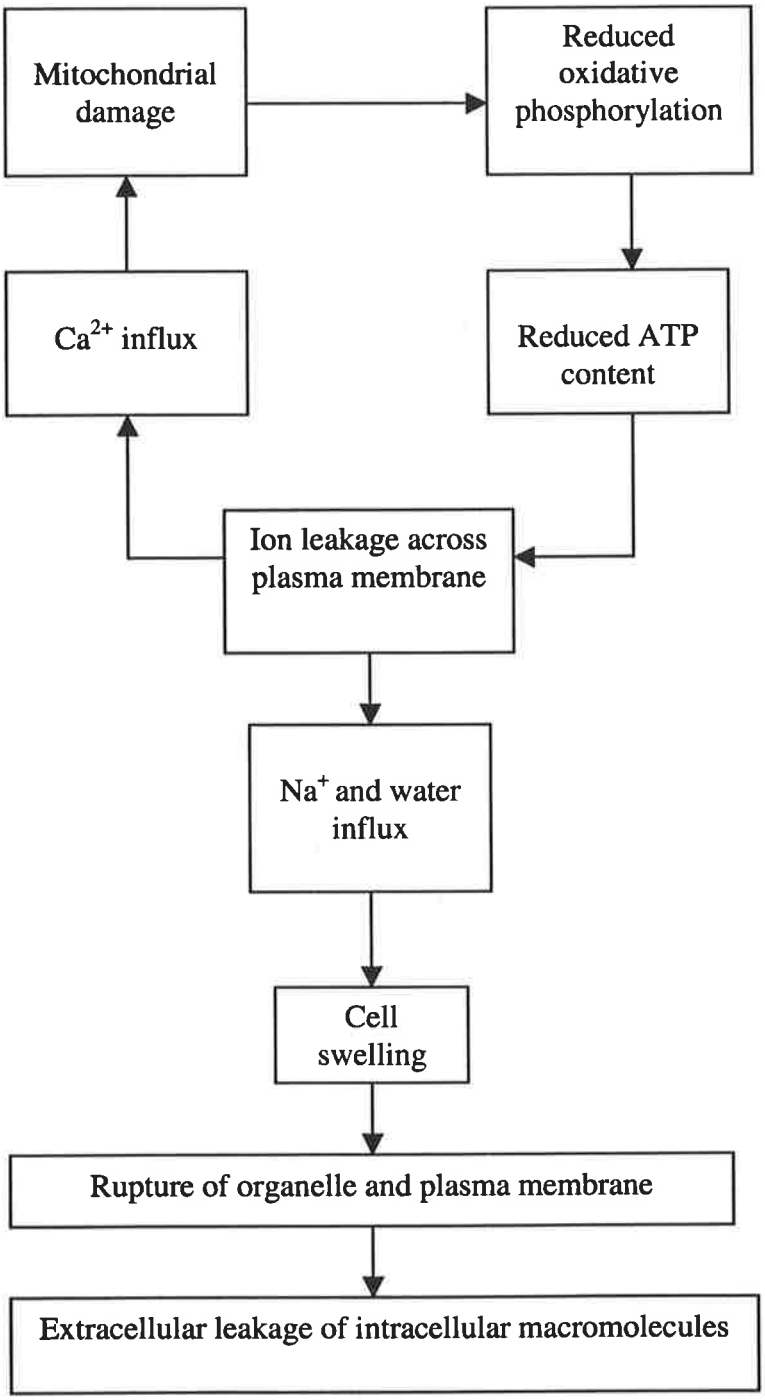

Figure 7.3. Summary of a partial mechanism in necrosis, adapted from Trump and Mergner (1974).

7.4. Cytoplasmic Free Calcium Ion and Its Role in Cell Death

Numerous studies have confirmed that an increase in cytosolic calcium plays a critical role in cell death, necrosis and apoptosis (Wyllie, 1981; Campbell, 1985; McConkey et al., 1991; McConkey et al., 1996). A physiological or pathological change in cell usually results in a rise in intracellular calcium concentration. The extent of change depends strongly on the time and magnitude of the change. An increase of $[Ca^{2+}]_{cyt}$ to 1-10μM for some minutes could disrupt intracellular metabolism under pathological circumstances (Campbell, 1985). There are several mechanisms that may lead to an elevation of free cytoplasmic Ca^{2+}. The most common cause is a change in the permeability of cell membrane to Ca^{2+} either by mechanical stress, physiological change or some other stimuli. Currently no mathematical correlation is available to describe the effect of change in free $[Ca^{2+}]_{cyt}$ on cell functions (Campbell, 1985).

The concentration of cytoplasmic calcium ions is regulated primarily by the mitochondria and the endoplasmic reticulum. Unfortunately, a prolonged rise in $[Ca^{2+}]_{cyt}$ within these organelles induces unfortunate consequences. The uptake of Ca^{2+} normally stimulates a chain of metabolic reactions in the organelles, particularly the mitochondria. The principal reactions include the oxidative phosphorylation, ATP synthesis and hydrolysis. However, an excessive uptake of Ca^{2+} by a mitochondrion could interfere with the respiratory chain, compete with ATP synthesis, and alter Ca^{2+}-regulated enzymes. Prolonged elevation of $[Ca^{2+}]$ in the mitochondrion may induce structural damage, and a Ca^{2+} overload will result (Trump et al., 1981; Campbell, 1985). A ten fold increase of $[Ca^{2+}]_{cyt}$ normally causes a complete loss of ATP synthesis and swelling of organelles. Reasonable correlations have been observed between loss of viability and both cellular calcium level and ATP content in injured tumour cells as illustrated in Figure 7.4 (Trump et al., 1981).

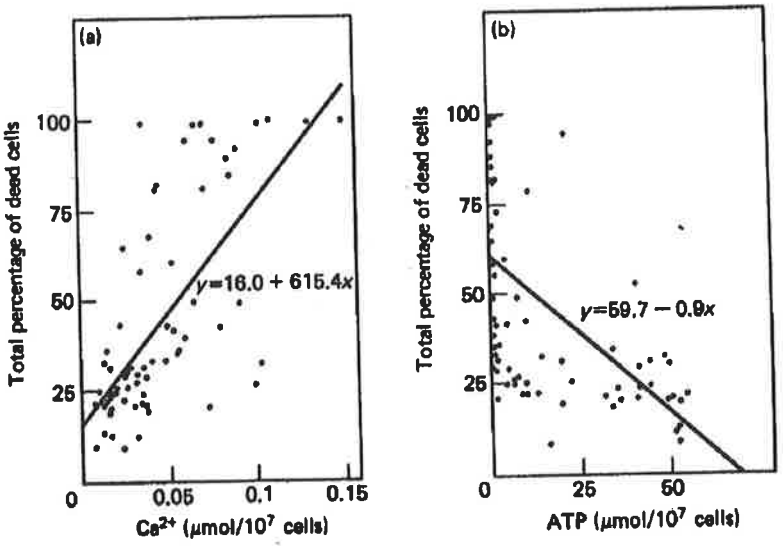

Figure 7.4. Scatter plots with regression lines showing (a) a positive relation between Ca^{2+} concentration (x) and the percentage of dead mammalian cell (y), and (b) a correlation between ATP content (x) and the total percentage of dead mammalian cells (y) (Trump et al., 1981).

The $[Ca^{2+}]_{cyt}$ profile in Figure 7.5 shows the progressive elevation of $[Ca^{2+}]_{cyt}$ during an onset of apoptotic cell death in cancer cells (Tombal et al., 1999). Necrotic processes also exhibit similar patterns.

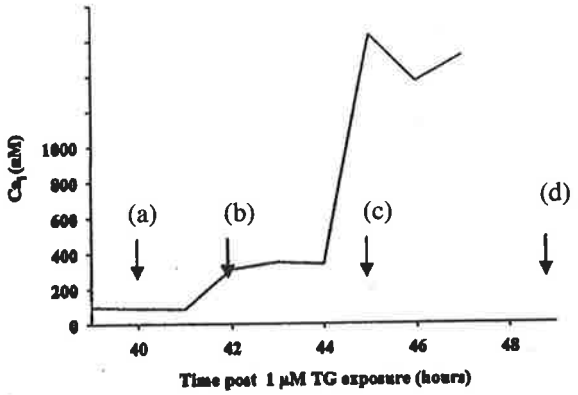

Figure 7.5. The delayed $[Ca^{2+}]_{cyt}$ elevation in cancer cells after exposed to induced apoptosis by 1μM of thapsigargin (TG) (Tombal et al., 1999). The arrows indicate various stages of apoptosis after exposure to TG; (a) 40 hours post exposure (b) 42 hours post exposure (c) 45 hours post exposure leads to an induction of plasma membrane hyperactivity (d) 49 hours post exposure shows fragmentation into apoptotic bodies.

In many cases, early damage to the cells, such as impairment of cell structure, mitochondrial metabolism and functions may be reverted when the source of injury is removed. Inhibition of the mitochondrial Ca^{2+} uptake by Ca^{2+} channel blockers can delay irreversible necrotic cell damage. However, a critical point exists where the resulting injury to the cell is so severe that cell death is inevitable within a few hours. In such cases, despite the continuance of some metabolic processes, the mitochondria are functionless, and consequently, the power supply of the cell is completely exhausted (Campbell, 1985). Such a phenomenon occurs in necrotic cell death. Unfortunately, this metabolic change is difficult to detect under the microscope, as its associated morphological changes only become detectable several hours after the irreversible chemical changes have occurred in the cells.

7.5. Kinetic Modelling of Cytosolic Calcium Ion

Despite the widespread argument over the type of regulatory system in cells, biological systems are generally believed to possess regulatory feedback control systems for ions and other chemicals, particularly when the cell is under stress (Ozaki et al., 1992; Wiesner et al., 1996; van Beek et al., 1999). Plant cells also possess robust, self-regulating mechanisms, which allow them to combat physiological insults and diseases (Malhó et al., 1998). In Chapter 6, it was proposed that hydrodynamic stress could damage plant cells by triggering the stress-activated calcium ion channels. A transient in intracellular $[Ca^{2+}]$ marks an early sign of sublytic responses, and Ca^{2+} signalling further participates in other consequential responsive processes. A functioning cell is capable of compensating for minor injuries caused by high levels of hydrodynamic stress. However, prolonged exposure to intense mechanical forces may lead to failure of cellular regulatory functions. Calcium is involved in most of these regulatory processes and injuries. Unfortunately, the characterisation of Ca^{2+} transient in plant cells exposed to shear stress remains unclear, as quantification of $[Ca^{2+}]$ in plant cells has proven to be difficult to achieve. To help understanding the Ca^{2+} response, a rudimentary kinetic model is proposed to describe the change in $[Ca^{2+}]_{cyt}$ as a result of mechanical insults through stretch-activated channels.

Regulatory systems of the cell can be described using mathematical models coupled with feedback control systems (Wiesner et al., 1996; Boitier et al., 1999; van Beek et al., 1999). While a few studies have attempted to model the kinetics of Ca^{2+} in mammalian cell response to shear flow, calcium modelling has been uncommon in plant cells. Cytosolic free Ca^{2+} in mammalian cells is primarily regulated by the mitochondria and endoplasmic reticulum (Campbell, 1985), whilst vacuole also participates in calcium regulation in plant cells (Trewavas et al., 1994). Normally, cellular transport kinetics are assumed to follow the well known Michaelis-Menten or Monod relationship, but unfortunately, actual cell functions are more complicated. For example, the rate of Ca^{2+} efflux through a Na^{+}-dependent process often follows Michaelis-Menten first-order kinetics, whilst the Na^{+}-independent route for Ca^{2+} efflux is a complex sigmoidal function of $[Ca^{2+}]$ (Gunter et al., 2000). The values of rate constants also vary substantially from one cell type to another. Furthermore, hundreds of chemical reactions occur simultaneously in the cell's metabolic processes. Clearly, it is very difficult to describe such a complex system with a single mathematical model. Hence, the mathematical model proposed in this section is only capable of predicting the general change in Ca^{2+} induced by various processes. It represents a first attempt and may direct future workers to pursue interesting lines of investigation.

A complex chemical process can be represented pictorially as a system of block diagrams, for example, Figure 7.6 represents a chemical process with various types of inputs and outputs. A single cell may be represented by such a system. The measured output or the controlled variable in this case is the cytosolic Ca^{2+} concentration. An external disturbance is an uncontrolled $[Ca^{2+}]$ change resulting from the external sources, such as a temperature shock or a mechanical stress. Mathematical descriptions of these processes are normally derived from mass balances of the fundamental species. These expressions exhibit strong non-linearity, but they can be simplified by linearisation about a steady-state operating point. The resulting equations form a set of differential algebraic equations. The linearisation enables conversion of the differential equations to a set of algebraic equations which are readily solved using transform operation, such as the Laplace transform.

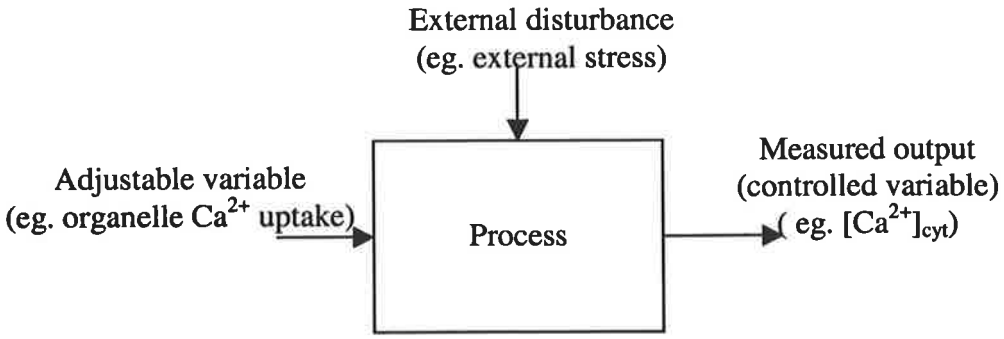

Figure 7.6. Input and output variables around a chemical process

The mathematical model is derived from a species mass balance of the cytosolic calcium content. Key assumptions of the model are summarised below

1. Ca^{2+} influx from the extracellular matrix occurs through (a) the ion-exchange channels (voltage dependent) and (b) stretch-activated channels;
2. Major energy-related reactions occur only in the mitochondria;
3. No Ca^{2+} ions exit through the stretch-activated ion channels;
4. Mechanical stress primarily causes abnormal regulation of Ca^{2+} from extracellular sources and does not influence cellular regulation by intracellular Ca^{2+} pools.

In plant cells, vacuoles provide a major storage volume for intracellular Ca^{2+}. Calcium concentration in the vacuole ranges from 0.1 to 10mM (Schumaker et al., 1986; Gelli et al., 1993). Undoubtedly, they play a significant role in the Ca^{2+} regulatory system. The entry of Ca^{2+} calcium into the vacuole is mediated by the Ca^{2+}-ATPase and nH^+/Ca^{2+} exchanger (Schumaker et al., 1986), whilst calcium efflux is mediated by Inositol 1,4,5-trisphosphate (IP_3)-dependent and IP_3-independent channels (White et al., 1992). The nH^+/Ca^{2+} exchanger in oat roots functions in a similar manner to that found for the Na^+/Ca^{2+} in mammalian cells (Schumaker et al., 1986). Despite strong evidence of the role of vacuole in Ca^{2+} signal transduction in plant cells (Gelli et al., 1993), few data are available on the kinetics of Ca^{2+} transport in isolated vacuoles. White et al. (1992) suggested significant Ca^{2+} efflux from the vacuoles in rye roots, whilst Gelli and Blumwald (1993) have reported the vacuolar release through the IP_3-insensitive (voltage-dependent) Ca^{2+} channel

to be reduced when the cytoplasmic Ca^{2+} concentration exceeded 10^{-6} M in *Beta vulgaris* cultures. In addition, the cytosolic Ca^{2+} concentration of 10^{-4} M could completely inhibit the voltage-dependent Ca^{2+} channel activity in the vacuoles (Gelli and Blumwald, 1993). This evidence suggests that the vacuolar Ca^{2+} release may serve as a negative feedback mechanism triggered by signal transduction of Ca^{2+}.

Figure 7.7 provides a schematic diagram of the proposed simplified Ca^{2+} transfer processes in a normal cell. The Ca^{2+} influx from the extracellular matrix passes through two different types of channels; K_1 and K_2 represent the rate constants for stretch-activated channels and voltage-dependent channels, respectively. The extracellular Ca^{2+} concentration is denoted by C_{ext}, and C refers to the cytosolic calcium. The mitochondrial Ca^{2+} concentration is represented by C_m, while C_{ER} denotes Ca^{2+} concentration in the endoplasmic reticulum. Finally, the vacuole Ca^{2+} concentration is represented by C_V. All concentrations are expressed in $mol.L^{-1}$.

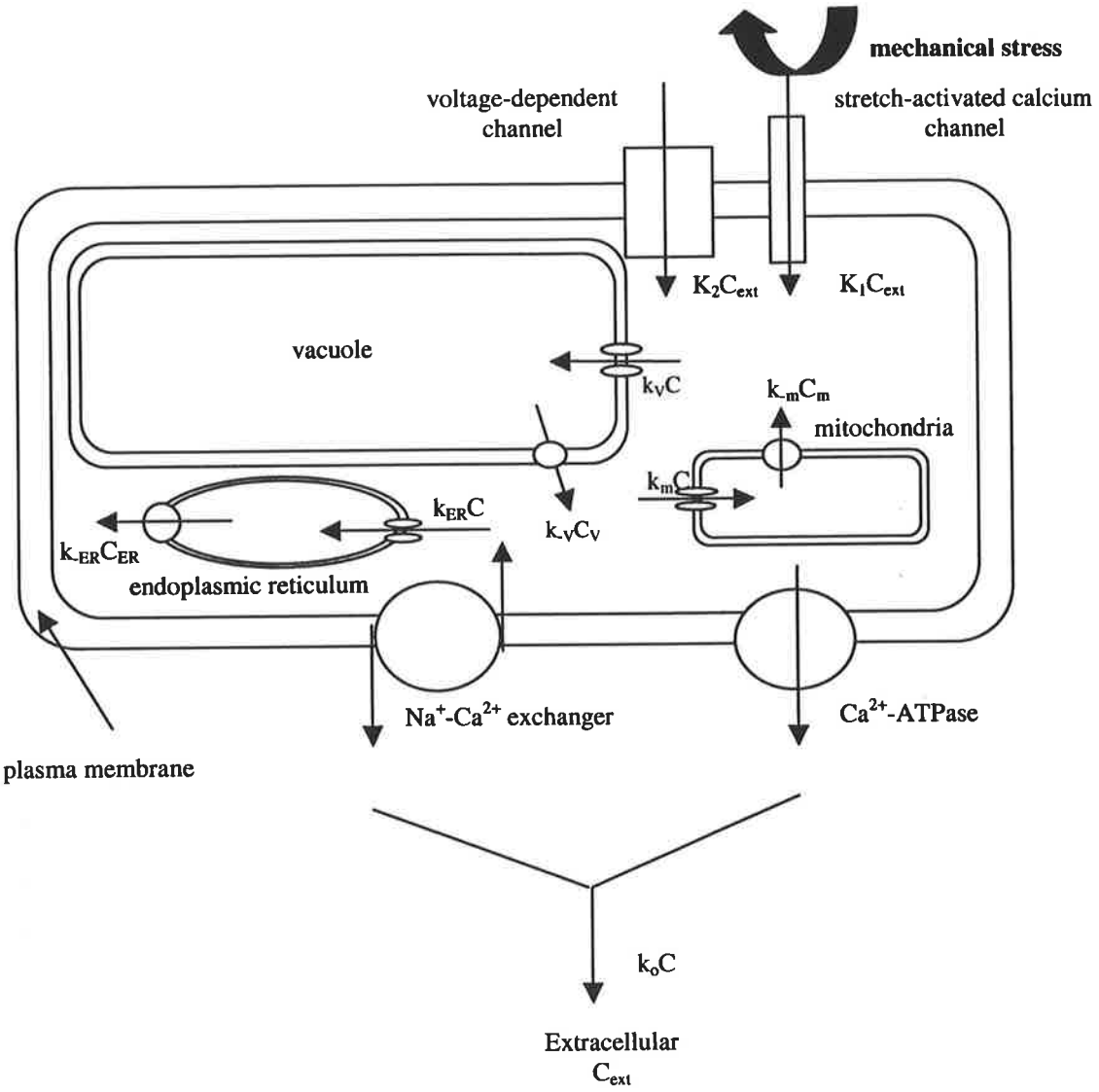

Figure 7.7. A diagram summarising the calcium ion transport processes in a normal cell.

The cytosolic Ca^{2+} influx is the sum of the influx through stretch-activated channels, the voltage dependent channels, Ca^{2+} from the mitochondria, the vacuole and the endoplasmic reticulum. The total Ca^{2+} efflux is the Ca^{2+} exiting the cytosol into the mitochondria, the endoplasmic reticulum, the vacuole, and the extracellular matrix. The rate of cytosolic calcium accumulation is the difference between the total Ca^{2+} influx and efflux:

Accumulation rate = Calcium influx rate – Calcium efflux rate – Calcium consumption rate

The rate of Ca^{2+} accumulation is generally represented by a differential equation (DE) summarising the principal cytosolic Ca^{2+} transport processes:

$$\frac{dC}{dt} = (K_1 C_{ext} + K_2 C_{ext}) + (k_{-m} C_m + k_{-ER} C_{ER} + k_{-V} C_V) - (k_m C + k_{ER} C + k_V C + k_o C) \tag{7.1}$$

The first two terms (K_1C_{ext} and K_2C_{ext}) account for the influx from extracellular matrix, the third and fourth terms refer to the influx of Ca^{2+} from the organelles and the remaining terms are the Ca^{2+} efflux from the cytosol to mitochondria, endoplasmic reticulum (ER), vacuole, and extracellular matrix, respectively.

Similarly, the rate of Ca^{2+} accumulation in the mitochondria is the difference between the total Ca^{2+} entering and exiting the mitochondria. The Ca^{2+} enters the mitochondria from the cytoplasm, whilst the efflux of Ca^{2+} leaves the mitochondria and enters the cytoplasm.

The principal mass balance for the mitochondria becomes

$$\frac{dC_m}{dt} = k_m C - k_{-m} C_m - \left(\sum Ca^{2+} \text{ consumed in mitochondrial reactions}\right)$$

Assuming that Monod kinetics pertain:

$$\frac{dC_m}{dt} = \left(\frac{\mu_m}{K_m + C}\right) C - \left(\frac{\mu_o}{K_o + C_m}\right) C_m - \left(\sum Ca^{2+} \text{ in reactions}\right)$$

where most Ca^{2+} is assumed to be consumed in ATP-related reactions, which may be represented by a Michaelis-Menten expression.

$$\frac{dC_m}{dt} = \left(\frac{\mu_m}{K_m + C}\right) C - \left(\frac{\mu_o}{K_o + C_m}\right) C_m - \left(\frac{V_{max}}{K_{rxn} + C_m}\right) C_m \tag{7.2}$$

To convert this non-linear differential equation to a linear one, a Taylor series expansion of the non-linear terms is performed. For example, if f is a non-linear function of concentration C, where

$$f(C)=\left(\frac{\mu}{K_m+C}\right)C$$

The linearised form of f(C) about a steady-state point, using a Taylor series expansion is f'(C), where

$$f'(C)\cong f(C)_{C=\overline{C}}+\left(\left.\frac{\partial f}{\partial C}\right|_{C=\overline{C}}\right)(C-\overline{C})$$

$$f'(C)=\left(\frac{\mu\overline{C}}{K_m+\overline{C}}\right)+\left(\frac{\mu K_m\overline{C}}{(K_m+\overline{C})^2}\right)(C-\overline{C})$$

$$f'(C)=\left(\frac{\mu\overline{C}}{K_m+\overline{C}}\right)+\left(\frac{\mu K_m\overline{C}}{(K_m+\overline{C})^2}\right)(\delta C)$$

where $\overline{C}$ represents the steady-state concentration.

Hence, linearisation of equation (7.2) about a steady-state yields:

$$\frac{d(\delta C_m)}{dt}=\left(\frac{\mu_m}{K_m+\overline{C}_o}\right)\overline{C}_o+\left(\frac{\mu_m K_m}{(K_m+\overline{C}_o)^2}\right)(C-\overline{C}_o)-\left(\frac{\mu_o}{K_o+\overline{C}_{mo}}\right)\overline{C}_{mo}$$
$$-\left(\frac{\mu_o K_o}{(K_o+\overline{C}_{mo})^2}\right)(C_m-\overline{C}_{mo})-\left(\frac{v_{max}}{K_{rxn}+\overline{C}_m}\right)C_m-\left(\frac{v_{max}K_{rxn}}{(K_{rxn}+\overline{C}_{mo})^2}\right)(C_m-\overline{C}_{mo}) \quad (7.3)$$

The deviation of $[Ca^{2+}]_m$ from the steady-state is $\delta C_m = C_m - \overline{C}_{mss}$. The variables $\overline{C}_o$ and $\overline{C}_{mo}$ refer to the steady-state $[Ca^{2+}]$ in the cytosol and mitochondria, respectively.

At steady-state, there is no accumulation in calcium concentration. A non-linear algebraic equation for mitochondrial $[Ca^{2+}]$ results:

$$\frac{d\delta C_{mss}}{dt} = 0 = \left(\frac{\mu_m}{K_m + \overline{C}_o}\right)\overline{C}_o - \left(\frac{\mu_o}{K_o + \overline{C}_{mo}}\right)\overline{C}_{mo} - \left(\frac{v_{max}}{K_{rxn} + \overline{C}_{mo}}\right)\overline{C}_{mo} \qquad (7.4)$$

Subtracting equation (7.4) from equation (7.3) produces the following linear differential equation for the deviation of mitochondrial concentration from steady state value.

$$\frac{d(\delta C_m)}{dt} = \left(\frac{\mu_m K_m}{(K_m + \overline{C}_o)^2}\right)(C - \overline{C}_o) - \left(\frac{\mu_o K_o}{(K_o + \overline{C}_{mo})^2}\right)(C_m - \overline{C}_{mo}) - \left(\frac{v_{max} K_{rxn}}{(K_{rxn} + \overline{C}_{mo})^2}\right)(C_m - \overline{C}_{mo})$$

(7.5)

Taking Laplace transform of equation (7.5) and rearranging to get

$$\delta C_m(s) = \left(\frac{B}{s + A}\right)\delta C(s) \qquad (7.6)$$

where $A = \frac{\mu_o K_o}{(K_o + \overline{C}_{mo})^2} + \frac{v_{max} K_{rxn}}{(K_{rxn} + \overline{C}_{mo})^2}$ and $B = \frac{\mu_m K_m}{(K_m + \overline{C}_o)^2}$

The expression in equation (7.6) can be represented as a conventional block diagram (Figure 7.8).

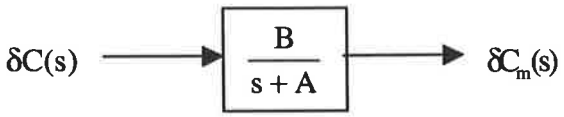

Figure 7.8. Block diagram representing equation (7.6)

In a similar manner, the differential balance for cytosolic Ca^{2+} transport in equation (7.1) may be linearised and subtracted from its corresponding steady-state equation to provide a linearised expression for accumulation of $[Ca^{2+}]_{cyt}$:

$$\frac{d(\delta C)}{dt} = C_{ext}(K_1 - \overline{K}_{10}) + \left(\frac{\mu_o K_o}{(K_o + \overline{C}_{mo})^2}\right)(C_m - \overline{C}_{mo}) + \left(\frac{\mu_{-ER} K_{-ER}}{(K_{-ER} + \overline{C}_{ERo})^2}\right)(C_{ER} - \overline{C}_{ERo})$$

$$+ \left(\frac{\mu_{-V} K_{-V}}{(K_{-V} + \overline{C}_{Vo})^2}\right)(C_V - \overline{C}_{Vo}) - \left(\frac{\mu_m K_m}{(K_m + \overline{C}_o)^2}\right)(C - \overline{C}_o) - \left(\frac{\mu_{ER} K_{ER}}{(K_{ER} + \overline{C}_o)^2}\right)(C - \overline{C}_o)$$

$$- \left(\frac{\mu_V K_V}{(K_V + \overline{C}_o)^2}\right)(C - \overline{C}_o) - \left(\frac{\mu_{max} K_c}{(K_c + \overline{C}_o)^2}\right)(C - \overline{C}_o) \qquad (7.7)$$

The transient effect of the voltage-dependent channels is assumed to be negligible compared to the effect of the stretch-activated channels, hence the dynamic change due to K_2 becomes zero. The rate of Ca^{2+} efflux from endoplasmic reticulum (ER) is relatively low compared to that from the mitochondria (Bush et al., 1995; Rizzuto et al., 2000), therefore the ER efflux term is negligible.

The linearised differential equation can be rearranged to yield

$$\frac{d(\delta C)}{dt} = C_{ext}(\delta K_1) + D(\delta C_m) - E(\delta C) + F(\delta C_V) \qquad (7.8)$$

where

$$D = \frac{\mu_o K_o}{\left(K_o + \overline{C}_{mo}\right)^2}$$

$$E = \frac{\mu_m K_m}{\left(K_m + \overline{C}_o\right)^2} + \frac{\mu_{ER} K_{ER}}{\left(K_{ER} + \overline{C}_o\right)^2} + \frac{\mu_V K_V}{\left(K_V + \overline{C}_o\right)^2} + \frac{\mu_{max} K_c}{\left(K_c + \overline{C}_o\right)^2} \qquad \text{and}$$

$$F = \frac{\mu_{-V} K_{-V}}{\left(K_{-V} + \overline{C}_{Vo}\right)^2}$$

However, the vacuolar Ca^{2+} efflux was found to be inhibited by a relatively low cytosolic $[Ca^{2+}]$ of 10^{-6} M (Gelli and Blumwald, 1993). Consequently, its efflux at high cytoplasmic $[Ca^{2+}]$ may not be as significant. In addition, as the vacuolar Ca^{2+} concentration (C_{V0}) is much higher than the cytosolic Ca^{2+} concentration, the rate of Ca^{2+} efflux from the vacuole (term F) is relatively small compared to the mitochondrial efflux in (term D). Hence, the rate of vacuolar Ca^{2+} efflux is assumed to be negligible, and equation (7.8) becomes:

$$\frac{d(\delta C)}{dt} = C_{ext}(\delta K_1) + D(\delta C_m) - E(\delta C) \qquad (7.8a)$$

Taking Laplace transform of equation (7.8a) yields an expression for cytosolic $[Ca^{2+}]$ change in terms of the mechanical stress $\delta K_1(s)$, and the transient mitochondrial calcium concentration; $\delta C_m(s)$:

$$\delta C(s) = \left(\frac{C_{ext}}{s+E}\right) \delta K_1(s) + \left(\frac{D}{s+E}\right) \delta C_m \qquad (7.9)$$

This expression can be represented diagrammatically as a conventional block diagram in Figure 7.9.

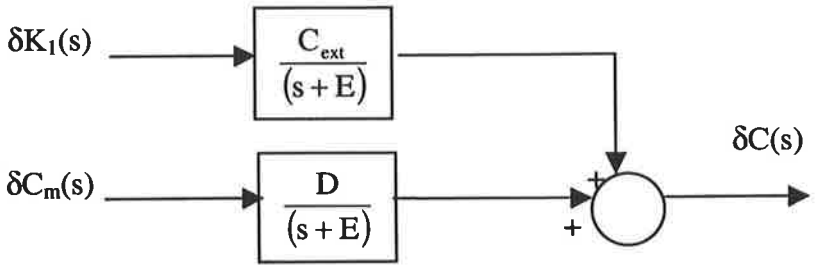

Figure 7.9. A diagrammatic representation of equation (7.9)

However, the transient of the mitochondrial concentration; δC_m is related to the cytosolic calcium transient; δC by the equation (7.6):

$$\delta C_m(s) = \left(\frac{B}{s+A}\right)\delta C(s) \tag{7.6}$$

A substitution of equation (7.6) into equation (7.9) yields:

$$\delta C(s) = \frac{C_{ext}}{(s+E)}(\delta K_1(s)) + \frac{D}{(s+E)}\frac{B}{(s+A)}(\delta C(s)) \tag{7.10}$$

The first term represents the disturbance generated by the mechanical stress $\delta K_1(s)$ and the second terms relates the cytosolic calcium transient δC to the mitochondrial transient δC_m. The mitochondrial calcium transient (δC_m) term is replaced by the cytosolic calcium transient (δC) relationship in equation (7.6).

Finally, another essential process in any molecular recognition and signal transduction is diffusion. The localised distribution of calcium concentration in the cytoplasm has often been observed in plant cells (Read et al., 1993). This evidence confirms that calcium diffusion in the cytoplasm is much slower than in free solution (Malhó et al., 1998).

Consequently, calcium diffusion may delay the calcium signal transduction process in plant cells. A study of the propagation of intracellular Ca^{2+} waves in stimulated mammalian cells reported an average wave velocity of 24.4 μm/s, which is the value assumed in this model (Boitier et al., 1999). For a cell 10μm in diameter, it will take 0.2s for Ca^{2+} to travel from the plasma membrane to the centre of the cell.

It was mentioned earlier that plant cells possess feedback regulatory process for calcium and other ions. In a feedback control system, the primary objectives are to stabilise the process and suppress the influence of the external disturbance (Stephanopoulos, 1984). The control objective of the proposed calcium kinetic model is to control the cytosolic calcium concentration. Equation (7.10) is a transfer function, representing the change in cytosolic $[Ca^{2+}]$; $\delta C(s)$, when a mechanical disturbance, $\delta K_1(s)$ is applied via the stretch-activated channels. The principal process involving $\delta C(s)$ describes the regulation of calcium ion concentration in a simplified fashion, and the disturbance process is a function of the applied mechanical stress $\delta K_1(s)$. The desired set point of this regulatory process is the steady-state $[Ca^{2+}]_{cyt}$ of 10^{-7} M. This cellular process is represented by a close-loop block diagram in Figure 7.10.

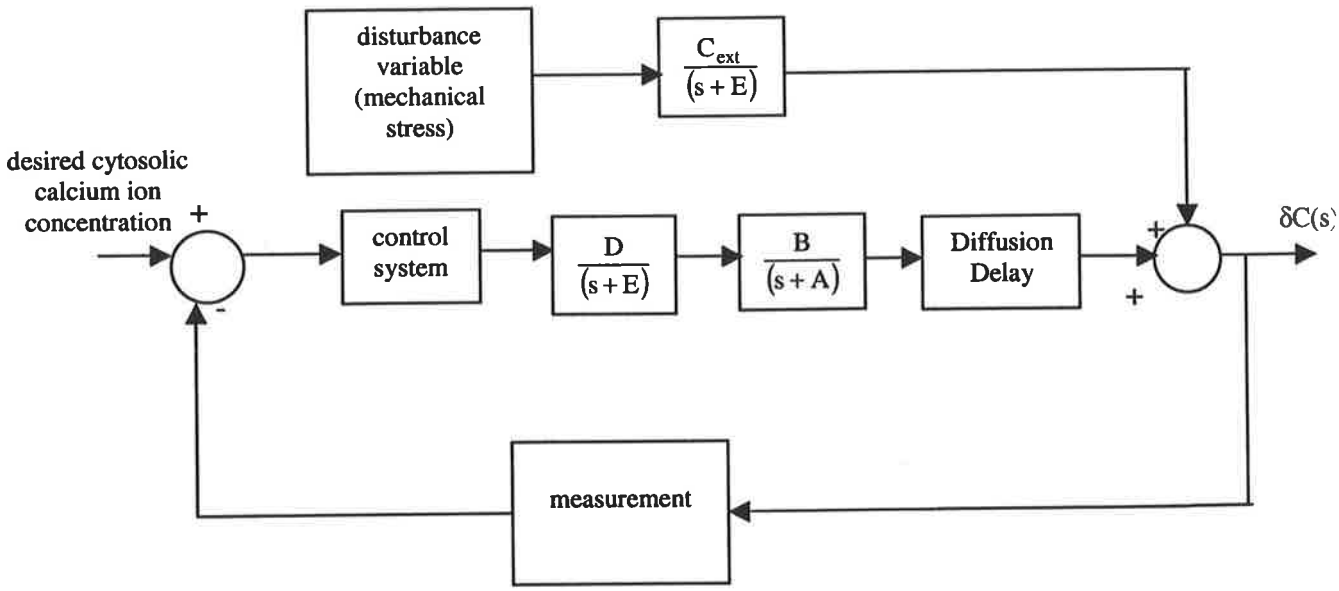

Figure 7.10. Schematic diagram of the proposed feedback-control system, describing the change in Ca^{2+} of the cytosol

Numerical values of rate constant used in the model are summarised in Table 7.3. These have been developed from literature values. The following assumptions were used in the calculation of the rate constants:

1. Protein concentration is approximately 1.2 mg/mL (Fagan et al., 1985).
2. Extracellular $[Ca^{2+}]$ is 10^{-3}M, $[Ca^{2+}]_{cyt}$ is 10^{-7}M and endoplasmic reticulum $[Ca^{2+}]$ is 10^{-4}M (Alberts et al., 1994).
3. Calcium concentration in the vacuole is 10mM (Schumaker et al., 1986; Gelli et al., 1993).
4. The mitochondrial Ca^{2+} concentration is 20×10^{-9} mol/mg (Moreno-Sanchez, 1985).
5. ATP concentration in the cell is approximately 10^{-3} M (Rizzuto et al., 2000).
6. The ATP concentration, [ATP] is approximately 1000 times the ADP concentration, [ADP] (Alberts et al., 1994).

Table 7.3: Rate constant values for the mathematical model

Type of Transport	Rate Constant	Reference
Mitochondria		
Ca^{2+} uptake	μ_m = 1400 nmol Ca^{2+}/mg/min K_m = 10μM	(Rizzuto et al., 2000)
Ca^{2+} efflux	μ_o = 18 nmol Ca^{2+}/mg/min K_o = 8μM	(Rizzuto et al., 2000)
ATP reactions		
hydrolysis	rate constant ≈ v_{max} = 150 nmol/mg/min	(Fagan et al., 1985)
synthesis	rate constant ≈ v_{max} = 21 nmol/mg/min	(Fagan et al., 1985)
Endoplasmic reticulum		
Ca^{2+} uptake	μ_{ER} = 126 pmol/mg/min K_{ER} = 2.5 μM	(Buckhout, 1984) (Buckhout, 1984)
Ca^{2+} efflux	μ_{-ER} = 300 pmol/mg/min K_{-ER} =0.15 μM	(Bush et al., 1995) (Bush et al., 1995)
Vacuole		
Ca^{2+} uptake	μ_V = 11 nmol/mg/min K_V = 10 μM	(Schumaker and Sze, 1986) (Schumaker and Sze, 1986)
Ca^{2+} efflux	μ_{-V} = 1350 pmol/mg/min K_{-V} = 2μM	(Bush et al., 1995) (Bush et al., 1995)
Cytosol		
Ca^{2+} influx (voltage-dependent)	V_{max} = 0.785 nmol/mg/min K_m = 6μM	(Giannini et al., 1987) (Giannini et al., 1987)
Ca^{2+} efflux	V_{max} = 1350 pmol/mg/min K_m = 2μM	(Bush et al., 1995) (Bush et al., 1995)
Diffusion Transport Delay		
Velocity of Ca^{2+} wave in the cell subject to touch	24.4 μm/s (Delay time = 0.2s)	(Boitier et al., 1999)

In this model, mechanical stress exerted by hydrodynamic shear stresses is considered the sole major disturbance which causes an abnormal elevation of $[Ca^{2+}]_{cyt}$. The kinetics of opening of a stretch-sensitive channel are given by (Guharay et al., 1984):

$$k_{1,2} = k_0 e^{\alpha T^2} \tag{7.11}$$

where k_0 is the rate constant in the absence of force which is $0.016ms^{-1}$, α is a constant $0.08\ (dyne.cm^{-1})^{-2}$. T is tension on the cell surface due to mechanical force, and is defined by

$$T = K_A \frac{\Delta A}{A} \tag{7.12}$$

where K_A is the elasticity constant which ranges from 130-340 $dyne.cm^{-1}$ and $\frac{\Delta A}{A}$ is a fractional increase in area (Guharay et al., 1984).

From Table 7.3, the numerical values of the rate constants can be calculated. The feedback control system was constructed in Matlab-Simulink software package using the simplified mathematical expressions from equation (7.10). A block diagram of the Simulink model is presented in Figure 7.11. The mechanical stress is represented by a periodic function derived from Chapter 6 at the local energy dissipation rate at 300rpm. The average cell surface strain at 300rpm is 6.45 $\%.s^{-1}$. For K_A = 340 $dyne.cm^{-1}$, the average strain rate generates the stretch-activated channel opening rate constant $k_{1,2}$ of 74.6 s^{-1}. The value of $k_{1,2}$ corresponds to in the amplitude of the disturbance function. The period of 0.2s represents the stirrer circulation time at 300rpm, and the calcium transport delay by diffusion is 0.2s. For the purpose of this modelling, it has been assumed that these cellular Ca^{2+}-regulatory processes are represented by a proportional-integral-derivative (PID) controller, which has been shown to provide a near optimal feedback controller for many processes (Stephanopoulos, 1984). It is assumed that the feedback control mechanisms provided by the cells have evolved to be robust and well tuned to near optimal conditions. In this case, the controller only implements the proportional function K_c, where the integral

and derivative actions are turned off. The controller has been tuned using the Ziegler-Nichols rules (Stephanopoulos, 1984).

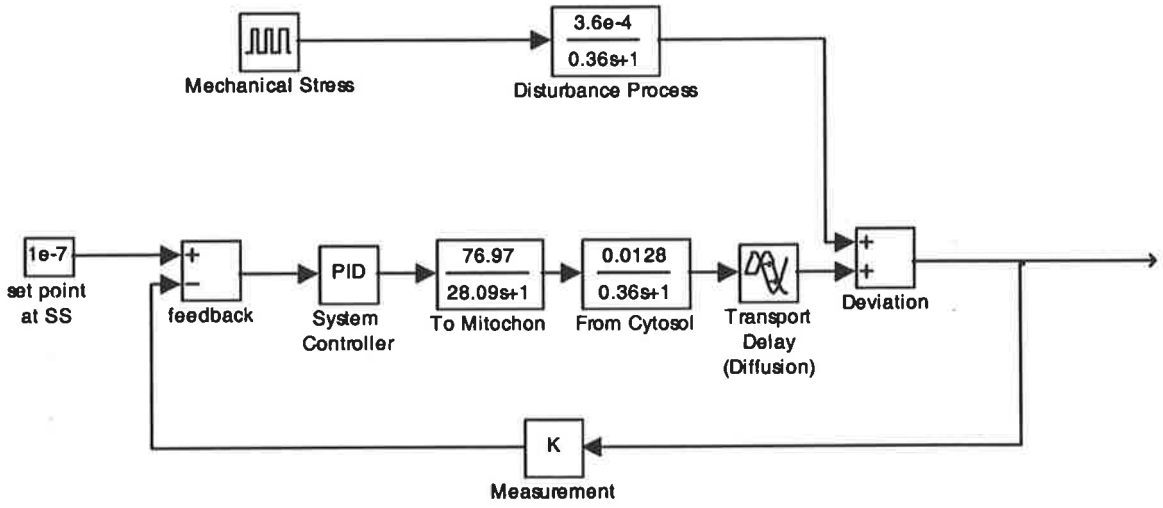

Figure 7.11. Simulink model of the cytosolic calcium ion concentration for a normal cell. This is based on the mathematical model developed in this chapter.

7.5.1. Results of Model Simulations

Calcium transient responses in plant cells are normally elicited by several environmental stimuli. A rise in cytosolic calcium concentration induced by touch, wind and cold shock has been reported in tobacco and Arabidopsis (Knight et al., 1992; Trewavas and Knight, 1994; Knight et al., 1996). The calcium responses in plant cells have been successfully detected using radiotracer, calcium fluorescent dyes, and luminometric technique (McAinsh et al., 1995; Knight et al., 1996; Blatt, 1999), but these techniques often involve

long and invasive procedures. Reliable measurements are difficult to obtain due to the small cytoplasm volume in plant cells (Blatt, 1999). Furthermore, shear-sensitivity experiments require healthy, intact plant cells, which are representative of the cells under normal culture growth conditions. Consequently, the calcium transient data for plant cells subjected to hydrodynamic shear environments remain scarce.

As there is growing evidence that transients of $[Ca^{2+}]_{cyt}$ resembles animal cells , studies often compare the function of plant cells with their mammalian counterpart. The intracellular Ca^{2+} kinetics in plant cells have shown some parallel mechanisms with animal cell models (Blatt, 1999). For instance, the hormone-induced Ca^{2+} increase in *Zea* and *Petroselinium* tissues was comparable to changes observed during the action potentials of animal cells (Blatt, 1999). Furthermore, numerous studies have suggested that membrane stretch-activated channels are involved in calcium response in both plant and mammalian cells to fluid shear (Sachs, 1988; Ding and Pickard, 1993; Haley et al., 1995). Consequently, it was considered appropriate to compare the modelling results with the calcium transient observed in mammalian cells exposed to fluid shear.

Typical shear stress-induced Ca^{2+} responses in endothelial cells are presented in Figure 7.12. The Ca^{2+} transients are characterised by a rapid increase followed by a plateau. Similar response patterns have been observed in other plant cells subjected to environmental stress. However, endothelial cells tend to require longer time for $[Ca^{2+}]$ to return to its steady-state level.

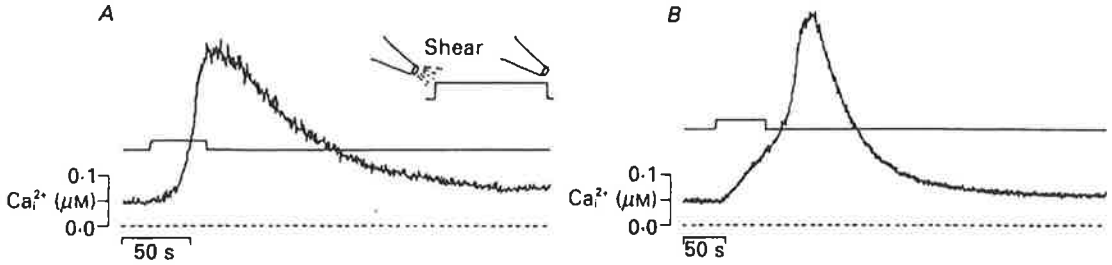

Figure 7.12. Observed patterns of the response of the endothelial cells to shear stress pulses by Schwarz et al. (1992). Shear stress ranges from 0.2 to 0.3 N/m^2. Shear stress pulses are indicated by the rectangular trace. The response A was observed in 60% of the cells, while more than 30% of the cell responses follow the pattern in B.

Figure 7.13 summarises the responses from the control model (for normal cell) in response to an applied fluid shear. This $[Ca^{2+}]_{cyt}$ response follows the trend observed in Arabidopsis cells exposed to temperature stimuli (Knight et al., 1996), and it also resembles $[Ca^{2+}]_{cyt}$ transient reported in endothelial cells subjected to laminar shear stress (Shen et al., 1992). Exposure of the endothelial cells to mild shear stresses (0.008-0.8 N/m^2) showed a transient $[Ca^{2+}]_{cyt}$ peak within seconds of the onset of shear stress (Shen et al., 1992). The maximum $[Ca^{2+}]_{cyt}$ change was obtained within 15-40s, and the concentration returned to the normal level within 40-80s despite the presence of the shear stress (Shen et al., 1992). These observations agreed reasonably well with the response obtained by the Matlab-simulation. The rise time of the calcium response is 5s and the total transient length is 37s. The overall kinetic response is in excellent agreement with the calcium response in tobacco seedlings exposed to wind and cold shock (Malhó et al., 1998). The maximum $[Ca^{2+}]_{cyt}$ change occurs after 5s and the $[Ca^{2+}]_{cyt}$ level returns to the steady-state level within 32s. The final steady-state $[Ca^{2+}]_{cyt}$ is approximately 1.8×10^{-7} M (the expected offset introduced by the proportional control will be negligible and could be entirely eliminated by the introduction of a modest amount of integral control). This slightly higher steady-state level is not entirely unexpected. A similar increase in resting calcium level after the Ca^{2+} transient has often been observed in stimulated plant cells (Malhó et al., 1998). The maximum $[Ca^{2+}]_{cyt}$ reached during the insult is approximately 5.3×10^{-6} M, which is

sufficient to cause irreversible damage to the mitochondria. Continuation of such insults could lead to an irreversible failure of mitochondria to regulate $[Ca^{2+}]_{cyt}$.

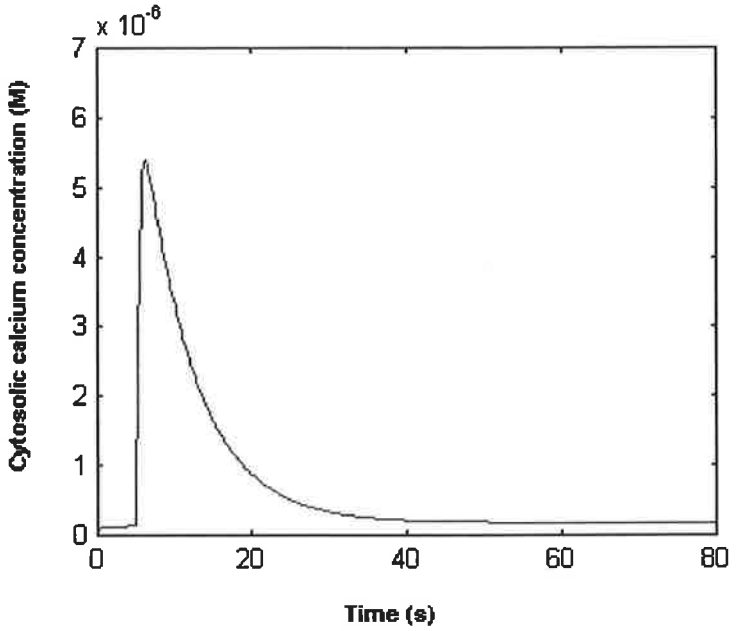

Figure 7.13. Change in $[Ca^{2+}]_{cyt}$ in a normal cell following an increase in Ca^{2+} concentration through stretch-activated channels. The final concentration is $1.8x10^{-7}$M. (Results obtained from Simulink simulations, using mechanical stress function with amplitude = 74.6, period = 0.2 seconds, start time = 5s).

Numerous studies have confirmed that the level of $[Ca^{2+}]_{cyt}$ change increases with increasing magnitude of shear stress (Shen et al., 1992; Schwarz et al., 1992). Evidence of oscillation of $[Ca^{2+}]_{cyt}$ in guard cells in response to external stimulus has been reported (McAinsh et al., 1996). Yellowley et al. (1997) observed that the levels of $[Ca^{2+}]_{cyt}$ response in bovine articular chondrocyte cells depended on the flow rate. They suggest that individual cells express various levels of flow receptor, depending on their growth stage. In addition, the cell surfaces are normally irregular, resulting in variation of shear stress on different locations on the cell surface. The variation of Ca^{2+} responses in bovine articular chondrocytes cells is presented in Figure 7.14. The cells were subject to flow-induced shear stress of 3.7 N/m^2 (Yellowley et al., 1997). Two of the cells showed a spontaneous Ca^{2+} response at the onset of the flow at 1min, whilst others showed varying degrees of delayed responses. This behaviour has also been reported in plant cells, where the cells

from the same population exhibited different sensitivities to the same stimulus (Malhó et al., 1998). Figure 7.15 compares two cases for the predicted $[Ca^{2+}]_{cyt}$ response in plant cells exposed to different energy dissipation rates. The model indicates that the maximum $[Ca^{2+}]_{cyt}$ stimulated by local energy dissipation rate (ε_{local}) is significantly greater than that caused by bulk energy dissipation rate (ε_{bulk}). This highlights the need for further investigation into how $[Ca^{2+}]_{cyt}$ changes in plant cells during shearing.

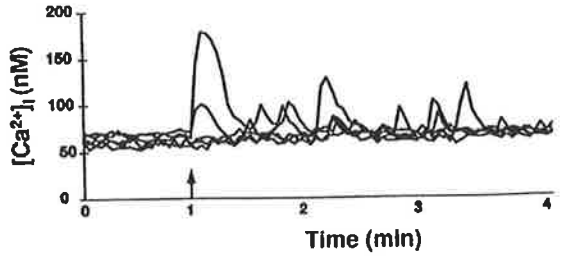

Figure 7.14. Variation of Ca^{2+} responses in bovine articular chondrocytes cells. Each line represents intracellular Ca^{2+} signal from an individual cell. Cells were subjected to constant laminar fluid flow. The flow-induced shear stress is 3.7 N/m^2 (from Yellowley et al. (1997)).

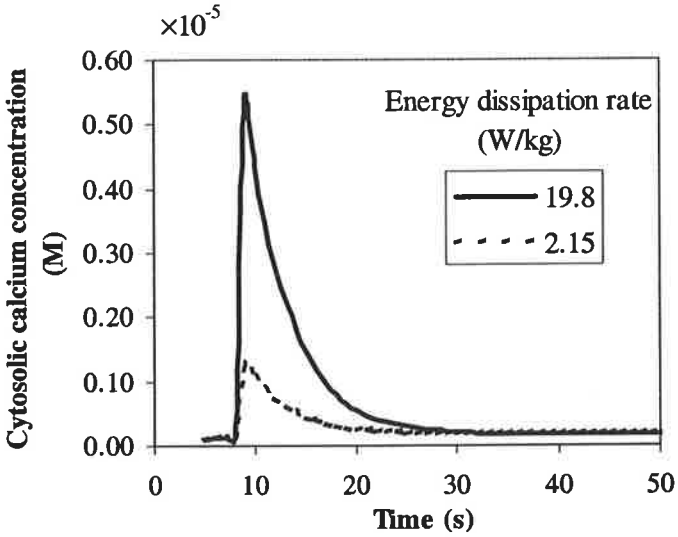

Figure 7.15. The effect of different levels of energy dissipation rate on calcium transient (from simulated results). The two energy dissipation levels represent the ε_{local} (19.8 W/kg) and ε_{ave} (2.15 W/kg) values obtained at 300rpm, and the stress is applied at t = 5s.

Evidence has strongly confirmed a sigmoidal relationship of $[Ca^{2+}]$ transient on the level of shear stress in endothelial cells (Schwarz et al., 1992). Wiesner et al. (1997) predicted a sigmoidal dependence of calcium influx through mechano-sensitive ion channels upon application of a shear stress. Shen et al. (1992) reported that the maximum increase in $[Ca^{2+}]_{cyt}$ with the applied shear stress closely followed a sigmoidal function. A similar study of the proposed model was conducted to verify whether the calcium transient would follow a sigmoidal relationship. The results in Figure 7.16 confirm a correlation that resembles the early stage of a sigmoidal curve. The range of energy dissipation rate studied here is much higher than the levels experienced by the endothelial cells. The $[Ca^{2+}]_{cyt}$ change exhibits an exponential increase with energy dissipation rate. However, as the energy dissipation rate increases, a plateau phase was not observed. Due to the lack of relevant data for plant cells, it remains difficult to establish the exact events of $[Ca^{2+}]_{cyt}$ change prior to cell death by shear damage. Studies often report heterogeneous distribution of $[Ca^{2+}]_{cyt}$ (Gilroy et al., 1986), hence, it would be difficult to measure any distinctive changes. It is suspected that the final stage of $[Ca^{2+}]_{cyt}$ transient may asymptote at a critical $[Ca^{2+}]_{cyt}$ value corresponding to the onset of cell death or lysis. However, additional information on sublytic-biological responses is required to confirm any appropriate modification to the proposed model.

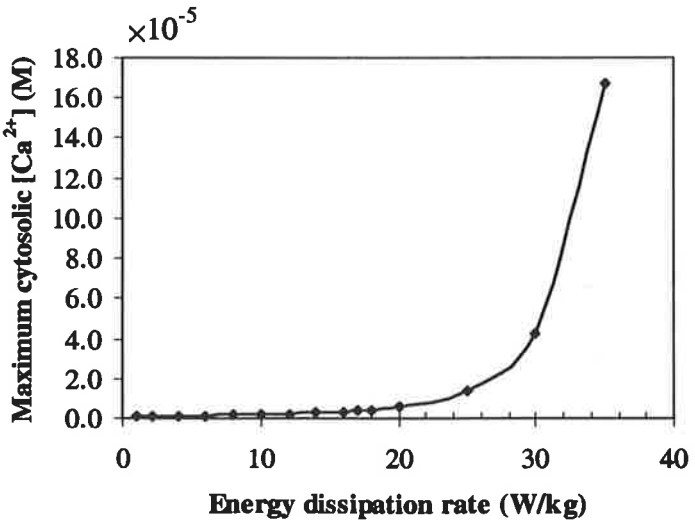

Figure 7.16. Amplitude of maximum cytosolic calcium concentration; $[Ca^{2+}]_{cyt}$ (from Simulink simulations) at different energy dissipation rates.

7.5.2. Modelling of a Damaged Cell

The proposed model can also be modified to predict calcium transient in a cell that has been substantially damaged. If the cell is injured and the mitochondria are unable to function normally, the Ca^{2+} regulatory system becomes ineffective. This abnormal system has been derived from the proposed model and is illustrated in Figure 7.17. It retains the negative feedback system without the functioning mitochondria. Figure 7.18 represents the $[Ca^{2+}]_{cyt}$ profile responding to the same magnitude of shear stress applied in the system proposed in Figure 7.11. The Ca^{2+} response follows similar profile to that observed in apoptotic tumour cells in Figure 7.5. Without the mitochondria, the $[Ca^{2+}]_{cyt}$ is stabilised at 5.4×10^{-6} M, which is an order of magnitude higher than the normal level. Such an increase of $[Ca^{2+}]_{cyt}$ only requires minutes to disrupt intracellular metabolism of the cell (Campbell, 1985). When this elevated level is sustained for 10-30 min, irreversible damage probably occurs. This could result in a complete loss of ATP synthesis and swelling of organelles (Campbell, 1985). The phenomenon presented here is clearly reflected in the change in mitochondrial activity in Figure 5.14 (Chapter 5). The lag period would correspond to the initial reversible process, followed by rapid first-order damage to the mitochondria. The beginning of the first-order decay possibly corresponds to an onset of the irreversible mitochondrial damage.

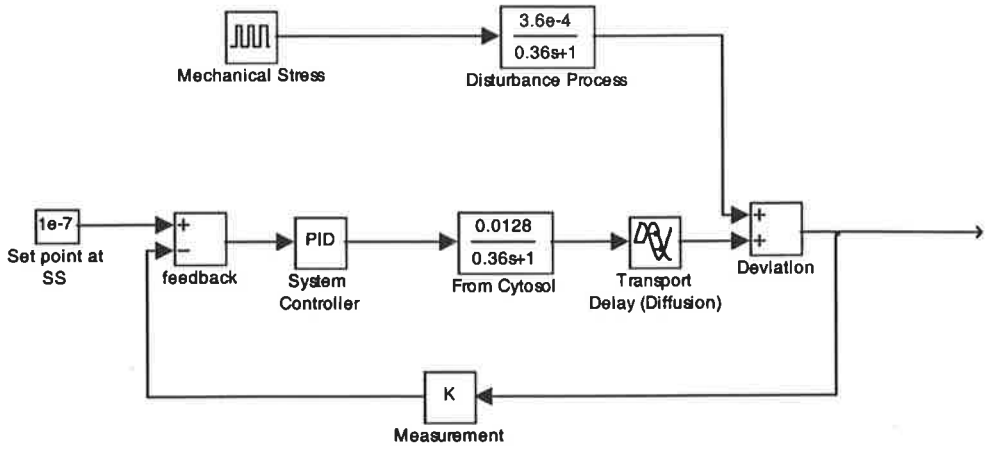

Figure 7.17. Simulink model of an injured cell without the mitochondrial regulatory system.

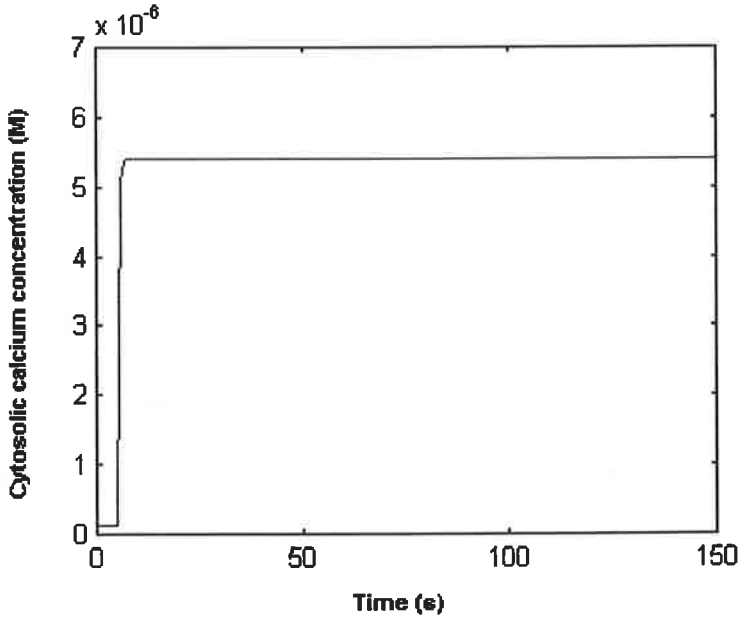

Figure 7.18. Change in $[Ca^{2+}]_{cyt}$ in a cell with injured mitochondria following Ca^{2+} increase through the stretch-activated channels. Final concentration is 5.4×10^{-6}M. (Mechanical stress function; amplitude = 74.6, period = 0.2 seconds, start time = 5s).

The results from this model confirmed the role of the mitochondria in controlling cytosolic calcium ions. Boitier et al. (1999) reported that the mitochondria exerted a negative feedback regulation on the propagation of the intracellular Ca^{2+} wave in rat cortical astrocytes cells. They also demonstrated that preventing mitochondrial Ca^{2+} uptake slowed the rate of decay of transient $[Ca^{2+}]_{cyt}$. This evidence supports that mitochondrial Ca^{2+} uptake plays a significant role in regulating Ca^{2+} in plant and mammalian cells subjected to external mechanical stress.

7.6. Conclusions

The intracellular calcium transient is a common response in plant cells to several external stimuli, such as temperature, hormones and mechanical stress. Plant cells exhibit similar calcium transients following exposure to hydrodynamic shear. However, the calcium transient during sublytic responses in plant cells remains unclear and has not been measured. Experimental data are scarce due to difficulty in quantifying $[Ca^{2+}]$ in whole plant cells and measurement techniques of intracellular calcium in plant cells are often invasive. Consequently, these procedures can inevitably disrupt normal cellular functions. Measurement protocols are complicated and often require several hours of incubation. Clearly, such techniques are considered impractical in the shear-sensitivity studies. A simplified mathematical model has been developed to describe the change in cytosolic calcium concentration associated with the sublytic responses in plant cells exposed to hydrodynamic shear. Shear stress was assumed to modulate the calcium response primarily through the mechano-sensitive ion channels. Mass balances were developed to establish the relationship between cytosolic Ca^{2+} and Ca^{2+} in other organelles, such as the mitochondria and the endoplasmic reticulum. The linearised mass balances were solved by Laplace transform techniques and presented diagrammatically as a block diagram. The predicted Ca^{2+} transient response to the local shear stress at 300rpm exhibited similar characteristics to the responses observed in endothelial cells exposed to shear stress. The Ca^{2+} model for the cell with impaired mitochondrial function confirmed that the mitochondria had an essential role in preventing a prolonged $[Ca^{2+}]_{cyt}$ elevation, leading to cell death.

This method of modelling involves the assumption of uniform, well-mixed Ca^{2+} distribution. Unfortunately, this assumption has been contradicted by a number of studies which confirmed that there is a heterogeneous distribution of $[Ca^{2+}]_{cyt}$ in plant cells (Read et al., 1993; Gilroy et al., 1986). Hence, it is difficult to accurately model such a complex system with a simple model, which assumes uniform distribution of Ca^{2+}. Furthermore, a fully described Ca^{2+} regulatory system in a cell involves several complex chemical processes (Wiesner et al., 1996). Consequently, this preliminary model presented a novel approach of modelling a complex system by converting the differential equations into linear algebraic transform expressions that are readily solved. Based on this proposed model, several modifications could be readily introduced to refine the model further to suit various biological systems.

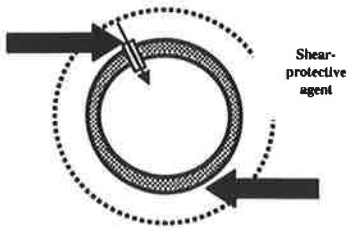

CHAPTER 8

FACTORIAL STUDIES OF THE EFFECTS OF SHEAR-PROTECTIVE AGENTS

Pluronic F-68 (PF-68), methocels, polyethylene-glycol and carboxymethyl-cellulose (CMC) are widely exploited as shear-protective agents for mammalian cell cultures grown in intensely agitated bioreactors. Despite the fact that plant cells are also severely damaged by exposure to shear conditions of similar intensity, surprisingly few studies have addressed the potential of shear protection in plant cell cultures. This chapter summarises an investigation of the shear-protective properties of surface-active PF-68, and viscosity enhancing carboxymethyl-cellulose on wild carrot cultures (*Daucus carota*). The two-level, three-factor (2^3) factorial designs were devised to determine if PF-68 and CMC provide a similar shear-protective effect for plant cells compared to animal cells. The three factors involved in the study are the impeller speed (300, 400 rpm), exposure time (3, 4hr) and the concentration of the proposed shear-protective agent (0.05, 0.1%(w/v)). The biological responses of the plant cells were quantified as relative mitochondrial activity, aggregate size and membrane integrity. Student's t-tests confirmed a significant improvement in the biological responses for the cell cultures grown in a medium supplemented with PF-68, but not CMC. Aggregate breakage was reduced considerably in cells grown in medium supplemented with PF-68. The principal variables affecting growth were agitator speed and time. In addition, the mitochondrial response showed strong interactions between concentration level and shear speed and exposure time. These interactions implied that the concentration of PF-68 providing optimal protection may depend on the shear conditions. It was concluded that the protective mechanism was dominated by biological interaction between the surfactant (PF-68) and the cell membrane, which can lead to either stronger

cell membrane structure or a protective polymer layer that surrounds the cell (Wu et al., 1995).

8.1. Background

Both plant and animal cell growth in suspension cultures are severely inhibited by the mechanical stresses resulting from bioreactor agitation. While, certain chemical compounds can be added to the culture medium to moderate damage in animal cells, little is known about their protective effects on plant cells. Protective medium additives are characterised as either surface-active or viscosity-enhancing polymers (Wu et al., 1995). Pluronic F-68, polyethylene-glycol and methylcellulose are the most recognised surface-active compounds, whereas carboxymethyl-cellulose and dextran are commonly known as viscosity-enhancing compounds. The degree of shear protection strongly depends on the type of polymer (Wu et al., 1995). Surface-active polymers are amphipathic molecular structures (i.e. both hydrophilic and hydrophobic parts); a property, which allows them to interact bind with hydrophobic phospholipid membranes, and provides protection to shear. However, viscosity-enhancing polymers are normally hydrophilic. Hydrophilic interaction between these polymers and the cell membrane is not possible. Wu et. al. (1995) have suggested that the shear protective effects are primarily attributed to surface-active polymers, as their molecules can bind with cell membrane, hence strengthening the membrane (Murhammer et al., 1990; Palomares et al., 2000). Despite the evidence that the viscosity-enhancing polymers are less effective in shear protection, they may provide minor protection to the cells by increasing fluid resistance to shear. Their action is a result of the dissolved polymer coiled chains. These chains exert resistance to flow of adjacent fluid layers resulting in an increase in viscosity (Wu et al., 1995).

Despite significant progress in the adoption of shear-protective agents to alleviate the damaging effects of shear on animal and insect cells, very few studies involving plant cells have been undertaken. Studies suggest that the shear protective mechanisms in insect cells differ from those occurring during the growth of mammalian cells. Further differences are expected for plant cells. Although plant cells (like mammalian cells) are severely damaged by exposure to intense shear conditions (Dunlop et al., 1994), their growth is not impacted

on by bubble activity (Rosenberg, 1989; Kieran et al., 2000). The search for improved performance of large-scale plant cell culture processes requires a fundamental study to determine if the damping effects of shear-protective agents can improve the tolerance of plant cells to an intense shear environment. The chapter will explore such behaviour.

Experiments to determine the effect of changes in concentration of shear protective polymer at different shearing speeds and for different exposure time can be performed using either a "one-factor-at-a-time" (single-factor) approach or factorial arrangement. For n factors at two levels, the first approach requires n times as many experiments as the factorial design (Cochran et al., 1957). In addition, a properly designed factorial experimental program is sufficiently powerful to relate the main effects with other binary interactions.

8.2. Factorial Design

The three factors used in the factorial (2^3) design were stirrer rotation speed (S), elapsed time (T) and the PF-68 concentration (C). The parameters, which represent the biological responses are summarised in Table 8.1. Variables Y_1, Y_2, and Y_3 refer to mitochondrial activity, aggregate size and membrane integrity respectively. Each main effect was calculated by taking an average of the difference between the four responses at the high level and four obtained at low level. The two-factor and three-factor interactions were calculated as described by Cochran and Cox (1957) or alternatively, the Yate's algorithm could be used (Box et al., 1978). Table 8.2 summarises the formulation required in the calculations of principal and interaction effects for a 2^3 factorial design. The standard error of an individual effect was estimated from variance of the effects of two-factor and three-factor interactions as described by Box et al. (1978). Table 8.3 presents the complete factorial design with the factors and levels before randomisation.

Table 8.1: Parametric representation of biological responses

Variable	Response
Y_1	Mitochondrial activity
Y_2	Aggregate size
Y_3	Membrane integrity

Table 8.2: Tabulated factors for the calculation of the effects (Montgomery, 1991b)

Factor	Mean	S	T	C	ST	SC	TC	STC
(1)	+	-	-	-	+	+	+	-
s	+	+	-	-	-	-	+	+
t	+	-	+	-	-	+	-	+
st	+	+	+	-	+	-	-	-
c	+	-	-	+	+	-	-	+
sc	+	+	-	+	-	+	-	-
tc	+	-	+	+	-	-	+	-
stc	+	+	+	+	+	+	+	+
Effect		$S = \frac{(s+st+sc+stc)-(1)-t-c-tc}{4}$						

From the tabulated values in Table 8.2, an effect is calculated by multiplying the factors on the left column with the sign of the desired effect. The effect is the total sum of these factors divided by four (2^{3-1}). For example, the principal effect S is given by (Montgomery, 1991b):

$$S = \frac{(s+st+sc+stc)-(1)-t-c-tc}{4}$$

Similarly, the interaction ST is given by:

$$ST = \frac{((1)+st+c+stc)-s-t-sc-tc}{4}$$

Table 8.3: Factors and their levels for the 2^3 factorial design

Level	Shearing speed (rpm)	Time (hour)	Concentration (%w/v)
-	300	3	0.05
+	400	4	0.10
Assay	**S**	**T**	**C**
1	-	-	-
2	+	-	-
3	-	+	-
4	+	+	-
5	-	-	+
6	+	-	+
7	-	+	+
8	+	+	+

8.3. Surface-active Polymer - Pluronic F-68

Pluronic F-68 (PF-68) is a non-ionic surfactant. It is known to protect mammalian and insect cells in suspension culture from the damage caused by hydrodynamic shear stresses (Michaels et al., 1992; Zhang et al., 1992; Palomares et al., 2000).

A number of protective mechanisms have been proposed to explain the protection of animal cells from applied shear stress in terms of relevant physical and biological mechanisms. Physical mechanisms occur when the additive interacts physically with the culture fluid. PF-68 reduces the surface tension of the medium, stabilises surface foams and reduces the interaction between cells and bubble disengagement events in bioreactors (Murhammer et al., 1990; Zhang et al., 1992; Wu et al., 1995; Palomares et al., 2000).

Biological interactions between the potential protective agents and the cells result from the absorption of the reagent onto the cell membrane with subsequent formation of a protective layer, which shields the cell from the shear forces in the fluid (Goldblum et al., 1990).

Furthermore, an interaction between the additive and the plasma cell membrane or cell metabolic events may enhance the resistance of the cells to mechanical stress (Wu et al., 1995). For instance, PF-68 interacts with insect cell membranes through absorption into the membranes, and protecting them from damage (Goldblum et al., 1990; Zhang et al., 1992). Results derived using a fluorescent polarisation technique confirmed an instantaneous decrease in the plasma membrane fluidity of hybridoma cell culture following the addition of PF-68. Ramírez and Mutharasan (1990) reported a direct correlation between a reduction of plasma membrane fluidity to an increase in resistance to shear for hybridoma cells. They suggested that PF-68 is either absorbed onto cell membranes, or is incorporated into those membranes. Zhang et al. (1992) demonstrated that the strength of hybridoma-cell membranes was also enhanced by use of PF-68. A 60% increase in the mean bursting tension of hybridoma cells supplemented with 0.05%(w/v) PF-68 compared to the cell culture without PF-68. In addition, they reported an increased elastic area compressibility modulus of approximately 120% greater than that for normal cells. A significant change in membrane strength was observed beyond a threshold concentration of 0.1%(w/v) PF-68.

For plant cell, the presence of PF-68 in the medium may have an additional benefit for downstream product recovery. Most plant cells require intracellular extraction of the desired secondary metabolites. The secretion of plant intracellular metabolites can be enhanced by alteration of their cell membranes by PF-68. Studies have demonstrated that the release of *Morinda citrifolia* cell metabolites was increased substantially when they were grown in high concentrations of PF-68 (2%(w/v)) (Bassetti et al., 1995; Bassetti et al., 1995).

Despite its benefits, PF-68 has the potential to retard cell growth. For instance, PF-68 exhibits slight toxicity for some mammalian cell lines. Zhang et al. (1992) observed a 14% reduction in the total cell number for hybridoma cells cultivated in a PF-68 supplemented medium. The reduced growth rate may be a consequence of an alteration in cell membrane strength with consequent reduction in the cell metabolism rates. However, unlike mammalian cells, plant cell cultures exhibit greater tolerance to PF-68 (King et al., 1990; Kumar et al., 1992). Low levels of PF-68 supplement in cell media stimulated growth in Petunia and Rubiaceae cells (Anthony et al., 1994; Bassetti et al., 1995; Anthony et al., 1997). King et al. (1990) reported high biocompatibility of low concentrations of PF-68 to

Solanum dulcamara cell suspension cultures. PF-68 also promotes growth in many plant cells by improving nutrient uptake and altering some cellular functions (King et al., 1990; Anthony et al., 1994; Bassetti et al., 1995). Additionally, it has been suggested that mechanical cell damage may be alleviated by presence of PF-68 (King et al., 1990). However, excessive membrane modification may also produce negative impacts. High levels of PF-68 were found responsible for severe alteration of cellular functions in *Morinda citrifolia* cultures (Bassetti et al., 1995). Nevertheless, responses of plant cells to PF-68 seemed to vary substantially from one species to another. Consequently, clear general rules have not been deduced for plant cells, and additional studies are required.

Modification of cell membrane may be insufficient to account for the entire protective mechanism in sparged, agitated bioreactors. Additional mechanisms, such as shear reduction could also be responsible, but little is known about which mechanism dominates under different conditions. It is possible that these cells are protected through a combination of mechanisms with the cell membranes strengthened and hydrodynamic effects moderated (Zhang et al., 1992).

8.3.1. Determination of Concentration Levels

Relative growth rates were measured for *Daucus carota* grown in WCM medium supplemented with different concentrations of PF-68 (MW 8400, Sigma). Three replicates were performed. Five concentrations studied were 0.01%, 0.05%, 0.1%, 0.2% and 1.0%(w/v), plus control samples with no additive. The average relative growth rate is summarised as a function of the PF-68 concentration in Figure 8.1.

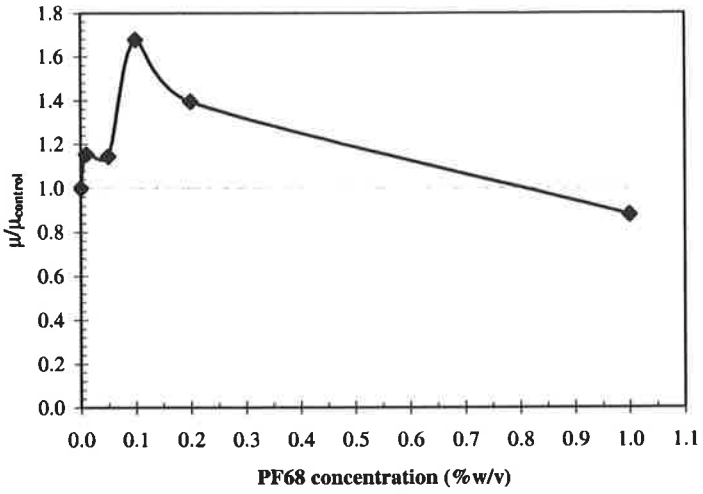

Figure 8.1. Relative growth rate of *D. carota* in medium with different levels of PF-68 supplement.

Growth medium supplemented with a small quantity of PF-68 generally stimulates growth compared to normal medium. In the current tests, the relative growth rate increased by roughly 15% when grown in 0.01-0.05%(w/v), and a 68% improvement was achieved when supplemented with 0.1%(w/v) PF-68. Growth rates relative to control increased with PF-68 concentration until 0.1%(w/v), after which the growth rate began to decline. Inhibition of growth occurred when the concentration exceeded approximately 0.8%(w/v). In medium supplemented with 1.0%(w/v) PF-68, the growth rate reduced to 12% compared to the control. Similar results were obtained for growth of *Solanum dulcamara* L. callus and protoplast (Kumar et al., 1992). Shoot regeneration of *Dendranthema grandiflora* or chrysanthemum explants was enhanced by 0.01-0.1% (w/v) PF-68 (Khehra et al., 1995). They also suggested that supplementation of medium with PF-68 could also inhibit the accumulation of polyphenolic compounds which indicates a possible biochemical effect of the surfactant (Khehra et al., 1995).

Finally, for the factorial design, the PF-68 concentration levels were kept sufficiently low to ensure that the linearity assumption was maintained. Lower and upper limits were 0.05% and 0.1%(w/v), respectively.

8.3.2. Shear Protection by Pluronic F-68

The factorial experiments were performed in a randomised order. The results are summarised in Table 8.4. Figure 8.2 compares the mitochondrial activity of cells in PF-68 against the data obtained at corresponding energy dissipation rates from shearing experiments without PF-68 supplementation. A slight shift was observed for the critical energy dissipation value in Figure 8.2 (~2000J/m^3). However, a Student's t-test was performed to confirm if the increase was significant.

Table 8.4: Results from the randomised 2^3 factorial experiments

Random Order	**Run**	**Factors**			**Responses**		
		S	**T**	**C**	**Y_1 (%)**	**Y_2 (%)**	**Y_3 (%)**
8	stc	+	+	+	13.9	61.2	98.7
5	c	-	-	+	64.1	75.8	99.7
2	s	+	-	-	28.6	82.6	106.7
4	st	+	+	-	5.2	58.6	53.9
6	sc	+	-	+	33.8	89.9	95.7
1	(1)	-	-	-	90.7	96.6	96.9
3	t	-	+	-	28.3	91.2	107.6
7	tc	-	+	+	75.4	102.1	90.7

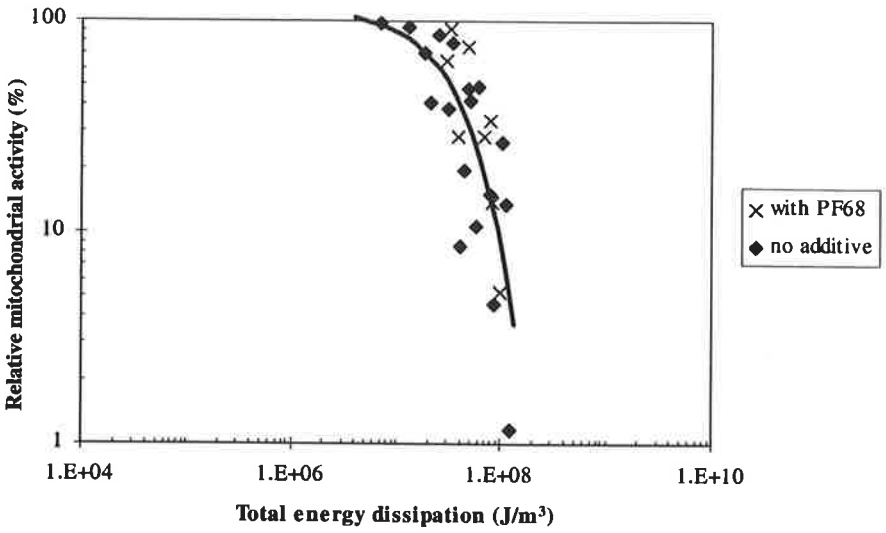

Figure 8.2. Comparison between mitochondrial activity for *D. Carota* cells in medium with and without PF-68. The solid curve represents the least square regression of the data with no PF-68 addition.

The base level of comparison for the Student's t-test was the difference between the responses with PF-68 supplement subtracting the values without any additive;

$$\mu_0 = \overline{x}_{PF68} - \overline{x}_{none} \qquad (8.1)$$

To determine whether an addition of PF-68 increased viability of the cell cultures, the standard reference of a null hypothesis was $H_0:\mu_0 \leq 0$, which corresponded to no increase in response. The alternative hypothesis referred to a significant increase in response, where $H_1:\mu_0 > 0$ (Perry et al., 1984). The viability of cells without additive was determined at corresponding energy dissipation rate rather than speed as addition of PF-68 slightly increased the drag force.

The paired Student's t-tests to determine any increase in biological responses are summarised in Table 8.5.

The 8 observations (n) allowed (n-1) degrees of freedom (df). For n = 8, the upper-tail test with 7 df at $\alpha = 0.1$ is defined by t = 1.415, and at $\alpha = 0.05$ by t = 1.895. The mitochondrial was found to increase significantly at 90% confidence level. The t-test on mean aggregate

size also suggested a significant improvement in cell viability, as less aggregate break-up was observed. The relative aggregate size was significantly larger for cell cultures grown in PF-68 ($P = 0.004$ at $\alpha = 0.05$). Similar results were observed for membrane integrity, where $P = 0.075$ ($\alpha = 0.05$), indicating less damage to cell plasma membrane when the medium was supplemented with PF-68. It could thus be concluded that PF-68 can provide certain degree of physiological protection for carrot cells in suspension.

Table 8.5: Student's t-tests of paired samples for mean difference

	Mitochondrial activity		**Aggregate Size**		**Membrane integrity**	
	PF-68	*No additive*	*PF-68*	*No Additive*	*PF-68*	*No additive*
Mean	42.51	30.28	82.24	65.95	93.75	80.55
Variance	936.08	1094.10	254.67	81.32	289.22	403.76
Observations	8	8	8	8	8	8
Alpha	0.1		0.05		0.1	
Degree of freedom	7		7		7	
t-statistic	1.811		3.602		1.617	
$t_{(critical,\ upper\ tail)}$	1.415		1.415		1.415	

The factorial analysis was extended further to determine the effects of each variable on the biological responses. The calculated principal and interaction effects with their standard errors are summarised in Table 8.6. The standard error of individual effect was estimated from variance of the effects of two-factor and three-factor interactions. Variance is the sum of squares of the effects of two-factor and three-factor interactions divided by the total number of factor-interactions, N (Box et al., 1978).

$$\text{Standard error} = \sqrt{\frac{\sum_{i=1}^{N} \text{Effects}^2}{N}}$$

The general linear regression model for this factorial design, which includes all effects, is defined as

$$Y_i = \beta_0 + \beta_1 S + \beta_2 T + \beta_3 C + \beta_4 ST + \beta_5 SC + \beta_6 TC + \beta_7 STC + \varepsilon_I \qquad (8.2)$$

where β_i is the regression coefficient and ε_i is the residual error, assuming individual data are normally distributed around zero mean with σ standard deviation ($\sim N(0,\sigma^2)$). An example of the estimated coefficients in the saturated model for mitochondrial activity (Y_1) at 5% level are summarised in Table 8.7.

Table 8.6: Principal and interaction effects of the 2^3 factorial experiments

Effect	Estimate ± Standard Error					
	Y_1		Y_2		Y_3	
Average	42.51	±6.56	82.24	±5.55	93.73	±6.82
Main effects						
S	-44.26	±13.11	-18.35	±11.09	-9.97	±13.64
T	-23.59	±13.11	-7.94	±11.0	-12.00	±13.64
C	0.031	±13.11	0.008	±11.0	4.92	±13.64
Two-factor interaction						
ST	1.96	±13.11	-18.37	±11.0	-12.85	±13.64
TC	19.31	±13.11	6.78	±11.0	9.04	±13.64
SC	-1.64	±13.11	4.98	±11.0	11.96	±13.64
Three-factor interaction						
STC	-17.55	±13.11	-9.13	±11.0	18.83	±13.64

Table 8.7: The coefficients for the saturated linear regression model for mitochondrial activity (Y_1) . The model was estimated by least square method.

Factor	μ	*S*	*T*	*C*	*ST*	*SC*	*TC*	*STC*
Coefficient	β_0	β_1	β_2	β_3	β_4	β_5	β_6	β_7
Value	42.52	-22.13	-11.80	4.29	0.978	-0.819	-9.65	-8.78

However, in a factorial design, there are random effects, as well as, the effects of real significance. The calculated principal and interaction effects in the factorial design in Table 8.6 suggested that rotational speed (S) and time (T) were the main effects for all biological responses. Nevertheless, large ST interaction for Y_2 and Y_3 inferred that the S and T could not be interpreted separately for these two responses (Box et al., 1978). This effect could evidently arise from the difference in sensitivity to shear stress at different times. Consider the two-way tables in Figure 8.3, which shows that interaction effect of shear and time for Y_2 and Y_3. The shear effect at low time was almost insignificant at 0.05 for Y_2, and 2.9 for Y_3, while the shear effect at high time was 36.8 and 22.9 for Y_2 and Y_3, respectively.

The binary interactions with concentration in aggregate size and membrane integrity seemed to be large, but insignificant compared to other large effects, owing to the fact that these assays were less sensitive in detecting cellular level responses. The mitochondrial responses showed that the TC and STC provided significant interaction effects. Concentration levels alone appear to have an insignificant effect on the mean. A rough observation in Figure 8.4 indicates that 0.1% (w/v) PF-68 appeared to provide improved cell protection compared to that for lower concentration of 0.05%(w/v) at high shearing speed and exposure time. These observations highlighted the difference in sensitivity to concentration effect at different shear stress and time levels. Unfortunately, it remains difficult to conclude with absolute certainty, as the separation between the two concentration levels might have been too narrow to induce any significant signs of improvement in the results.

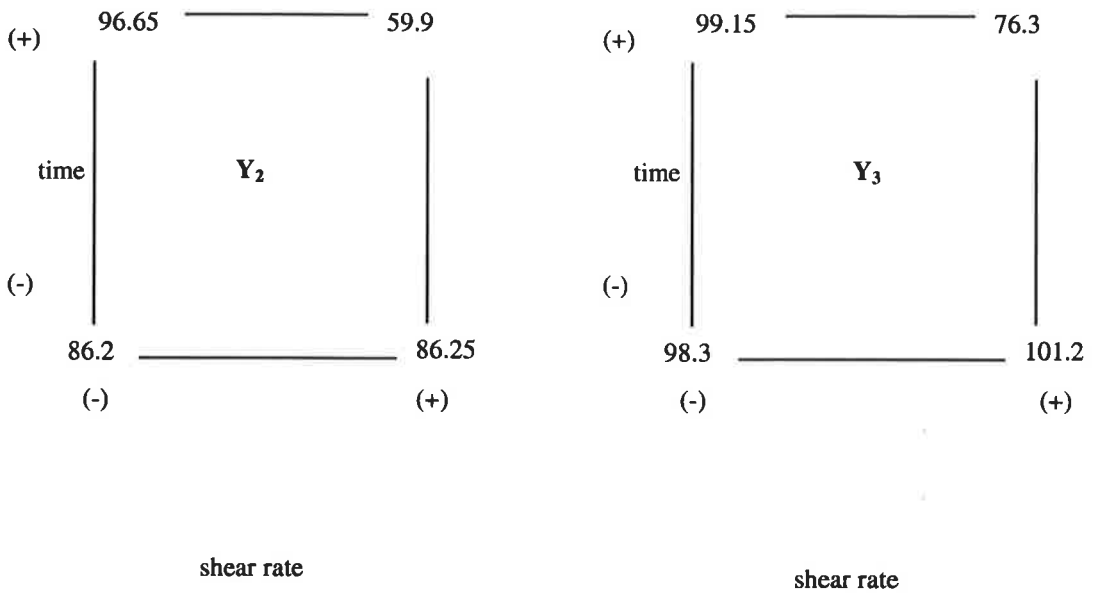

Figure 8.3. The shear rate- time (ST) interaction pilot plot for aggregate size (Y_2) and membrane integrity (Y_3).

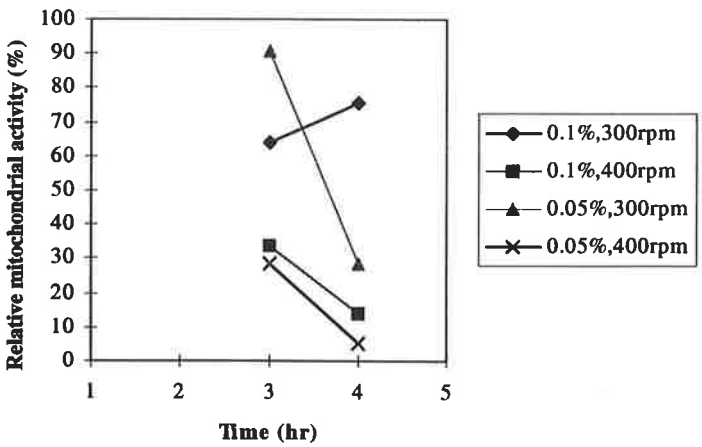

Figure 8.4. Comparison of the PF-68 concentration effects at different rotational speeds and times

For the regression models, the random factors had to be eliminated. The significance of each effect on the model was determined by plotting the normal score plots of the effects. The normal scores can be calculated from the corresponding normal probability of each effect, where P_i is defined by (Box et al, 1978):

$$P_i = 100\left((i-0.5)/(N-1)\right) \qquad (8.3)$$

where i is the order number of the effects ranked in order (from 1 to N), and N is the total number of runs, which is 8 in this case.

The final results were obtained from the StatPak tool provided by the Department of Applied Mathematics at the University of Adelaide. The normal score plots in Figures 8.5(a), (b) and (c) illustrate the effects of the mitochondrial activity (Y_1), aggregate size (Y_2) and membrane integrity (Y_3) respectively. Figure 8.5(a) indicates that S, T, STC and TC may have significant effects on mitochondrial activity, whereas the important effects on the aggregate size in Figure 8.5(b) include S, ST and TC. However, the regression analysis (at $\alpha = 0.05$), showed that the only significant effects for Y_2 were S and ST. The normal score plot of membrane integrity in Figure 8.5(c) suggests a possible broken line at zero normal score, which strongly suggests a possible outlier (Prat et al., 1989). The linear regression analysis for Y_3 responses confirms a standardised residual of an outlier, which lies ≥ 2 (Figure 8.6). The normal score plot for Y_3 after the outlier had been removed is shown in Figure 8.5(d). The only significant effects for Y_3 are the main effects S and T.

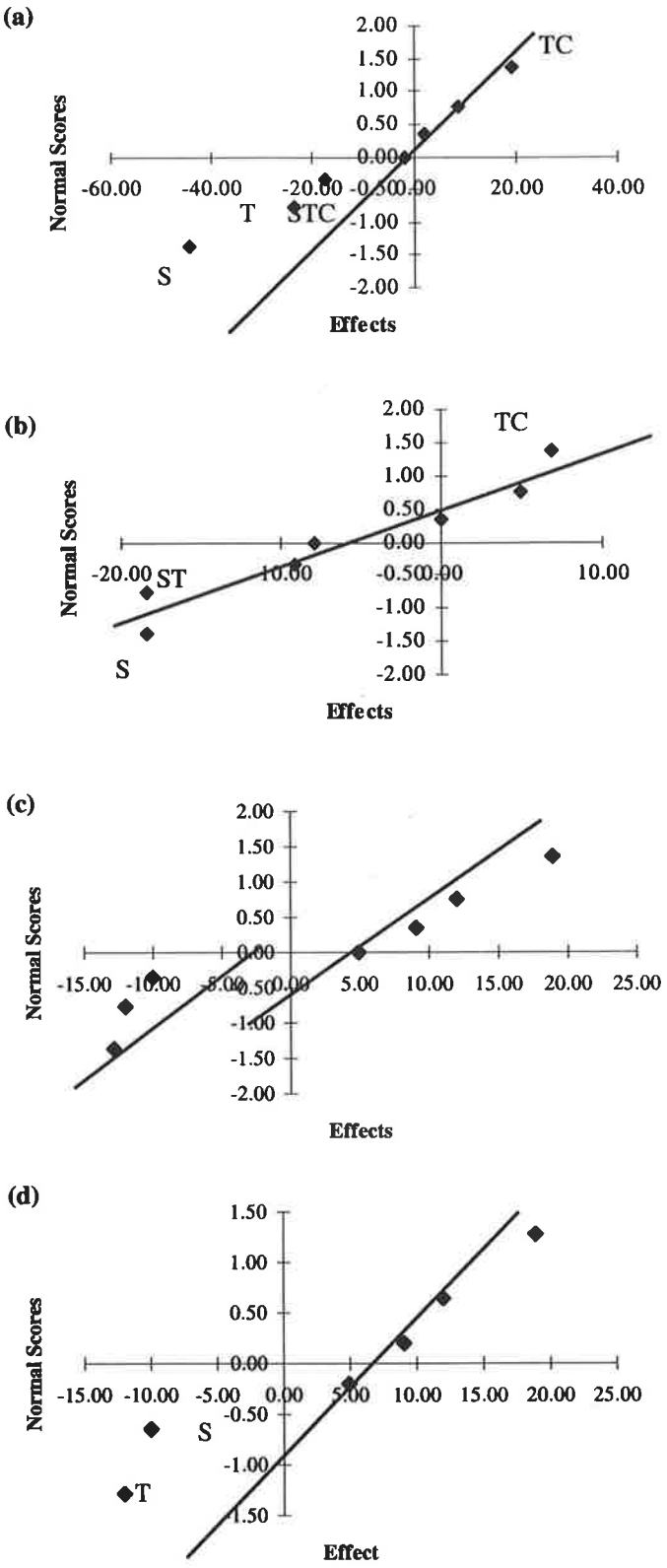

Figure 8.5. Normal score plots for the effects of **(a)** mitochondrial activity, **(b)** aggregate size, **(c)** membrane integrity with the outlier, and **(d)** membrane integrity without the outlier for 2^3 factorial designs with PF-68.

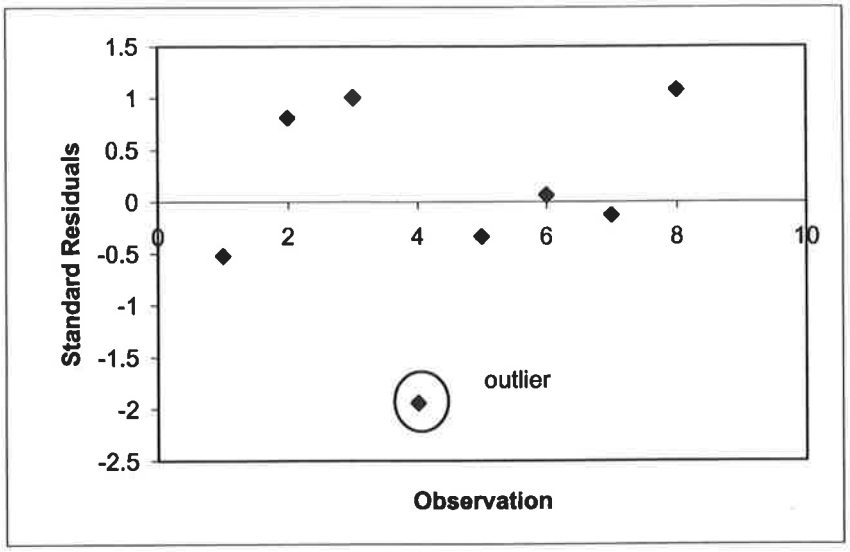

Figure 8.6. Standardised residual plot for the membrane integrity (Y_3) effects. The standard residual of an outlier ≥ 2.

Regression models were refitted to each response, using only significant factors. The new regression model for Y_1, hence becomes

$$Y_{1i} = \beta_0 + \beta_1 S + \beta_2 T + \beta_6 TC + \beta_7 STC + \varepsilon_1 \qquad (8.4)$$

A standard residual plot of the predicted values for Y_1 in Figure 8.7 shows complete random effects, as no recognisable pattern. The model is therefore retained. The estimated regression coefficients and their P-values are summarised in Tables 8.8, 8.9 and 8.10 for Y_1, Y_2 and Y_3 respectively.

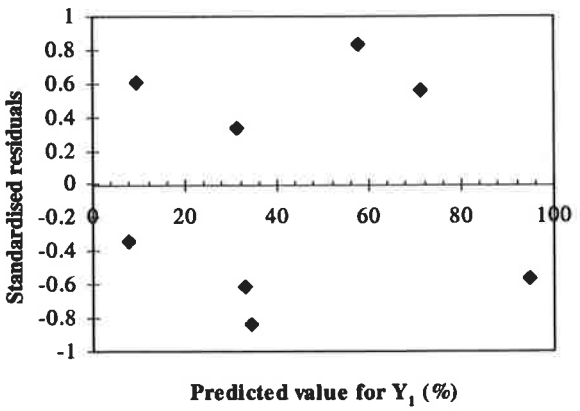

Figure 8.7. Standardised residual plot for predicted value for mitochondrial activity (Y_1).

Table 8.8: The calculated linear regression coefficients for Y_1 (standard error = 2.58)

	Coefficients	*P-value*
Intercept	42.51	0.0005
S	-22.13	0.0033
T	-11.80	0.0197
TC	9.65	0.0334
STC	-8.78	0.0426

Table 8.9: The calculated linear regression coefficients for Y_2 (standard error = 3.29)

	Coefficients	*P-value*
Intercept	82.24	1.92×10^{-6}
S	-9.18	0.0386
ST	-9.19	0.0385

Table 8.10: The calculated linear regression coefficients for Y_3

	Coefficients	*P-value*
Intercept	99.49	3.78×10^{-6}
S	0.774	0.796
T	-0.240	0.936

While no significant effect on the mean was observed for membrane integrity (Y_3) at 10% level, the regression models for Y_1 and Y_2 were significant. The ordinary least square linear regression models for mitochondrial activity (Y_1) and aggregate size (Y_2) are, therefore, described by;

$$Y_1 = 42.51 - 22.13S - 11.80T + 9.65TC - 8.78STC \quad (8.5)$$

$$Y_2 = 82.24 - 9.18S - 9.19ST \quad (8.6)$$

The outcome for the mitochondrial activity verified that shearing speed (S) and exposure time (T) produced strong influences on biological responses. The two-factor interaction

TC and three-factor interaction STC appeared to be significant despite the absence of the main effect C. It was suspected that the concentration levels might be too low to adequately distinguish any significant relationship. However, as time is considered an independent variable, it is possible that concentration effect may only prevail in presence of other main effects S and T (Cochran et al., 1957). As the protective effect of PF-68 is reportedly dependent on its concentration (Goldblum et al., 1990), this implies that higher PF-68 concentration may improve the activity at more severe shear conditions and longer exposure.

The results for break-up of aggregates were somewhat unexpected. The mean aggregate size distribution of carrot cultures grown in shaker flasks in normal medium and medium supplemented with 0.05% and 0.1% (w/v) PF-68 did not differ significantly. However, data showed that the aggregate size were only affected by shearing speed, and were not influenced by time or concentration. Similar results were observed in membrane integrity, where only minute differences were observed at different levels. No significant relationship shown at either levels could indicate that the assays were not sensitive enough to detect any small physiological change in cells. Additionally, the small difference between each factorial level would worsen the capability of these assays.

As plant cells are reportedly tolerant to bubble activity (Dunlop et al., 1994; Kieran et al., 2000), these results strongly suggested a biological interaction between PF-68 and cell membrane. The overall results implied a reduction in shear sensitivity of the cells grown in PF-68. Although PF-68 has been identified as a potentially excellent agent for improving shear tolerance of plant cells, these tests are only a preliminary indication. Further verification is required prior to its application in any large-scale processes. Additional considerations, such as other downstream processes and product safety, need to be accounted for when designing a scale-up process. Future work could prove PF-68 as a shear-protective agent for plant cell cultures.

8.4. Viscosity-Enhancing Polymer - Carboxymethyl Cellulose (CMC)

Unlike the surface-active polymers, viscosity-enhancing agents, such as CMC and dextran cannot bind to the cell membrane. Their sole means of protecting cells from hydrodynamic shear stress is by increasing the medium viscosity, thereby reducing the shear rate experienced by the cell.

As cell damage mechanisms may vary for different cell systems, several contradictory results have been reported. Dextran has been successfully used to dampen turbulent forces on microcarrier cultures (Cherry et al., 1988; Croughan et al., 1989). Goldblum et al. (1990) argued against the protective effect solely resulting from an increase medium viscosity. They also found that an 8-fold increase in viscosity by dextran decreased shear sensitivity of insect cells in laminar viscometric flow by a factor of 28. By contrast, Michaels et al. (1992) reported that dextran promoted cell damage in hybridoma cultures in bioreactors.

A 2^3 factorial design devised to determine whether CMC had a shear protective effect on plant cells (by increasing the medium viscosity). The results, combined with those for PF-68 may lead to the discovery of the fundamentals of the shear protective mechanisms for plant cells.

8.4.1. Determination of Concentration Levels

The relative growth rates of *Daucus carota* grown in WCM medium supplemented at five different concentrations of CMC (approx. MW 90000, Sigma) was determined (three replicates). The five concentrations levels were 0.05%, 0.1%, 0.2%, 0.3% and 0.5%(w/v), and control samples with no additive. Figure 8.8 summarises the average relative growth rate as a function of the CMC concentration.

CMC has no adverse effect on growth up to concentration of 0.5%(w/v). Optimum growth rate of 0.22 day^{-1} (25% higher than control) was observed at 0.1%(w/v) CMC. Cells cultured in medium supplemented with 0.5%(w/v) CMC showed signs of abnormal

growth. The exponential growth phase (6-day) cultures in 0.5% CMC became extremely viscous and yellow, and cell aggregates appeared abnormal. These cultures were, therefore, terminated after 7 days. From the results obtained, the concentration levels selected for the factorial study were 0.05% and 0.1% (w/v).

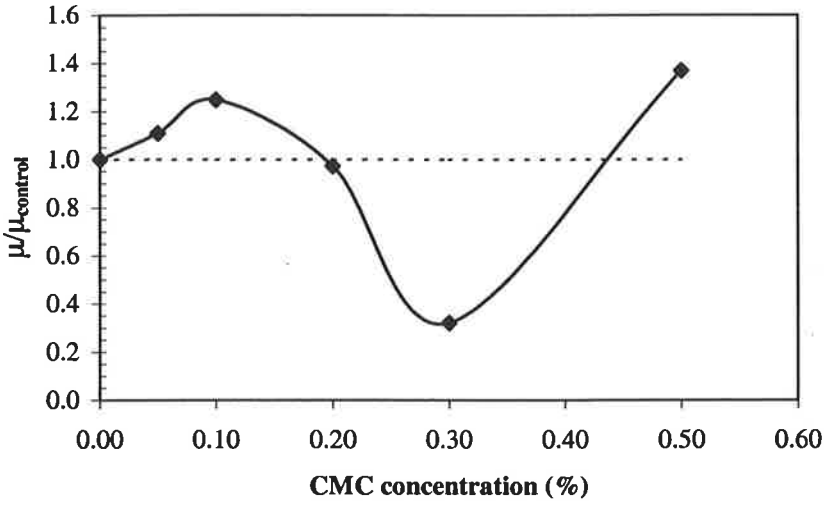

Figure 8.8. Relative growth rate of *D. carota* in WCM medium supplemented with different amounts of CMC.

8.4.2. Shear Protection by Carboxymethyl Cellulose

The randomised factorial experiments and their results are summarised in Table 8.11. The calculated principal and interaction effects are listed in Table 8.12 with their standard errors. The values roughly indicated that Y_1 was significantly influenced by the interactions ST, SC and STC, whereas S was the significant main effect for Y_2 and Y_3.

The concentration effects in Figure 8.9 show that cells exposed to low level of CMC (0.05%(w/v)) thrive better at lower speed, whereas cells grown in high level of CMC (0.1%(w/v)) perform better at higher speed.

Table 8.11: Results from the randomised 2^3 factorial experiments

Random Order	Run	Factors			Responses		
		S	T	C	Y_1 (%)	Y_2 (%)	Y_3 (%)
6	sc	+	-	+	56.5	92.8	106.1
7	tc	-	+	+	72.6	88.9	109.8
5	c	-	-	+	48.2	96.5	98.7
2	s	+	-	-	18.9	64.5	87.8
3	t	-	+	-	84.5	94.5	86.7
1	I	-	-	-	70.5	99.4	93.6
4	st	+	+	-	9.7	61.9	96.2
8	stc	+	+	+	13.8	70.6	93.6

The mitochondrial responses (Y_1) were compared with corresponding data for cells without additive in Figure 8.10. The results were less promising compared to those with PF-68. No apparent improvement was observed in cell responses grown in CMC. The Student's t-tests in Table 8.13 confirmed this observation by retaining the null hypothesis at 95% confidence level ($P>0.05$).

Table 8.12: The calculated principal and interaction effects for 2^3 factorial designs with CMC

Effect	Estimate ± Standard Error					
	Y_1		Y_2		Y_3	
Average	46.84	±7.99	83.66	±3.42	96.55	±2.61
Main effects						
S	-44.24	±15.98	-22.35	±6.84	-1.30	±5.22
T	-3.37	±15.98	-9.34	±6.84	0.03	±5.22
C	1.88	±15.98	7.14	±6.84	10.93	±5.22
Two-factor interaction						
ST	-22.56	±15.98	-3.06	±6.84	-2.05	±5.22
TC	-5.77	±15.98	-5.57	±6.84	-0.75	±5.22
SC	18.93	±15.98	11.35	±6.84	-3.11	±5.22
Three-factor interaction						
STC	-10.97	±15.98	-4.25	±6.84	-9.74	±5.22

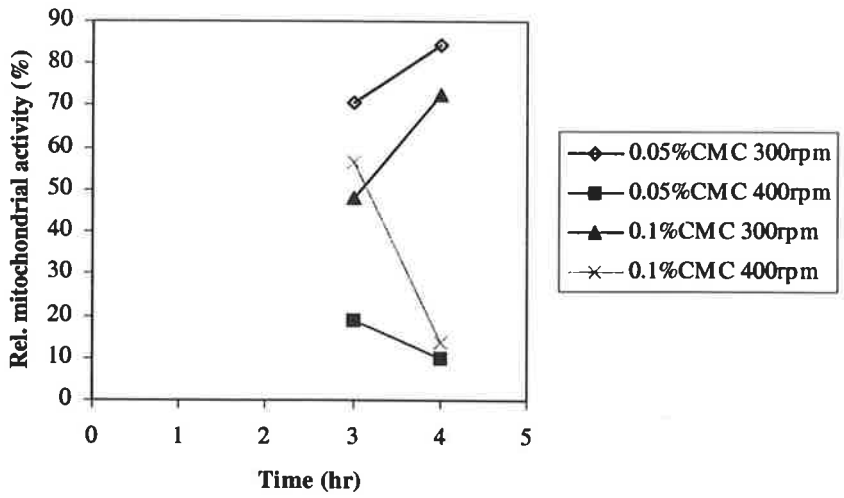

Figure 8.9. The effects of CMC concentration on the mitochondrial activity of *D. carota* at different exposure time.

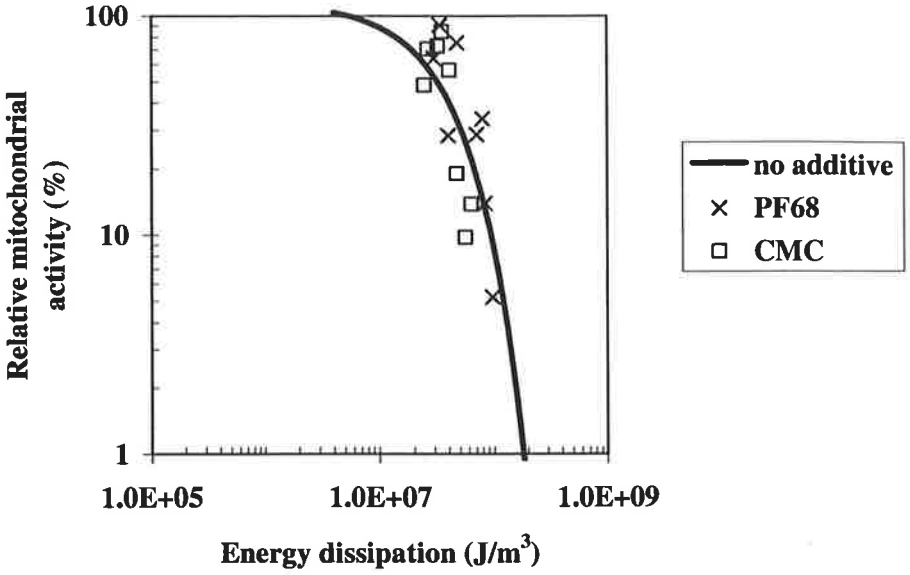

Figure 8.10. Comparison of the mitochondrial activity for *D. carota* in medium with PF-68 (0.05 and 0.1% (w/v)) (cross), CMC (0.05 and 0.1% (w/v)) (square) and without polymer supplement (solid curve).

Table 8.13. The results for the Student's t-test with CMC

Response	t-statistic	P-value
Mitochondrial activity	0.794	0.227
Aggregate size	1.12	0.149
Membrane integrity	0.03	0.488

Despite the results from the t-tests, further investigation was undertaken on the dependence of concentration effects on other parameters (i.e. rotational speed and time). The normal score plots of the factorial effects on mitochondrial activity (Y_1), aggregate size (Y_2) and membrane integrity (Y_3) are presented in Figures 8.11(a), (b) and (c) respectively. Although the normal score plots indicated the possible effects of shear stress and concentration on all three types of responses, the evidence was not sufficient to draw conclusions. The normal score plots for Y_1 and Y_2 showed strong effect of the shear stress, and some dependence of concentration on shear stress. However, the results from Y_3 were slightly inconsistent, as the tertiary interaction was observed without any binary interaction.

The linear regression analyses yield the coefficients (for $\alpha = 0.05$) listed in Tables 8.14, 8.15, and 8.16 for Y_1, Y_2 and Y_3 respectively.

As expected, shear stress was a major negative factor in the regression models. Even though concentration had positive effects on all responses (Table 8.12), the lack of the main effect C for Y_1 and regression model on Y_2 argued against its significance (at 95% confidence level).

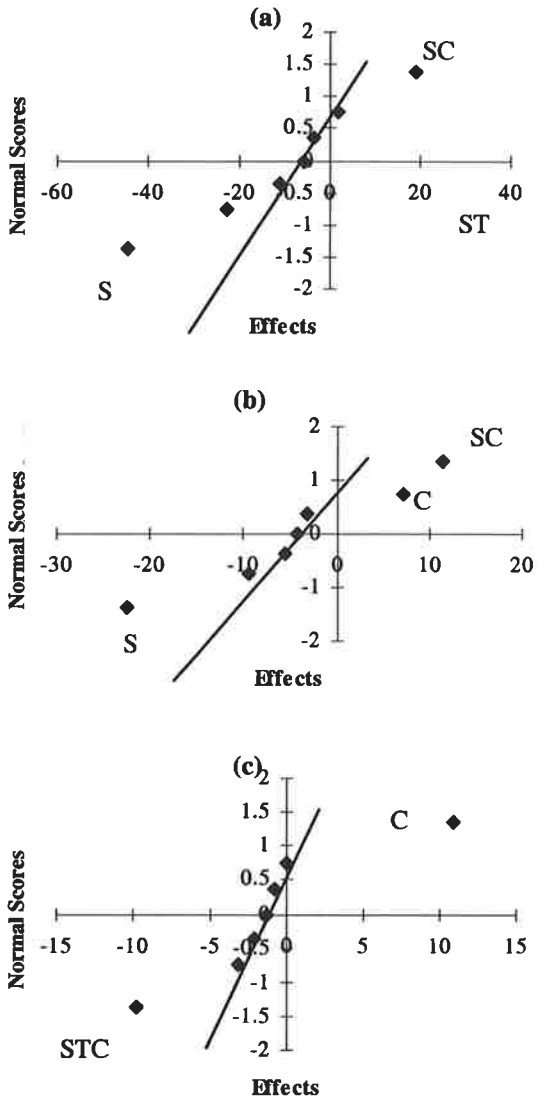

Figure 8.11. Normal score plots of the effects on **(a)** mitochondrial activity, **(b)** aggregate size, and **(c)** membrane integrity for 2^3 factorial designs with CMC.

Table 8.14: Linear regression coefficients for Y_1 (standard error = 3.24)

	Coefficient	*P-value*
Intercept	46.84	0.00013
S	-22.12	0.00242
ST	-11.28	0.02483
SC	9.47	0.04343

Table 8.15: Linear regression coefficients for Y_2 (standard error = 3.02)

	Coefficient	*P-value*
Intercept	83.66	1.01×10^{-5}
S	-11.18	0.021
C	3.57	0.302
SC	5.67	0.133

Table 8.16: Linear regression coefficients for Y_3 (standard error = 0.899)

	Coefficient	*P-value*
Intercept	96.55	1.32×10^{-9}
C	5.47	0.0017
STC	-4.87	0.0029

Despite the uncertainty surrounding the results for Y_2 and Y_3, a linear regression model for Y_1 can be described as

$$Y_1 = 46.84 - 22.12S + 9.47SC - 11.28ST \qquad (8.7)$$

While the factorial analysis suggested possible effects of CMC concentration level on shear protection, the t-tests showed insignificant improvement. It was, therefore, concluded that there was insufficient evidence to make any definite statement on the efficacy of CMC as a shear-protective agents for plant cells. As viscosity-enhancing agents reportedly perform poorer than surface-active agent in protecting animal cells (Michaels et al., 1992; Wu et al., 1995), the outcomes from these experiments on carrot cells were not completely

unexpected. Additionally, as CMC is hydrophilic, it has no physiological interaction with cell membrane. This finding verified the hypothesis that plant cells were protected through similar mechanisms to animal and insect cells. The mechanism of strengthening membrane structure and increasing membrane fluidity may be achieved by either (i) biological binding to cell phospholipid membrane, or (ii) forming a protective polymer layer surrounding the cell (Wu et al., 1995; Palomares et al., 2000).

8.5. Conclusions

The efficacy of shear protective effects of surface-active (PF-68) and viscosity-enhancing (CMC) polymers were investigated using 2^3 factorial designs. A significant improvement in biological responses of *D. carota* when grown in PF-68 supplemented medium, but not CMC. Concentration of both agents showed positive, but somewhat insignificant as the main effect. Shearing speed and exposure time were the two main effects influencing all physiological responses. Although different concentration levels of PF-68 showed no significant effect on the response, strong interactions between concentration and other factors were observed. Additionally, higher concentration of PF-68 seemed to provide a superior protective effect compared with lower concentration, while the reverse pattern was observed for CMC. These results indicated that effectiveness of concentration of these compounds may depend on the level of shear rate and time. In general, the protective effects were better detected at a cellular level (mitochondrial activity), rather than late physical attributes, such as membrane integrity. On the basis of these results, it was concluded that the protection was minor, and was primarily a result of the biological mechanism, where the surfactant polymers physically interact with the cell plasma membrane. However, like other biological systems, these results were a mere preliminary indication of further tests that are required before any serious conclusions were made.

CHAPTER 9

CONCLUSIONS

The prime objective of this project was to improve the characterisation and understanding of shear damage mechanisms in plant cells. To satisfy this goal, this work has focussed on the local interaction of the cell with shear flow structures. Studies were conducted with special considerations as to how the fluid-cell interaction might affect the sublytic responses mediated by calcium ions. Calcium signal transduction in sheared cells is believed to involve the mechano-sensitive calcium channels. Reduction of the interaction between turbulent eddies and the cells may alleviate this injurious effect. Consequently, the shear-protective ability of compounds, such as Pluronic F-68 and carboxymethyl cellulose was investigated to assess their role in alleviating the damaging effects of hydrodynamic shear in plant cells.

A novel experimental apparatus was designed to generate turbulent flow fields that resembled the bioreactor flow conditions. The advantages of the device over a conventional bioreactor were the smaller control volume and less variation in the flow field. The experimental device was consisted of a stainless steel annular bowl and a cylindrical stirrer. The stirrer rotated inside the annulus to generate turbulence within the annulus gap. The characterisation of the resulting flow pattern was quantified using a computational fluid dynamic software package CFX. The simulated results were obtained for several operating velocities to establish a relationship between local and measured hydrodynamic parameters.

The magnitude of shear damage sustained by plant cells can be quantified in terms of a number of biological responses. Three types of biological responses measured in this study included the relative mitochondrial activity, aggregate size and membrane integrity. The hierarchy of these responses confirmed that mitochondrial activity provided the most sensitive responses, whilst membrane integrity was the least sensitive. Cell damage

occurred over the total energy dissipation range from 10^6 to 10^8 J/m^3, which was comparable to the values found for *Morinda citrifolia* and *Atropa belladonna* (Wongsamuth et al., 1997; MacLoughlin et al., 1998). However, the range of turbulent shear damage was found to be two orders of magnitude higher than earlier results reported for *Daucus carota* (Dunlop et al., 1994). As stated, the three biological response indicators yielded different values for the onset of cell damage. Approximately 90% of cell remained viable at total energy dissipation of 9.5×10^6, 1.76×10^7 and 4.5×10^7 J/m^3 for mitochondrial activity, aggregate size and membrane integrity, respectively. This suggests that significant variation exists between different types of biological response. Furthermore, these responses can vary significantly with differing shear environment. 3D regression analysis of viability as a function of energy dissipation rate (ε) and time (t) demonstrated strong dependence for biological responses with both time and energy dissipation rate. These analyses confirmed that a global critical cumulative dissipation limit might not be optimal for all types of cells. This finding prompted further investigation into other appropriate parameters to model the shear response of plant cells. Regression Analysis indicated that the alternative design parameter proposed by Jüsten et al. (1996) was a more appropriate design parameter, including the local energy dissipation rate, the impeller geometry, and fluid circulation time. This parameter has several advantages over the other parameters as it is independent of the operating volume and is applicable to any impeller configuration.

The kinetics of the biological responses were found to follow first-order with an initial lag phase. The rate of decay increased with increase in the rate of energy dissipation. As expected, mitochondrial activity experienced the fastest decay rate, followed by aggregate size and membrane integrity. The decay rate of aggregate size exhibited strong correlation to that for mitochondrial activity, suggesting that a relationship between break-up of aggregates and cellular activity may exist.

The relationship between cell aggregate size and shear stress experienced by the aggregate was studied by characterising the irregularity of cell aggregate structures. Analysis of their geometric factors confirmed that most cell aggregates were highly irregular and their shapes deviated substantially from the spherical aggregates. Classification of the morphology of cell aggregates indicated that larger aggregates broke preferentially to form smaller and rounder aggregates. These smaller aggregates were found to be more stable

and shear-resistant. This finding agreed with the results reported for *Morinda citrifolia* (MacLoughlin et al., 1998).

Modelling of surface shear stress and membrane stretching in cell aggregates confirmed that larger aggregates experienced higher surface shear stress. The surface shear stress could cause severe membrane stretching that was sufficient to open a stretch-activated calcium channel. Consequently, it was concluded that the membrane stretching might play an important role in various sublytic responses associated with calcium ion regulation.

Evidence has confirmed that the shear stress signal pathway in plant cells is mediated by calcium ions. The change in calcium concentration during the sublytic responses in plant cells was investigated by kinetic modelling. A kinetic model was developed to describe a change in calcium level in complex biological systems subject to mechanical forces. The model assumed that calcium transient response to fluid shear stress in plant cells occurred solely through mechano-sensitive channels. The effect of fluid shear stress on these channels is related to the membrane stretching estimated by the surface shear stress model. This proposed kinetic model included the primary functions of the mitochondria, the vacuole and the endoplasmic reticulum. A mathematical expression was derived from Ca^{2+} mass balances, which yielded a system of differential equations. These differential equations were simplified to algebraic equations by Laplace transformation. These simplified equations were simulated with Matlab-Simulink. However, due to the lack of appropriate experimental data and difficulty in measuring transient Ca^{2+} responses in plant cells suspended in shear flow, the modelling results were validated with similar data obtained from mammalian cells. The prediction of calcium transient by the Matlab-Simulink model generally agreed well with calcium responses in endothelial cells subjected to shear stress.

Calcium transient obtained from the model for a damaged cell with abnormal mitochondrial function showed a response that resembled the pattern found in apoptotic cells. The results confirmed the important role of the mitochondria in calcium regulation within the cell. However, despite these reasonable outcomes, the model proposed still requires further validation with data for plant cells exposed to hydrodynamic shear. Unfortunately, the validation can only be argued by comparison with data from

mammalian cells, until the techniques for the measurement of calcium in suspended plant cells are developed.

Factorial studies on shear protection demonstrated that a surface-active agent: Pluronic F-68 (PF-68) could alleviate the damaging effect of turbulent shear stress. Student's t tests on the mitochondrial activity confirmed a significant improvement in the viability of carrot cells grown in PF-68 supplemented medium. However, a viscosity-enhancing agent, carboxymethyl cellulose (CMC) failed to provide any significant protection for the carrot cells. The lack of improvement by CMC indicated that the shear protective mechanism was mediated by an interaction between the agent and the cell membrane. The strengthening of the cell membrane may result from increasing membrane fluidity. PF-68 may also provide an alternative protective mechanism by forming of protective polymer layer surrounding the cells and preventing their interaction with the turbulent eddies.

Recommendations for future research include further studies of the role of calcium in sublytic responses in plant cells. Validation of the proposed kinetic model requires quantification of intracellular calcium concentration of plant cells in response to various fluid shear stresses. Although the current techniques for calcium measurement may be inappropriate for shear-sensitivity studies, they could be used to correlate the effects of mechanical stress on the intracellular calcium level. Furthermore, characterisation of calcium transduction pathway in plant cells requires the understanding of the events associated with cellular dysfunctions induced by a change in calcium concentration. The critical calcium transient leading to irreversible cellular damage is a vital factor in establishing these biological events. Application of appropriate protein and coenzyme inhibitors would enable some of these pathways to be predicted. Finally, it is recommended that the shear-protective effects of PF-68 be verified with other cell lines and shear environments. The moderation of the turbulent stress experienced by the cell afforded by these shear-protective agents could play a crucial role in reducing the intensity of the associated calcium transients.

An improvement of current plant cell culture technology are only likely to be achieved as a result of better understanding of the rate limiting steps, particularly knowledge of the cell's sensitivity to hydrodynamic shear. This work has addressed some of the important aspects of the studies of shear sensitivity in plant cells. The primary focus was directed toward the

local turbulent forces experienced by the cells, and their effects on calcium transient responses. The shear-protective study on plant cells has also proven to be encouraging. It may provide an alternative option for improvements in productivity, avoiding the need to design low-shear bioreactors or to develop more shear-resistant plant cell strains using genetic means. The findings presented here have introduced valuable means of improving the shear-sensitivity studies. They have enhanced the current understanding of cell-fluid interaction and the associated calcium signalling, which is one of the most important keys to elucidate the response mechanisms of plant cells to hydrodynamic shear stress.

APPENDICES

APPENDIX A
WILD CARROT MEDIUM INGREDIENTS

Table A.1: Ingredients for wild carrot medium (WCM)

Compound	Quantity (g/L)
2,4-dichlorophynoxyacetic acid	0.5×10^{-3}
$CaCl_2.2H_2O$	0.225
$CuSO_4.5H_2O$	1.5×10^{-5}
FeNaEDTA	0.01825
H_3BO_3	0.024
KH_2PO_4	0.068
KI	0.38×10^{-3}
KNO_3	4.0
$MgSO_4.7H2O$	0.185
$MnSO_4.H2O$	0.07
$NaMoO_4.2H_2O$	1.4×10^{-5}
NH_4Cl	0.54
Sucrose	20.0
Thiamine.HCl	0.003
$ZnSO_4.7H_2O$	0.04

APPENDIX B

EXAMPLES OF CFX CODE

1. Simplified Model with Rotating Coordinates

The following program code is an example of a CFX command file for transient flow using rotating coordinates (no baffles). Water was used as the standard fluid. In this example, the rotational speed is 400rpm, which corresponds to 2 m/s.

```
>>CFX4
 >>OPTIONS
  TWO DIMENSIONS
  BODY FITTED GRID
  ROTATING COORDINATES
  TURBULENT FLOW
  ISOTHERMAL FLOW
  INCOMPRESSIBLE FLOW
  TRANSIENT FLOW
  NUMBER OF USER FUEL COMPONENTS 0
  NUMBER OF FUELS 1
  NUMBER OF OXIDANTS 1
  USER SCALAR EQUATIONS 3
  MASS FRACTION EQUATIONS 0
  CHEMICAL SPECIES EQUATIONS 0
  MAXIMUM DEGREE OF POLYNOMIAL DEPENDENCE ON T 0
  MAXIMUM NUMBER OF MATERIAL TYPES 10
  NUMBER OF PHASES 1
  NUMBER OF PARTICLE MASS FRACTIONS 0
 >>VARIABLE NAMES
  U VELOCITY 'U VELOCITY'
  V VELOCITY 'V VELOCITY'
  W VELOCITY 'W VELOCITY'
  PRESSURE 'PRESSURE'
  DENSITY 'DENSITY'
  VISCOSITY 'VISCOSITY'
  K 'K'
  EPSILON 'EPSILON'
```

```
  USER SCALAR1 'SHEAR RATE'
  USER SCALAR2 'XY NODAL SHEAR STRESS'
  USER SCALAR3 'YPLUS'
>>MODEL DATA
 >>SET INITIAL GUESS
  >>INPUT FROM FILE
   READ DUMP FILE
  >>DIFFERENCING SCHEME
   ALL EQUATIONS 'HYBRID'
   U VELOCITY 'QUICK'
   V VELOCITY 'QUICK'
   YPLUS 'NO MATRIX'
   SHEAR RATE 'NO MATRIX'
   XY NODAL SHEAR STRESS 'NO MATRIX'
 >>PHYSICAL PROPERTIES
   >>STANDARD FLUID
    FLUID 'WATER'
    STANDARD FLUID REFERENCE TEMPERATURE 2.7300E+02
  >>ROTATING COORDINATES PARAMETERS
   OMEGA 0.0 0.0 41.8879
   POSITION VECTOR ON ROTATING AXIS 0.0 0.0 0.0
  >>TRANSIENT PARAMETERS
    >>ADAPTIVE TIME STEPPING
     NUMBER OF TIME STEPS 1000000000
     INITIAL TIME STEP 1.0000E-04
     MINIMUM TIME STEP 1.0000E-05
     MAXIMUM TIME STEP 1.0000E-04
     MULTIPLY TIME STEP BY 2.0000E+00
     DIVIDE TIME STEP BY 2.0000E+00
     MINIMUM INTERVAL BETWEEN INCREMENTS 5
     MAXIMUM NUMBER OF CONTIGUOUS DECREMENTS 500
     BACKWARD DIFFERENCE
     INITIAL TIME 0.0000E+00
     MAXIMUM TIME 10.0000E-01
    >>EXTRAPOLATION ORDER
     ALL EQUATIONS 2
   >>TURBULENCE PARAMETERS
    >>TURBULENCE MODEL
     TURBULENCE MODEL 'LOW REYNOLDS NUMBER K-EPSILON'
>>SOLVER DATA
```

```
>>PROGRAM CONTROL
 MINIMUM NUMBER OF ITERATIONS 50
 MAXIMUM NUMBER OF ITERATIONS 500
 MASS SOURCE TOLERANCE 1.0000E-06
 ITERATIONS OF TURBULENCE EQUATIONS 3
 ITERATIONS OF VELOCITY AND PRESSURE EQUATIONS 1
 ITERATIONS OF TEMPERATURE AND SCALAR EQUATIONS 1
 ITERATIONS OF HYDRODYNAMIC EQUATIONS 1
 SOLVER DEBUG PRINT STREAM 20
>>EQUATION SOLVERS
 U VELOCITY 'AMG'
 V VELOCITY 'AMG'
 PRESSURE 'AMG'
 K 'LINE SOLVER'
 EPSILON 'LINE SOLVER'
>>TRANSIENT CONTROL
 >>CONVERGENCE TESTING ON VARIABLE
  PRESSURE
 >>CONTROL PARAMETERS
  MINIMUM RESIDUAL VALUE 5.0000E-02
  MAXIMUM RESIDUAL VALUE 5.0000E-01
  REDUCTION FACTOR 2.0000E+00
  DIVERGENCE RATIO 1.0000E+05
>>UNDER RELAXATION FACTORS
 U VELOCITY 6.5000E-01
 V VELOCITY 6.5000E-01
 PRESSURE 1.0000E+00
 VISCOSITY 1.0000E+00
 K 7.0000E-01
 EPSILON 7.0000E-01
>>MODEL BOUNDARY CONDITIONS
 >>WALL BOUNDARIES
  PATCH NAME 'WALL_IN'
  ANGULAR VELOCITY 0.0 0.0 -41.8879
 >>WALL BOUNDARY CONDITIONS
 PATCH NAME 'WALL_OUT'
  ANGULAR VELOCITY 0.0 0.0 -41.8879
>>OUTPUT OPTIONS
 >>LIMITS
  MAXIMUM NUMBER OF LINE GRAPHS 20
```

```
>>FRONTEND PRINTING
 NO TOPOLOGY STRUCTURE
 NO REAL BOUNDARY CONDITIONS
>>DUMP FILE OPTIONS
 TIME INTERVAL 5.0000E-02
 U VELOCITY
 V VELOCITY
 YPLUS
 XY NODAL SHEAR STRESS
 SHEAR RATE
 PRESSURE
 K
 EPSILON
>>LINE GRAPH DATA
 XYZ 0.050725 -3.00000E-03 0.000000
 EACH TIME STEP
 FILE NAME 'MONITOR_1'
 PRESSURE
 K
 EPSILON
 XY NODAL SHEAR STRESS
 SHEAR RATE
>>LINE GRAPH DATA
 XYZ 0.049133 -3.00000E-03 0.000000
 EACH TIME STEP
 FILE NAME 'MONITOR_2'
 PRESSURE
 K
 EPSILON
 SHEAR RATE
 XY NODAL SHEAR STRESS
>>LINE GRAPH DATA
 XYZ 0.048858 -6.00000E-03 0.00000
 EACH TIME STEP
 FILE NAME 'MONITOR_3'
 PRESSURE
 K
 EPSILON
 SHEAR RATE
 XY NODAL SHEAR STRESS
```

```
>>LINE GRAPH DATA
 XYZ 0.048395 -9.000000E-03 0.00000
 EACH TIME STEP
 FILE NAME 'MONITOR_4'
 PRESSURE
 K
 EPSILON
 SHEAR RATE
 XY NODAL SHEAR STRESS
>>LINE GRAPH DATA
 XYZ 1.000000E-03 -0.049225 0.00000
 EACH TIME STEP
 FILE NAME 'MONITOR_5'
 PRESSURE
 K
 EPSILON
 SHEAR RATE
 XY NODAL SHEAR STRESS
>>LINE GRAPH DATA
 XYZ -0.049225 1.000000E-03 0.00000
 EACH TIME STEP
 FILE NAME 'MONITOR_6'
 PRESSURE
 K
 EPSILON
 SHEAR RATE
 XY NODAL SHEAR STRESS
>>LINE GRAPH DATA
 XYZ 1.000000E-03 0.049225 0.00000
 EACH TIME STEP
 FILE NAME 'MONITOR_7'
 PRESSURE
 K
 EPSILON
 SHEAR RATE
 XY NODAL SHEAR STRESS
>>STOP
```

2. Modified Model using Sliding Mesh

The following CFX program code is an example of a command file for transient flow using sliding mesh (for the cases with and without baffles). The rotational speed for this case is 400rpm, which corresponds to 2 m/s.

```
>>CFX4
 >>OPTIONS
  TWO DIMENSIONS
  BODY FITTED GRID
  UNMATCHED GRIDS
  TRANSIENT GRID
  TURBULENT FLOW
  ISOTHERMAL FLOW
  INCOMPRESSIBLE FLOW
  TRANSIENT FLOW
  NUMBER OF USER FUEL COMPONENTS 0
  NUMBER OF FUELS 1
  NUMBER OF OXIDANTS 1
  USER SCALAR EQUATIONS 2
  MASS FRACTION EQUATIONS 0
  CHEMICAL SPECIES EQUATIONS 0
  MAXIMUM DEGREE OF POLYNOMIAL DEPENDENCE ON T 0
  MAXIMUM NUMBER OF MATERIAL TYPES 10
  NUMBER OF PHASES 1
  NUMBER OF PARTICLE MASS FRACTIONS 0
 >>VARIABLE NAMES
  U VELOCITY 'U VELOCITY'
  V VELOCITY 'V VELOCITY'
  W VELOCITY 'W VELOCITY'
  PRESSURE 'PRESSURE'
  DENSITY 'DENSITY'
  VISCOSITY 'VISCOSITY'
  K 'K'
  EPSILON 'EPSILON'
  USER SCALAR1 'SHEAR RATE'
  USER SCALAR2 'XY NODAL SHEAR STRESS'
>>MODEL TOPOLOGY
 >>GLUE PATCHES FOR UNMATCHED GRIDS
```

```
   FIRST PATCH NAMES 'BLKBDYCIN'
   SECOND PATCH NAMES 'BLKBDYCOUT'
>>MODEL DATA
 >>SET INITIAL GUESS
  >>INPUT FROM FILE
   READ DUMP FILE
 >>DIFFERENCING SCHEME
  ALL EQUATIONS 'VAN LEER'
  U VELOCITY 'QUICK'
  V VELOCITY 'QUICK'
  SHEAR RATE 'NO MATRIX'
  XY NODAL SHEAR STRESS 'NO MATRIX'
 >>PHYSICAL PROPERTIES
  >>STANDARD FLUID
   FLUID 'WATER'
   STANDARD FLUID REFERENCE TEMPERATURE 2.7300E+02
  >>GRID MOTION PARAMETERS
   PATCH NAME 'USER3D1'
   DIRECTION VECTOR ON MOTION AXIS 0.0 0.0 1.0
   ROTATION SPEED 41.8879  /*400rpm*/
  >>TRANSIENT PARAMETERS
   >>ADAPTIVE TIME STEPPING
    NUMBER OF TIME STEPS 1000000000
    INITIAL TIME STEP 1.0000E-04
    MINIMUM TIME STEP 1.0000E-06
    MAXIMUM TIME STEP 6.0000E-04
    MULTIPLY TIME STEP BY 2.0000E+00
    DIVIDE TIME STEP BY 2.0000E+00
    MINIMUM INTERVAL BETWEEN INCREMENTS 5
    MAXIMUM NUMBER OF CONTIGUOUS DECREMENTS 500
    BACKWARD DIFFERENCE
    /*QUADRATIC TIME DIFFERENCING*/
    INITIAL TIME 0.0000E+00
    MAXIMUM TIME 1.0000E+00
   >>EXTRAPOLATION ORDER
    ALL EQUATIONS 2
  >>TURBULENCE PARAMETERS
   >>TURBULENCE MODEL
    TURBULENCE MODEL 'LOW REYNOLDS NUMBER K-EPSILON'
>>SOLVER DATA
```

```
>>PROGRAM CONTROL
  MINIMUM NUMBER OF ITERATIONS 50
  MAXIMUM NUMBER OF ITERATIONS 200
  MASS SOURCE TOLERANCE 1.0000E-06
  ITERATIONS OF TURBULENCE EQUATIONS 3
  ITERATIONS OF VELOCITY AND PRESSURE EQUATIONS 1
  ITERATIONS OF TEMPERATURE AND SCALAR EQUATIONS 1
  ITERATIONS OF HYDRODYNAMIC EQUATIONS 1
  SOLVER DEBUG PRINT STREAM 20
  OUTPUT MONITOR POSITION FIXED WITHIN GRID
 >>DEFERRED CORRECTION
  K START  30
  K END 40
  EPSILON START 30
  EPSILON END 40
 >>EQUATION SOLVERS
  U VELOCITY 'GENERAL AMG'
  V VELOCITY 'GENERAL AMG'
  PRESSURE 'GENERAL AMG'
  K 'LINE SOLVER'
  EPSILON 'LINE SOLVER'
 >>TRANSIENT CONTROL
  >>CONVERGENCE TESTING ON VARIABLE
   U VELOCITY
  >>CONTROL PARAMETERS
   MINIMUM RESIDUAL VALUE 1.0000E-05
   MAXIMUM RESIDUAL VALUE 1.0000E-04
   REDUCTION FACTOR 2.0000E+00
   DIVERGENCE RATIO 1.0000E+10
/* >>UNDER RELAXATION FACTORS
  U VELOCITY 6.0000E-01
  V VELOCITY 6.0000E-01
  PRESSURE 1.0000E+00
  VISCOSITY 1.0000E+00
  K 1.0000E-01
  EPSILON 1.0000E-01 */
 >>COURANT NUMBER FALSE TIMESTEPS
  ALL EQUATIONS 1.0
>>MODEL BOUNDARY CONDITIONS
>>OUTPUT OPTIONS
```

```
>>LIMITS
 MAXIMUM NUMBER OF LINE GRAPHS 20
>>FRONTEND PRINTING
 /*NO TOPOLOGY STRUCTURE*/
 /*NO REAL BOUNDARY CONDITIONS*/
>>DUMP FILE OPTIONS
 TIME INTERVAL 2.0000E-02
 INITIAL GUESS
 FINAL SOLUTION
 GEOMETRY DATA
 U VELOCITY
 V VELOCITY
 EPSILON
 XY NODAL SHEAR STRESS
 SHEAR RATE
>>LINE GRAPH DATA
 RESIDUAL
 FILE NAME 'resid'
>>LINE GRAPH DATA
 XYZ 0.04893 -0.00449 0.000000
 EACH TIME STEP
 FILE NAME 'MONITOR_1'
 PRESSURE
 K
 EPSILON
 XY NODAL SHEAR STRESS
 SHEAR RATE
>>LINE GRAPH DATA
 XYZ 0.05044 -0.004494 0.000000
 EACH TIME STEP
 FILE NAME 'MONITOR_2'
 PRESSURE
 K
 EPSILON
 SHEAR RATE
 XY NODAL SHEAR STRESS
>>LINE GRAPH DATA
 XYZ 0.05009 -0.007473 0.00000
 EACH TIME STEP
 FILE NAME 'MONITOR_3'
```

```
 PRESSURE
 K
 EPSILON
 SHEAR RATE
 XY NODAL SHEAR STRESS
>>LINE GRAPH DATA
 XYZ 0.04956 -0.01042 0.00000
 EACH TIME STEP
 FILE NAME 'MONITOR_4'
 PRESSURE
 K
 EPSILON
 SHEAR RATE
 XY NODAL SHEAR STRESS
>>LINE GRAPH DATA
 XYZ 0.04885 -0.01334 0.00000
 EACH TIME STEP
 FILE NAME 'MONITOR_5'
 PRESSURE
 K
 EPSILON
 SHEAR RATE
 XY NODAL SHEAR STRESS
>>LINE GRAPH DATA
 XYZ 0.04798 -0.01621 0.00000
 EACH TIME STEP
 FILE NAME 'MONITOR_6'
 PRESSURE
 K
 EPSILON
 SHEAR RATE
 XY NODAL SHEAR STRESS
>>LINE GRAPH DATA
 XYZ 0.04115 -0.02951 0.00000
 EACH TIME STEP
 FILE NAME 'MONITOR_7'
 PRESSURE
 K
 EPSILON
 SHEAR RATE
```

```
  XY NODAL SHEAR STRESS
 >>LINE GRAPH DATA
  XYZ 0.03581 -0.03581 0.00000
  EACH TIME STEP
  FILE NAME 'MONITOR_8'
  PRESSURE
  K
  EPSILON
  SHEAR RATE
  XY NODAL SHEAR STRESS
>>STOP
```

APPENDIX C

REGRESSION ANALYSIS ON ENERGY DISSIPATION RATE AND TIME

The proposed linear regression model in terms of energy dissipation ε and time t has the form

$$Y_i = \beta_0 + \beta_1 \varepsilon + \beta_2 t + \alpha_i$$

where Y_i refers to the biological response, $\beta\alpha_i$ represents the regression coefficients, and α_i represents the residual. All analyses were calculated at 5% significant level. Tables C.1, C.2 and C.3 summarise the results for regression statistics, the Anova analysis and the statistics for regression coefficients for mitochondrial activity (Y_1), respectively.

Table C.1: Regression results for mitochondrial activity

Regression Statistics	
Multiple R	0.847
R^2	0.717
Adjusted R^2	0.679
Standard Error	18.04
Observations	18

Table C.2: Anova results for mitochondrial activity

	Degree of freedom	*SS*	*MS*	*F*	*Significance F*
Regression	2	12350.6	6175.3	18.97	7.81×10^{-5}
Residual	15	4883.2	325.55		
Total	17	17233.8			

Table C.3: Statistics for regression coefficients of mitochondrial activity results

	Coefficients	*Standard Error*	*t-stat*	*P-value*	*Lower 95%*	*Upper 95%*
Intercept	129.64	15.09	8.592	3.54×10^{-7}	97.48	161.8
Energy dissipation rate (W/kg)	-12.36	2.824	-4.378	0.00054	-18.38	-6.343
Time (hour)	-10.60	2.491	-4.256	0.00069	-15.91	-5.292

Similar statistical analyses for relative aggregate size (Y_2) are summarised in Tables C.4, C.5 and C.6.

Table C.4: Regression results for aggregate size

Regression Statistics	
Multiple R	0.752
R^2	0.566
Adjusted R^2	0.508
Standard Error	13.42
Observations	18

Table C.5: Anova results for aggregate size

	degree of freedom	*SS*	*MS*	*F*	*Significance F*
Regression	2	3525.5	1762.8	9.783	0.0019
Residual	15	2702.7	180.18		
Total	17	6228.2			

Table C.6: Statistics for regression coefficients of aggregate size results

	Coefficients	*Standard Error*	*t-stat*	*P-value*	*Lower 95%*	*Upper 95%*
Intercept	122.94	11.23	10.95	1.49×10^{-8}	99.011	146.9
Energy dissipation rate (W/kg)	-6.711	2.101	-3.195	0.0060	-11.19	-2.234
Time (hour)	-5.565	1.853	-3.004	0.0089	-9.51	-1.616

The regression results for membrane integrity (Y_3) are shown in Tables C.7, C.8 and C.9. The *P-value* of energy dissipation rate was higher than 0.025, which seemed to indicate that energy dissipation rate was not a significant parameter in this analysis. However, a data point in the standardised residual plot in Figure C.1 showed the standardised residual of 2.3, which was considered an outlier (Perry et al., 1984).

Table C.7: Regression results for membrane integrity before removing outlier

Regression Statistics	
Multiple R	0.682
R^2	0.466
Adjusted R^2	0.394
Standard Error	10.09
Observations	18

Table C.8: Anova results for membrane integrity

	Degree of freedom	*SS*	*MS*	*F*	*Significance F*
Regression	2	1330.8	665.39	6.5318	0.00911
Residual	15	1528.0	101.87		
Total	17	2858.8			

Table C.9: Statistics for regression coefficients of membrane integrity results

	Coefficients	*Standard Error*	*t-stat*	*P-value*	*Lower 95%*	*Upper 95%*
Intercept	115.15	8.440	13.643	7.35×10^{-10}	97.159	133.14
Energy dissipation rate (W/kg)	-2.833	1.580	-1.793	0.0931	-6.199	0.5340
Time (hour)	-4.328	1.393	-3.107	0.00722	-7.298	-1.359

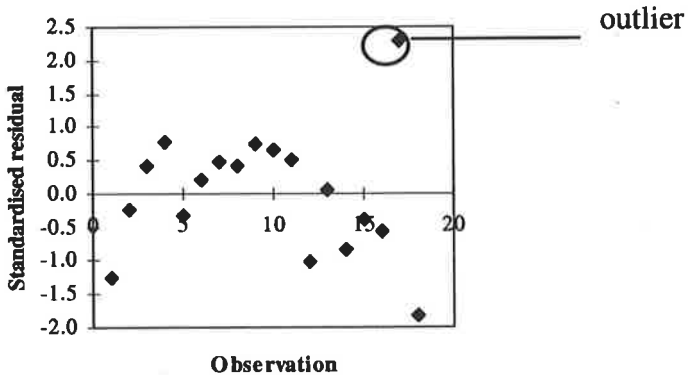

Figure C.1. Standardised residual plot of membrane integrity data

The regression analysis was repeated with membrane integrity data after the outlier had been eliminated. These results are summarised in Tables C.10, C.11 and C.12.

Table C.10: Regression results for membrane integrity after removing outlier

Regression Statistics	
Multiple R	0.8183
R^2	0.6696
Adjusted R^2	0.6224
Standard Error	7.986
Observations	17

Table C.11: Anova results for membrane integrity without an outlier

	degree of freedom	*SS*	*MS*	*F*	*Significance F*
Regression	2	1809.4	904.69	14.185	0.00043
Residual	14	892.89	63.778		
Total	16	2702.3			

Table C.12: Statistics for regression coefficients of membrane integrity results without an outlier

	Coefficients	*Standard Error*	*t-stat*	*P-value*	*Lower 95%*	*Upper 95%*
Intercept	120.66	6.903	17.48	6.62×10^{-11}	105.85	135.46
Energy dissipation rate (W/kg)	-3.880	1.293	-3.001	0.00954	-6.654	-1.107
Time (hour)	-5.097	1.129	-4.515	0.000486	-7.518	-2.675

A summary of all coefficients for the linear regression model using least square method is presented in Table C.13 below, where Y_1, Y_2 and Y_3 represent relative mitochondrial activity, aggregate size and membrane integrity respectively.

Table C.13: Regression coefficients for three biological responses

Coefficients	Y_1	Y_2	Y_3
β_0	129.6	122.9	120.7
β_1	-12.36	-6.711	-3.880
β_2	-10.60	-5.565	-5.097

APPENDIX D

REGRESSION ANALYSIS OF RATE-RATIO AND TIME

The linear regression model in terms of the rate-ratio $\left(\frac{P}{k'D^3}\frac{1}{t_c}\right)$ (Jüsten et al., 1996) and time t is expressed as:

$$Y_i = \beta_0 + \beta_1\left(\frac{P}{k'D^3}\frac{1}{t_c}\right) + \beta_2 t + \varepsilon_i$$

where Y_i represents the biological response, β_i refers to the regression coefficients, and ε_i is the residual. The regression results for mitochondrial activity (Y_1) at 5% significant level are summarised in Tables D.1, D.2 and D.3.

Table D.1: Regression results for mitochondrial activity

Regression Statistics	
Multiple R	0.8579
R^2	0.7360
Adjusted R^2	0.7008
Standard Error	17.417
Observations	18

Table D.2: Anova results for mitochondrial activity

	degree of freedom	*SS*	*MS*	*F*	*Significance F*
Regression	2	12683.7	6341.9	20.907	4.59×10^{-5}
Residual	15	4550.08	303.34		
Total	17	17233.8			

Table D.3: Statistics for regression coefficients of mitochondrial activity results

	Coefficients	*Standard Error*	*t-stat*	*P-value*	*Lower 95%*	*Upper 95%*
Intercept	119.28	12.742	9.3609	1.18×10^{-7}	92.117	146.44
Time (hour)	-10.714	2.404	-4.457	0.000461	-15.837	-5.590
$P/k'D^3t_c$	-0.3797	0.0816	-4.655	0.000311	-0.5536	-0.2059

Tables D.4, D.5 and D.6 present the results of regression analyses on aggregate size data at 5% significant level.

Table D.4: Regression results for aggregate size

Regression Statistics	
Multiple R	0.7699
R^2	0.5927
Adjusted R^2	0.5384
Standard Error	13.00
Observations	18

Table D.5: Anova results for aggregate size

	degree of freedom	*SS*	*MS*	*F*	*Significance F*
Regression	2	3691.4	1845.7	10.913	0.00119
Residual	15	2536.8	169.12		
Total	17	6228.2			

Table D.6: Statistics for regression coefficients of aggregate size results

	Coefficients	*Standard Error*	*t-stat*	*P-value*	*Lower 95%*	*Upper 95%*
Intercept	117.69	9.514	12.3696	2.85×10^{-9}	97.408	137.97
Time (hour)	-5.626	1.795	-3.1347	0.00682	-9.452	-1.801
$P/k'D^3t_c$	-0.2097	0.0609	-3.4431	0.00362	-0.3396	-0.0799

Similarly, Tables D.7, D.8 and D.9 summarised the regression analyses results for membrane integrity at 5% significant level.

Table D.7: Regression results for membrane integrity

Regression Statistics	
Multiple R	0.8337
R^2	0.6951
Adjusted R^2	0.6515
Standard Error	7.6719
Observations	17

Table D.8: Anova results for membrane integrity

	degree of freedom	*SS*	*MS*	*F*	*Significance F*
Regression	2	1878.3	939.13	15.956	2.45×10^{-4}
Residual	14	824.01	58.858		
Total	16	2702.3			

Table D.9: Statistics for regression coefficients of membrane integrity

	Coefficients	*Standard Error*	*t-stat*	*P-value*	*Lower 95%*	*Upper 95%*
Intercept	117.93	5.804	20.317	8.69×10^{-12}	105.48	130.37
Time (hour)	-5.161	1.085	-4.755	0.00031	-7.489	-2.833
$P/k'D^3t_c$	-0.1237	0.0374	-3.306	0.00521	-0.2039	-0.0434

APPENDIX E

LIST OF PUBLICATIONS

1. Sowana, D.D., D.R.G Williams, E.H. Dunlop, B.B. Dally, B.K. O'Neill and D.F. Fletcher (2001), "Turbulent Shear Stress Effects on Plant Cell Suspension Cultures", *Chemical Engineering Research and Design*, **79**: A8 (November 2001).

2. Sowana, D.D., D.R.G Williams, B.K. O'Neill, and E.H. Dunlop (2001), "Factorial Design of Shear Protective Properties of Pluronic-F68 on Wild Carrot Cell Cultures", *6th World Congress of Chemical Engineering*, 23-27 September 2001, Melbourne, Australia.

3. Sowana, D.D., D.R.G Williams, E.H. Dunlop, B.B. Dally, B.K. O'Neill and D.F. Fletcher (2001), "Turbulent Shear Stress Effects on Plant Cell Suspension Cultures", *4th International Symposium on Mixing in Industrial Processes*, 14-16 May 2001, Toulouse, France.

Papers Currently under Review

1. Sowana, D.D., D.R.G Williams, B.K. O'Neill, and E.H. Dunlop, "Factorial Design of Shear Protective Properties of Pluronic-F68 on Wild Carrot Cell Cultures", *Biochemical Engineering Journal*

2. Sowana, D.D., D.R.G Williams, B.K. O'Neill and E.H. Dunlop, "Modelling the Role of Calcium in Shear Damage and Death", *Plant, Cell and Environment*

NOMENCLATURE

Symbol		*Units*
a	Strain rate parameter	1/s
A	Cross sectional area	mm^2
C	Circularity, Equation (6.3)	-
C	Concentration	mol/L
C_μ, C_D	Drag coefficient	-
d, d_c	Particle diameter	m
D	Impeller diameter	m
D_{agg}	Aggregate diameter	m
D_f	Box-counting fractal dimension	-
D_{O2}	Oxygen diffusivity	cm^2/s
D_{pf}	Perimeter-based fractal dimension	-
D_s	Stirrer diameter	m
DW	Dry cell weight	g/L
E	Cell surface strain rate	-
E	Surface elasticity	MPa
FCW	Fresh cell weight/wet weight	g/L
g	Gravitational constant	m/s^2
K	First-order deactivation rate constant	1/s
k_0	Initial channel opening rate constant	1/s
$k_{1,2}$	Channel opening rate constant	1/s
k_La	Overall mass transfer coefficient	1/s

Symbol		*Units*
K_A	Elasticity constant	Dyne/cm
L	Eddy length scale	m
min	Time scale in minute	min
P	Perimeter, Equation (6.1)	mm
P	Power input	W
P_T	Power input	W
q_{O2}	Specific oxygen uptake rate	Mmol/g (dw) /s
r	Eddy radius	m
R	Dimensionless radius, Equation (6.12)	-
R^2	Correlation factor, Figure 6.16	-
Re	Reynolds number	-
t	Time	s
t_c	Circulation time	s
T	Time scale (Chapter 6)	s
T	Tension (Chapter 7)	Dyne/cm
U	Instantaneous velocity	m/s
U_∞	Stream velocity	m/s
u_c	Velocity	m/s
V_{ss}	Volume of the shearing section	m^3
V_T	Volume	m^3
X/X_0	Relative cell viability	-
Y_1	Relative mitochondrial activity	%
Y_2	Relative aggregate size	%

Symbol		*Units*
Y_3	Relative membrane integrity	%
$\bar{u}$, $\overline{U}$	Mean velocity	m/s
u', v', w'	Fluctuation velocity component in the x, y and z direction respectively	m/s

Greek Symbols

δ	Wake width	m
ε	Energy dissipation rate	W/kg
γ	Shear rate	1/s
η	Kolmogorov length scale	m
μ	Dynamic Viscosity	Pa s
μ	Growth rate, Equation (3.5)	1/day
μ_c	Cell surface viscosity	Pa.s
ν	Kinematic Viscosity	m^2/s
θ	Time scale of turbulence	s
θ_M	Relaxation time of cell surface	s
υ_e	Eddy velocity	m/s
ρ	Fluid density	kg/m^3
τ	Shear stress	N/m^2
τ_k	Turbulent shear stress	N/m^2
τ_l	Instantaneous maximum shear stress	N/m^2
τ_{Re}	Reynolds stress	N/m^2
τ_s	Surface shear stress	N/m^2
τ_t	Turbulent shear stress	N/m^2

Greek Symbols

τ_v	Viscous shear stress	N/m^2
ω_o	Vorticity parameter	-

Subscripts

0	Initial; (time = 0)
ave	Average
cyt	Cytosolic
ER	Endoplasmic reticulum
ext	Extracellular
i	Impeller
L	Liquid
local	Local
m	Mitochondria
max	Maximum
T	Total
V	Vacuole

REFERENCES

Abu-Reesh, I. and F. Kargi (1989). "Biological Responses of Hybridoma Cells to Defined Hydrodynamic Shear Stress." *Journal of Biotechnology* **9**: 167-178.

Alberts, B., D. Bay, J. Lewis, M. Raff, M, K. Roberts, and J.D. Watson. (1994). Molecular Biology of the Cell. New York, Garland Publishing.

Alexander, R. W. (2001). "Teasing apart the Taxol Pathway." *Trends in Biochemical Science* **26**(3): 152.

Aloi, L. E. and R. S. Cherry (1994). "Intracellular Calcium Response of Sf-9 Insect Cells Exposed to Intense Fluid Forces." *Journal of Biotechnology* **33**: 21-31.

Al-Rubeai, M., R. P. Singh, A.N. Emery, and Z. Zhang (1995). "Cell Cycle and Cell Size Dependence of Susceptibility to Hydrodynamic Forces." *Biotechnology and Bioengineering* **46**: 88-92.

Amtmann, A., H. G. Klieber and D. Gradmann (1992). "Cytoplasmic Free Ca^{2+} in the Marine Alga Acetabularia: Measurement with Ca^{2+}-Selective Microelectrodes and Kinetics Analysis." *Journal of Experimental Botany* **43**(252): 875-885.

Anathan, A., A. L. Goldberg, and R. Voellmy (1986). "Abnormal Proteins Serve as Eukaryotic Stress Signals and Trigger the Activation of Heat Shock Genes." *Science* **232**: 522-524.

Anderson, J. W. and J. Beardall (1991). Molecular Activities of Plant Cells. Oxford, Blackwell Scientific Publications.

Anthony, P., M. R. Davey, J.B Power, C. Washington, and K.C. Lowe. (1994). "Synergistic Enhancement of Protoplast Growth by Oxygenated Perfluorocarbon and Pluronic F-68." *Plant Cell Reports* **13**: 251-255.

Anthony, P., K. C. Lowe, M.R. Davey, and J.B Power. (1997). "Strategies for Promoting Division of Cultured Plant Protoplasts: Synergistic Beneficial Effects of Haemoglobin (Erythrogen) and Pluronic F-68." *Plant Cell Reports* **17**: 13-16.

Arora, P. D., K. J Bibby and C. A. G. McCulloch (1994). "Slow Oscillations of Free Intracellular Calcium Ion Concentration in Human Fibroblasts Responding to Mechanical Stretch." *Journal of Cellular Physiology* **161**: 187-200.

Bailey, J. E. and D. F. Ollis (1986). Biochemical Engineering Fundamentals. Singapore, McGraw-Hill Book.

Bassetti, L., M. Hagendoorn, and J. Tramper. (1995). "Surfactant-Induced Non-Lethal Release of Anthraquinones from Suspension Cultures of *Morinda citrifolia*." *Journal of Biotechnology* **39**: 149-155.

Bassetti, L. and J. Tramper (1995). "Increased Anthraquinone Production by *Morinda citrifolia* in a Two-Phase System with Pluronic F-68." *Enzyme and Microbial Technology* **17**: 353-358.

Benson, E. E. (1994). Cryopreservation. *Plant Cell Culture*. R. A. Dixon and R. A. Gonzales. Oxford, Great Britain, Oxford University Press: 147-167.

Billiones R. G., M. L. Tackx, and M. H. Daro (1999). "The Geometric Features, Shape Factors and Fractal Dimensions of Suspended Particulate Matter in the Scheldt Estuary (Belgium)." *Estuarine, Coastal and Shelf Science* **48**: 293-305.

Bird, R. B., W. E. Stewart, and E.N. Lightfoot (1960). Transport Phenomena. New York, USA, John Wiley & Sons.

Blatt, M. R. (1999). "Reassessing Roles for Ca^{2+} in Guard Cell Signalling." *Journal of Experimental Botany* **50**: 989-999.

Bloor, M. S. and J. H. Gerrard (1966). "Measurements on Turbulent Vortices in a Cylinder Wake." *Proceedings of the Royal Society of London, Series A* **294**: 319-342.

Boitier, E., R. Rea, and M.R. Duchen. (1999). "Mitochondria Exert a Negative Feedback on the Propagation of Intracellular Ca^{2+} Waves in Rat Cortical Astrocytes." *Journal of Cell Biology* **145**(4): 795-808.

Box, G. E. P., W. G. Hunter, and J.S. Hunter. (1978). Statistics for Experiments: An Introduction to Design, Data Analysis and Model Building. New York, John Wiley and Sons.

Büchner, K.-H., U. Zimmermann, and F. W. Bentrup (1981). "Turgor Pressure and Water Transport Properties of Suspension-Cultured Cells of *Chenopodium rubrum* L." *Planta* **151**: 95-102.

Buckhout, T. J. (1984). "Characterisation of Ca^{2+} Transport in Purified Endoplasmic Reticulum Membrane Vesicles from *Lepidium sativum* L. Roots." *Plant Physiology* **76**: 962-967.

Bush, D. S. and T. Wang (1995). "Diversity of Calcium-Efflux Transporters in Wheat Aleurone Cells." *Planta* **197**: 19-30.

Calabrese, R. V. and C. M. Stoots (1989). "Flow in the Impeller Region of a Stirred Tank." *Chemical Engineering Progress* **85**(5): 43-50.

Campbell, A. K. (1985). Intracellular Calcium: Its Universal Role as Regulator. Chichester, UK, John Wiley & Sons.

Cantwell, B. and D. Coles (1983). "An Experimental Study of Entrainment and Transport in the Turbulent Near Wake of a Circular Cylinder." *Journal of Fluid Mechanics* **136**: 321-374.

Caulet, P. J. C., R. G. J. M. van der Lans and K. C. A. M. Luyben (1996). "Hydrodynamical Interactions between Particles and Liquid Flows in Biochemical Applications." *Chemical Engineering Journal* **62**: 193-206.

Cazalé, A.-C., M.-A. Rouet-Mayer, H. Barbier-Brygoo, Y. Mathieu, and C. Lauriere(1998). "Oxidative Burst and Hypoosmotic Stress in Tobacco Cell Suspensions." *Plant Physiology* **116**: 659-669.

CFX (1997). CFX-4.2 SOLVER Manual. AEA Technology, Harwell, Didcot, Oxfordshire, UK.

Cherry, R. S. and E. T. Papoutsakis (1988). "Physical Mechanisms of Cell Damage in Microcarrier Cell Culture Bioreactors." *Biotechnology and Bioengineering* **32**: 1001-1014.

Cherry, R. S. and K.-Y. Kwon (1990). "Transient Shear Stress on a Suspension Cell in Turbulence." *Biotechnology and Bioengineering* **36**: 563-571.

Cochran, W. G. and G. M. Cox (1957). Experimental Designs. New York, John Wiley and Sons.

Cooney, C. L. and A. E. Humphrey, Eds. (1985). Comprehensive Biotechnology: The Principles, Applications and Regulations of Biotechnology in Industry, Agriculture and Medicine. Oxford, Pergamon Press.

Cosgrove, D. J. and R. Hedrich (1991). "Stretch-Activated Chloride, Potassium, and Calcium Channels Coexisting in Plasma Membranes of Guard Cells of *Vicia faba* L." *Planta* **186**: 143-153.

Cowger, N. L., K. C. O'Connor, T.G. Hammond, D.J. Lacks, and G.L. Navar. (1999). "Characterisation of Bimodal Cell Death of Insect Cells in a Rotating-Wall Vessel and Shaker Flask." *Biotechnology and Bioengineering* **64**(1): 14-26.

Croughan, M. S., J. F. Hamel, and D.I.C. Wang (1987). "Hydrodynamic Effects on Animal Cells Grown in Microcarrier Cultures." *Biotechnology and Bioengineering* **29**: 130-141.

Croughan, M. S., E. S. Sayre, and D.I.C. Wang. (1989). "Viscous Reduction of Turbulent Damage in Animal Cell Culture." *Biotechnology and Bioengineering* **33**: 862-872.

Curtin, M. E. (1983). "Harvesting Profitable Products from Plant Tissue Culture." *Biotechnology* **1**: 649-657.

Cutter, L. A. (1966). "Flow and Turbulence in a Stirred Tank." *AIChE Journal* **12**(1): 35-45.

Davidson, R. M. (1993). "Membrane Stretch Activates a High-conductance K^+ Channel in G292 Osteoblastic-Like Cells." *Journal of Membrane Biology* **131**: 81-92.

Desikan, R., A. Reynolds, J.T. Hancock, and S.J. Neill. (1998). "Hairpin and Hydrogen Peroxide Both Initiate Programmed Cell Death but have Differential Effects on Defence Gene Expression in *Arabidopsis* suspension cultures." *Biochemical Journal* **330**: 115-120.

Ding, J. P. and B. G. Pickard (1993). "Mechanosensory Calcium-Selective Cation Channels in Epidermal Cells." *The Plant Journal* **3**(1): 83-110.

Doran, P. M. (1993). Design of Reactors for Plant Cells and Organs. *Advances in Biochemical Engineering*. G. Wilson. Berlin, Springer Verlag: 114-168.

Doran, P. M. (1999). "Design of Mixing Systems for Plant Cell Suspensions in Stirred Reactors." *Biotechnology Progress* **15**: 319-335.

Dunlop, E. H., P. K. Namdev, and M.Z. Rosenberg (1994). "Effect of Fluid Shear Forces on Plant Cell Suspensions." *Chemical Engineering Science* **49**(14): 2263-2276.

Dracup, M., J. Gibbs, C. E. E. Stuiver, H. Greenway and T. J. Flowers (1986). "Determination of Free Space, Growth, Solute Concentrations and Parameters of Water Relations of Suspension-Cultured Tobacco Cells." *Plant, Cell and Environment* **9**: 693-701.

Dyster, K. N., E. Koutsakos, Z. Jaworski, and A.W. Nienow (1993). "An LDA Study of the Radial Discharge Velocities Generated by a Rushton Turbine." *Trans. IChemE* **71 part A**: 11-23.

Dziuba, J., A. Babuchowski, M. Smoczynski and Z. Smietana (1999). "Fractal Analysis of Caserinate Structure." *International Dairy Journal* **9**: 287-292.

Elias, C. B., R. B. Desai, M.S. Patole, J.B. Joshi, and R.A. Mashelkar (1995). "Turbulent Shear Stress - Effect on Mammalian Cell Culture and Measurement Using Laser Doppler Anemometer." *Chemical Engineering Science* **50**(15): 2431-2440.

Fagan, M. H. and T. G. Dewey (1985). "Steady State Kinetics of ATP Synthesis and Hydrolysis Coupled Calcium Transport Catalysed by the Reconstituted Sarcoplasmic Reticulum ATPase." *Journal of Biological Chemistry* **260**(10): 6147-6152.

Frisch, U. (1995). Turbulence: The Legacy of A.N. Kolmogorov. Cambridge, Great Britain, Cambridge University Press.

Fujita, Y. and M. Tabata, Eds. (1987). Secondary Metabolites from Plant Cells-Pharmaceutical Application and Progress in Commercial Production. Plant Tissue and Cell Culture, New York, Alan R. Liss: 169-185.

Gelli, A. and E. Blumwald (1993). "Calcium Retrieval from Vacuolar Pools." *Plant Physiology* **102**: 1139-1146.

Giannini, J. L., J. Ruiz-Cristin, and D.P. Briskin. (1987). "Calcium Transport in Sealed Vesicles from Red Beet (*Beta vulgaris* L.) Storage Tissue." *Plant Physiology* **85**: 1137-1142.

Gibbs, W. W. (2001). "Cybernetic Cells." *Scientific American* **August 2001**: 43-47.

Gilroy, S., W. A. Hughes and A. J. Trewavas (1986). "The Measurement of Intracellular Calcium Levels in Protoplasts from Higher Plant Cells." *FEBS Letters* **199**(2): 217-221.

Goldblum, S., Y.-K. Bae, W.F. Hink, and J. Chalmers (1990). "Protective Effect of Methylcellulose and Other Polymers on Insect Cells Subjected to Laminar Shear Stress." *Biotechnology Progress* **6**(5): 383-390.

Gregoriades, N., J. Clay, N. Ma, K. Koelling, and J.J. Chalmers. (2000). "Cell Damage of Microcarrier Cultures as a Function of Local Energy Dissipation Created by a Rapid Extensional Flow." *Biotechnology and Bioengineering* **69**(2): 171-182.

Guardiola, J., J. L. Iborra and M. Canovas (1995). "A Model That Links Growth and Secondary Metabolite Production in Plant Cell Suspension Cultures." *Biotechnology and Bioengineering* **46**: 291-297.

Guharay, F. and F. Sachs (1984). "Stretch-Activated Single Ion Channel Currents in Tissue-Cultured Embryonic Chick Skeletal Muscle." *Journal of Physiology* **352**: 685-701.

Gunkel, A. A. and M. E. Weber (1975). "Flow Phenomena in Stirred Tanks." *AIChE Journal* **21**(5): 931-937.

Gunter, T. E., L. Buntinas, G. Sparagna, R. Eliseev, and K. Gunter. (2000). "Mitochondrial Calcium Transport: Mechanisms and Functions." *Cell Calcium* **28**(5/6): 285-296.

Haley, A., A. J. Russell, N. Wood, A. C. Allan, M. Knight, A. K. Campbell and A. J. Trewavas (1995). "Effects of Mechanical Signaling on Plant Cell Cytosolic Calcium." *Proccedings of the National Academy of Science (USA)* **92**: 4124-4128.

Hinze, J. O. (1959). Turbulence: An Introduction to Its Mechanism and Theory. New York, McGraw-Hill Book Company.

Hinze, J. O. (1975). Turbulence: An Introduction to Its Mechanism and Theory. New York, McGraw-Hill Book Company.

Ho, C.-H., K. A. Henderson, and L.G. Rorrer. (1995). "Cell Damage and Oxygen Mass Transfer during Cultivation of *Nicotiana tabacum* in a Stirred-Tank Bioreactor." *Biotechnology Progress* **11**: 140-145.

Hooker, B. S., J. M. Lee, and G. An. (1989). "Response of Plant Tissue Culture to a High Shear Environment." *Enzyme and Microbial Technology* **11**: 484-490.

Hooker, B. S. and J. M. Lee (1990). "Cultivation of Plant Cells in a Stirred Vessel: Effect of Impeller Design." *Biotechnology and Bioengineering* **35**: 296-304.

Horsch, R. B. and G. E. Jones (1980). "A Double Filter Paper Technique For Plating Cultured Plant Cells." *In Vitro* **16**(2): 103-108.

Illing, S. (1996). An Investigation of the Effect of Hydrodynamic Stress on the Growth, Morphology and Metabolism of Microorganisms. PhD thesis, Cape Town, South Africa, University of Cape Town.

Illing, S. and S. Harrison (1999). "The Kinetics and Mechanism of *Corynebacterium glutamicum* Aggregate Breakup in Bioreactors." *Chemical Engineering Science* **54**: 441-454.

Jelinek, H. F. and E. Fernandez (1998). "Neurons and Fractals: How Reliable and Useful are Calculations of Fractal Dimensions." *Journal of Neuroscience Methods* **81**: 9-18.

Jiang, S., S. C. Chow, P. Nicotera, and S. Orrenius. (1994). "Intracellular Ca^{2+} Signals Activate Apoptosis in Thymocytes: Studies using the Ca^{2+}-ATPase Ibhibitor Thapsigargin." *Experimental Cell Research* **212**: 84-92.

Joshi, J. B., C. B. Elias and M. S. Patole (1996). "Role of Hydrodynamic Shear in the Cultivation of Animal, Plant and Microbial cells." *Chemical Engineering Journal* **62**: 121-141.

Jüsten, P., G. C. Paul, A.W. Nienow, and C.R Thomas. (1996). "Dependence of Mycelial Morphology on Impeller Type and Agitation Intensity." *Biotechnology and Bioengineering* **52**: 672-684.

Kawase, Y. and M. Moo-Young (1990). "Mathematical Models for Design of Bioreactors: Applications of Kolmogoroff's Theory of Isotropic Turbulence." *The Chemical Engineering Journal* **43**: B19-B41.

Kerr, J. F. R. and B. V. Harmon (1991). Definition and idence of Apoptosis: Historical Perspective. *Apoptosis: The Molecular Basis of Cell Death*. L. D. Tomei and F. O. Cope. USA, Cold Spring Harbor Laboratory Press: 5-30.

Kessell, R. H. J. and A. H. Carr (1972). "The Effect of Dissolved Oxygen Concentration on Growth and Differentiation of Carrot (*Daucus carota*) Tissue." *Journal of Experimental Botany* **23**(77): 996-1007.

Khehra, M., K. C. Lowe, M.R. Davey, and J.B. Power. (1995). "An Improved Micropropagation System for *Chrysanthemum* based on Pluronic F-68-Supplemented Media." *Plant Cell, Tissue and Organ Culture* **41**: 87-90.

Kieran, P. M., H. J. O'Donnell, D.M. Malone, D.M., and P.F. MacLoughlin. (1995). "Fluid Shear Effects on Suspension Cultures of *Morinda citrifolia*." *Biotechnology and Bioengineering* **45**: 415-425.

Kieran, P. M., P. F. MacLoughlin, and D.M. Malone. (1997). "Plant Cell Suspension Cultures: Some Engineering Considerations." *Journal of Biotechnology* **59**: 39-52.

Kieran, P. M., D. M. Malone and P. F. MacLoughlin (2000). Effects of Hydrodynamic and Interfacial Forces on Plant Cell Suspension Systems. *Advances in Biochemical Engineering/Biotechnology*. T. Scheper. Berlin, Springer-Verlag. **67:** 139-177.

King, A. T., M. R. Davey, B.J. Mulligan, and K.C. Lowe. (1990). "Effects of Pluronic F-68 on Plant Cells in Suspension Culture." *Biotechnology Letters* **1**: 29-32.

Knight, M. R., S. M. Smith, and A.J. Trewavas. (1992). "Wind-induced Plant Motion Immediately reases Cytosolic Calcium." *Proceedings of the National Academy of Science of U.S.A.* **89**: 4967-4971.

Knight, H., A. J. Trewavas, and M.R. Knight. (1996). "Cold Calcium Signaling in Arabidopsis Involved Two Cellular Pools and a Change in Calcium Signature after Acclimation." *Plant Cell* **8**: 489-503.

Kumar, R. V., R. Panniers, A. Wolfman, A, and E.C. Henshaw. (1991). "Inhibition of Protein Synthesis by Antagonists of Calmodulin in Ehrlich Ascites Tumor Cells." *European Journal of Biochemistry* **195**: 313-319.

Kumar, V., L. Laouar, M.R. Davey, B.J. Mulligan, and K.C. Lowe. (1992). "Pluronic F-68 Stimulates Growth of *Solanum dulcamara* in Culture." *Journal of Experimental Botany* **43**(249): 487-493.

Launder, B. E. and B. T. Sharma (1974). "Application of the Energy Dissipation Model of Turbulence to the Calculation of Flow near a Spinning Disc." *Letters in Heat and Mass Transfer* **1**: 131-138.

Lee, K. C. and M. Yianneskis (1998). "Turbulence Properties of the Impeller Stream of a Rushton Turbine." *AIChE Journal* **44**(1): 13-24.

Levins, D. M. and J. R. Glastonbury (1972). "Application of Kolmogoroff's Theory to Particle-Liquid Mass Transfer in Agitated Vessels." *Chemical Engineering Science* **27**: 537-543.

Lockshin, R. A. and Z. Zakeri (1991). Programmed Cell Death and Apoptosis. *Apoptosis: The Molecular Basis of Cell Death*. L. D. Tomei and F. O. Cope. USA, Cold Spring Harbor Laboratory Press: 47-60.

LoSchiavo, F., B. Baldan, D. Campagnin, R. Ganz, P. Mariani, and M. Terzi. (2000). "Spontaneous and Induced Apoptosis in Embryogenic Cell Cultures of Carrot (*Daucus carota* L.) in different Physiological States." *European Journal of Cell Biology* **79**: 294-298.

MacLoughlin, P. F., D. M. Malone, J.T. Murtagh, and P.M. Kieran. (1998). "The Effects of Turbulent Jet Flows on Plant Cell Suspension Cultures." *Biotechnology and Bioengineering* **58**(6): 595-604.

Malek, A. M. and S. Izumo (1996). "Mechanism of Endothelial Cell Shape Change and Cytoskelatal Remodelling in Response to Fluid Shear Stress." *Journal of Cell Science* **109**(4): 713-726.

Malhó, R., A. Moutinho, A. van der Luit, and A. J. Trewavas (1998). "Spatial Characteristics of Calcium Signalling: the Calcium Wave as a Basic Unit in Plant Cell Calcium Signalling." *Philosophical Transactions of the Royal Society of London B* **353**: 1463-1473.

Mandelbrot, B. B. (1983). The Fractal Geometry of Nature, New York, W.H. Freeman.

Markx, G. H., H. J. G. ten Hoopen, J.J. Meijer, J.J., and K.L. Vinke. (1991). "Dielectric Spectroscopy as a Novel and Convenient Tool for the Study of the Shear Sensitivity of Plant Cells in Suspension Culture." *Journal of Biotechnology* **19**: 145-158.

Masuda, Y. (1978). "Vicsoelastic Properties of Plant Cell Walls-III. Hysteresis Loop in the Stress-Strain Curve at Constant Strain Rate." *Biorheology* **15**: 87-97.

Matsuo, T. and H. Unno (1981). "Forces Acting on Floc and Strength of Floc." *ASCE* **107 (EE3)**: 527-545.

McAinsh, M. R., A. A. R. Webb, J. E. Taylor, and A. M. Hetherington (1995). "Stimulus-Induced Oscillations in Guard Cell Cytosolic Free Calcium." *The Plant Cell* **7**: 1207-1219.

McCabe, P. F., A. Levine, P.J. Meijer, N.A. Tapon, and R.J. Pennell. (1997). "A Programmed Cell Death Pathway Activated in Carrot Cells Cultured at Low Cell Density." *Plant Journal* **12**: 267-280.

McConkey, D. J. and S. Orrenius (1991). Cellular Signalling in Thymocytes Apoptosis. *Apoptosis: The Molecular Basis of Cell Death*. L. D. Tomei and F. O. Cope. USA, Cold Spring Harbor Laboratory Press: 227-246.

McConkey, D. J. and S. Orrenius (1996). "The Role of Calcium in Regulation of Apoptosis." *Journal of Leukocytle Biology* **59**: 775-783.

McMeekin, T. A., O. J. N., T. Ross T, and D.A. Ratkowsky. (1993). Predictive Microbiology - theory and application. Taunton, Somerset, England, Research Studies Press Ltd.

Meijer, J. J. (1988). Effects of Hydrodynamic and Chemical/Osmotic Stress on Plant Cells in a Stirred Bioreactor. *Biochemical Engineering*. Delft, The Netherlands, Delft University of Technology: 122.

Meijer, J. J., ten Hoopen, H. J. G., K.Ch.A.M Luyben, and K.R. Libbenga. (1993). "Effects of Hydrodynamic Stress on Cultured Plant Cells : A Literature Survey." *Enzyme and Microbial Technology* **March 1993**: 234-238.

Meijer, J. J., H. J. G. ten Hoopen, Y.M. van Gameren, K.Ch.A.M. Luyben, and K.R. Libbenga. (1994). "Effects of Hydrodynamic Stress on the Growth of Plant Cells in Batch and Continuous Culture." *Enzyme and Microbial Technology* **16**: 467-477.

Meneses-Acosta, A., R. Z. Mendonça, H. Merchant, L. Covarrubias, and O.T. Ramírez. (2001). "Comparative Charaterisation of Cell Death Between Sf9 Insect Cells and Hybridoma Cultures." *Biotechnology and Bioengineering* **72**(4): 441-457.

Mersmann, A., G. Schneidet, H. Volt, and E. Wenzig (1990). "Selection and Design of Aerobic Bioreactors." *Chemical Engineering Technology* **13**: 357-370.

Michaels, J. D., K. T. Kunas, and E.T. Papoutsakis. (1992). "Fluid-Mechanical Damage of Freely-Suspended Animal Cells in Agitated Bioreactors: Effects of Dextran Derivatised Celluloses and Polyvinyl Alcohol." *Chemical Engineering Communications* **118**: 341-360.

Michaels, J. D., J. E. Nowak, A.K. Mallik, K. Koczo, D.T. Wasan, and E.T. Papoutsakis. (1995). "Interfacial Properties of Cell Culture Media with Cell-Protecting Additives." *Biotechnology and Bioengineering* **47**: 420-430.

Montgomery, D. C. (1991a). Design and Analysis of Experiments. New York, John Wiley & Sons.

Montgomery, D. C. (1991b). Introduction to Statistical Quality Control. New York, John Wiley & Sons.

Moreno-Sanchez, R. (1985). "Regulation of Oxidative Phosphorylation in Mitochondria by External Free Ca^{2+} Concentrations." *Journal of Biological Chemistry* **260**(7): 4028-4034.

Mufti, N. A. and M. L. Shuler (1995). "Induction of Cytochrome P-450IA1 Activity in Response to Sublethal Stresses in Microcarrier-Attached Hep G2 Cells." *Biotechnology Progress* **11**: 659-663.

Mujumdar, A. S., B. Huang, D. Wolf, M.E. Weber, and W.J.M. Douglas. (1970). "Turbulence Parameters in a Stirred Tank." *Canadian Journal of Chemical Engineering* **48**: 475-483.

Murhammer, D. W. and C. F. Goochee (1990). "Structural Features of Nonionic Polyglycol Polymer Molecules Responsible for the Protective Effect in Sparged Animal Cell Bioreactors." *Biotechnology Progress* **6**(2): 142-148.

Murphy, R. and J. A. C. Smith (1998). "Determination of Cell Water-Relation Parameters Using the Pressure Probe: Extended Theory and Practice of the Pressure-Clamp Technique." *Plant, Cell and Environment* **21**: 637-657.

Nagata, S. (1975). Mixing : Principles and Applications. Tokyo, Japan, Kodansha Scientific Books.

Namdev, P. K., E. H. Dunlop, K. Wenger, and P. Villenueve. (1994). Role of Turbulence in Fermentations. *Advances in Bioprocess Engineering*. O. T. Ramirez, and G. Ramirez. The Netherlands, Kluwer Academic Publishers: 149-156.

Namdev, P. K. and E. H. Dunlop (1995). "Shear Sensitivity of Plant Cells in Suspensions : Present and Future." *Applied Biochemistry and Biotechnology* **54**: 109-131.

Nelkin, M. and M. Tabor (1990). "Time Correlations and Random Sweeping in Isotropic Turbulence." *Phys. Fluids A* **2**(1): 81-83.

Nicolaou, K. C., K. Rodney, K. Guy, and P. Potier. (1996). "Taxoids: New Weapons against Cancer." *Scientific American* June 1996: 84-88.

Nienow, A. W. (1998). "Hydrodynamics of Stirred Bioreactors." *Applied Mechanics Reviews* **51**(1): 3-32.

Nishitani, K. and Y. Masuda (1981). "Auxin-Induced Changes in the Cell Wall Structure: Changes in the Sugar Composition, Intrinsic Viscosity and Molecular Weight Distributions of Matrix Polysaccharides of the Epicotyl cell Wall of Vigna Angularis." *Physiologia Plantarum* **52**: 482-494.

OTA, U. S. Official of Technology Assessment (1983). Plant-the Potential for Extracting Protein, Medicines, and Other Useful Chemicals. Proceedings of an OTA Workshop, Washington, D.C., US Congress.

Ozaki, H., L. Zhang, I. L. O. Buxton, K. M. Sanders, and N. G. Publicover (1992). "Negative-Feedback Regulation of Excitation-Contraction Coupling in Gastric Smooth Muscle." *American Journal of Physiology* **263**(6): C1160-C1171.

Palomares, L. A., M. González, and O.T. Ramírez. (2000). "Evidence of Pluronic F-68 Direct Interaction with Insect Cells: Impact on Shear Protection, Recombinant Protein, and Baculovirus Production." *Enzyme and Microbial Technology* **26**: 324-331.

Papoutsakis, E. T. (1991). "Fluid-mechanical Damaged of Animal Cells in Bioreactors." *Trends in Biotechnology* **9**(12): 427-437.

Park, J. M., S. Y. Yoon, K.L. Giles, D.D. Songstad, D. Eppstein, D. Novakovski, L. Friesen, and I. Roewer. (1992). "Production of Sanguinarine by Suspension Culture of *Papaver somniferum*." *Journal of Fermentation and Bioengineering* **74**: 292-296.

Parr, A. J., J. I. Smith, R.J. Robins, and M.J.C. Rhodes. (1984). "Apparent Free Space and Cell Volume Estimation: A Non-Destructive Method for Assessing the Growth and Membrane Integrity/Viability of Immobilised Plant Cells." *Plant Cell Report* **3**: 161-164.

Pepin, M.-F., J. Archambault, C. Chavarie and F. Cormier (1995). "Growth Kinetics of *Vitis vinifera* Cell Suspension Cultures: I. Shake Flask Cultures." *Biotechnology and Bioengineering* **47**: 131-138.

Perry, R. H. and D. W. Green, Eds. (1984). Perry's Chemical Engineers' Handbook. Singapore, McGraw-Hill Book Co.

Petersen, P. and A. W. Alfermann (2000). Plant Cell Cultures. *Biotechnology*. H. Sahm. Germany, Wiley: 577-585.

Placek, J. and L. L. Tavarides (1985). "Turbulent Flow in Stirred Tanks." *AIChE Journal* **31**(7): 1113-1120.

Potter, J. F. and G. J. S. Ross (1979). Maximum Likelihood Estimation of Breakpoints and the Comparison of the Goodness of Fit with that of Conventional Curves. *Low Temperature Stress in Crop Plants: the Role of Membrane*. J. M. Lyons, D. Graham and J. K. Raison. New York, Academic Press: 535-542.

Prat, A. and X. Tort (1989). Case Study: Experimental Design in a Pet Food Manufacturing Company. *Center for Quality and Productivity Improvement*. Madison, Univeristy of Wisconsin-Madison.

Prokop, A. and R. K. Bajpai (1992). "Shear Sensitivity of Biocatalysts to Hydrodynamic Shear Stress." *Advance in Applied Microbiology* **37**: 165-232.

Ramírez, O. T. and R. Mutharasan (1990). "The Role of the Plasma Membrane Fluidity on the Shear Sensitivity of Hybridomas Grown under Hydrodynamic Stress." *Biotechnology and Bioengineering* **36**: 911-920.

Read, N. D., W. T. G. Allan, H. Knight, M. R. Knight, R. Malho, A. Russell, P. S. Shacklock and A. J. Trewavas (1992). "Imaging and Measurement of Cytosolic Free Calcium in Plant and Fungal Cells." *Journal of Microscopy* **166**: 57-86.

Read, N. D., P. S. Shacklock, M. R. Knight and A. J. Trewavas (1993). "Imaging Calcium Dynamics in Living Plant Cells and Tissues." *Cell Biology International* **17**(2): 111-125.

Reuzeau, C. and R. F. Pont-Lezica (1995). "Comparing Plant and Animal Extracellular Matrix-Cytoskeleton Connections - Are They Alike?" *Protoplasma* **186**: 113-121

Rizzuto, R., P. Bernardi, and T. Pozzan. (2000). "Mitochondria as All-Round Players of the Calcium Game." *Journal of Physiology* **529**(1): 37-47.

Robb, S. J., L. D. Robb-Gaspers, R.C. Scaduto, Jr., A. P. Thomas, and J. R. Connor (1999). "Influence of Calcium and Iron on Cell Death and Mitochondrial Function in Oxidatively Stress Astrocytes." *Journal of Neuroscience Research* **55**: 674-686.

Rodrigues-Monroy, M. and E. Galindo (1999). "Broth Rheology, Growth and Metabolite Production of *Beta vulgaris* Suspension Culture: a Comparative Study Between Cultures Grown in Shake Flasks and in a Stirred Tank." *Enzyme and Microbial Technology* **24**: 687-693.

Rosenberg, M. Z. (1989). The Hydrodynamic Shear Sensitivity of Suspension Cultured Plant Cells, PhD thesis, Saint Louis, Missouri, Sever Institute of Washington University.

Russ, J. C. (1994). The Image Processing Handbook, U.S.A, CRC Press.

Rygol, J. and U. Lüttge (1983). "Water-Relation Parameters of Giant and Normal Cells of *Capsicum annuum* pericarp." *Plant, Cell and Environment* **6**: 545-553.

Sackin, H. (1995). "Stretch-Activated Ion Channels." *Kidney International* **48**: 1134-1147.

Sahai, O. and M. Knuth (1985). "Commercializing Plant Tissue Culture Processes: Economics, Problems and Prospects." *Biotechnology Progress* **1**(1): 1-9.

Sajc, L., D. Grubisic and G. Vunjak-Novakovic (2000). "Bioreactors for Plant Engineering: an Outlook for Further Research." *Biochemical Engineering Journal* **4**: 89-99.

Schlatmann, J. E., P. R. H. Moreno, J.L Vinke, and H.J.G. ten Hoopen. (1994). "Effect of Oxygen and Nutrient Limitation on Ajmalicine Production and Related Enzyme Activities in High Density Cultures of *Catharanthus roseus*." *Biotechnology and Bioengineering* **44**: 461-468.

Schlichting, H. (1968). Boundary Layer Theory. New York, USA, McGraw-Hill Book Company.

Schroeder, J. I. and P. Thuleau (1991). "Ca^{2+} Channels in Higher Plant Cells." *Plant Cell* **3**: 555-559.

Schroeder, R., F. Gartner, B. Steinbrenner, B. Knoop, and R. Beiderbeck. (1989)."Viability Factors in Plant Cell Suspension Cultures - Some Propertis." *Journal of Plant Physiology* **135**: 422-427.

Schumaker, K. S. and H. Sze (1986). "Calcium Transport into the Vacuole of Oat Roots." *Journal of Biological Chemistry* **261**(26): 12172-12178.

Schwarz, G., G. Callewaert, G. Droogmans and B. Nilius (1992). "Shear Stress-Induced Calcium Transients in Endothelial Cells from Human Umbilical Cord Veins." *Journal of Physiology* **458**: 527-538.

Schwartzberg, H. G. and R. E. Treybal (1968). "Fluid and Particle Motion in Turbulent Stirred Tanks." *Industrial and Engineering Chemistry Fundamentals* **7**(1): 1-12.

Scragg, A. H., E. J. Allan, and F. Leckie. (1988). "Effect of Shear on the Viability of Plant Cell Suspensions." *Enzyme and Microbial Technology* **10**: 361-367.

Scragg, A. H. (1995). "The Problems Associated with High Biomass Levels in Plant Cell Suspensions." *Plant Cell, Tissue and Organ Culture* **43**: 163-170.

Serra, T. and X. Casamitjana (1998). "Structure of the Aggregates during the Process of Aggregation and Breakup under a Shear Flow." *Journal of Colloid and Interface Science* **206**: 505-511.

Sharp, J. M., B. R. Crowley, and K.H. Kwok (1995). Plant Cell Culture. Collingwood, VIC., TAFE Publications.

Shen, J., F. W. Luscinskas, A. Connolly, C. F. D. Jr. and M. A. G. Jr. (1992). "Fluid Shear Stress Modulates Cytosolic Free Calcium in Vascular Endothelial Cells." *American Journal of Physiology* **262C**: C384-C390.

Singh, R. P., M. Al-Rubeai, C. D. Gregory and A. N. Emergy (1994). "Cell Death in Bioreactors: A Role for Apoptosis." *Biotechnology and Bioengineering* **44**:720-726.

Smaili, S. S., Y.-T. Hsu, R.J. Youle, and J.T. Russell. (2000). "Mitochondria in Ca^{2+} Signaling and Apoptosis." *Journal of Bioenergetics and Biomembranes* **32**(1): 35-46.

Smith, J. J. and M. D. Lilly (1990). "The Effect of Agitation on the Morphology and Penicillin Production of *Penicillium chrysogenum*." *Biotechnology and Bioengineering* **35**: 1011-1023.

Spicer, P. T., W. Keller, and S. E. Pratsinis (1996). "The Effect of Impeller Type on Floc Size and Structure during Shear-Induced Flocculation." *Journal of Colloid and Interface Science* **184**(112-122).

Stephanopoulos, G. (1984). Chemical Process Control: An Introduction to Theory and Practive. New Jersey, Prentice-Hall.

Stockbridge, L. L. and A. S. French (1988). "Stretch-Activated Calcium Channels in Human Fibroblasts." *Biophysical Journal* **54**: 187-190.

Su, W. W. (1995). "Bioprocessing Technology for Plant Cells Suspension Cultures." *Applied Biochemistry and Biotechnology* **50**: 189-230.

Takeda, T., M. Seki, and S. Furusaki. (1994). "Hydrodynamic Damage of Cultured Cells of *Carthamus t torius* in a Stirred Tank Reactor." *Journal of Chemical Engineering of Japan* **27**(4): 466-471.

Takeda, T., T. Kitagawa, Y. Takeuchi, M. Seki and S. Furusaki (1997). Metabolic Responses of Plant Cell Culture to Hydrodynamic Stress. 46th Annual Meeting of the Canadian Society of Chemical Engineering, Kingston, Ontario, Canada.

Takeda, T., T. Kitagawa, Y. Takeuchi, M. Seki and S. Furusaki (1998). "Metabolic Responses of Plant Cell Culture to Hydrodynamic Stress." *The Canadian Journal of Chemical Engineering* **76**: 267-275.

Tanaka, H., H. Semba, T. Jitsufuchi, H. Harada. (1988). "The Effect of Physical Stress on Plant Cells in Suspension Cultures." *Biotechnology Letters* **10**(7): 485-490.

Thion, L., C. Mazars, P. Thuleau, A. Graziana, M. Rossignol, M. Moreau, and R. Ranjeva (1996). "Activation of Plasma Membrane Voltage-Dependent Calcium-Permeable Channels by Disruption of Microtubules in Carrot Cells." *FEBS Letters* **393**: 13-18

Timmers, A. C. J., H.-D. Reiss and J. H. N. Schel (1991). "Digitonin-aided Loading of Fluo-3 into Embryogenic Plant Cells." *Cell Calcium* **12**: 515-521.

Tombal, B., S. R. Denmeade, and J.T. Isaacs. (1999). "Assessment and Validation of a Microinjection Method for Kinetic Analysis of $[Ca^{2+}]_i$ in Individual Cells undergoing Apoptosis." *Cell Calcium* **25**(1): 19-28.

Tomi, D. T. and D. F. Bagster (1978). "The Behaviour of Aggregates in Stirred Vessels." *Transactions of the Institute of Chemical Engineers* **56**: 1-8.

Towill, L. E. and P. Mazur (1975). "Studies on the Reduction of 2,3,5-triphenyltetrazolium Chloride as a Viability Assay for Plant Tissue Cultures." *Canadian Journal of Botany* **53**: 1097-1102.

Townsend, A. A. (1947). "Measurements in the Turbulent Wake of a Cylinder." *Proceedings of the Royal Society of London, Series A* **190**: 551-561.

Townsend, A. A. (1951). "The Diffusion of Heat Spots in Isotropic Turbulence." *Proceedings of the Royal Society of London* **A209**: 418-430.

Trewavas, A. and M. Knight (1994). "Mechanical Signalling, Calcium and Plant Form." *Plant Molecular Biology* **26**: 1329-1341.

Trump, B. F., I. R. Berezesky, and A.R. Osornio-Vargas. (1981). Cell Death and the Disease Process. The Role of Calcium. *Cell Death in Biology and Pathology*. I. D. Bowen and R. A. Lockshin. New York, Chapman and Hall: 209-242.

van Beek, J. H. G. M., M. H. Wijhe, M.H.J. Eijgelshoven, and J.B. Hak. (1999). "Dynamic Adaptation of Cardiac Oxidative Phosphorylation is not Mediated by Simple Feedback Control." *American Journal of Physiology* **277**(4 part 2): H1375.

van't Riet, K. and J. M. Smith (1975). "The Trailing Vortex System Produced by Rushton Turbine Agitators." *Chemical Engineering Science* **30**: 1093-1105.

Verpoorte, R., R. van der Heijden, J. Schriprsema, J.H.C. Hoge, and H.J.G. ten Hoopen. (1993). "Plant Cell Biotechnology for the Production of Alkaloids: Present Status and Prospects." *Journal of Natural Products* **56**: 186-207.

Wagner, F. and H. Vogelmann (1977). Cultivation of Plant Tissue Cultures in Bioreactors and Formation of Secondary Metabolites. *Plant Tissue Culture and Its Bio-technological Application*. W. Barz, E. Reinhard, and M.H. Zenk. New York, USA, Springer-Verlag: 245-252.

Webb, A. A. R., M. R. McAinsh, J. E. Taylor, and A. M. Hetherington (1996). "Calcium Ions as Intracellular Second Messengers in Higher Plants." *Advances in Botanical Research* **22**: 45-85.

White, P. L., J. Banfield, and M. Diaz (1992). "Unidirectional Ca^{2+} Fluxes in Roots of Rye (*Secale cereale* L.). A Comparison of Excised Roots with Roots of Intact Plants." *Journal of Experimental Botany* **43**(253): 1061-1074.

Widholm, J. M. (1972). "The Use of Fluorescein Diacetate and Phenosafranine for Determining Viability of Cultured Plant Cells." *Stain Technology* **47**(4): 189-194.

Wiesner, T. F., B. C. Berk, and R. M. Nerem (1996). "A Mathematical Model of Cytosolic Calcium Dynamics in Human Umbilical Vein Endothelial Cells." *American Journal of Physiology* **270**: C1556-C1569.

Wiesner, T. F., B. C. Berk, and R. M. Nerem (1997). "A Mathematical Model of Cytosolic-free Calcium Response in Endothelial Cells to Fluid Shear Stress." *Proceedings of the National Academy of Science of the USA* **94**(8): 3726-3731.

Wilcox, D. C. (1998). Turbulence Modeling for CFD. Anaheim, California, DCW Industries.

Williams, D. A. and F. S. Fay (1990). "Intracellular Calibration of the Fluorescent Calcium Indicator Fura-2." *Cell Calcium* **11**: 75-83.

Winston, F. K., L. E. Thibault, and E. J. Macarak (1993). "An Analysis of the Time-Dependent Changes in Intracellular Calcium Concentration in Endothelial Cells in Culture Induced by Mechanical Simulation." *Journal of Biomedical Engineering* **115**: 160-168.

Wong, V., D. Williams, C. Colby, and D. Saint. (2000). Correlation of Oxygen Uptake Rate and Mitochondrial Activity in Carrot Cell Cultures Exposed to Laminar Fluid Shear, *Biotechnology Techniques* **22**(24): 1919-1924.

Wong, V. (2001). Hydrodynamic Shear Sensitivity of Suspension Cultured Plant Cells, PhD thesis, Chemical Engineering, Adelaide, Australia, University of Adelaide.

Wongsamuth, R. and P. M. Doran (1997). "The Filtration Properties of *Atropa belladonna* Plant Cell Suspensions; Effect of Hydrodynamic Shear and Elevated Carbon Dioxide Levels on Culture and Filtration Parameters." *Journal of Technology and Biotechnology* **69**: 15-26.

Wu, H. and G. K. Patterson (1989). "Laser-Doppler Measurement of Turbulent-Flow Parameters in a Stirred Mixer." *Chemical Engineering Science* **44**(10): 2207-2221.

Wu, S.-C., B. E. Dale, and J.C. Liao. (1993). "Kinetic Characterisation of Baculovirus-Induced Cell Death in Insect Cell Cultures." *Biotechnology and Bioengineering* **41**: 104-110.

Wu, J., A. J. Daugulis, P. Faulkner, and M.F.A. Goosen. (1995). "Protective Effects of Polymer Additives on Animal Cells Exposed to Rapidly Falling Liquid Films." *Biotechnology Progress* **11**: 127-132.

Wyllie, A. H. (1981). Cell Death: a New Classification Separating Apoptosis from Necrosis. *Cell Death in Biology and Pathology*. I. D. Bowen and R. A. Lockshin. New York, Chapman and Hall: 9-34.

Yamamoto, R. and Y. Masuda (1971). "Stress-Relaxation Property of the *Avena* Coleoptile Cell Wall." *Plysiologia Plantarum* **25**: 330-335.

Yao, X., H. Y. Kwan, F. L. Chan, N. W. K., and Chan and Y. Huang (2000). "A Protein Kinase G-Sensitive Channel Mediates Flow-Induced Ca^{2+} Entry into Vascular Endothelial Cells." *FASEB Journal* **14**(7): 932-938.

Yellowley, C. E., C. R. Jacob, Z. Li, Z. Zhou & H. J. Donahue (1997). "Effects of Fluid Flow on Intracellular Calcium in Bovine Articular Chondrocytes." *American Journal of Physiology* **273**: C30-C36.

Zhang, Z., M. Al-Rubeai, and C.R. Thomas. (1992). "The Effect of Pluronic F-68 on Mechanical Properties of Mammalian Cells." *Enzyme and Microbial Technology* 14(6): 980-983.

Zhang, Z., M. Al-Rubeai, and C.R. Thomas. (1993). "Estimation of Disruption of Animal Cells by Turbulent Capillary Flow." *Biotechnology and Bioengineering* **42**: 987-993.

Zhang, J. J., K. Fujiyama, T. Seki, T, and T. Yoshida. (1994). "A Quantitative Analysis of Shear Effects on Cell Suspension and Cell Culture of *Perilla frutescens* in Bioreactors." *Biotechnology and Bioengineering* **44**: 649-654.

Zhong, J.-J., K. Fujiyama, T. Seki, and T. Yoshida. (1994). "A Quantitative Analysis of Shear Effects on Cell Suspension and Cell Culture of *Perilla frutescens* in Bioreactors." *Biotechnology and Bioengineering* **44**: 649-654.

Zhong, J.-J., J.-T. Yu, and T. Yoshida (1995). "Recent Advances in Plant Cell Cultures in Bioreactors." *World Journal of Microbiology and Biotechnology* **11**: 461-467.

Zhou, G. and S. M. Kresta (1996a). "Distribution of Energy between Convective and Turbulent Flow for Three Frequently Used Impellers." *Transactions of Institution of Chemical Engineers* **74**(3): 379-389.

Zhou, G. and S. M. Kresta (1996b). "Impact of Tank Geometry on the Maximum Turbulence Energy Dissipation Rate for Impellers." *AIChE Journal* **42**(9): 2476-2490.